Universidade de Lisboa
Faculdade de Ciências
Departamento de Química e Bioquímica

Synthesis and Study of Metallo-Organic Compounds for Second-Order NLO molecular Switching

Tiago Jorge Laranjeira Silva

Doutoramento em Química
Especialidade em Química Inorgânica

2015

Universidade de Lisboa
Faculdade de Ciências
Departamento de Química e Bioquímica

Synthesis and Study of Metallo-Organic Compounds for Second-Order NLO molecular Switching

Tiago Jorge Laranjeira Silva

Tese orientada pela Prof. Dr. Maria Helena Viegas Garcia e pelo Prof. Dr. Paulo Jorge Gomes Mendes, especialmente elaborada para a obtenção do grau de doutor em Química, especialidade de Química Inorgânica

2015

Para os meus pais

Para a Professora Maria do Carmo Gama

Acknowledgements

Para este trabalho contribuiram inúmeras pessoas às quais quero expressar o meu mais sentido agradecimento:

À prof. M. Helena Garcia pelos ensinamentos que foram além da ciência, pela motivação nas alturas menos boas e pela liberdade dada no laboratório que tornou o caminho difícil mas muito mais enriquecedor.

Ao Prof. Paulo Mendes o meu mais profundo agradeçimento por me ter acompanhado ao longo de todos estes anos de trabalho juntos e pela amizade que deles surgiu; pela confiança depositada, pela paciência inesgotável, pelo perfeccionismo e espírito crítico (construtívo) que almejo alcançar um dia.

À prof. M. Paula Robalo agradeço não só todo o apoio na voltametria ciclica mas também a disponibilidade mostrada sempre que preciso e poucas vezes por mim aproveitada. As marcações da voltametria ficaram sempre "para depois".

Aos profs. João Paulo Ramalho e Alfredo Carvalho agradeço o apoio dado na química quântica e as inúmeras conversas proveitosas que me ajudaram imenso "a manter a entropia do meu cérebro a níveis aceitáveis" (piada dita pelos próprios ainda eu era aluno em Évora) para mais facilmente ultrapassar os obstáculos que foram surgindo.

Aos actuais e aos antigos membros grupo de Química Organometálica da Faculdade de Ciências, nomeadamente à Dra. A. Isabel Tomaz, à Dra. Andreia Valente, ao "Metro-e-Meio" (Cristina Matos), Adhan Pillon, Guilherme Nogueira, sem esquecer e Patrícia Gaudino-Martinez, pelos bons momentos e companhia, dentro e fora da faculdade.

À Maria pela amizade incondicional, em território nacional e além fronteiras.

Ao Diogo Vila-Viçosa, Paulo Costa, Rafael Nunes e João França pela amizade.

Aos meus pais e ao meu irmão por, mesmo sem compreenderem as minhas escolhas, nunca me terem deixado de acreditar em mim e me terem apoiado no caminho que escolhi.

Finalmente, à Filipa por me ter acompanhado mais do que ningum nesta última etapa, pela sua compreensão, apoio e paciência nos momentos mais desesperantes, mas especialmente por tudo o resto. Quem diria que o acaso nos juntava....

A todos o meu obrigado

Abstract

Nonlinear optics (NLO) deals with the interaction of high-intensity electromagnetic radiation with mater. It is an active field of research that find application in technological areas such as optical storage and all-purpose optical devices.

Molecular switches are defined as compounds presenting the ability to commute, in a reversible way, between two or more states in response to external stimulus. These reversible switching processes, and thereby the alteration of the molecular properties of the compounds, find great interest in many technological applications that are based on commutation mechanisms.

This work was developed with the objective of combining the highly NLO-active η^5-monocyclopentadienyliron (II) and ruthenium (II) organometallic fragment with ligands that intrinsically present adequate spectroscopical and redox properties to promote switching processes, with the ultimate goal of obtaining organometallic complexes exhibiting high contrasts of their second-order NLO properties. Objectively, the work combines the synthesis of new organic chromophores and their respective organometallic compounds, their spectroscopical and electrochemical characterization and the evaluation of their nonlinear optical properties. Density functional theory was also used as a useful tool for fully understand the underlying electronic properties of the compounds responsible for their nonlinear optical features.

This thesis is divided in six chapters: In Chapter 1 a brief introduction to the nonlinear optical phenomenon will be addressed. A short mathematical description of the nonlinear optical phenomena is presented followed by the common experimental techniques to evaluate the nonlinear optical properties of molecules. A state-of-the art in organometallic compounds for nonlinear optical purposes is made, in particular for nonlinear optical switching. Fi-

nally, quantum chemical methods for obtaining the optical nonlinearities are presented.

Chapter 2 covers the synthesis, spectrocopic, electrochemical and nonlinear optical characterization of three novel η^5-monocyclopentadienyliron (II) and ruthenium (II) organometallic complexes containing the 5-[3-(thiophen-2-yl)-benzo[c]thiophenyl]thiophene-2-carbonitrile ligand(**L1**). The novel ligand was achieved by a five step procedure in good yield. The complexes were obtained by halide abstraction in the adequate organometallic fragment by thallium (I) hexafluorophosphate. The combination of experimental techniques such as infrared, linear absorption and nuclear magnetic resonance spectroscopies, cyclic voltammetry and hyper-Rayleigh Scattering with density functional theory calculations allowed the unambiguous assignement and interpretation of the electronic properties of the new complexes. The synthesized complexes present moderate hyperpolarizabilities at 1500 nm ($\beta = 105 - 164 \times 10^{-30}$ esu; $\beta_0 = 57 - 87 \times 10^{-30}$ esu). The similarity of the hyperpolarizabilities of the complexes were rationalized by the density functional theory studies which clearly showed that the energies and intensities of the lowest-energy electronic transition, responsible for the nonlinear optical properties, have mainly intra-ligand charge transfer character. The nonlinear optical switching of the complexes was investigated by density functional theory calculations. Results show that upon oxidation or reduction, the compound increased their hyperpolarizabilities by up-to a 8-fold factor.

Chapter 3 is devoted to the synthesis and spectroscopical characterization of five 1,2,4,5-tetrazine (*s*-tetrazine) ligands and three novel η^5-monocyclopentadienyl-ruthenium (II) organometallic complexes. Ligands **L1** and **L2** were synthesized by a Nucleophilic Aromatic substitution reaction on 3,6-bis(3,5-dimethylpyrazolyl)-*s*-tetrazine whereas ligand **L3** and the precursor of **L4** and **L5** were obtained by Piner's method, starting from the adequate nitriles. An unprecedent selective Sonogashira coupling afforded ligands **L4** and **L5** in moderate to good yields. Ligand **L4** is an unprecedent case of a diethynyl-*s*-tetrazine compound. Three novel organometallic complexes were obtained, one complex bearing **L2** and two binuclear complexes bearing ligand **L3**. The

complexes were synthesized by halide abstraction of the adequate organometallic fragments with thallium (I) trifluoromethanesulfonate in moderate yields. The electronic properties of the complexes were investigated by spectroscopic techniques, namely infrared and UV-Vis. and nuclear magnetic resonance spectroscopies. Density functional theory calculations were used in order to gain greater insight of the obtained spectroscopic properties for both the ligands and the complexes. Nonlinear optical properties and the redox-switching abilities were also investigated by density functional theory. Results show that both the ligands and complexes present low to moderate hyperpolarizabilities, in the range of β_{tot} = 0 - 35 $\times 10^{-30}$ esu for the ligands and β_{tot} = 15 - 108 $\times 10^{-30}$ esu for the complexes, in good accordance with perditions made by the spectroscopic data. Concerning the one-redox oxidation of the complexes, results show that the behaviour of the hyperpolarizablities depends on the coordinated ligant to the metal centre. For complex **bRuL2**, DFT predicts an enhancement of the estimated hyperpolarizability by a 8- to 31-fold factor depending on the functional. In the case of complexes **aRuL3** and **bRuL3**, the one-electron oxidation leads to different results for different funtionals: a dimishing by of the hyperpolarizability is expected by *ca.* 2-fold factor for B3LYP and M06. CAM-B3LYP predicts an enhancement of the hyperpolarizabilities of both complexes **aRuL3** and **bRuL3** by a 11-fold and a 2.5-fold factor respectively.

Chapter 4 presents other works developed during the time of this thesis. In particular, the experimental measurements of the nonlinear optical properties of several η^5-monocyclopentadienylmetal (II) complexes and three density functional theory studies, the mechanistic study of ring-opening polymerization of ϵ-caprolactone by a bis-arene-ruthenium (II) complex and the dissociation energies and charge decomposition analysis of several η^5-monocyclopentadienyl-ruthenium (II) organometallic complexes bearing heterocyclic compounds are briefly showed.

Finally, in Chapter 5 the concluding remarks, future prospects and a critical analysis of the work are made, and in Chapter 6 the general methods for the synthesis and Density Functional calculations is presented.

Resumo

A Ótica Não-Linear trata da interação de feixes intensos de luz com a matéria. Actualmente, é uma área de enorme interesse tecnológico uma vez que os seus fundamentos são aplicados em várias área do conhecimento, desde a informática à biotecnologia.

Comutadores moleculares podem ser definidos como moléculas que possuem a capacidade de alterar, de forma reversível, as suas propriedades fisico-químicas por aplicação de um estímulo externo. A reversibilidade destes processos, em particular, têm um grande interesse em aplicações tecnológicas, nomeadamente no desenvolvimento de dispositivos e memórias óticos que possuem no seu funcionamento base fenómenos de transmissão de informação.

Esta tese foi desenvolvida no âmbito do desenvolvimento de compostos organometálicos de ferro (II) e ruténio (II), baseados em η^5-monociclopentadienilos metálicos, contendo ligandos orgânicos que possuam propriedades espectroscópicas e electroquímicas adequadas para promover a comutação das suas propriedades de ótica não linear. Mais objetivamente, este trabalho combina a síntese de novos ligandos orgânicos e dos seus respetivos compostos organometálicos com a sua caracterização espectroscópica e electroquímica, assim como com a determinação das suas propriedades de ótica não linear por dispersão de hyper-Rayleigh. Adicionalmente, estudos pela Teoria da Densidade do Funcional foram aplicados para racionalizar os resultados experimentais obtidos, em particular as referidas propriedades de ótica não linear. Esta tese encontra-se dividida em seis capítulos:

No Capítulo 1 será feita uma breve introdução ao fenómeno da ótica não linear. Será apresentada uma breve descricção matemática dos processos de ótica não linear seguida da apresentação das técnicas experimentais mais comuns para a determinação destas propriedades em compostos químicos. Far-se-á também

pequeno estado da arte sobre compostos organometálicos com elevadas propriedades de ótica não linear, em particular compostos cujas propriedades de comutação molecular foram já demostradas. Finalmente, serão descritos os métodos quânticos comummente usados para a determinação das propriedades de ótica não linear. Será dada particular atençcão aos métodos utilizados na teoria da densidade do funcional.

O Capítulo 2 trata da síntese e caracterização espectroscópica e electroquímica de três novos compostos organometálicos contendo fragmentos η^5-monociclopentadienilos de ferro (II) e rutnio (II) e um ligando baseado em 1,3-ditienilbenzo[c]-tiofeno. O novo ligando foi obtido com bom rendimento em cinco passos sintéticos. Os respectivos complexos organometálicos foram síntetizados por abstração de halogeneto com trifluorofosfato de tálio (I). A combinação de várias técnicas espectroscópicas, nomeadamente espectroscopias de infravermelho, ultravioleta-vísivel e ressonância magnética nuclear, electroquímicas (voltametria cíclica) e de dispersão de hyper-Rayleigh com cálculos quânticos permitiu correlacionar e interpretar todos os dados experimentais obtidos. Os compostos síntetizados mostraram propriedades de ótica não linear moderadas ($\beta = 105 - 164 \times 10^{-30}$ esu; $\beta_0 = 57 - 87 \times 10^{-30}$ esu) quando comparados com outos compostos semelhantes já publicados. A semelhança dos valores obtidos para todos os compostos sintetizados foi racionalizada com base em estudos da teoria da densidade do funcional, onde se mostrou claramente que as energias e as intensidades das transições de menor energia, responsáveis pelas propriedades de ótica não linear dos compostos, possuem essencialmente um carácter relacionado com o ligando. A comutação das propriedades de ótica não linear dos compostos foram investigadas através da teoria da densidade do funcional, tendo os resultados mostrado que, após um estímulo redox, os compostos sintetizados aumentam até oito vezes o valor das sua propriedades de ótica não linear.

No Capítulo 3 são apresentadas as sínteses e caracterização espectroscópica de cinco novos ligandos baseados em anéis de 1,2,4,5-tetrazina (*s*-tetrazina), assim como a sínteses e caracterização espectroscópica de três novos compostos organometálicos. Os ligandos **L1** e **L2** foram sintetizados em bom rendimento

a partir de 3,6-bis(3,5-dimetilpirazolil)-*s*-tetrazina por uma reacção de Substituição Nucleofílica Aromática. O ligando **L3** e o percursor dos ligandos **L4** e **L5** foram síntetizados pelo método de Piner a partr de compostos contendo nitrilos nas posições adequadas. Por sua vez, os ligandos **L4** e **L5** foram síntetizados selectivamente por uma reação de acoplamento de Sonogashira em rendimentos moderados. O ligando **L4** é o único derivado de 1,2,4,5-tetrazina conhecido na literatura que contém duas funções acetilénicas. Foram obtidos três complexos organometálicos, um contendo o ligando **L2** e dois contendo o ligando **L3**, por abstração de halogeneto com trifluorometanossulfonato de tálio (I) em rendimentos moderados. As propriedades electrónicas dos compostos foram estudadas por técnicas espectroscópicas, nomeadamente espectroscopias de infravermelho, ultravioleta-vísivel e ressonância magnética nuclear. Estudos pela teoria da densidade do funcional foram utilizados para uma melhor compreensão e correlação com resultados experimentais obtidos. As propriedades de ótica não linear e de comutação foram também avaliados por cálculos quânticos. Os resultados obtidos mostram que quer os ligandos quer os complexos organometálicos apresentam propriedades moderadas (β_{tot} = 0 - 35 $\times 10^{-30}$ esu para os ligandos e β_{tot} = 15 - 108 $\times 10^{-30}$ esu para os complexos organometálicos) quando comparados com outros publicados na literatura. Estes resultados estão em concordância com as propriedades espectroscópicas obtidas. No que respeita ás propriedades de comutação, mostrou-se que as propriedades de ótica não linear para estes compostos são dependentes dos ligandos coordenados. Por exemplo, após um estimulo redox, prevê-se que o o complexo **bRuL2** aumente a sua primeira hiperpolarizabilidade por um factor de 8 a 31 vezes consoante o funcional utilizado, enquanto que os compostos **aRuL3** e **bRuL3** apresentam diferentes comportamentos para os funcionais utilizados: de acordo com o funcional CAM-B3LYP deverão diminuir esta propriedade para metade e de acordo com os funcionais B3LYP e M06 deverão aumentar a sua hiperpolarizabilidade 11 e 2.5 vezes, respectivamente.

No Captulo 4 mostrar-se-ão outros trabalhos efectuados no decurso deste doutoramento, envolvendo medições experimentais de hiperpolarizabilidades de compostos organometálicos e cálculos pela teoria da densidade do funcional.

Finalmente, nos Capítulos 5 e 6 serão feitas as conclusões gerais e considerações finais do trabalho realizado e a descrição dos métodos experimetais gerais para a obtenção e caracterização dos compostos.

Contents

List of Figures

Page

Chapter 1

Chapter 2

Chapter 3

Chapter 4

List of Schemes

Page

Chapter 1

Chapter 2

Chapter 3

List of Tables

Page

Chapter 1

Chapter 2

Chapter 3

Symbols and Abbreviations

In Equations

α_{ij}	Linear polarizability tensor
β_0	Zero frequency quadratic nonlinearity
β_{ijk}	Quadratic hyperpolarizability tensor component
γ_{ijkl}	Cubic hyperpolarizability tensor component
λ	Wavelength
μ_i	Dipole moment in the ith direction
ω_{ij}	Frequency
$I_{2\omega}$	Intensity of second-harmonic light
I_{ω}	Intensity of light
P_i	Macroscopic polarization vector component

Acronyms

CC	Coupled Cluster
CI	Configurational Iteration
CT	Charge Transfer
DCM	Dichloromethane
DFT	Density Functional Theory

DMF Dimethylformamide

EFISH or EFISH Electric field-induced second-harmonic generation

FF Finite Field method

FTIR Fourier-transform Infrared Spectroscopy

GDA Generalised Gradient Approximation

HF Hartree-Fock

HRS Hyper-Rayleigh scattering

ILCT Intra-Ligand Charge Transfer

ITN Isothianaphtalene, refering to 1,3-dithienoylbenzo[c]thiophene

KE Electro-Optical Kerr Effect

KS Kohn-Shan

LDA Local Density Approximation

MLCT Metal-to-Ligand Charge Transfer

MP Moller-Plesset

MPF Multi-Photon Fluorescence

NLO Nonlinear Optics

NMR Nuclear Magnetic Resonance Spectroscopy

PE Pockels Effect

PEDOT Poly(3,4-ethylenedioxythiophene)

SD Slater Determinant

SHG Second-Harmonic Generation

SONLO Second-Order Nonlinear Optics

SOS Sum-Over-States method

TD-TDF Time Dependent Density Functional Theory

THG Third Harmonic Generation

TLM Two-Level Model

TPA Two Photon Absorption

Uv-Vis. Ultraviolet-Visible Spectroscopy

XC Exchange Correlation functional

Chapter 1

Introduction

And God said "Let there be light", and there was light (Genesis, 1:3). This is probably the most known reference to light and its origin. Since the beginning of time light always played a vital role in human and all living beings life. Without light probably the Universe as it is known would not exist, since many phenomena in Nature are driven by light. Life itself would certainly not exist. Nowadays, light is a crucial resource for all technological applications, from simple compact disc players to store's checkout lines, where laser beams read bar codes for prices. Digital cameras that capture our world and allow pictures to be taken also use light. More importantly, light is the basis of the technology that allows computers and telephones to be connected to one another through fibre optics cables.

Photonics is defined as the generation, manipulation, transport, detection, and use of light information and energy, whose quantum unit is the photon. Today, the global market for photonics is estimated to be approximately €300 billion. This market is expected to grow significantly over the next few years, with the estimated market size approaching €480 billion by 2015. Europe has an overall share of 20% of this global market and the annual market growth rate of photonics in Europe is estimated to be between 8 and 10%. Europe also has particularly strong positions in industrial laser technologies, information and communications technology and biophotonics.[1]

Not only for these economic reasons but also due to the current and constant need for the improvement of the available technology, photonics is one of the most active fields of academic research, namely in energy, information and communication technologies and in the development of new components for medical and life sciences, imaging and production technologies. Among these components are new light sources, transistors,

amplifiers, modulators, storage devices and switches. The current technological advances are made at the expenses of the development and understanding on the Nonlinear Optics (NLO) field. Nonlinear optical phenomena and materials can be considered as the basic elements for all-optical processing systems. Nevertheless, most materials exhibit relatively weak nonlinear optical properties and need large size devices with high operational power and cost, making them unsuitable for all-optical integrated devices. Still, when compared to common electronic devices, these systems are much more desirable due to a much more efficient and fast energy and information transfers.

This Chapter is divided in four parts: in the first part a brief introduction to NLO will be addressed and a short mathematical description of the NLO phenomena is presented; the second part will show the state of the art on the organometallic compounds for NLO applications, particularly *Second-Harmonic Generation* (SHG); the third part deals with Molecular Switching based on molecular entities. A brief description and examples of compounds that can act as Molecular Switches, and particularly NLO Molecular Switches are presented; finally, the fourth part is dedicated to *Density Functional Theory* applied to NLO phenomena, and how to obtain these quantities by quantum chemical modelling.

1.1 Microscopic Theory of Nonlinear Optics

All-optical phenomena arise from light-matter interactions. In particular, nonlinear optical phenomena arise from the interaction of strong electromagnetic fields, like the ones produced by laser beams, with matter. Herein, only a brief physical and mathematical description will be made, in order to give the reader the enough insights to understand the following sections. A detailed mathematical description of the principles of nonlinear optics can be found elsewhere.[2–8]

Light, or an electromagnetic (EM) radiation in general, can be described either by a stream of particles (photons) or by a time- and space-varying oscillating electric ($\vec{E}$) and magnetic ($\vec{B}$) fields. A material, in its turn, can be seen as a collection of charged particles: nuclei and electrons. Hence, two different approaches can be used when one is dealing with light-matter interactions: a particle-like model and a wave-like model.

In one hand, if light is considered as a stream of photons, where each photon carries a linear momentum that can be transferred to the molecule, the nonlinear optical properties can be simply explained as the annihilation (absorption) of n photons of ω frequency with

the creation (emission) of a new photons of $n\omega$ frequency. This process requires that the energy of the photons is such that the molecule is considered to be excited to pseudo-energy levels, also known as *virtual excited-sates*. The particle-like model of nonlinear optical phenomena for the interaction of a molecule with two photons is represented in **Figure 1.1**.

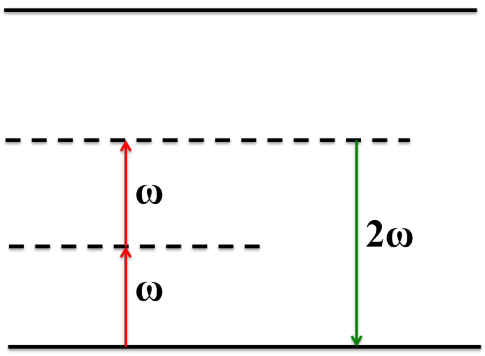

Figure 1.1: Particle-like model for the description of nonlinear optical phenomena.

In another hand, if light is considered an oscillating electromagnetic field, the light-matter interaction can be described by an acting electric force that perturbs the nuclei and electrons motion in opposite directions, the positive charges (nuclei) will tend to move in one direction, whereas the negative charges (electrons) will tend to move towards the opposite direction. This oscillating movement will occur at the electric field frequency. According to the Born-Oppenheimer approximation the nuclei have much slower movements than the electrons, and hence only the electron movement is usually considered. Therefore, when an intense light beam interacts with highly polarizable electrons of a molecule, its electric field, $\vec{E}$, generate a distortion in the electronic cloud of the molecule, resulting in an induced polarization. Within these interactions the electromagnetic field components of the incident light beam are modied and new components, differing for example in phase, frequency or amplitude, are produced. The induced dipole moment can be estimated in term of the molecular polarization ($\vec{\rho}$). If the intensity of the incident light is low, the relation between the polarization and the electromagnetic field is linear, and its is given by:

$$\rho = \mu_0 + \alpha E. \tag{1.1}$$

where μ_0 is the permanent molecular dipole moment and α is the first-order polarizability, or linear polarizability, at a certain radiation frequency, ω. The vectorial forms of the quantities as well as their frequency dependency were omitted for simplification. The first-order polarizability is related to linear optical properties, namely the refractive index. In the presence of intense fields, such the ones produced by lasers, the electrons movement is much greater than the nuclei movement, especially if the molecule has delocalized π-electrons. The charge separation its enhanced and new nonlinear terms are generated. The induced polarization is, thus, given by:

$$\rho = \mu_0 + \alpha E + \beta E^2 + \gamma E^3 + \ldots \tag{1.2}$$

where β is the first hyperpolarizability (or second-order polarizability or also quadratic hyperpolarizability) and γ is the second hyperpolarizability (or third-order polarizability or also cubic hyperpolarizability). As before, the vectorial form and the frequency dependence of the polarization and the electric field were omitted for simplification. The first and second hyperpolarizabilities, β and γ, are quantities that are associated with the second- and third-order NLO phenomena, respectively. In particular, β is responsible for phenomena like second-harmonic generation, sum- and difference-frequency generation and parametric amplification, whereas γ is responsible for phenomena like third-harmonic generation, degenerate four-wave mixing and stimulated Raman scattering, among others.

In equation 1.2 both the polarizability and the hyperpolarizabilities were treated as scalar quantities. However, α, β and γ are vectorial quantities that are dependent on the cartesian coordinates of the molecular system. The linear polarizability and the second- and third-order hyperpolarizabilities are, in fact, first, second and third rank tensors, with 9, 27 and 81 components each, respectively. Hence, α should be denoted α_{ij}, β should be denoted β_{ijk} and γ should be denote γ_{ijkl}. These quantities are also dependent on the frequency of the incident light. Including this frequency dependence in equation 1.2, the

following general relation is obtained:

$$\begin{aligned}\vec{\rho} = \vec{\mu_0} &+ \sum_j \alpha_{ij}(-\omega;\omega)E_j(\omega) \\ &+ \sum_{j\leq k} \beta_{ijk}(-2\omega;\omega_1,\omega_2)E_j(\omega_1)E_k(\omega_2) \\ &+ \sum_{j\leq k\leq l} \gamma_{ijkl}(-3\omega;\omega_1,\omega_2,\omega_3)E_j(\omega_1)E_k(\omega_2)E_l(\omega_3) \\ &+ \ldots\end{aligned} \tag{1.3}$$

Due to the conservation of energy principle, the sum of the generated and vanishing frequencies must be zero and therefore $-\omega = \omega$, $-2\omega = \omega_1 + \omega_2$ and $-3\omega = \omega_1 + \omega_2 + \omega_3$. The negative sign arises by the definition that the emitted frequency should be negative.

Equation 1.3, is still an simplification, and can be used only in the static field domain. Optical fields are time-dependent, and contain an oscillatory term at a frequency ω:

$$E(t) = E_0 \cos(\omega t) + \frac{E_0}{2}\left(e^{i\omega t} + e^{-i\omega t}\right) \tag{1.4}$$

Substituting equation 1.4 into equation 1.3 and expanding using trigonometric relations one obtains:

$$\rho = \mu_0 + \frac{1}{2}\alpha E_0 e^{i\omega t} + \frac{1}{2}\beta E_0^2 + \frac{1}{4}\beta E_0^2 e^{2i\omega t} + \frac{3}{8}\gamma E_0^3 e^{i\omega t} + \frac{1}{8}\gamma E_0^3 e^{3i\omega t} + c.c. + \ldots \tag{1.5}$$

with *c.c.* denoting complex conjugate terms. It is evident from the equation above that the presence of higher-order terms leads to generation of new frequencies of molecular dipole oscillation: the "β term" causes the appearance of frequency doubling (2ω) while the "γ term" gives frequency tripling (3ω). In addition, the second-order term generates a time-independent contribution to the dipole (called optical rectication) and a cubic term, due to γ, oscillating at the frequency ω. Finally, it is shown that the β and γ tensors are complex quantities, with real and imaginary parts. For second-order NLO effects, only the real part is important, but for third-order NLO effects, both real and imaginary parts have to be taken into account.

Equation 1.5 provides the fundamental origin of microscopic hyperpolarizabilities that

govern the nonlinear optical properties at the molecular level.

1.2 From the Microscopic to the Macroscopic Domain

The earliest measurements of the linear and nonlinear optical properties of organic crystals showed that the crystal optical properties mimic the properties of the individual molecules. However, the response of the bulk material to an electric field is not a simple summation of all the individual molecular (hyper)polarizations. They are, nevertheless, proportional and can be obtained by simple scaling. It is, hence, possible to write analogue equations for the linear (Equation 1.1) and nonlinear (Equation 1.2) regime of the polarization. If instead of an individual molecule, the applied electromagnetic field is interacting with a bulk material, the dipole moment can now be written as:

$$P = \epsilon_0 + \chi^{(1)}E \tag{1.6}$$

$$\begin{aligned} P &= \epsilon_0 + \epsilon_0\chi^{(1)}E + \epsilon_0\chi^{(2)}E^2 + \epsilon_0\chi^{(3)}E^3 + \dots \\ &= \epsilon_0(\chi^{(1)}E + \chi^{(2)}E^2 + \chi^{(3)}E^3 + \dots) \\ &= \epsilon_0(P^{(1)} + P^{(2)} + P^{(3)}) \end{aligned} \tag{1.7}$$

where ϵ_0 is the vacuum permittivity, and $\chi^{(1)}$, $\chi^{(2)}$ and $\chi^{(3)}$ are the linear and nonlinear first and second susceptibilities, respectively. As in the microscopic case, the vectorial form and the frequency dependence were omitted for simplification.

The quantities $\chi^{(2)}$ and β will be extensively discussed along this work since they are responsible for the second-order nonlinear optical phenomena. Thus, a relation between the two quantities is necessary and its given by the following expression:

$$\chi^{(2)} = Nf\beta \tag{1.8}$$

where N is the number of density and f is the local field factor. It is clear that $\chi^{(2)}$ and β must have the same dimension and, in fact, they are both second rank tensors. The local field factor arises from the fact that a molecule that is hosted in a collection

of several other molecules, like the case of a crystal, experiences not only the force of the applied electric field but also the electric fields generated by its surroundings. In other words, the electric field at the molecular site is a superposition of the applied electric field and the electric field due to local fluctuations in charge density of the nearby molecules. The Lorentz−Lorenz model and the Onsager model are the most used field factors, the latter being of greater importance to nonlinear optics. Equations 1.9 and 1.10 are the equations resulting from the Lorentz−Lorenz and the Onsager models, respectively.

$$f_\omega = \frac{\epsilon_\omega + 2}{3} \tag{1.9}$$

$$f_0 = \frac{\epsilon_0(\epsilon_\infty + 2)}{2\epsilon_0 + \epsilon_\infty} \tag{1.10}$$

where ϵ_ω is the dielectric constant at frequency ω, ϵ_0 is the dielectric constant of the surroundings and ϵ_∞ is the internal dielectric constant of the molecule, that is assumed to be the square of its refractive index.

The orientational average of the molecules in the crystal lattice is also an essential factor in the macroscopic hyperpolarizabilities. As for all even-order optical phenomena there is a non centrosymmetric requirement in order to have a non-zero first hyperpolarizability, that is, in order to $\chi^{(2)}$ be a non zero-quantity, the material has to be non-centrosymmetric. In the case of crystals, $\chi^{(2)}$ is completely determined by its symmetry, and therefore, there is a need of knowing the molecular symmetry group in order to correctly estimate the first hyperpolarizability of molecules. In other words, the molecular symmetry will determine which of the 27 tensors of either $\chi^{(2)}$ or β are nonzero values.

Finally, molecular reorientational contributions to the hyperpolarizabilities are also important for measurements of the second-order hyperpolarizability in solution, and must be taken into account, particularly for higher intensity fields.

1.3 Experimental Techniques for Measuring Second-Order NLO Properties

There are several experimental techniques and computational methods that allow to evaluate the NLO properties of chemical compounds. Herein, only the experimental techniques for obtaining second-order nonlinear optical properties will be discussed. A more com-

plete description of all the techniques, including the ones for the evaluation of higher order phenomena is described elsewhere[8–13] and in the references therein. The computational methods will be addressed further on the text (*c.f.* Section 1.6.3).

The measurement of the NLO response can be performed both in solid state or in solution. The most popular method for measurements in the solid state is *Kurtz and Perry Powder Technique*, whereas for measurements in solution *Electric Field Induced Second-Harmonic Generation* (EFISH), *hyper-Rayleigh Scattering* (HRS) and the *Z-scan Method* are the most used. In this work only HRS and the Kurtz Powder technique will be discussed in detail. The other techniques will be only briefly described. Although solvatochromic measurements do not afford direct quantification of the nonlinear optical properties, they are important for the qualitative estimation of the NLO properties of organic and organometallic compounds. For that reason, they will be also included at the end of this section.

1.3.1 Kurtz and Perry Powder Technique

The Kurtz and Perry powder technique was one of the earliest methods to determine the nonlinear optical susceptibilities of powders, namely the first-order nonlinear optical susceptibility, $\chi^{(2)}(-2\omega;\ \omega,\ \omega)$. Samples are prepared by grinding the solids in to small size particles of thickness, r, (usually $75 < r < 150\ \mu m$) by the use of standard sieves, and are loaded into a cell with a known thickness, L, usually 0.2 mm. The same procedure is used for a standard of known nonlinear optical susceptibility. The most common standards are urea, quartz, zinc oxide and dihydrogenophosphate salts, like ammonium dihydrogenophosphate (ADP) or potassium dihydrogenophosphate (KDP). In a typical laser set up, showed in **Figure 1.2**, the sample is irradiated with a 1064 nm laser beam of a diameter d and operating at a frequency, ω. In order to ensure that a statistically large number of particles of random orientation are encountered, the laser beam diameter is much larger than the thickness of the particles.

The generated second-harmonic light is separated from the fundamental laser wavelength by filters and a monochromator and detected in a photomultiplier tube (PMT). The readout is made in an oscilloscope. The efficiency of the harmonic generation is obtained by comparison of the intensity of the sample's and of the standard's harmonic

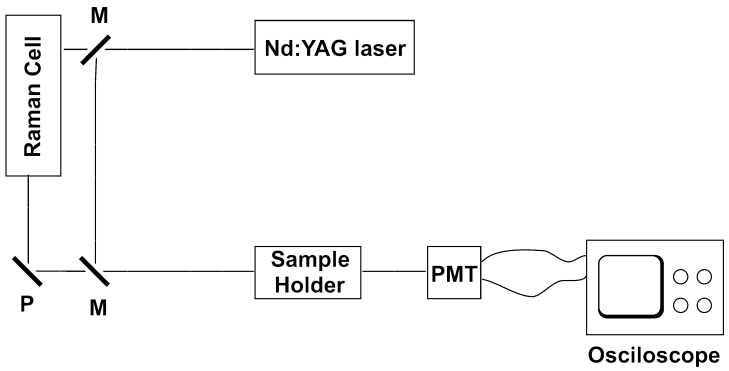

Figure 1.2: Typical laser set-up for the Kurtz Powder Technique

(adapted from ref.[14])

light:

$$SHG_{efficiency} = \frac{I_{2\omega}(sample)}{I_{2\omega}(standard)} \tag{1.11}$$

Hence, the Kurtz-Perry powder technique is used to compare the intensity of the SHG of a powder sample with that of a reference sample of known $\chi^{(2)}$:

$$\frac{I_{2\omega}(sample)}{I_{2\omega}(standard)} \propto \frac{d_{ef}(sample)}{d_{ef}(standard)^2} \tag{1.12}$$

where d_{ef} represents the nonlinear optical coefficient, that is proportional to $\chi^{(2)}$. Despite the simplicity of the experimental laser set up, the data analysis and interpretation of the signal is not straightforward. Factors like the particle size and its packing, the crystallographic structure of the compound or the phase conjugation of the laser beam can be critical. Also, re-absorption of the harmonic light in the solid state can also be present, in particular if compounds have absorption bands nearby the second-harmonic wavelength. Optical degradation upon irradiation with the laser beam cannot be excluded as well. Given that the relation between β and $\chi^{(2)}$ depends on crystal packing, this technique is not applicable to compounds crystallizing in centrosymmetric space groups, this being the case of most of the compounds possessing large dipole moments. For all these reasons, Kurtz-Perry powder technique results do not have a quantitative significance, and are used only qualitatively to establish the magnitude of generation of second-harmonic light of a solid towards a known reference. Although this technique is limited it is a simple and

rapid method for screening a large number of powder materials.

1.3.2 Hyper-Rayleigh Scatterring

Hyper-Rayleigh Scattering (HRS) is currently the most used technique to estimate the molecular nonlinearities, β. The HRS experiment consists in recording the scattered light intensity of all molecules interacting with the laser radiation as a function of the incident laser light intensity, as shown by equation 1.13:

$$I_{2\omega} = \frac{16\pi^5}{c\lambda^4 r^2} N f_\omega^4 f_{2\omega}^2 \left\langle \beta_{HRS}^2 \right\rangle I_\omega^2 \tag{1.13}$$

where $I_{2\omega}$ is the second-harmonic intensity, N is the number of molecules per unit of volume, f_ω^4 and $f_{2\omega}^2$ are local field factors for the linear and nonlinear regime respectively, I_ω is the fundamental wavelength intensity, r the distance to the scattering centre, and c the speed of light in vacuum. The brackets indicate the orientational average of the molecular hyperpolarizability. The second-order signal is therefore generated from an isotropic solution of a solute randomly dissolved in a solvent. Simply speaking, although a solution is an isotropic medium, the time average of the fluctuating induced dipole response $\mu(r,t)$ during the excitation is not, in average, zero. Since HRS is based on fluctuations away from centrosymmetry in solutions, pulsed lasers and very accurate focusing are needed to obtain enough intensity of the harmonic generation. The most commonly used laser apparatus is Q-switched Neodymium-doped Yttrium Aluminium Garnet (Nd:YAG) laser working at milijoule energy in nanosecond pulses, resulting in megawatt peak power energy. The fundamental wavelength of the laser is usually 1064nm, although higher wavelengths are also common. The changing of the fundamental wavelengths further to the red is achieved by optical parametric oscillators (OPO's). The use of these nanosecond lasers requires also the use of gated integrators (boxcar averagers) to increase the signal-to-noise ratio of the experiments. Also, since this technique is based on a incoherent scattered light it is essential to vary the intensity of the fundamental light intensity externally. This is achieved by the use of a half-wave rotation plate between two polarizers (P). The first polarizer ensures an 100% intensity of horizontal polarization of light is obtained. The half-wave plate (HWP) changes the polarization of this light by a few degrees and the second polarizer defines its exact vertical polarization. By this way, the rotation of the HWP modulates the incoming light intensity from zero to maximum intensity. The light

is then splited by a beam splitter (BS) that directs a fraction of this light towards the sample and the remaining to a photodiode that collects and analyses both its pulse time and intensity. The scattered second-harmonic light intensity is of very low intensity and its detection has to be efficient enough to collect very low levels of scattered photons. This system consists of a photomultiplier tube (PMT) with an interference filter (F) for the second-harmonic wavelength on one side and a mirror of the other side of the cell to maximize the number of scattered photons reaching to the photomultiplier. A general laser set-up of an HRS experiment is shown in **Figure 1.3**.

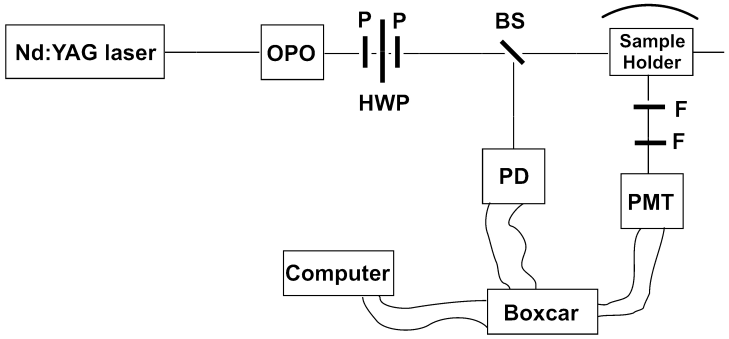

Figure 1.3: Typical laser set-up for the HRS experiment

(adapted from ref.[15])

Since HRS measurements are done in solution, both the contributions of the solute and the solvent must be present in the scattered light intensity. It is clear that HRS experiments might require the knowledge *a priori* of the solvent's hyperpolarizability. However, that is only possible if the solvent has itself a large enough hyperpolarizability. If that is the case, then a simple plotting of the quadratic coefficient (QC) of different concentration solutions of the solute is enough to obtain $\langle\beta^2_{HRS}\rangle_{solute}$:

$$\begin{aligned} QC &= GN_{solvent}\langle\beta^2_{HRS}\rangle_{solvent} + GN_{solute}\langle\beta^2_{HRS}\rangle_{solute} \\ &= intercept + slope\,\langle\beta^2_{HRS}\rangle_{solute} \end{aligned} \tag{1.14}$$

If the solvent in use does not have a measurable hyperpolarizability, it is possible to use an external reference method. In this case a standard of well-known hyperpolarizability is used and the obtained slope of a series of different solutions of the standard and the

solute are compared.

$$I_{2\omega} = GN_{standard} \langle \beta^2_{HRS} \rangle_{standard} = slope_{standard} \langle \beta^2_{HRS} \rangle_{standard} \tag{1.15}$$

$$I_{2\omega} = GN_{solute} \langle \beta^2_{HRS} \rangle_{solute} = slope_{solute} \langle \beta^2_{HRS} \rangle_{solute} \tag{1.16}$$

Dividing equations 1.16 by 1.15 the following relation that allows to determine the nonlinearity of the solute is obtained:

$$\begin{aligned} \frac{slope_{solute}}{slope_{standard}} &= \frac{\langle \beta^2_{HRS} \rangle_{solute}}{\langle \beta^2_{HRS} \rangle_{standard}} \\ \langle \beta^2_{HRS} \rangle_{solute} &= \sqrt{\frac{slope_{solute}}{slope_{standard}}} \langle \beta^2_{HRS} \rangle_{standard} \end{aligned} \tag{1.17}$$

Its important to state that, besides second-harmonic generation, there is other sources of incoherent photon emission at the second-harmonic wavelength. This phenomenum, called multi-photon fluorescence (MPF), are, in fact, an additional contribution to the HRS signal, and hence it can result in an overestimation of the hyperpolarizability values. Since two-photon fluorescence has the exact same wavelength then the second-harmonic generation, the interference filter itself does not provide any guarantee of a pure HRS signal. However, it is not necessary the use of other techniques to ensure that the HRS signal has MPF contamination. A simple methodology was purposed by Song *et al.* based on the spectral resolution of the MPF and HRS signals.[16] MPF present a very broad band whereas HRS presents a very narrow peak of only a few wavelengths. When interference filters are used at discrete wavelengths close to the second-harmonic signal, it is possible to investigate the presence of the MPF signal, with a simple relation between the fluorescence intensities of the solute and the solvent and the intensity of the HRS signal it is possible to subtract the MPF contribution. This relation is:

$$\alpha = \frac{I_{Fluorescence}}{I_{HRS} - I_{solvent}} \tag{1.18}$$

Other methodology was purposed by Noordman *et. al* using the different time scales

of the MPF and the HRS phenomena.[17] HRS is considered a time-immediate phenomenon but MPF have a nano scale time regime. By applying the proper time-gating in the boxcar averagers, it is possible to differentiate these signals. Other possibility is to change the laser set-up and its pulse time from nanoseconds to femtoseconds.

$\langle\beta^2_{HRS}\rangle$ is strongly dependent of the coordinate system, the polarization state of the fundamental and second-harmonic light, as well as the geometry of the experiment itself. Let us define (X, Y, Z) as the laboratory coordinates and (x, y, z) as the internal molecular coordinate system. In a classic HRS experiment, a 90°-geometry experiment is used, that is, the fundamental light is propagating in the X direction and is polarized in the Z direction, whereas the second-harmonic light is collected in the Y direction. The relations between the laboratory and the internal molecular coordinate systems were determined by Cyvin *et al.* and are the following:[18]

$$\langle\beta^2_{ZZZ}\rangle = \frac{1}{7}\sum_i \beta^2_{iii} + \frac{6}{35}\sum_{i\neq j}\beta_{iii}\beta_{ijj} + \frac{9}{35}\sum_{i\neq j}\beta^2_{iij} + \frac{12}{35}\sum_{ijk,cyclic}\beta^2_{ijk} \tag{1.19}$$

$$\begin{aligned}\langle\beta^2_{XZZ}\rangle = \frac{1}{35}\sum_i \beta^2_{iii} - \frac{2}{105}\sum_{i\neq j}\beta_{iii}\beta_{ijj} + \frac{11}{105}\sum_{i\neq j}\beta^2_{iij} \\ - \frac{2}{105}\sum_{ijk,cyclic}\beta_{iij}\beta^2_{jkk} + \frac{8}{35}\beta^2_{ijk}\end{aligned} \tag{1.20}$$

The first subscripts of equations 5.5 and 5.6 (Z or X) refer to the polarization of the second-harmonic light, and if they are measured with same sensitivity, then:

$$\langle\beta^2_{HRS}\rangle = \langle\beta^2_{ZZZ}\rangle + \langle\beta^2_{XZZ}\rangle \tag{1.21}$$

Most molecular systems are dipolar *push-pull* systems where the dipole moment is aligned with the z-axis. On the assumption that, in these cases, β_{zzz} is much larger than β_{xzz}, a good approximation is made by:

$$\langle\beta^2_{HRS}\rangle \approx \left(\frac{1}{7}+\frac{1}{35}\right)\langle\beta^2_{ZZZ}\rangle = \frac{6}{35}\langle\beta^2_{ZZZ}\rangle \tag{1.22}$$

$$\rho = \frac{\langle\beta^2_{XZZ}\rangle}{\langle\beta^2_{ZZZ}\rangle} \tag{1.23}$$

It is clear, by equations 5.5 and 5.6 together with equation 1.23, that depending on the symmetry of the molecule, and hence the number of non-vanishing tensors, the depolarization ratios will be different for a given molecule. For the prototypical *push-pull* one dimensional system, where the major tensor is β_{ZZZ}, the depolarization ratio is $\frac{1}{5}$. Although the estimation of the depolarization ratio seems to be quite straightforward, by changing the detection polarizers of the experimental setup, it can still be affected by the same factors that affect the hyperpolarizability measurement itself, namely the contribution to the total hyperpolarizability by the solvent and the MPF phenomena.

1.3.3 Electric Field Induced Second Harmonic Generation

The Electric Field Induced Second-Harmonic Generation (EFISH) allows the determination of the first-order hyperpolarizability, β(-2ω; ω, ω) of molecules in solution through the determination of the second-order susceptibility, $\chi^{(3)}$ (-2ω; ω, ω, 0). In this technique, alongside the incident polarized laser beam of frequency ω, a strong static electric field, $\vec{E}$, is applied to a wedge-shaped cell containing a solution of the sample, which is placed perpendicularly to the incoming laser beam. The electric field is applied all over the cell glass walls, and forces the molecules with a permanent dipole moment to partly align according to its direction, hence breaking the centrosymmetry of the medium, and allowing nonlinear properties to be obtained. Because a strong electric field is required to align the molecules, they should have a permanent dipole moment. For that reason EFISH can not be applied to measure the second-order nonlinear optical properties of non-polar or octupolar molecules. Also, EFISH cannot be used with ionic molecules or with a polar solvent. This is in fact the major drawback of this technique comparatively to HRS, since it prevents the usage of the vast majority of organometallic complexes to be analysed by this technique.

The second-order susceptibility is related to the third-order molecular polarizability, γ_{ijkl}, by the following relation:

$$\chi^{(3)}(-2\omega;\omega,\omega,0) = N f_0 f_{2\omega} f_\omega^2 \gamma_{ijkl} \tag{1.24}$$

where N is the number density of the solute and f_0, $f_{2\omega}$ and f_ω^2 are local field factors. The third-order molecular polarizability, in its turn, has three main terms: an electronic,

γ^e_{ijkl}, a vibronic term, γ^v_{ijkl} and a rotational term, γ^v_{ijkl}.

$$\gamma_{ijkl} = \gamma^e_{ijkl} + \gamma^v_{ijkl} + \gamma^v_{ijkl} \tag{1.25}$$

In EFISH, it is only the rotational contribution to the third-order molecular polarizability that is proportional to the second-order molecular polarizability. The relation between this two quantities is given by:

$$\gamma^v_{ijkl} = \frac{\mu \cdot \beta_{vec}}{5k_bT} \tag{1.26}$$

where μ is the molecular dipole moment, β_{vec} is the vectorial component of the second-order hyperpolarizability projected in the dipole moment axis, k_b is Boltzmann's constant and T is the temperature. Hence, in EFISH, the net second-order effect is dependent on the $\mu \cdot \beta_{vec}$ product. To obtain the value of β_{EFISH} it is thus necessary to know the value of the ground state dipole moment of the molecule. This is in fact another drawback of this technique: the fact that other quantities are required for the interpretation of the results, namely the dielectric constant of the solvent, the permanent dipole moment and the intrinsic second-order hyperpolarizability of the material, that must be obtained by a separate experiment, makes the EFISH technique very limited and troublesome.

Like in the case of HRS, several reference methods can be used. On one side, the use of a quartz reference wedge-shaped crystal allows one to use the quartz itself as a reference. On other side, if the solvent where the experiment is performed has a nonlinear third-order response, it can also be used as reference for determining the solute molecular cubic hyperpolarizability and therefore, if the dipole moment of the solute is known, the molecular quadratic hyperpolarizability.

1.3.4 Solvatochromism

Solvatochromism is defined as the change in position, intensity and also shape of the UV-Vis absorption band of a molecule in solvents of different dielectric constant. It provides a quick and simple proof of solvent-solute interactions between the ground and the excited-state. This solvent-solute interaction can be divided in pure electrostatic interactions, dispersion interactions and hydrogen-bonding interactions. All of them affect the NLO properties of a molecule in solution and by this fact it is an important when one wants to estimate nonlinear properties, especially when working with donor-acceptor *push-pull*

chromophores. The change in the nonlinear properties of *push-pull* chromophores as a function of the dielectric constant of the solvent can be understood by the changes in the stabilization of the ground and excited state upon excitation. An electronic transition from the ground state to an excited state leads to a substantial change in the electronic density of a molecule, and therefore an alteration in its dipole moment. In its turn, this change in the dipole moment will lead to an enhanced polarization of both the solvent in the solvation sphere of the molecule and other solute molecules in its surroundings. If a red shift is observed in the absorption band of a solute, in solutions of two different solvents with increasing dielectric constant, the molecules present a higher polarization in the excited state than in the ground state, $\mu_g<\mu_e$. This is called positive solvatochromism. In this case, solvents with higher dielectric constant enhance the excited state stabilization and the excitation energy is decreased. Contrariwise, if a blue shift is observed either the ground state is more stabilized or the excited state is destabilized by the solvent, leading to an increase the excitation energy, and hence $\mu_e<\mu_g$. So, in general, red shifts lead to an increase of the linear and nonlinear polarizabilities whereas blue shifts lead to a decrease of these properties.

Hydrogen bonding can affect the energies of the ground and excited states, either positively or negatively. In the case of transition metal carbonyl compounds, it is known that hydrogen bonding stabilizes the ground state leading to blue shifts (negative solvatochromism). However, in the case of *p*-nitroaniline, the excited state is stabilized, leading to a red shift of the absorption band (positive solvatochromism). For these reasons, the establishment of hydrogen bonds can also affect the nonlinear properties of a molecule.

Donor-acceptor *push-pull* compounds are known for their large ground state dipole moment and for possessing low-lying charge-transfer transitions, occurring at the molecular dipole axis. For this fact, they usually have large values of first hyperpolarizabilities. A simple two-state model was purposed by Oudar and Chemla for describing the hyperpolarizability of 1D *push-pull* chromophores, taking into account their solvatochromic behaviour through the spectroscopic parameters of the electronic excitation. This model is now know simply as the Two Level Model (TLM), and is usually expressed by the equation:[19]

$$\beta_{zzz}(-2\omega;\omega,\omega) = \frac{3e^2}{2m\hbar}\frac{\omega_{eg} f \Delta\mu_{eg}}{(\omega_{eg}^2-\omega^2)(\omega_{eg}^2-4\omega^2)} \tag{1.27}$$

where e is the charge of an electron, m is the mass of the electron, f is the oscillator

strength of the transition, $\Delta\mu_{eg}$ is the variation of the dipolar moment between the ground and excited states and ω_{eg} and ω are the frequencies of the electronic transition between the ground and the excited states and the frequency of the laser source, respectively. Since the oscillator strength of the transition is proportional to the transition dipole moment operator, $\langle g|\hat{\mu}|e\rangle$, equation 1.28 can be re-written as:

$$\beta_{zzz}(-2\omega;\omega,\omega) \propto \frac{f\Delta\mu_{eg}}{E_{eg}^3} \tag{1.28}$$

The TLM has been widely used to extrapolate the resonance-enhanced values of the nonlinear hyperpolarizabilities to the off-resonance regime. It provides a good approximation to the experimental hyperpolarizabilities of small molecules that have a dominant electronic transition along the dipole moment axis of the molecule. However, the TLM is clearly insufficient to describe properly the behaviour of medium sized molecules, or even large systems, with more than one dominant electronic transition or with electronic transitions that have complex absorption bands, with more than two exited-states involved. Furthermore, the applicability of the TLM to non-polar molecules is also discouraged. Recently, Perez-Moreno *et al.* used Thomas-Kuhn sum-rules over the Sum-Over-States expression to prove that one needs to use models with a minimum of two excited states in order to obtain good approximations to the nonlinear response.[20]

1.4 Organometallic Compounds for NLO

Nonlinear optical materials have been extensively studied for the last three decades. The vast majority are dipolar or quadrupolar π-conjugated organic or organometallic-based materials, end-capped with donor and acceptor moieties (the so-called *push-pull* systems) for which the nonlinear optical responses are attributed to the highly delocalizable π-electrons, low energy intramolecular charge transfer processes (low HOMO-LUMO gaps) and highly polarized excited states. Other structures, like octupolar geometries, also proven to give high NLO responses. The octupolar systems usually consists of molecules with D_3, D_{3h}, T_d, D_{2d} point group symmetries and can been seen as cubes featuring donor and/or acceptor moieties on its edges. The NLO response of octupolar compounds is based on a spatially controlled organization of the low energy intramolecular charge transfers. **Figure 1.4** represents these three architectural systems. This work refers only

to dipolar complexes.

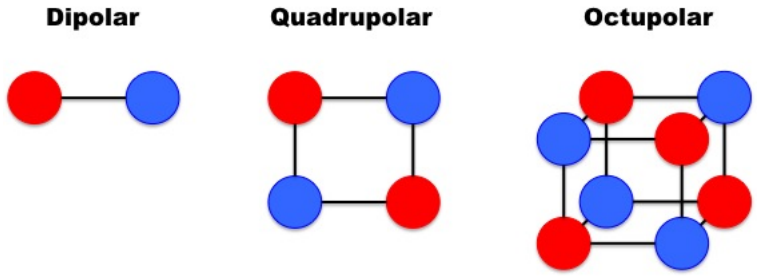

Figure 1.4: Generic structures for dipolar, quadrupolar and octupolar systems. Blue spheres represent donor groups and red spheres represent acceptor groups

The main strategy of the dipolar approach is based on the so-called two-level model (TLM) purposed by Oudar[19]. In general lines, this model states that the second-order nonlinear optical response is correlated to the energy of the charge transfer process, λ_{max}, the transition dipole moment and the difference between the ground- and excited-state dipole moment. The consequences of these factors lead to a *push-pull* architecture, where the molecules are structured as Donor-(π-conjugated system)-Acceptor. Small organic molecules, typically exemplified by *p*-nitroaniline, belong to these architectural type and are known for high nonlinear optical responses. Organometallic complexes, in their turn, can also be designed to have such a *push-pull* architecture. Depending on the metal centre, its oxidation state and the co-ligands present, one can obtain organometallic fragments with donor or acceptor capability, or even belonging to the conjugation path.

In this section, an overview of the organometallic complexes for second-order nonlinear optical applications will be addressed. In particular, the focus will be set on Group VIII metal complexes presenting mainly dipolar architectures.

1.4.1 Metallocenyl Derivatives

Metallocenyl derivatives are among the first and most studied organometallic compounds for SONLO applications. Their architecture is based on mono- or dissubstituted cyclopentadienyl rings as shown in **Figure 1.5**.

The interest of studying the nonlinear optical properties of such compounds was due to the initial report of a SHG powder efficiency of 62 times that of urea by the simple *cis*-1-ferrocenyl-2(4-nitrophenyl)ethylene (see **Figure 1.6**).[21] Since this report by Marder *et al.*

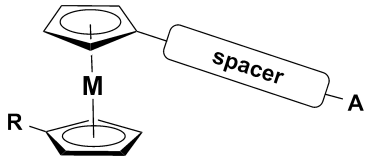

Figure 1.5: General structure of metallocenyl organometallic complexes. R =H or NLO-chromophore, A = acceptor

inumerous experimental and theoretical reviews have been published. It is now well established that the moderate electron donation ability of the metallocene organometallic fragment is higher than the typical organic fragments, like tertiary amines or methoxyphenyl groups. However, the obtained nonlinear optical hyperpolarizabilities are of the same magnitude than the equivalent organic fragments.[22] This behaviour is attributed to a poor electronic coupling between the metal *d*-orbitals and the π-conjugated system of the substituent.[23] Furthermore, the typical spectra for *push-pull* metallocene compounds presents two bands, one between 300 and 400 nm (assigned to $\pi \rightarrow \pi^{\star}$ transitions) and the second in the 450 to 600 nm region (assigned to a metal-to-ligand charge transfer (MLCT)), that can both contribute to the optical nonlinearity, and so the TLM is not appropriate to calculate the frequency-independent nonlinear hyperpolarizabilities.[24]

Despite the aforementioned drawback, metallocenyl derivatives, in particular ferrocenyl derivatives, present remarkable high bulk quadratic NLO efficiencies due to the tailorability of the ferrocene moiety, affording noncentrosymmetric crystal packings. The SHG efficiencies ferrocenyl derivatives containing different substituents on one of the cyclopentadienyl rings or in both cyclopentadienyl rings were evaluated by Kurtz powder technique.[25,26] Results show the expected influence of the crystal packing of the compounds, with consequent repercussion on the nonlinear optical properties. Some examples of ferrocene derivatives with high bulk efficiency are also shown in **Figure 1.6**.

It was purposed that in order to present significative second-order molecular nonlinear optical properties metallocenyl compounds must bear stronger electron-withdrawing groups than the typical nitro, cyano or dicyanovinyl groups, in a structural arrangement that allows a more effective coupling between the donor and acceptor counterparts.[27] The most effective electron-withdrawing group was shown to be a tungsten carbene organometallic fragment.[28] In an attempt to replicate the carbenium ion effect several indanones and triaryl carbinols were purposed.[29–31] Some examples of metallocenyl

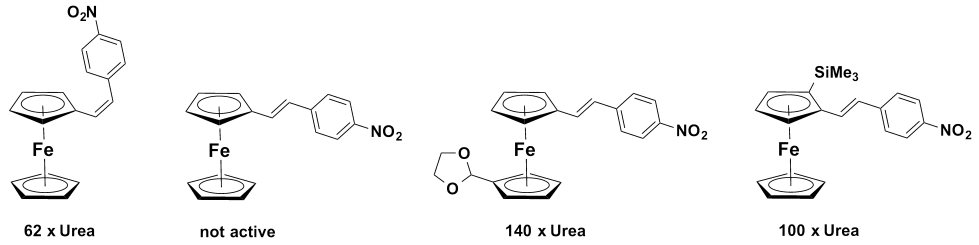

Figure 1.6: Selected ferrocenyl complexes with high bulk SHG properties

derivatives bearing strong electron acceptor groups and presenting high first hyperpolarizabilities are shown in **Figure 1.7**).

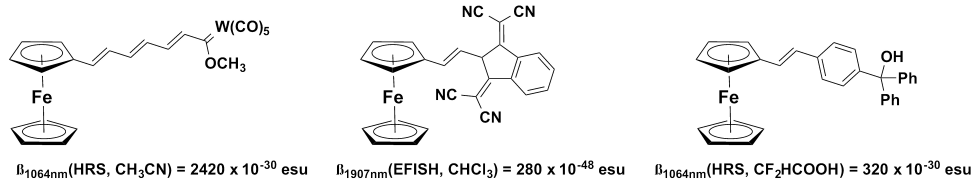

Figure 1.7: Selected ferrocenyl complexes derivatives bearing strong electron acceptor groups and their molecular first hyperpolarizabilities

Other recently reported electron-withdrawing groups were pyridinium- and other quaternary ion-based groups, like N-methylquinolinium or N-methylbenzothiazolium.[32–34] Like the purely organic counterparts, an increase of the molecular nonlinear optical hyperpolarizability in the pyridinium-based ferrocenyl compounds is observed with the increasing extend of the conjugated system. The substitution of pyridinium by other quaternary ions shows that the increasing electron-acceptor character of the substituents lead to an apparent increase of the observed molecular first hyperpolarizability. In accordance, it was also shown that the coordination of a second electron-acceptor organometallic fragment, like second- and third-row metallic carbonyls resulted in an increase the molecular nonlinear optical hyperpolarizability by at least a 2-fold factor, depending on the present transition metal (**Figure 1.8**).[33]

Varying the metal centre of the metallocenyl moiety also affects the molecular SONLO properties of the complexes. For example, ruthenocenyl compounds were synthesized and their nonlinear optical properties were compared to parent ferrocenyl derivatives (**Figure 1.9**). The results clearly show that the substitution of iron by a second-row transition

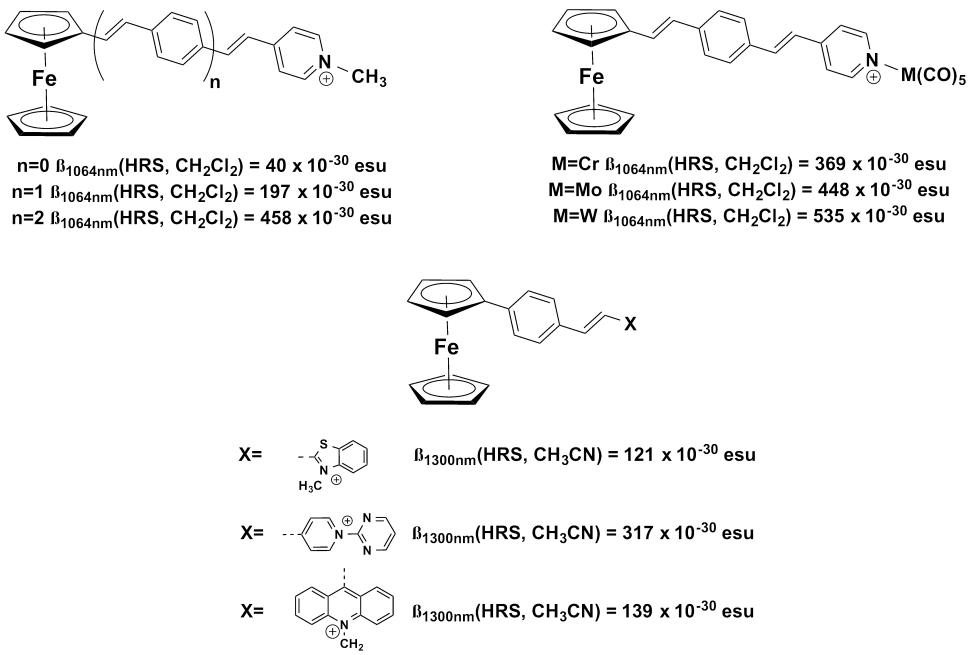

Figure 1.8: Selected ferrocenyl complexes bearing quartenery ion-based groups and their molecular first hyperpolarizabilities

metal lead to a blue shift of the absorption band accompanied with the consequent lowering of the measured nonlinear hyperpolarizability.[23,24]

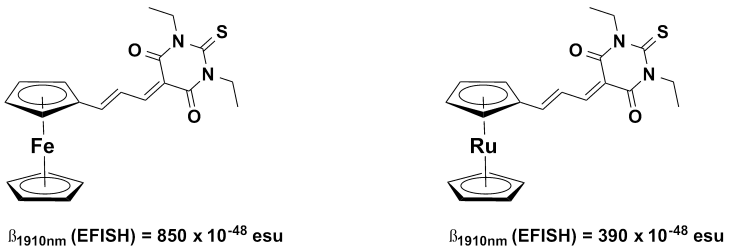

Figure 1.9: Selected ferrocenyl and ruthenocenyl complexes

1.4.2 Half-sandwich Complexes

Half-sandwich organometallic complexes and in particular their η^5-monocyclopentadienyl derivatives, whose general structure is depicted in **Figure 1.10**, emerged in the early

nineties as very promising candidates for overcoming the drawbacks of metallocenes. This section will focus only on the η^5-monocyclopentadienyl family of compounds. Reviews on other half-sandwich organometallic complexes, namely indenyl and η^5-pentamethylcyclopentadienyl can be found elsewhere.[35–38]

By presenting the metal centre in the same plane as the organic NLO-chromophore, a more favourable coupling between the metal centre and the organic conjugated backbone occurs and, therefore, better second-order hyperpolarizabilities are observed when compared to metallocenyl derivatives. The NLO properties can be tuned by changing the donor ability of the organometallic fragment (varying the co-ligands and the metal itself), changing the organic spacer or choosing different acceptor moieties. Furthermore, optimization of the crystal packing can be obtained by introducing chiral co-ligands and/or by varying the counter ion as well, which itself can additionally introduce chirality.

Group 8 metal complexes are the most studied to date, and several reviews are known that summarize the synthesis, spectroscopical, electrochemical and nonlinear optical properties of theses complexes.[11,38–40]

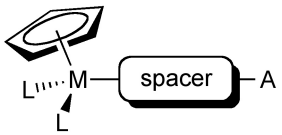

Figure 1.10: General structure of half-sandwich organometallic complexes.

L = Co-ligands, A = acceptor

Two major classes of group 8 half-sandwich metal complexes emerged with relevance for their NLO properties, in particular second-order nonlinearities: cationic nitrile complexes and neutral acetylide complexes. In both cases, the presence of low-lying, intense absorption bands, in the visible region, attributed to metal to ligand charge-transfer (MLCT), are correlated with the obtained high hyperpolarizabilities. Also, these bands exhibit a positive solvatochromic behaviour, red-shifted by increasing the solvent polarity, which is characteristic of MLCT transitions that lead to an increase of the dipole moment upon photo-excitation. Infrared spectroscopy of the normal vibrational modes of the nitrile or acetylide linkage allowed the estimation of a high degree of π-backdonation from the nd metal orbitals to the antibonding $\pi^\star$-orbitals from the ligands. Evidence for this phenomenon was revealed by significant negative shifts on $\nu_{X\equiv C}$ (X=C or N) band of the

ligands, indicating a decrease in the bond order. The magnitude of these negative shifts depend on the metal, π-system and acceptor group. Further spectroscopic evidence for π-backdonation was found by Nuclear Magnetic Resonance Spectroscopy (NMR), where a shielding of the chromophore protons was systematically verified accompanied by a general trend in the deshielding of the carbons, upon coordination to the metal, and especially for the ones close to the metal centre. The magnitude of the shielding effect is metal and ligand dependant, but solvent polarity can also be an important factor.

1.4.2.1 Half-sandwich Nitrile Complexes

The first studies were performed in η^5-(monocyclopentadienyl)(LL)$Fe^{(II)}$ and $Ru^{(II)}$ nitrile complexes (LL = k^2-dppe, 2 PPh_3, 1,2-diphenylphosphinoferrocene, or other phosphanes or amines), with the synthesis of 4-nitrophenyl derivatives.[41,42] The complexes showed very good SONLO properties, with the iron (II) complex outperforming the ruthenium complexes by a 2-fold factor (see **Figure 1.11**). The extension of the π-conjugated system from phenyl to biphenyl in both iron and ruthenium complexes was found to lead to a significant decrease in the measured hyperpolarizability as consequence of the loss of donor-acceptor conjugation. The significant torsion angles between the phenyl rings were responsible for this loss. In the case of the $Fe^{(II)}$ complexes the introduction of a vinylene unit in between the phenyl rings lead to an increase in the hyperpolarizability value, suggesting that the increase in the conjugation length, without affecting planarity, could be done by inserting of a vinylene unit between aromatic rings.[14] The analogous $Ru^{(II)}$ showed a smaller enhancement in the measured hyperpolarizability comparatively to the biphenyl derivative.

Several $Fe^{(II)}$ and $Ru^{(II)}$ nitrile thiophene derivatives were synthesized and their NLO properties were evaluated. These compounds were found to yield higher β values than the phenyl-based derivatives due to a more effective conjugation between the organometallic donor and the nitro group. In fact, thiophene groups are known to provide a higher level of electronic coupling than benzenoid-based structures because of their more effective conjugation, thus yielding high second-order NLO responses. Contrary to that found for benzenoid-based compounds, quadratic hyperpolarizabilities were found to increase with the chain-lengthening of the π-bridge in the series of thienyl derivatives. For example, measurements in a series of $[\eta^5\text{-}(C_5H_5)Fe(k^2\text{-dppe})(N{\equiv}C\{SC_4H_2\}_nNO_2)]^+$ (n = 1, 2 and 3) showed an increase in the nonlinearities with increasing conjugation length, illustrated by

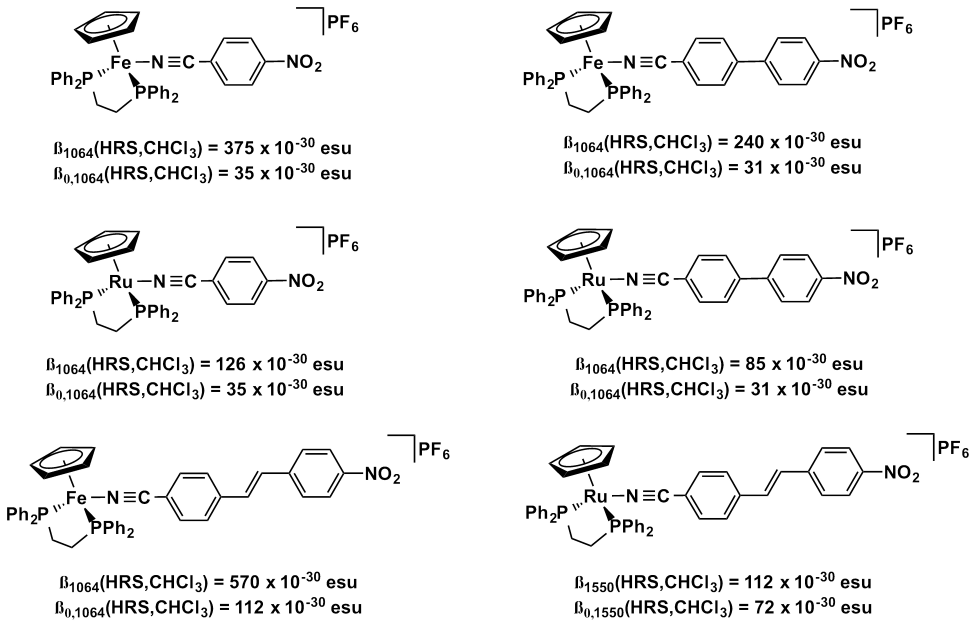

Figure 1.11: Selected structures for half-sandwish dipolar nitrile organometallic complexes

the values of $\beta_{1064} = 455, 710$ and 910×10^{-30} esu, respectively. However, the less resonant β_{1550} values do not follow this trend, and neither do their derived static hyperpolarizability, for which only slight variations are verified (**Figure 1.12**). Quadratic hyperpolarizabilities were also found to increase very slightly with the chain-lengthening of the π-bridge in the ruthenium thienyl derivatives series, $[\eta^5\text{-}(C_5H_5)Ru(k^2\text{-dppe})(N{\equiv}C\{SC_4H_2\}_nNO_2)]^+$ (n = 1, 2 and 3). This near constancy of β_0 was attributed to a competition between charge transfer efficiency and growing conjugation length, resulting in a balance of these contradictory effects, considering oligo-thiophene torsion angles to be too small to be a significant factor in the observed trend.[13] The constancy on the quadratic hyperpolarizability response due to the insertion of a vinylene unit further supports this assumption (also shown in **Figure 1.12**).

Keeping in mind that the exploitation of promising thiophene based ligands for NLO purposes should not be limited to the chain lengthening alternative, the potentialities of the benzo[1,2-b:4,3b]dithiophene (BDT) based chromophores were explored. The fused-rings structure guarantees the rigidity of the ligand to be coordinated on the same plan of the metal centre, in a family of iron and ruthenium derivatives.[43] The quadratic hy-

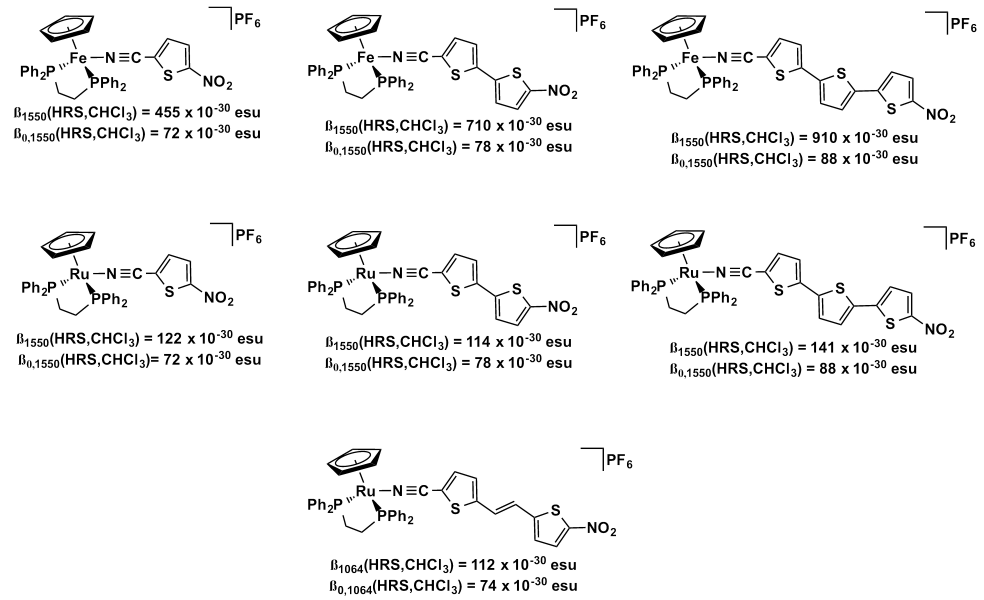

Figure 1.12: Selected structures for half-sandwich dipolar nitrile organometallic complexes bearing heteroaromatic ligands

perpolarizability for $[\eta^5\text{-}(C_5H_5)M(k^2\text{-dppe})(N{\equiv}C\text{-BDT})]^+$ (M = Fe and Ru) are negligible due to weak π-backbonding effect which barely compensates the ligand σ-coordination, as suggested by the spectroscopic and electrochemical data. However, a very weak nonlinear optical signal was obtained for $[\eta^5\text{-}(C_5H_5)Fe(k^2\text{-dppe})(N{\equiv}C\text{-BDT-}NO_2)]^+$, attributed to the presence of a red shifted electronic excitation comparatively to the previous parent compounds (**Figure 1.13**).

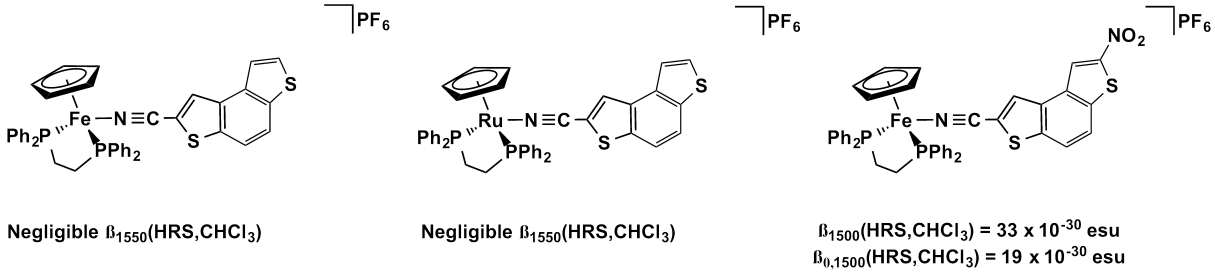

Figure 1.13: Selected structures for half-sandwich dipolar nitrile organometallic complexes bearing fused-ring thiophenes

The effect of different acceptor end groups has been also studied. For example, re-

cently the well-known good acceptor nitro group has been replaced by the less classical chromophore N-(3-cyanophenyl)formamide. The compound originated a value of $\beta_{0,1500nm}$ (HRS, $CHCl_3$) = 212 × 10^{-30} esu placing this compound in the best range of values reported in the literature for an organometallic.[44] However, the absence of any MLCT absorption band led to postulate that the high hyperpolarizability value found for this compound first might be originated by a strong variation of the dipolar moment between the ground state and the excited state upon photo-excitation. Heterobinuclear organometallic complexes were also tested as possible electron acceptor groups. In particular, the good electron acceptor chromium tricarbonyl moiety was used in the series of bimetallic compounds $[\eta^5\text{-}(C_5H_5)Ru(k^2\text{-dppe})N{\equiv}C\text{-(spacer)-}C{\equiv}C\text{-}(\eta^6\text{-}(C_6H_6))Cr(CO)_3]^+$ showing enhanced nonlinearities relatively to the parent monometallic chromium compounds, but lower than similar compounds with the nitro group as acceptor **Figure 1.14**.[45]

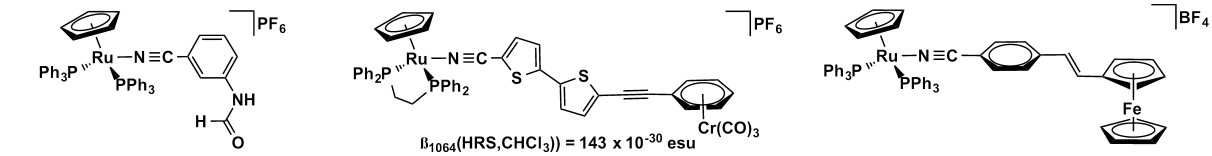

Figure 1.14: Selected structures for half-sandwich dipolar nitrile organometallic complexes

1.4.2.2 Half-sandwich Acetylide Complexes

Acetylide complexes probably constitute the most widely studied class of compounds for NLO applications. The NLO properties of these complexes have also been extensively reviewed.[11,38] Several transition metals have been used, but this work centre its attention exclusively on group VIII metals.

Conversely to the nitrile derivatives, the analysis of the measured hyperpolarizabilities of organometallic complexes bearing acetylene-based chromophores is not straightforward. In general, a dispersion-enhancement is observed for the majority of measurements of the molecular quadratic nonlinearities at 1064 nm, as it can be seen for several examples for which the determined β and β_0 values differ from an order of magnitude. The uncertainty

of the magnitude of resonance enhancement makes both the analysis and comparison to other complexes difficult, and care must be taken when one is interpreting the results. One of the most noticeable examples is demonstrated in **Figure 1.15**.[46,47]

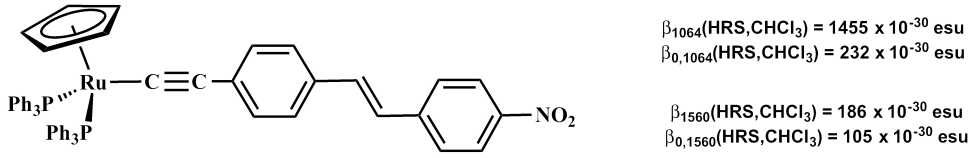

Figure 1.15: Selected example of acetylide organometallic complex presenting a dispersion-enhanced HRS quadratic hyperpolarizability at 1064nm fundamental wavelength

Varying the metal centre in a series of iron (II), ruthenium (II) and osmium (II) η^5-(monocyclopentadienyl) acetylide complexes, bearing k^2-dppe as co-ligand resulted in an increase of the measured hyperpolarizability when proceeding from the first to the third row transition metal, as exemplified in **Figure 1.16**. These results are also suggestive of higher dispersion enhancement of the iron (II) complexes judging by the magnitudes of β_{1064} and β_0.

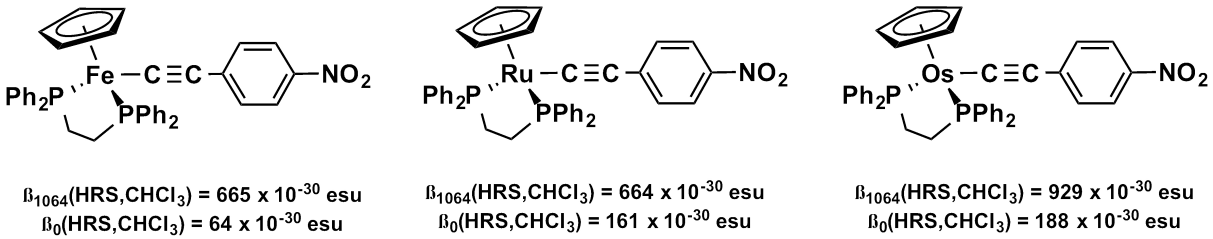

Figure 1.16: Selected example of acetylide organometallic complexes presenting different transition metals

As in the case of the nitrile complexes, structural modications to the π-conjugated backbone have a similar impact to that observed in purely organic systems, that is, an increasing of the first hyperpolarizability is observed upon increasing chromophore chain length. For example, going from the simple phenyl ring to longer conjugated systems, like biphenyl, 4-phenylethynyl or (E)-4-phenylethene, the first hyperpolarizabilities of the corresponding ruthenium η^5-(monocyclopentadienyl) acetylide complexes has the following trend:

$\beta(C_6H_4) < \beta\ (C_6H_4\text{-}C_6H_4) < \beta(C_6H_4\text{-}C{\equiv}C\text{-}C_6H_4) < \beta((E)\text{-}C_6H_4CH{=}CH\text{-}C_6H_4)$.

Again, the biphenyl complex present lower hyperpolarizability than the ethynyl and ethene linked phenyl compounds due to the torsion effects as examined theoretically for comparable Ru complexes. The difference on the hyperpolarizabilities of the ethynyl and ethene linked biphenyl compounds is attributed, in their turn, to an energy mismatch of the sp-hybridized π-orbitals of the acetylenic carbons with orbitals of sp^2 hybridized phenyl carbons.[48]

The change in the phenyl rings linkage to heteronuclear linkages, when going from (E)-C=C to(E)-N=C and (E)-N=N linkages was also evaluated. The results show a decrease on the second-order NLO response, being the imino linkage the less effective (**Figure 1.18**).

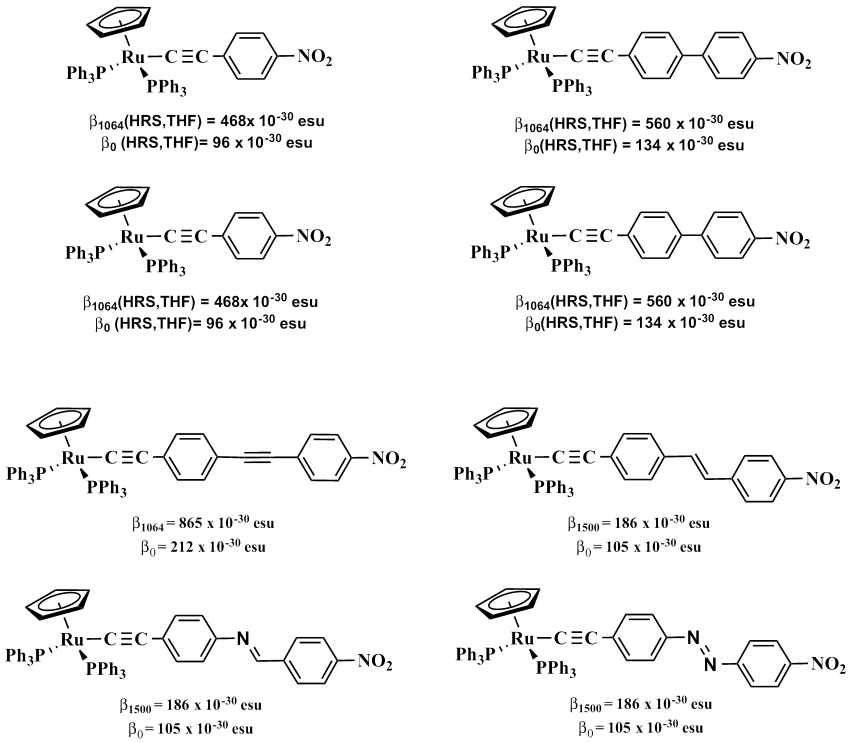

Figure 1.17: Selected example of acetylide organometallic complex presenting different transition metals

Replacing phenyl by heterocyclic rings results in the expect enhancement of the non-linearities due to the lower π-electronic delocalization energies of the heterocyclic moiety.

For example, replacing the phenyl ring by thienyl derivatives results in a slight increase on the second-order nonlinearity. However, as aforementioned, the comparison of the results obtained for a series of benzene- and heterocyclic-based alkynyls is not straightforward due to the fact that phenylacetylides were measured at 1064 nm and the complexes presenting thienyl rings were measured at 1500/1560 nm, and hence a strong dispersion-enhancement can be present in the case of the former. The above stated behaviour for the chain lengthening effect on the quadratic hyperpolarizability for the phenyl-based complexes can be observed for the series of thienyl derivatives η^5-(C_5H_5)Ru(LL)(C≡C-2-Th_n-5-NO_2)] (LL = 2 PPh_3, k^2-dppe; n = 1, 2).[49]

Despite the several acceptor groups explored on the π-spacer, the good acceptor nitro group has been the most widely used across this series of acetylide complexes. Replacement with weaker groups, like the formyl group in its protected of free forms, in the series of phenylacetylenes results in a decrease of the nonlinearities as can be seen in **Figure 1.19**.[50] These results are easily justified by a dimishing of the dipolar D-π-A asymmetry.

Conversely, the use of the good electron acceptor N-methyl pyridinium derivatives leads to an enhancement of the second-order hyperpolarizability, in particular for longer conjugated systems.

The use of pro-quinoidal ligands was envisaged because this feature leads to the conservation of aromatic stabilization energy and can, thereby, enhance the optical nonlinearities. This idea had already been exploited with organic molecules by Marder *et al.*[51] The use of indoanilinoacetylide ligands has been examined because in the charge-transfer excited state the ring closest to the metal centre becomes quinoidal while the second ring becomes aromatic. Although the quadratic nonlinearity for this complex is large (β_0 = 159 $\times 10^{-30}$ esu), it is lower than the ones determined for similarly sized two-ring ene- and azo-linked complexes (**Figure 1.20**).[52]

1.4.3 Acetylide Metal Phosphine Complexes

Acetylide metal complexes containing bidentate tertiary phosphines is another family of very well successful organometallic compounds for nonlinear optical applications. A general structure of these complexes is depicted in **Figure 1.22**. Most of the studies are centred on (diphenylphosphane)ethane (k^2-dppe) and (diphenylphosphane)methane (k^2-dppm)-ruthenium, platinum or gold complexes. Herein, only the ruthenium complexes will be presented.[53,54]

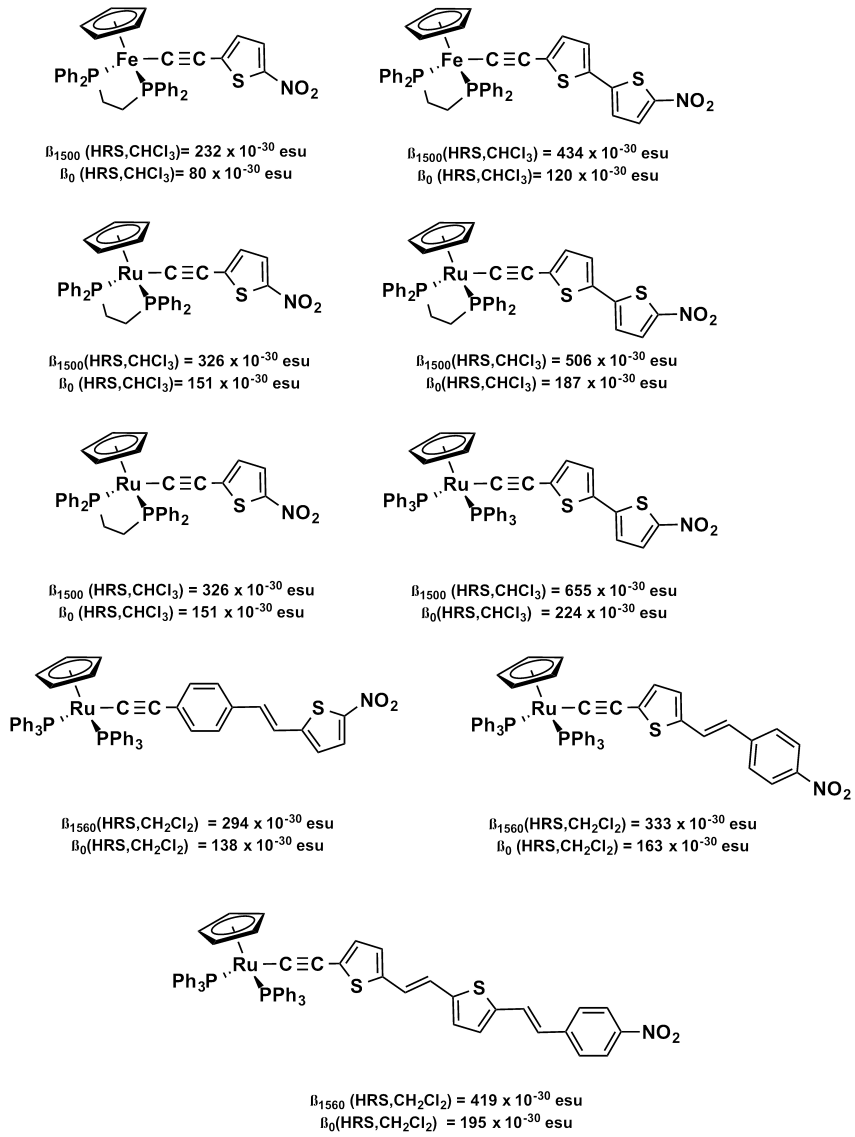

Figure 1.18: Selected example of acetylide organometallic complexes presenting heterocyclic aromatic ligands

Spectroscopic measurements for these compounds show that they have very similar nonlinear optical properties to those of the previously mentioned η^5-monocyclopentadienyl compounds, with errors of *ca.* 10% for both β and β_0. They also display the NLO-active chromophore in the same plane of the metal centre and hence, very low-lying metal-to-ligand charge transfers are observed. This characteristic transition is also responsible for their high nonlinear optical properties.

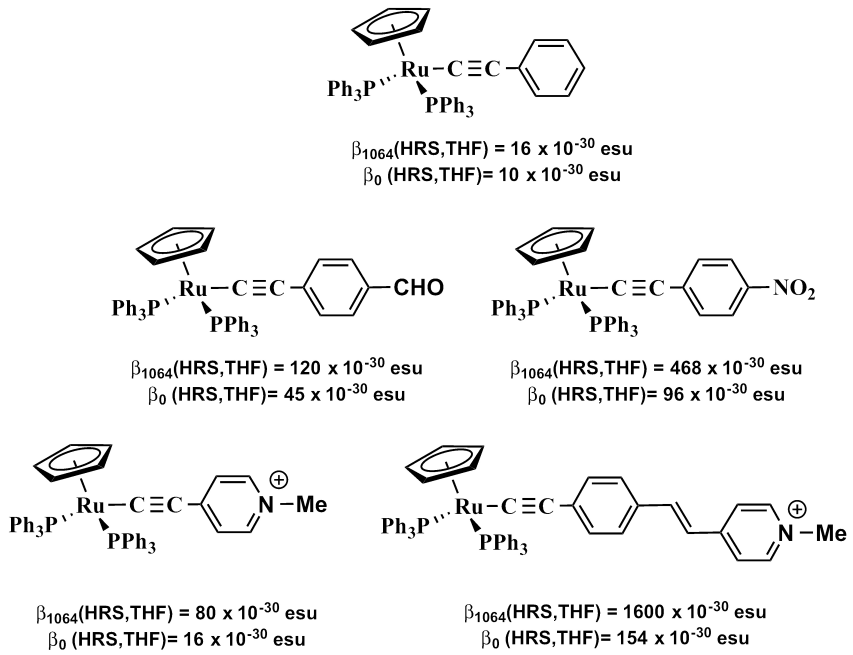

Figure 1.19: Selected example of acetylide organometallic complexes presenting different electron acceptor groups

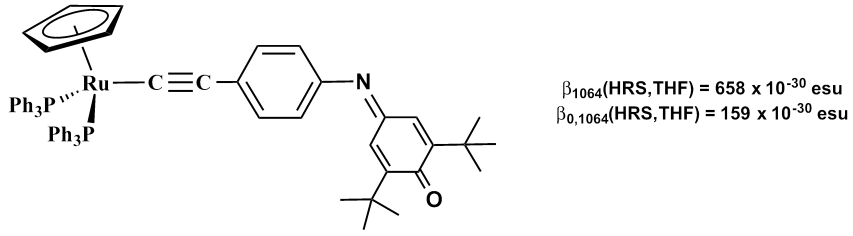

Figure 1.20: Selected example of acetylide organometallic complex presenting a dispersion-enhanced HRS quadratic hyperpolarizability at 1064nm fundamental wavelength

Chain lengthening of the NLO-active chromophore leads of an increase in the measured hyperpolarizability (**Figure 1.23**). However, the opposite behaviour is observed when the number of aromatic rings increases over two repeating units, that is, in the case of the present acetylide bidentate phosphane complexes a saturation of the measured hyperpolarizability is not observed until the number of repeating units is approximately twenty units (evaluated theoretically).[55] Also, for the cases of high-conjugated length

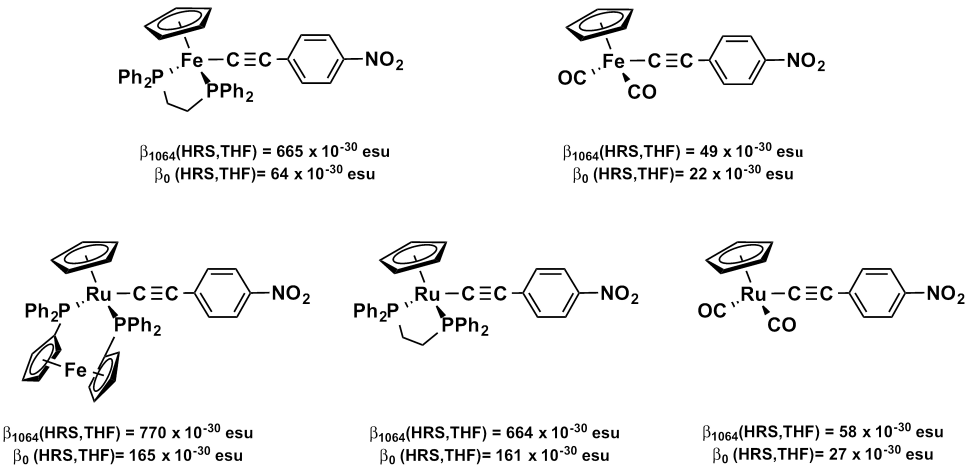

Figure 1.21: Selected example of acetylide organometallic complexes presenting diferent co-ligands

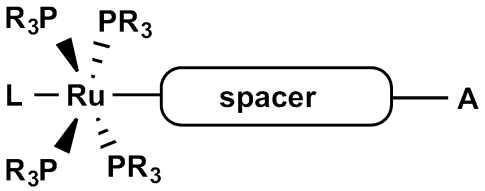

Figure 1.22: General structure of acetylide metal phosphine organometallic complexes. PR_3=tertiary phosphine, L=Cl or other NLO-active co-ligand, A=acceptor

ligands, the measured hyperpolarizability do not correlate with the absorption spectra of the complexes, for which a blue shift is observed with the increasing number of repeating units.

Replacement of the usual triple bond between the phenyl rings leads to an increase of the observed molecular hyperpolarizability. As in the previous cases, ethylene linkages provides higher nonlinear optical properties than imine linkages (**Figure 1.24**).

Control of the crystal packing can be made by inclusion of chiral phosphanes, like 1,2-bis(methylphenylphosphane)benzene.[56]

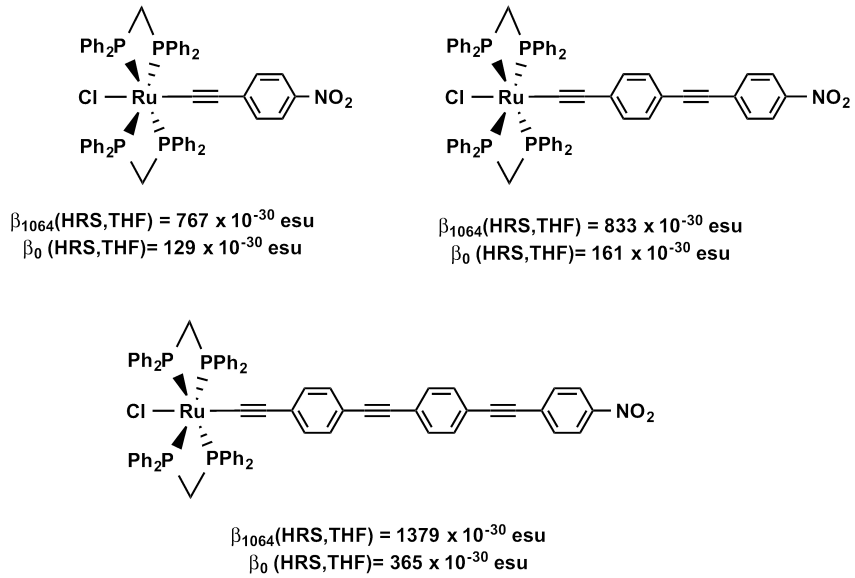

Figure 1.23: Selected examples of acetylide metal phosphine organometallic complexes with increasing length chromophores

1.4.4 Metal Ammine Complexes

Metal amine complexes emerged very recently as interesting organometallic fragments for nonlinear optical applications. Based on the $[(NH_3)_xRu(L)_y]^+$ (y=1 when x=5 and y=2 when x=4) fragment, their nonlinear optical properties have been extensively studied by Coe *et al.*[34,57–60]

The electron donating character of the organometallic fragment can be tuned by substituting the axial ammonia ligand by an electron-donating or electron-withdrawing group. The general structure for these compounds is depicted in **Figure 1.26**.

The good electron-donating abilities of the ruthenium ammine fragment, that lies in the same plane of the delocalized aromatic system, gives rise to very low metal-to-ligand charge transfers that are responsible for the observed molecular nonlinear optical properties of these compounds. Interestingly, like in the case of the aforementioned half-sandwish organometallic fragments, attempts to improve the molecular hyperpolarizability by extending the conjugated system resulted in maximization of this property for relatively short conjugation lengths. In fact, longer conjugation lengths lead to a decreasing of the measured molecular hyperpolarizability.[61] These results were justified by a blue-shift of the low-energy transitions with the increasing conjugation length. DFT cal-

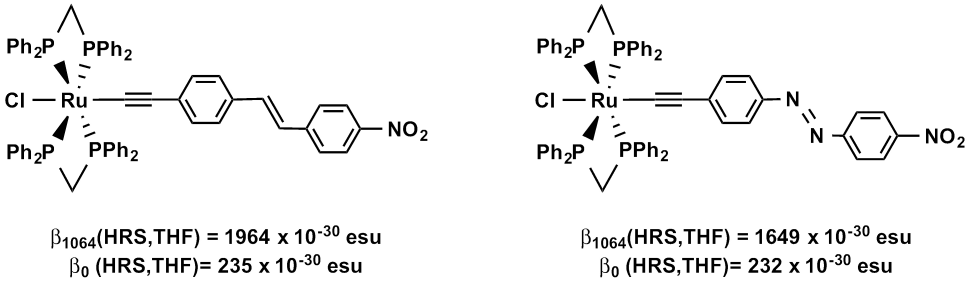

Figure 1.24: Selected examples of acetylide metal phosphine organometallic complexes bearing ethylene and imine linkages

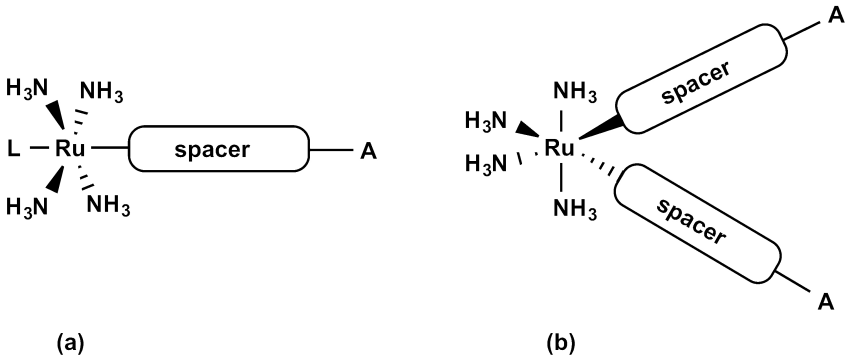

Figure 1.25: General structure of ruthenium ammine organometallic complexes.

L=NH_3 or other co-ligand, A=acceptor

culations were also used to rationalize the results, showing that, for longer chromophores, the lowest energy transition are dominated by an intra-ligand charge transfer, clearly affecting the nonlinear optical response of the molecules. Hence, it was showed that for longer chromophores, the inclusion of the good-electron donor organometallic fragment is not advantageous comparatively to simpler and less costing organic fragments, like 4-(dimethylamino)phenyl groups.[62]

Increasing the number of acceptor units coordinated in the *cis*-$[Ru(NH_3)_4]^{2+}$ was also investigated.[63,64] The presence of the two electron-acceptor groups cause the complexes to exhibit several metal to ligand charge transfers making the molecular hyperpolarizabilities much harder to analyse. Furthermore, the molecules typically belong to the C_{2v} point symmetry group, for which two main β tensors are dominant, β_{zzz} and β_{zyy} (considering that the ligands are in the yz plane), and hence the TLM is not applicable in these

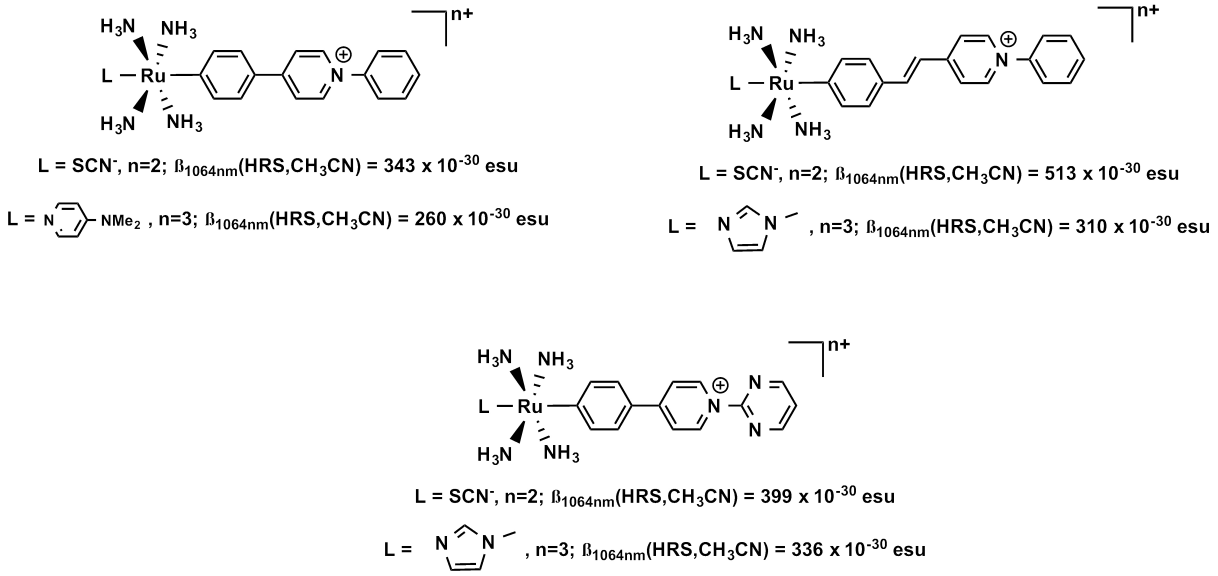

Figure 1.26: Selected examples of ruthenium ammine organometallic complexes

compounds. For that reason, these complexes were studied with Stark spectroscopy, which allows the molecular hyperpolarizabilities associated with each electronic transition to be estimated. In **Figure 1.27** are depicted the molecular structure of two of these 2D V-shaped molecules. The presented molecular hyperpolarizabilities were obtained by the summation of the hyperpolarizability components for all the MLCT bands.

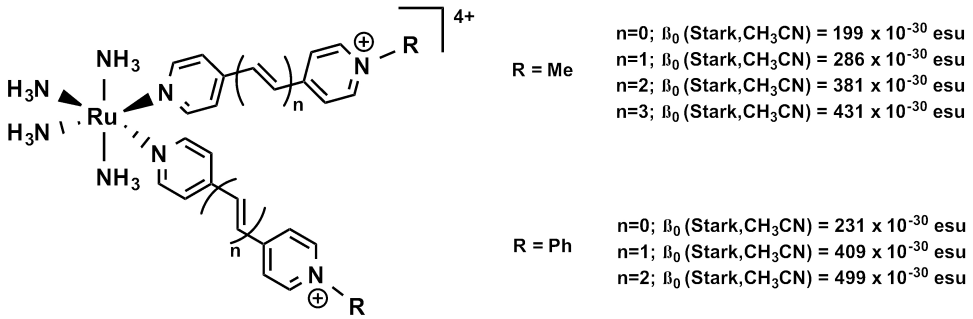

Figure 1.27: Selected examples of 2D V-shaped ruthenium ammine organometallic complexes

It is clear that, in the case of these complexes, the molecular hyperpolarizability increases with the increasing of the conjugated system length. Conversely to the previous

1D complexes, the energy of the MLCT electronic transitions is not blue-shifted by the elongation of the delocalized π-system, leading to a gradual enhancement of the molecular hyperpolarizability.

1.5 Nonlinear Optical Molecular Switching

The development of highly effective materials for NLO is still challenging. More recently, with the need of new miniaturized technologies, another challenge was brought to light - the development of nano and molecular-scale devices. The miniaturization processes of such technologies requires the development of nano and molecular scaled components, such as circuits, memories and, more importantly, switches.

Molecular Switches are generally defined as molecules that, upon a external stimuli, are capable of being reversibly interconverted between at least two forms, generically called the *on-state* and the *off-state*. NLO molecular switches are, for that matter, molecules capable of switching their NLO properties upon one or more suitable external stimuli. Like any other molecular switch, in order to be useful NLO molecular switches several requirements must be fulfilled namely: rapid and reversible commutation between the different forms; be stable both in solution and in the solid state; and display large NLO contrasts, that is, the hyperpolarizabilities between the different forms must be sufficiently large.

NLO switchable compounds can be classified by the type of the used external stimuli, and hence there are pH-, photo- and redox-induced switches. In one of the first reviews on this subject, Coe purposed a different and broader classification based on the type of alteration to the basic functional units of the material, rather than the stimuli the compounds respond to. This classification is based on the alteration on the donor, the π-conjugated bridge or the acceptor parts,[58] and applies to both organic and organometallic compounds. **Scheme 1.1** depicts this classification.

In the Type I mechanism, the hyperpolarizability is altered by reducing the ability of the donor moiety (D) of the on form. This will be done by oxidation (or protonation) of the donor, which therefore will become a competing acceptor moiety (A) leading to a lower hyperpolarizability (off form). In the Type II mechanism, the β value is changed upon reduction (or deprotonation) of the acceptor (A) moiety which becomes competitive with the donor (A changes into D). Finally, in type III mechanism a change in the conjugation

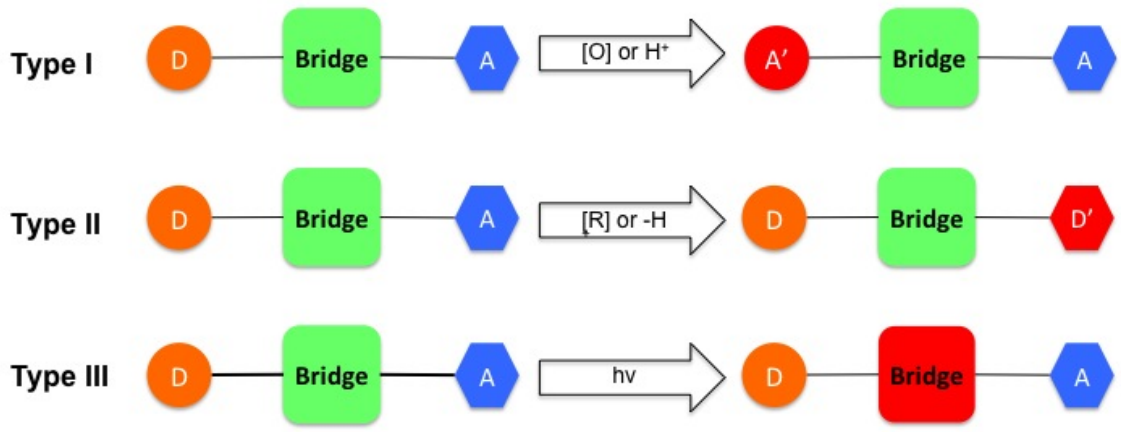

Scheme 1.1: Classification of NLO molecular switches

length of the π-conjugated bridge. This alteration in the conjugation path can be done, for example, by isomerization or cyclization in the organic chromophores and lead to a break in the donor-acceptor coupling.

Organometallic compounds of Group 8 metals are also among the most versatile compounds for obtaining NLO molecular switches, since they can incorporate innumerous organic compounds as ligands and, more importantly, because the presence of one (or several) transition metal centre(s) allows a great design flexibility and accessibility of different metal oxidation states. The electronic properties of the ligands directly or indirectly bonded to the metal centre can be altered, providing a feasible way to fine-tune the properties of the complexes. Furthermore, organometallic complex can respond orthogonally to any of the mentioned stimulus, allowing a greater combination of states to be achieved.

1.5.1 Switching by alteration of the donor or acceptor groups - Redox Switching

The first purposed redox active NLO molecular switch was based on the pentaammine-$Ru^{(III)}/Ru^{(II)}$ redox couple.[58] Combining these organometallic electron donors with pyridyl

ligands bearing several electron-accepting pyridinium groups, excellent nonlinear optical properties were obtained. Upon oxidation, a dramatic decrease in the harmonic scattering intensity was observed, with no meaningful values for β.[65] Recently, the modulation of Langmuir-Blodgett (LB) thin films of ruthenium pentaamine complexes was investigated.[66] Results showed that oxidation lead to a *ca.* 50% decrease in the nonlinear optical response intensity, and that the signal is almost completely restored on reduction. Albeit this reversible process was possible for two cycles, the signal diminished with further cycling. Octamethylferrocene derivatives substituted with an ethynyl nitrothiophene derivative were also shown as possible molecular switches. Again, upon oxidation of the $Fe^{(II)}$ metal centre, the first hyperpolarizability was reduced by almost 10 times.[67] **Figure 1.28** depicts the examples stated above.

The promising results for these compounds resulted in the burst of several organometallic based molecular switches. Dipolar and octupolar complexes of group VIII metals are among the most studied compounds for redox-based NLO molecular switching, since they often present reversible redox processes between the $M^{(II)}/M^{(III)}$ forms, allowing the interconversion of the complexes between two oxidation states easily achieved. By this fact, they are indeed the most promising metals for NLO molecular switching. Intuitively, a decrease of the NLO response upon oxidation is expected due to the decrease of the electron-donor ability of the metal centre, from the good electron donor d^6-$M^{(II)}$ to the poor electron donor d^5-$M^{(III)}$. Metal alkynyl compounds, in particular η^5-pentamethylmonocyclopentadienylmetal (Metal= Iron (II) or Ruthenium (II)) and alkynylbis(diphosphine)ruthenium complexes, have attracted attention in this field due not only their intrinsic large optical nonlinearities, but also to their reversible and well defined redox properties. As far as this work is concerned no metal alkynyl or nitrile compounds bearing η^5-monocyclopentadienylmetal (Metal = Iron (II) or Ruthenium (II)) have been reported.

The synthesis and NLO switching ability of mono-, bi and trinuclear η^5-C_5Me_5(k^2-dppe)$Fe^{(II)}$ organometallic complexes containing phenylethynyl bridging ligands was synthesized and tested for their NLO-switching ability.[68,69] The mononuclear radical cationic complexes presented a much lower (close to negligible) NLO activity when compared to their neutral counterpart. The lower NLO activity is attributed to the lowering of the electron donation ability of the d^6-$Fe^{(II)}$ alongside an inversion of the dipole moment in the excited state. The polynuclear compounds were isolated in different oxidation states

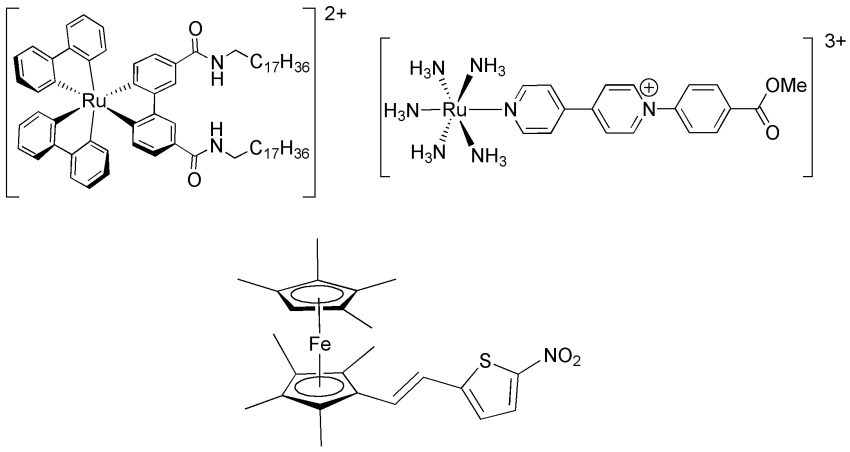

Figure 1.28: Examples of the first synthesized metallo-organic NLO switches

allowing their NLO properties to be investigated separately. The results show that the polynuclear complexes had an expected increase of the quadratic NLO response by at least a factor of 3 when compared with the mononuclear complex. The three possible states for the binuclear complexes ($Fe^{(II)}/Fe^{(II)}$, $Fe^{(II)}/Fe^{(III)}$ and $Fe^{(III)}/Fe^{(III)}$) present different second-order responses in all three forms, being the $Fe^{(II)}/Fe^{(III)}$ the most active. The trinuclear complex showed similar nonlinearities for all the forms (**Figure 1.29**).

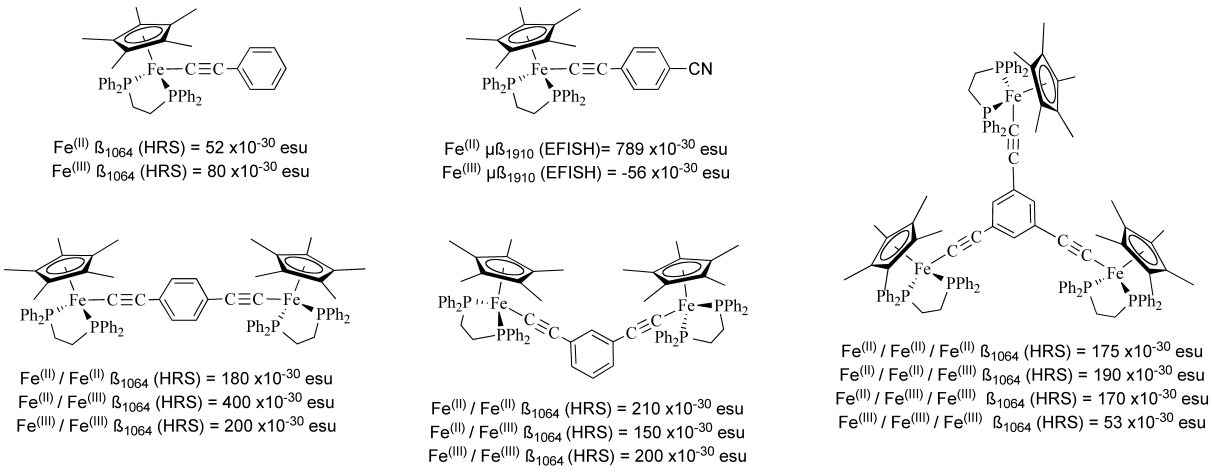

Figure 1.29: Selected structures of phenylethynyl based Iron (II) molecular switches

The third-order nonlinearities of bimetallic half-sandwich $Fe^{(II)}$ end-capped with an oc-

taedral *trans*-$Ru^{(II)}(k^2\text{-dppe})_2$ complex across three possible states was evaluated (**Figure 1.30**).[53,70,71] The complexes showed different NLO properties in all forms, going from a low response for the $Fe^{(II)}/Ru^{(II)}$ form to a highly active response in the $Fe^{(II)}/Ru^{(III)}$. The final $Fe^{(III)}/Ru^{(III)}$ form showed the highest third-order response of the three forms, with values that almost enhance by a almost 2-fold compared with the mixed valence form. Further enhancement of the conjugated system to an octupolar mixed hexametallic system prove to greatly enhance the nonlinear optical properties of the compounds, in particular for the $Fe^{(III)}/Ru^{(III)}$ form, for which an enhancement of the third-order hyperpolarizability by *ca* 10-fold was observed.

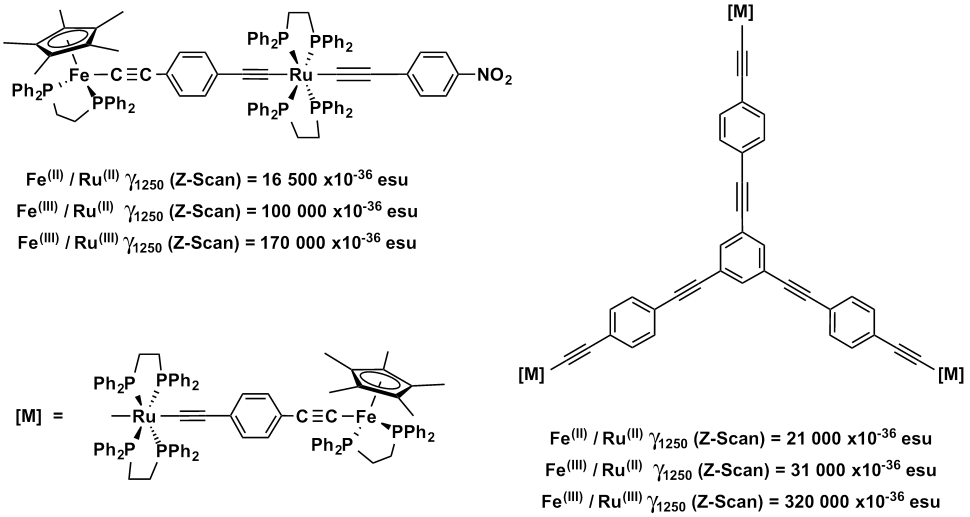

Figure 1.30: Selected structures of mixed valence phenylethynyl based Fe (II)/Ru (II) molecular switches

1.5.2 Switching by alteration of the conjugated system

Switching the NLO properties by an alteration at the π-conjugated bridge is a common way to easily investigate the NLO switching ability of a molecule. In fact, the first approach to the attain the reversible NLO switching of organometallic compounds was by incorporation of a photochromic organic ligand directly coordinated to the metal(s) centre(s). A recent review was published.[72] To date, there are several families of organic chromophores studied for their photochromic behaviour, like diarylethenes,[73,74] spiropyrans,[75] anil derivatives, fulgides, azobenzenes, indolino-oxazolidines and flavinium salt,

for which several reviews have been published.[76–80] However, the majority of the work has been performed in the diarylethene family, in particular with the 5,5-dithienylperfluorocyclopentene (DTE) moiety.

DTE possess two light-induced interconvertible forms, as shown in **Figure 1.31**, generically called the open- and closed-forms. The absorption maximum of the open form presents high energy transition (300-400 nm depending on the substituent) and it is attributed to intra-ligand charge transfers occurring in the independent photochromic units, whereas the closed form presents low-lying energy transitions in the 500-700 nm range, characteristic of a charge transition of an enhanced conjugated system. Coordination of these ligands to different metal centres usually is accompanied with a red shift of these bands.[81] For these reasons, DTE ligands are the most appealing starting materials for NLO molecular switching. Surprisingly although innumerous papers are devoted to the photochromic switching of DTE containing organometallic complexes, only a few examples report the nonlinear optical properties of such complexes. Ruthenium complexes bearing *bis*-5,5-dithienylperfluorocyclopentene (DTE) -2,2'-bipyridine ligands were synthesized and their NLO properties evaluated by HRS.[82] The hyperpolarizabilities at 1910 nm fundamental wavelength of the complexes in open- and close form of the DTE ligand showed to be different by a factor of *ca.* 3.4 (β_{open} = 325 $\times 10^{-30}$ esu; β_{closed} = 1113 $\times 10^{-30}$ esu). Also, iron (II) tris(bipyridyl) complexes featuring six DTE photochromic units were synthesized and HRS measurements were performed at 1910 nm.[72,82] Results showed again an enhancing of the hyperpolarizability upon photo irradiation (β_{open} = 250 $\times 10^{-30}$ esu; β_{closed} = 2000 $\times 10^{-30}$ esu).

Changes in the conjugated system can also been achieved by protonation of metal alkynyl compounds. The presence of the akynyl group allows also the switching to be achieved by protonation, as shown for example by Hurst *et al.*[50,83]. **Figure 1.32** shows some examples of NLO protic switches. However, the pH switching abilities of the majority of these compounds were rather puzzling, since there are no consistent results on the expectation value of the first hyperpolarizability upon protonation or deprotonation. In other words, there is not predictability if the pH variation will lead to an increase or a decrease in the hyperpolarizability value. The impossibility of a systematic analysis of the results of such complexes was attributed to an unpredictable behaviour of the two-photon absorption resonance effect, leading to the appearance of large errors, either by resonance enhancement or absorption of the harmonic light, thus preventing structure-

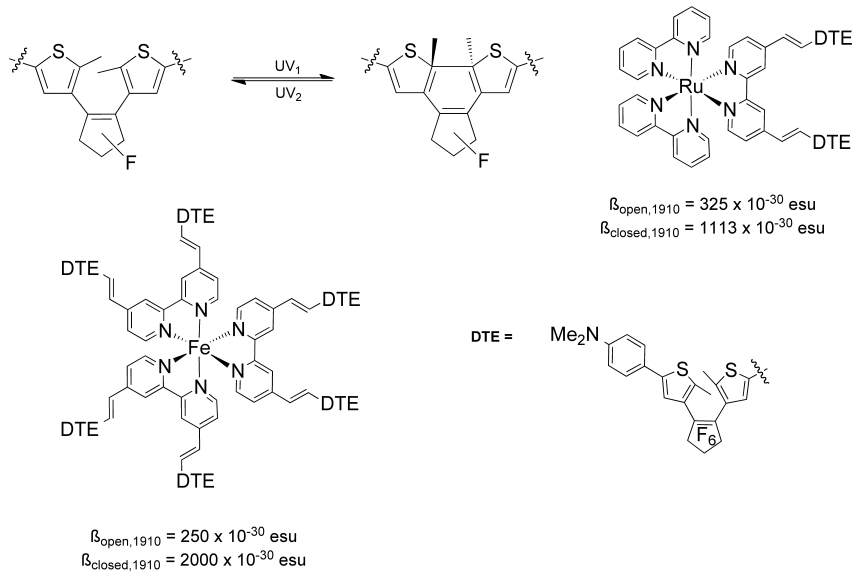

Figure 1.31: 5,5-Dithienylperfluorocyclopentene (DTE) based molecular switches

property relations to be addressed properly. Furthermore, pH-dependent switches are not suitable for technological applications, since the chemical manipulations involved are not straightforward. In this sense, electro-reversible Fe(II) and Ru(II) alkynyl complexes, with mono-, bi- and tri-organometallic centres, seemed to provide a much more suitable way of achieving systematic NLO switching abilities.

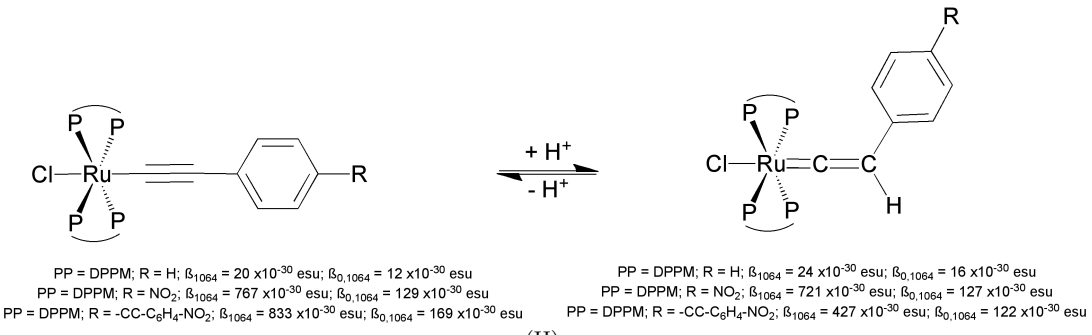

Figure 1.32: Examples of $Ru^{(II)}$ complexes for protic switching

1.5.3 Multi-stimuli Switching

Multi-stimuli switching of the nonlinear optical properties of compounds can also be achieved. The multi-stimuli approach is based on both the switching by alteration of the conjugated system and the electrochemical switching. Together they combine the pH and/or redox switching abilities of organometallic moieties with the modulation of the optical properties by photochromic ligands, like DTE derivatives.

Although organic multi-redox NLO switching is known, the switching of the quadratic hyperpolarizabilities of organometallic complexes has not been reported yet.[84] However, the synthesis and third-order nonlinear optical properties, in particular the nonlinear absorption, has been recently evaluated for an alkynyl ruthenium containing bidentate tertiary phosphine and a DTE ligand (**Figure 1.33**).[85] Results show that the synthesized complex responds orthogonally to protic (yne-linkage *vs.* ene-linkage), electrochemical (metal-centred redox: Ru (II) *vs.* Ru (III)), and photochemical (DTE ring-opening *vs.* ring-closing) stimuli allowing six possible states to be obtained. The six states are interconverted along different pathways according to the applied stimulus and result in distinct changes to cubic nonlinear optical absorption.

1.6 Density Funcional Theory in NLO

Nowadays, *Density Functional Theory* (DFT) is probably the most successful formulation of quantum mechanics and has allowed chemists to study a wide variety of complex chemical systems and their properties. In the base of that success is the fact that DFT provides a sufficiently accurate description of the motion of electrons at low computational costs when compared to other *ab initio* methods, like Moller-Plesset (MP), Multi-Configurational Iteration (CI) and Coupled Cluster (CC) methods.

As any *ab initio* method, DFT is based on the Schrödinger equation, that in its time independent form, for a system of N electrons and M nuclei, is the following:

$$\hat{H}\Psi(x_1, x_2, \ldots, x_N|R_1, R_2, \ldots, R_M) = E\Psi(x_1, x_2, \ldots, x_N|R_1, R_2, \ldots, R_M) \qquad (1.29)$$

where Ψ is the wave function for the system, E is the energy and $\hat{H}$ is the Hamiltonian

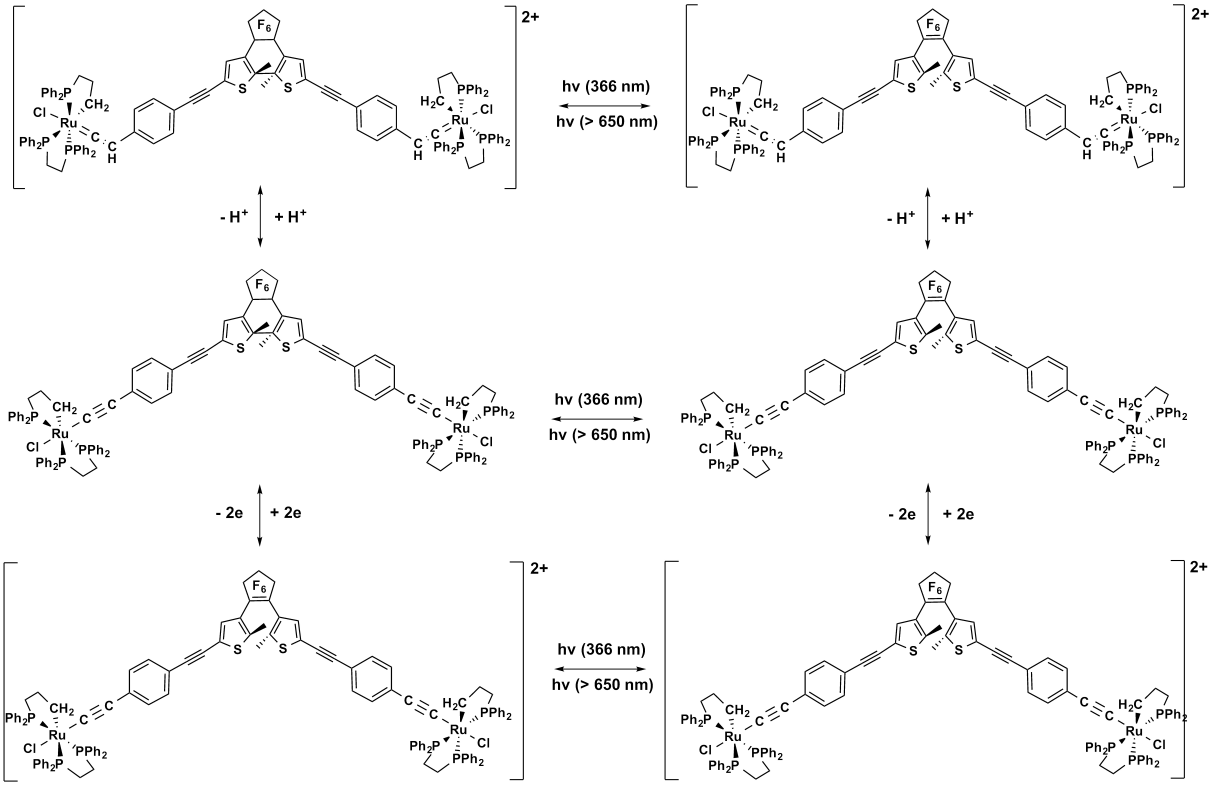

Figure 1.33: Interconvertion between six states of a multi-stimuli $Ru^{(II)}$ molecular switch

operator that is given by:

$$\begin{aligned} \hat{H}_elec &= \hat{T}_e + \hat{V_{eN}} + \hat{V}_{ee} \\ &= -\frac{1}{2}\sum_{i=1}^{N}\nabla_i^2 - \sum_{i=1}^{N}\sum_{A=1}^{M}\frac{Z_A}{r_{iA}} \\ &+ \sum_{i=1}^{N}\sum_{j=1}^{N}\frac{1}{r_{ij}} \end{aligned} \tag{1.30}$$

In equation 1.30 T_e represents the kinetic energy operator, V_{eN} the electron-nuclei attractive potential (called external potential in DFT theory) and V_{ee} and V_{NN} the electron-electron repulsion and nuclei-nuclei repulsion potentials, respectively. The indexes i and j represent the sum over electron i and electron j at the r_i, r_j positions and A, B represent

the sum over nuclei at positions R_A, R_B with nuclear charges Z_A, Z_B. Note that the previous equation includes the Born-Oppenheimer approximation and thus the kinetic energy and the nuclei potential are not shown. In this case the Hamiltonian operator is called the electronic Halmitonian operator. However, in order to obtain the total energy of the system, E_{tot}, the nuclei potential as to be added to the electronic energy, E_{elec}, and hence, the total energy of the system is given by:

$$E_{tot} = E_{elec} + E_{Nuc} \tag{1.31}$$

The initial quantum molecular problem is to solve the Schrödinger equation in order to find the nuclear positions, R_A, R_B, ..., R_N that lead to the lowest eigenvalue - the energy minimum. This eigenvalue is the ground state energy, E_0, of the molecule and the resulting nuclear positions provide the ground state geometry. The fundamental principle that allow to obtain an approximate solution to the Schrödinger equation, and therefore E_0, is the Variational Principle, that states that the energy computed by equation for any given set of trial SO's is higher or equal to the "exact" energy of the system:

$$\langle \Psi_{real} | \hat{H} | \Psi_{real} \rangle \leq \langle \Psi_{trial} | \hat{H} | \Psi_{trial} \rangle \tag{1.32}$$

According to the Hellmann–Feynman theorem, once the ground state energy is obtained, all the properties of the system (in its ground state) can be determined by deriving the energy in respect to other quantities, like the positions of the nuclei or the electric field. However, the complexity of this N-electron problem is such that there is no exact solutions for the Schrödinger equation and hence approximations are needed. This work deals only with the DFT approximation. Other methods will be mentioned only when strictly needed. This is the case of the Hartree-Fock approximation that will be briefly presented next.

1.6.1 The Hartree-Fock Approximation

The electronic wave function, $\psi(x)$, should contain all the information of the system, but in order to be a solution to the Schrödinger equation, the electronic wave function must, among another requirements, be normalized as well as be antisymmetric with respect to the exchange of any pair of electron. The first requirement results from the Born interpretation of the wave function that states that the fact that $|\psi^2|$ is related to the

probability density of finding an electron in a particular region of space at a particular time, and thus this probability has to be $0 < |\psi^2| < 1$. The latter requirement is related to the Paulis Exclusion Principle: no two electrons of the same spin can occupy the same space point at the same time.

The principle of the HF approximation is that the total wave function of a system of N electrons can be separated as a product of mono-electronic wave functions, called *Spin-Orbitals* (SO), $\phi(x)$:

$$\Psi_{HF}(x_1, x_2, \ldots, x_N) = \phi_1(x_1) \times \phi_2(x_2) \times \cdots \times \phi_N(x_N) \tag{1.33}$$

This HF product of wave functions violates the antisymmetric requirement, and hence the appropriate form to describe a system by means of SO's is by the use of the Slater Determinant (SD). The HF method is a single SD method, which means that the entire N electron system will be described by a single SD. For the HF method, the SD has the form:

$$\Psi_{SD}(x_1, x_2, \ldots, x_N) = \frac{1}{\sqrt{N!}} \begin{bmatrix} \phi_1(x_1) & \phi_2(x_1) & \ldots & \phi_N(x_1) \\ \phi_1(x_2) & \phi_2(x_2) & \ldots & \phi_N(x_2) \\ \vdots & \vdots & \ddots & \vdots \\ \phi_1(x_N) & \phi_2(x_N) & \ldots & \phi_N(x_N) \end{bmatrix} \tag{1.34}$$

Once the SD is formed, it is possible to use the variational principle to minimize its value, and hence obtain the energy minimum. The expectation value of the $\hat{H}$ operator over such a SD can be formed by construction of each the individual parts of the $\hat{H}$ operator. The result of such operation yields:

$$E_{HF} = \langle \Psi_{SD} | \hat{H} | \Psi_{SD} \rangle = \sum_i \langle \phi_i | \hat{h} | \phi_i \rangle + \frac{1}{2} \sum_i \sum_j \langle \phi_i \phi_i || \phi_j \phi_j \rangle - \langle \phi_i \phi_j || \phi_j \phi_i \rangle \tag{1.35}$$

where the index the first sum reflects the one-electron Hamiltonian operator, $\hat{h}$, and the second sum reflects the two-electron operators. The one-electron operator defines the kinetic and the electron-nucleus attraction for a single electron, and is given by:

$$\langle \phi_i | h | \phi_i \rangle = \int \phi_i^* \left\{ -\frac{1}{2} \nabla^2 - \sum_A^M \frac{Z_A}{r_{iA}} \right\} \phi_i \partial x_i \tag{1.36}$$

As for the two-electron operator can be separated into the form of:

$$\langle \phi_i \phi_i || \phi_j \phi_j \rangle = \int \int |\phi_i|^2 \frac{1}{r_{12}} |\phi_j|^2 \, \partial x_i \partial x_j \tag{1.37}$$

$$\langle \phi_i \phi_j || \phi_j \phi_i \rangle = \int \int \phi_i^* \phi_j^* \frac{1}{r_{1,2}} \phi_j \phi_i \partial x_i \partial x_j \tag{1.38}$$

The term $\langle \phi_i \phi_i || \phi_j \phi_j \rangle$ is the Coulombic electrostatic interaction between the electron i and the average non-local charge distribution of the other $N-1$ electrons, whereas the term $\langle \phi_i \phi_j || \phi_j \phi_i \rangle$ is called the *Exchange* integral and has no classic physical meaning. It arises from the antisymmetry requirement of the wave function, and its similar to the Coulomb term, except that it switches (exchanges) the spin orbitals ϕ_i and ϕ_j.

In order to solve Equation 1.35 and obtain the minimum of the SD, the SO's must remain orthonormal. This is accomplished by Lagrange's method of undetermined multipliers, here denoted ϵ_i, that lead's to the *Hartree-Fock equations*:

$$\hat{f} \phi_i = \epsilon_i \phi_i \tag{1.39}$$

where $\hat{f}$ denotes the Fock operator, and ϵ_i have the physical meaning of being the orbital energies. The Fock operator is an one-electron operator that is defined as:

$$\hat{f} = -\frac{1}{2} \nabla^2 - \sum_A^M \frac{Z_A}{r_{iA}} + V_{HF} \tag{1.40}$$

It is easily seen, that the first two term are the kinetic energy and the electron-nucleus attraction energies, whereas V_{HF} is, in fact, an one-electron potential that is non less then the repulsive energy of the $N-1$ electron acting on the i'th electron. Hence, the complicated two-electron repulsion integrals on equation 1.35 are elegantly replaced, in the HF method, by an average potential given by a one-electron operator. This HF potential comprises two components: the Coulomb operator, $\hat{J}$, and the Exchange operator, $\hat{K}$ that are defined as:

$$V_{HF} = \sum_j^n \left(\hat{J}_i(x) - \hat{K}_i(x) \right) \tag{1.41}$$

$$\hat{J}_i(x_1) = \int |\phi_i(x_2)|^2 \frac{1}{r_{12}} \partial x_2 \tag{1.42}$$

$$\hat{K}_i(x_1)\Phi_i(x_1) = \int \phi_j^*(x_2)\frac{1}{r_{12}}\phi_i(x_2)\partial x_2\Phi_j(x_1) \tag{1.43}$$

In this case, the Coulomb integral represents the potential felt by an electron at the x_1 position by the presence of another electron, in a SO ϕ_i, at a distance x_2 from it, weighted by the probability of the second electron be found at the x_2 position. Since the $\hat{J}_i$ operator depends only on the value of ϕ_i at the x_1 position, this term is also called *local*. As for the $\hat{K}_j$ operator, it has no classic physical meaning and can only be defined when applied on a SO. it is very similar to the $\hat{J}_i$ operator, but it exchanges the variables in two SO. For that reason, the exchange operator is a *non-local*. It should be also noticed that the double summation on equation 1.35 allows that $i = j$, that is, it allows a Columbic interaction of the electron i with itself, and hence a *self-interaction* error is obtained in the HF method.

The HF method its a self-consistent field method (SCF) since it relies on an iterative procedure of finding the best wave functions that lead to a minimum of energy. This means that, after an initial guess, the spin-orbitals are tested and modified repeatedly until the input and output orbitals differ by less than a predetermined threshold - the so-called convergence of the SCF. The machinery behind a SCFHF procedure is not on the scope of this work and will not be addressed here.

1.6.2 Density Functional Theory

Unlike all the other *ab initio* methods, the DFT formulation is based on electronic density rather than wave functions. The earliest form of DFT was purposed by Thomas and Fermi almost one century ago, but their theories had deficiencies in the approximations made and were ignored by the scientific community.[86,87] It was not until 1964, with the publications of Hohenberg and Kohn (HK) theorems that was proven undoubtedly that electronic density is of fundamental importance on the quantum calculations of molecular system properties.[88] Moreover, the use of the electronic density reduces the number of variables from 3N to only 3, allowing large molecular systems to be studied at significant lower computational cost.

In one sentence, DFT can be understood as follows: for a given system, the electron density uniquely determines the position and charges of the nuclei, and hence trivially determines the Hamiltonian, without having the knowledge of any wave function. In

other words, the electronic density is the fingerprint of the system. This sentence is, in fact, a different way of stating HK first theorem: *The ground state density of a system of interacting electrons in an external potential uniquely defines this potential, except for an additive constant*, which proof is found is most quantum chemical books. The second HK theorem introduces the *variational principle* of DFT theory, and states that *there exists a universal functional for the energy, in terms of the electronic density, $E(\rho)$, which is valid for any external potential. For a given external potential, the global minimum of this functional is the ground state energy of the system, and the corresponding density is the ground state density.* Since this exact functional is not known, any functional will provides an energy that is higher or equal to the energy of the universal functional.

It is possible to write an equation similar to equation 1.30, that allows the energy of the system to be calculated. $E[\rho]$ is named the energy functional:

$$E[\rho] = T[\rho] + V_{ext}[\rho] + V_{ee}[\rho] \tag{1.44}$$

where $T[\rho]$ is the kinetic energy functional, $V_{ext}[\rho]$ is the interaction with an external potential functional and $V_{ee}[\rho]$ is the electron-electron interaction functional. Unfortunately, only the external potential functional can be obtained exactly. Kohn and Sham used an approximation similar to the HF method, treating the N-electron system as a fictitious system of non-interacting particles, each one moving in an effective potential of all the other particles. In this case, a similar SD can be written in the form of:

$$\Theta_S(x_1, x_2, \ldots, x_N) = \frac{1}{\sqrt{N!}} \begin{bmatrix} \varphi_1(x_1) & \varphi_2(x_1) & \ldots & \varphi_N(x_1) \\ \varphi_1(x_2) & \varphi_2(x_2) & \ldots & \varphi_N(x_2) \\ \vdots & \vdots & \ddots & \vdots \\ \varphi_1(x_N) & \varphi_2(x_N) & \ldots & \varphi_N(x_N) \end{bmatrix} \tag{1.45}$$

where the terms $\varphi_i(x_i)$ are now called the Kohn-Sham (KS) orbitals. Using this artefact, it is now possible to compute the kinetic energy of the non-interacting particles in the system, that is simply the same expression that was used in 1.30:

$$T_{KS}[\rho] = -\frac{1}{2} \sum_{i}^{N} \langle \varphi_i | \nabla^2 | \varphi_i \rangle \tag{1.46}$$

Still, the kinetic energy of a non-interacting system of particles is not the exact kinetic

energy of the system, and therefore, Kohn and Sham proposed that the total energy functional should be written as:

$$E[\rho] = T_{KS}[\rho] + V_{ext}[\rho] + E_{XC}[\rho] \tag{1.47}$$

where the term $E_{XC}[\rho]$ is called the *Exchange-Correlation Energy* and includes all the remaining unknown terms (the non-classical electrostatic contributions and the difference to the exact kinetic energy). In other words the XC functional contains all the errors of considering the system as a classic non-interacting system of particles, a kind of junkyard where everything is stowed away. The XC functional is given by:

$$E_{XC}[\rho] = (T[\rho] - T_{KS}[\rho]) + (V_{ee}[\rho] - V_H[\rho]) \tag{1.48}$$

The new term, $V_H[\rho]$, is the Hartree energy, that arises from the classical treatment of the electron-electron interaction and has a Columbic form that can be written in terms of the electronic density.

At this point it is important to mention that the KS orbitals are not, by all means, identical to the HF spin orbitals. The only physical significance is that the sum of the KS orbitals add up to the exact electronic density of the system. They are, however, more adequate to be qualitatively interpreted in a molecular orbital scheme than the HF spin orbitals, since the later neglect the correlation effects as well as the ground state density. Also, the SD generated by the KS orbitals cannot be related to the SD generated by the HF theory simply because it does not lead to a true N-electron wave function - it deals with density orbitals.

Current research in DFT is focused in the development of new methods for improve the XC functional through different approaches. This active field of research lead to the development of a myriad of functionals that are in more or less extend appropriate for particular studies. The ultimate evaluation of a functional is then made in terms of its results towards the available experimental data or by direct comparison with more accurate quantum theories. There are three main approximations to the XC functional: the Local Density Approximation (LDA), the Generalised Gradient Approximation (GGA) and the Hybrid Exchange Approximation.

The LDA approximation is based on the homogeneous electron gas approximation, where electrons are treated as moving in a constant positive charge distribution. The XC

functional can be defined, in the LDA approximation, in the form of:

$$E_{XC}^{LDA}[\rho] = \int \rho(r)\epsilon_{XC}(\rho)dr \tag{1.49}$$

where $\epsilon(\rho)$ is the XC energy per particle of uniform electron gas of density ρ. This term can be separated linearly in the exchange part, ϵ_X and in the correlation part, ϵ_C. The exchange part has an analytic expression is known as the *Slater Exchange*, whereas the correlation part has no analytic expression

Error of the LDA based functionals are usually related with over-biding energies and underestimated bond lengths.

In the GGA approximation, the XC functional takes into account not only the electronic density but also its gradient. The XC functional is, hence, generally described by:

$$E_{XC} \approx \int \rho(r)\epsilon_{XC}(\rho, \nabla\rho)dr \tag{1.50}$$

Within the GGA approximation, a different set of functionals was developed. These functionals are called meta-GGA functionals and depend explicitly on the semi-local parameters, namely the Laplacian of the spin density matrix or the local kinetic energy density. Typically, they are presented in the form:

$$E_{XC} \approx \int \rho(r)\epsilon_{XC}(\rho, \nabla\rho, \nabla^2\rho, \tau)dr \tag{1.51}$$

where τ is the kinetic energy given by 1.46. Modern GGA and meta-GGA functionals greatly improve the LDA functionals and typically predict the ground-state energy with an error less than 0.3 eV, bond lengths and angles within 1% of experimental values and atomization energies with an absolute error of less than 0.3 eV.[89]

Finally, hybrid exchange functionals provide an improvement to the GGA approximation by including a given percentage of the HF correlation. Furthermore, these functionals present the correct $\frac{-1}{r}$ behaviour of the exchange part. They also use a method that gradually "turns on" the electron-electron interactions. The XC functional then takes the form:

$$E_{XC} = \frac{1}{2}\int drdr \int_{\lambda=0}^{1} \frac{\lambda e^2}{|r-r'|}(\langle\rho(r)\rho(r')\rangle_{\rho,\lambda} - \rho(r)\delta(r-r')) \tag{1.52}$$

where, r and r' represent electrons with different spin, the term between brackets is the

density-density correlation function and λ is the coupling constant of the density-density correlation function. At $\lambda = 0$ one is in the HF domain whereas at $\lambda = 1$ one is at the GGA approximations. Hence, is reasonable to separate the XC energy in:

$$E_{XC} \approx \alpha E_{HF} + \beta E_{XC}^{GGA} \tag{1.53}$$

where α and β are constants that must satisfy the relations $0 \leq \alpha \leq 1$ and $0 \leq \beta \leq 1$ and $0 \leq \alpha + \beta \leq 1$. The parameter α allows the incorporation of a given percentage of the HF exchange contribution, whereas β allows the incorporation of a DFT exchange by a factor of $1 - (\alpha + \beta)$. Becke used this approach and developed what is the most popular and successful functional to date, the B3LYP. Its α and β parameters are based on several experimental data, namely atomisation energies, ionisation potentials, proton affinities and atomic energies in order to better reproduce the experimental properties of the molecules. This functional is known as Becke's three parameter functional and its E_{XC} is given by:

$$E_{XC} = E_{XC}^{LDA} + 0.2(E_X^{Fock} - E_X^{LDA}) + 0.7\Delta E_X^{B88} + 0.81\Delta E_C^{PW91} \tag{1.54}$$

1.6.3 Nonlinear Optical Properties from DFT

The nonlinear optical response of a material is still a great challenge for theoretical and computational chemists, since the problem relies on describing multi photon absorption processes in the presence of a highly intense external field, with a proper consideration of solvation effects. Therefore, the computational effort is much more demanding than for simple linear absorption responses, that can be easily obtained by the TD-DFT formalism. Although *ab initio* methods have been successfully used for quantitatively calculate the linear and nonlinear optical properties of molecules, their usage is limited to small molecules due to high computational cost. Semi-empirical methods, in their turn, are known to be less computational demanding, but highly dependent on parameterizations, leading to less accurate results. DFT methods fall in between these two levels of theory, giving good quantitative results at a low computational cost.[90] Most of the implementation of theoretical prediction of the linear and NLO polarizabilities in quantum chemistry software packages, like Gaussian (G09)[91], has been done in early 1990's. In the next paragraphs, a short overview on the theory behind the NLO calculations is made.

Two main approaches for calculating the molecular hyperpolarizabilities are used: derivative and perturbation techniques. When a molecule is exposed to an electric field, its charge density will respond to this perturbation and the overall energy of the system is thereby different from its initial state. This energy in the presence of the electric field can be described in terms of a Taylor expansion by (to avoid confusion with energy, E, the electric field is hereby denoted as F):

$$\begin{aligned} E(\vec{F}) = E_0(\vec{0}) &+ \sum_i \left(\frac{\partial E}{\partial F_i}\right)_{\vec{F}} F_i \\ &+ \frac{1}{2!}\sum_{ij} \left(\frac{\partial^2 E}{\partial F_i \partial F_j}\right)_{\vec{F}} F_i F_j \\ &+ \frac{1}{3!}\sum_{ijk} \left(\frac{\partial^3 E}{\partial F_i \partial F_j \partial F_k}\right)_{\vec{F}} F_i F_j F_k \\ &+ \frac{1}{4!}\sum_{ijkl} \left(\frac{\partial^4 E}{\partial F_i \partial F_j \partial F_k \partial F_l}\right)_{\vec{F}} F_i F_j F_k F_l + \ldots \end{aligned} \tag{1.55}$$

where the indexes in summations represent the Cartesian axes and the indexes outside represent the partial derivatives represent the static domain (if $\vec{F} = \vec{0}$) or the dynamic domain (if $\vec{F} \neq \vec{0}$). In accordance to the HellmannFeynman theorem, each of the derivatives can be related to one of the electric properties of the molecules. In other words, the dipole moment, the linear polarizability and the nonlinear hyperpolarizabilities can be written as derivatives of the energy with respect to the incident electric field by:

$$\mu_i = \left(\frac{\partial E}{\partial F_i}\right) \tag{1.56}$$

$$\alpha_{ij} = -\left(\frac{\partial E_i}{\partial F_i \partial F_j}\right) \tag{1.57}$$

$$\beta_{ijk} = -\left(\frac{\partial^3 E}{\partial F_i \partial F_j \partial F_k}\right) \tag{1.58}$$

$$\gamma_{ijkl} = -\left(\frac{\partial^4 E}{\partial F_i \partial F_j \partial F_k \partial F_l}\right) \tag{1.59}$$

Therefore, from a practical point of view the electric properties of a molecule can be obtained by differentiation of the field-dependent energy or dipole moment. This is

the basis of the finite field method, which is by far the most used method for obtaining such quantities. Since the dipolar moment operator is the derivative of the energy in respect to the electric field, the quantum chemical linear and nonlinear responses can be obtained from similar energy expressions with higher derivative orders. The DFT scheme enables the determination of the ground-state density, and consequently the dipole moment, of a molecule with or without external electric fields. After differentiation, it is then possible to determine the static polarizability and hyperpolarizability tensors, by performing calculations in small electric fields of varying magnitudes and directions.[92] This procedure is the so-called finite-field (FF) approach, where the tensors are determined from finite differentiation techniques and the energy expression is truncated by the forth power F^4. The major drawback of FF calculations is that it only provides access to static polarizabilities and hyperpolarizabilities. The frequency dependent tensors are not possible to calculate with this method. This is of crucial importance since it makes a direct comparison with experimental results impossible, especially for hyperpolarizabilities where it is known that there are substantial differences between the frequency-dependent and zero frequency results.[92] If no analytical derivatives are implemented, FF calculation have to be solved numerically. Like all numerical derivative procedures, this might lead numerical problems, especially for lower or higher fields. In the case of the lower fields, the numerical problem arises from the fact that $F \to 0$, and usually, for static quantities, a value of 0.001 a.u. is used. For higher fields, the source of this error arises not only from the missing terms in the truncated equations, but more importantly from the high energy of this field that might lead to ionization or a changing in the ordering of the electronic states of the molecule.

The *Sum-Over-States* method (SOS) uses a completely different approach to the FF method, in the sence that it uses Time Dependent Perturbation theory for obtaining the nonlinear optical responses of a molecule. In SOS, the dipole moment operators and energies are evaluated and summed. This summation is, in general, infinite leading to a strong criticism of this methodology since it is well known that only a few states are involved in the NLO phenomena.[93] For the first hyperpolarizability, the SOS expression is given by:

$$\beta_{ijk}(\omega_\sigma;\omega_1,\omega_2) = \sum_P \sum_{g,e} \frac{\langle 0|i|g\rangle \langle g|j|e\rangle \langle e|k|0\rangle}{(E_g - E_0 - h\omega_\sigma)(E_e - E_0 - h\omega_2)} \tag{1.60}$$

where g and e represent the ground and excited state respectively, and $j = j - \langle 0|j|0\rangle$.

The main advantage of the SOS method is that one can directly obtain frequency dependent properties. However, this equation might lead to inaccurate results, since a complete description not only the ground state but also several excited sates is necessary. Moreover, the SOS expression must be also truncated in some manner, since the description of all the excited states of the molecule is impossible. This truncation also leads to severe problems in the calculation of the SOS values of hyperpolarizabilities, since the choice of the truncation might affect the final result.

1.6.4 Comparison of Theoretical and Experimental Hyperpolarizabilities

The enormous initial success of DFT methods in obtaining field-dependent and -independent properties of small molecules led to a rapid burst in the number of papers in this subject. However, DFT methods are known to fail when trying to predict the amplitude of NLO properties of long organic and organometallic molecules, specially when a comparison with experimental values is made. Several problems have been addressed to justify this failure of the DFT methods.

Computational methods afford the 10 or 18 components of hyperpolarizability tensor, for the static and field-dependent regime respectively. The remaining 17 or 9 tensors for each case are obviated due to the Kleinmman symmetry. For comparison with experiment, that only provide the orientational average of the hyperpolarizability tensor, the components of the hyperpolarizability need to be converted to the so-called total hyperpolarizability, β_{total}. The most used method of obtaining β_{total}, is the determination of the norm of the hyperpolarizability vector, that is given by:

$$\beta_{total} = \sqrt{\beta_x^2 + \beta_y^2 + \beta_z^2} \tag{1.61}$$

with

$$\beta_i = \frac{1}{3}\sum \left(\beta_{iii}^2 + \beta_{ijj}^2 + \beta_{ikk}^2\right), \quad with \quad i,j,k = x,y,z \tag{1.62}$$

The major drawback of this scaling method is that there it has no physical significance in relation to the value obtain from any experimental setup. Also, this equation is limited to the static domain and it has no molecular symmetry dependence. As far as this

work is concern, the best method to obtain β_{total} is by direct use of equations 1.22 and 5.6 (hereafter called β_{HRS}), after an analysis of the molecular symmetry and usage of the Kleinmann symmetry to obtain all the non-vanishing tensor components. Finally, results can then be compared with the experimental value. In this case, both Kleinman symmetry and the geometric dependence of the hyperpolarizability are included. Also, if the adequate computational method is applied, it is possible to obtain both the static and dynamic value of β_{total}.

Comparison of the experimental and theoretical values of the hyperpolarizabilities is only possible if the results are in the same convention. Thus, as stated previously in Section 1.7, a clear and unambiguous description of both the experimental setup and the theoretical formulations for obtaining the NLO properties in terms of the used convention for each case is mandatory. The Gaussian software package, used throughout this work, uses the nonlinear optical definitions used by Kurtz and Dudis[94] that is assumed as the T convention.

The basis set dependence of the quantum estimated hyperpolarizabilities is still a subject of current investigation. It is well known that, for small molecules, including both diffuse and polarization functions on the non-hydrogen atoms is essential for obtaining sufficiently converged hyperpolarizability values.[94,95] However, there is no systematic trend that one can follows in order to establish which particular basis set to use. In fact, many authors suggest that the decision of the basis set to use should take into account the quality/cost ratio of the calculation, rather than the accurateness of the result. Also, it is important to state that the basis set is also dependent on the nature of the system, this meaning that the size and complexity of the chosen basis set should weight accordingly. For example, the use of small basis sets in the calculation of very large π-delocalized systems hyperpolarizabilities was found to be sufficient.[96] This is also true for open-shell systems, were the simple 6-31G+(d,p) basis set proven to be suficiently accurate to estimate the hyperpolarizabilities of π-delocalized systems.[97]

The choice of the functional, and in particular the XC part of the functional, is also crucial for the correct description of the hyperpolarizabilities. The reliability of several functionals to evaluate molecular electronic hyperpolarizabilities has been questioned in a large number of studies. Although early works proven the good performance of both LDA- and GGA-based functionals in the prediction of the hyperpolarizabilities of small molecules, it was further discussed that the need for a correct description of the asymp-

totic behaviour of the XC potential is necessary for more accurate results, especially larger extended systems.[98,99] The observed deviations were of several order of magnitude when comparing the calculated and experimental hyperpolarizabilities, and were also attributed an incorrect electric field dependence of the response part of the exchange potential.[92] The huge success of hybrid functionals, such as B3LYP, arises from the inclusion a certain percentage of the exact HF exchange, that corrects both the long-range asymptotic behaviour and the electric field dependence of the calculations. In fact B3LYP is one of the most successful functionals for large systems such as organic push-pull π-conjugated systems and transition-metal complexes.(colocar referencia adequada) However, in the case of large π-conjugated systems, a fraction of HF exchange remains often insufficient, even qualitatively.[100] Among the new strategies to circumvent the so-called short-sightedness of the XC functionals is the development of long-range corrected functionals, like the Coulomb- attenuating model (CAM).[101] Using these long-range corrected functionals, such as the CAM-B3LYP functional, better predictions of β for extended π-conjugated push-pull systems are observed.[102] However, there is no consensus among the scientific community on the systematic improvement of long-range corrected functionals over HF in the determination of the molecular hyperpolarizabilities as well as in the evaluation of the molecular nonlinear optical switching contrasts.[103,104]

Although the choice of the functional is still very dependent on the system, some remarks can be made concerning the choice of the functional for the determination of the molecular hyperpolarizabilities: i) the best functionals are hybrid functionals that in general include substantial amounts of HF exchange; ii) long-range corrected hybrid functionals are more suitable to describe qualitatively the evolution of the molecular hyperpolarizability in extended systems; iii) octupolar molecules are usually better described by HF than by popular B3LYP or even CAM-B3LYP functionals. These latter are usually adequate to satisfactorily describe the NLO responses quasi-pure dipolar character; iv) the recently developed Minnesota functionals (M05 and M06) provide slightly larger deviations for the estimated hyperpolarizability values of dipolar molecules.[105]

Solvation is another important factor when dealing with the comparison of experimental and theoretical hyperpolarizabilities. In fact, since most of the experimental techniques are performed in solution, the inclusion of the solvent effects on both the optimized structure and the electric properties obtained by quantum mechanics are needed to an accurate estimation, and therefore, comparison to the experimental values. Hence, an

accurate consideration of the solvated geometrical structure and more importantly of the charge distribution in the NLO chromophore are important aspects on molecular response properties, that need to be properly modelled by the solvent effects. Nowadays, there are many alternative solvation models that can be used.[106] However, among the available approaches, the most popular for this kind of study is still represented by continuum solvation models, namely the polarizable continuum model (PCM).[107,108] In this solvation model, like in all continuum models, a molecule (or a few molecules) of the solute are placed into a void cavity within a continuous dielectric medium mimicking the solvent. The shape and size of the cavity are differently defined in the various continuum models, but a common definition is that a cavity should have a physical meaning. In particular, the cavity should exclude the solvent and must contain within its boundaries the largest possible part of the solute charge distribution.[106]

1.7 Units and Conventions In Nonlinear Optics

It was shown above that nonlinear optical properties can be obtained by several experimental techniques. Also, quantum mechanical calculations were showed be used for the estimation of nonlinear optical properties. It is not uncommon that great confusion among authors arise when dealing with comparison of several results obtained by different techniques, quantum methods, unit systems or conventions used for defining the NLO quantities. Therefore, when dealing either experimental or theoretical results it is necessary a careful analysis of the data.

The unit system is by far the simplest problem to solve when one is dealing with the comparison of data obtained from different sources. **Table 1.1** shows the typical units used in the NLO field for both the CGS and the SI systems in experimental and quantum methods.

A much more complex problem arises when dealing with the convention system used to describe the NLO quantities. There are currently five different conventions in use for defining the microscopic and macroscopic NLO quantities. These conventions are used by different authors, and hence care must be taken when dealing with the comparison of experimental data between different works. The relation between these conventions was first made by Willetts *et al.*[109] and more recently by Kuzyk *et al.*[110]. Herein, only the two most used conventions will be addressed. If equation 1.2 is expanded in a Taylor series

Table 1.1: Unit systems and convertion factors for NLO properties

Parameter	Metric System		Convertion Factor
	CGS	SI	
Electric Field	$statV.cm^{-1}$	$V.m^{-1}$	$E_{SI} = 3 \times 10^4 E_{CGS}$
Polarization	$statV.cm^{-1}$	$C.m^{-2}$	$P_{SI} = \frac{1}{3} \times 10^{-11} P_{CGS}$
μ	$stat.C.cm = statV.cm^2$	$C.m$	$\mu_{SI} = 3 \times 10^4 \mu_{CGS}$
α	cm^3	m^3	$\alpha_{SI} = (4\pi) \times 10^{-6} \alpha_{CGS}$
β	$statV^{-1}.cm^4 = esu$	$V^{-1}.m^4$	$\beta_{SI} = \frac{4\pi}{3} \times 10^{-10} \beta_{CGS}$
γ	$statV^{-2}cm^5 = esu$	$V^{-2}.m^5$	$\gamma_{SI} = \frac{4\pi}{9} \times 10^{-14} \gamma_{CGS}$

fashion, one gets:

$$\rho = \mu_0 + \alpha^T E + \frac{1}{2!}\beta^T E^2 + \frac{1}{3!}\gamma^T E^3 + \dots \tag{1.63}$$

where the superscript, T, refers that the Taylor expansion is in use, and obviously this is called the T convention. A different convention arises from the inclusion of the factorial terms into the linear and nonlinear polarizabilities themselves, resulting in the so called the B convention:

$$\rho = \mu_0 + \alpha^B E + \beta^B E^2 + \gamma^B E^3 + \dots \tag{1.64}$$

Although these two equation appear very similar, the inclusion of the factorial term in equation 1.64 results that, in the static limit, the terms β and γ differ by $\frac{1}{2}$ and $\frac{1}{6}$ respectively. For second-order nonlinear processes, its is easily seen that the relation between these two conventions is:

$$\beta^B(0;0,0) = \frac{1}{2}\beta^T(0;0,0) \tag{1.65}$$

The transition from the static limit to the frequency-dependent limit involves an additional factor of $\frac{1}{2}$, leading to a factor of 4 for second-order processes. A further uncertainty is whether or not so-called degeneracy factors are included in the definition of the NLO parameters. Because SONLO susceptibilities and hyperpolarizabilities are defined for a given combination of the input frequencies, degeneracy factors arise as a result of summing over the field amplitudes of fields with the same frequency. For example, the g used to describe the process of THG and that used to describe nonlinear refraction may differ by a factor of 3, depending on whether the degeneracy factor is included in the definition

of G or not. It is usually considered prudent to define the hyperpolarizabilities in such a way that they collapse to the same value as the frequencies tend to zero.

1.8 Motivation for this work

Despite the great advances in the chemical and physical knowledge of the NLO phenomena of metallo-organic based materials, molecular materials are not yet used in NLO technologies. The main reason for this fact are the inadequate properties, low stability but more importantly the fact that cheaper and more efficient inorganic materials still provide the reliability needed for device fabrication. Nonetheless, organometallic compounds have demonstrated great potential in the NLO field, despite the need for more systematic measurement and modelling approaches.

In the past few years, great technological achievements, in both synthetic methods and quantum methods, allowed a greater knowledge of the NLO concepts needed for guiding the scientific community, and in particular chemists, in the development of tailored made molecules with high nonlinear optical performances. Within certain limitations, it is now possible to prepare nonlinear optical materials by design, taking advantage of the *a priori* data provided by quantum methods. These include, for example, the bond-length alternation parameter; the development of new molecular architectures, such as quadrupolar or octupolar molecular structures, quinoidal and pro-quinoidal and pseudo-aromatic structures; the deeper knowledge of excited-states properties. All these new concepts allowed chemists intuition and know-how about the nonlinear response to be strengthened.

This thesis does not focus on purely organic or inorganic materials neither in the development of device assemblies and technologies, but concentrates on the development of tailor-made organometallic materials and their characterization as possible redox NLO-active molecular switches. In particular, this work is based on the synthesis and characterization of novel η^5-monocyclopentadienyliron (II) and ruthenium (II) organometallic complexes bearing two different families of redox active ligands: benzo[c]thiophene and *s*-tetrazine. In the case of the first, the usage of a pro-quinoidal structure was envisaged to significantly enhance the NLO quadratic response, whereas in the case of the latter the strong electron acceptor ability of the *s*-tetrazine ring would produce greater donor-acceptor coupling, resulting also in an enhancement of the NLO quadratic response. In

both cases, the good redox properties of the ligands would promote the electrochemical reversibility needed for the complexes to act as redox-NLO switches.

References

[1] M. Butter, M. Leis, M. Sandtke, M. McLean, J. Lincoln, and A. Wilson. The leverage effect of photonics technologies: the european perspective, study prepared for the european commission. *DG Information Society and Media*, March 2011.

[2] R. W. Boyd. *Nonlinear Optics*. Academic Press, Burlington, Third edition, 2008.

[3] P. P Banerjee. *Nonlinear Optics: Theory, Numerical Modeling and Applications*, volume 86. Marcel Dekker, Inc., First edition, 2004.

[4] E. Van Stryland M. Bass, G. Li. *Handbook of Optics*, volume IV. McGraw Hill, Inc., Third edition, 2010.

[5] W. T. Hill and C. H. Lee. *Light-Matter Interaction*. Wiley-VCH Verlag GmbH, 2007.

[6] R. Menzel. *Photonics - Linear and Nonlinear Interactions of Laser Light and Matter*. Springer-Verlag, second edition edition, 2007.

[7] G. New. *Introduction to Nonlinear Optics*. Cambridge University Press, 2011.

[8] V. Rodriguez T. Verbiest, K. Clays. *Second-Order Nonlinear Optical Characterization Techniques: An Introduction*. Taylor and Francis Group, 2009.

[9] J. Zyss. *Molecular Nonlinear Optics: Materials, Physics, and Devices*. Optics and Photonics Series. Academic Press, 1994.

[10] E. Goovaerts, W. E. Wenseleers, M. H. Garcia, and G. H. Cross. Chapter 3 - Design and characterization of organic and organometallic molecules for second order nonlinear optics. In Hari Singh Nalwa, editor, *Handbook of Advanced Electronic and Photonic Materials and Devices*, pages 127 – 191. Academic Press, Burlington, 2001.

[11] C. E. Powell and M. G. Humphrey. Nonlinear optical properties of transition metal acetylides and their derivatives. *Coordination Chemistry Reviews*, 248(7–8):725 – 756, 2004.

[12] J. P. Morrall, G. T. Dalton, M. G. Humphrey, and M. Samoc. Organotransition metal complexes for nonlinear optics. volume 55 of *Advances in Organometallic Chemistry*, pages 61 – 136. Academic Press, 2007.

[13] M.G. Papadopoulos, A.J. Sadlej, and J. Leszczynski. *Non-Linear Optical Properties of Matter: From molecules to condensed phases*. Challenges and Advances in Computational Chemistry and Physics. Springer, 2007.

[14] M.H. Garcia, M.P. Robalo, A.R. Dias, M.F. M. Piedade, A. Galvão, W. Wenseleers, and E. Goovaerts. Organometallic complexes for second-order non-linear optics: synthesis and molecular quadratic hyperpolarizabilities of η^5-monocyclopentadienyliron(ii) nitrile derivatives with different phosphines. x-ray crystal structure of [Fecp(DPPE)(p-ncc$_6$h$_4$no$_2$)][pf$_6$]ch$_2$cl$_2$. *Journal of Organometallic Chemistry*, 619(1–2):252 – 264, 2001.

[15] T. Verbiest, L. Derhaeg, E. Kelderman, J.F.J. Engbersen, W. Verboom, D.N. Reinhoudt, K. Clays, and A. Persoons. Determination of molecular hyperpolarizabilities by hyper rayleigh scattering. In G.J. Ashwell and D. Bloor, editors, *Organic Materials for non-linear optics III*, pages 326–331. Royal Society of Chemistry, Cambridge, 1994.

[16] N. W. Song, T. K., S. C. Jeoung, S. Jeon, B. R. Cho, and D. Kim. Improved method for measuring the first-order hyperpolarizability of organic NLO materials in solution by using the hyper-Rayleigh scattering technique. *Chemical Physics Letters*, 261(3):307 – 312, 1996.

[17] O.F.J. Noordman and N.F. van Hulst. Time-resolved hyper-Rayleigh scattering: measuring first hyperpolarizabilities β of fluorescent molecules. *Chemical Physics Letters*, 253(1–2):145 – 150, 1996.

[18] S. J. Cyvin, J. E. Rauch, and J. C. Decius. Theory of hyperraman effects (nonlinear inelastic light scattering): Selection rules and depolarization ratios for the secondorder polarizability. *The Journal of Chemical Physics*, 43(11):4083–4095, 1965.

[19] J. L. Oudar and D. S. Chemla. Hyperpolarizabilities of the nitroanilines and their relations to the excited state dipole moment. *The Journal of Chemical Physics*, 66(6):2664–2668, 1977.

[20] J. Perez-Moreno, K. Clays, and M. G. Kuzyk. Why do we need three levels to understand the molecular optical response? *Proceedings of SPIE*, 8113:81130L–81130L–9, 2011.

[21] M. L. H. Green, S. R. Marder, M. E. Thompson, J. A. Bandy, D. Bloor, P. V. Kolinsky, and R. J. Jones. Synthesis and structure of (cis)-[1-ferrocenyl-2-(4-nitrophenyl)ethylene], an organotransition metal compound with a large second-order optical nonlinearity. *Nature*, 330(6146):360–362, 11 1987.

[22] J. C. Calabrese, L. T. Cheng, J. C. Green, S. R. Marder, and W. Tam. Molecular second-order optical nonlinearities of metallocenes. *Journal of the American Chemical Society*, 113(19):7227–7232, 1991.

[23] V. Alain, M. Blanchard-Desce, C. Chen, S. R. Marder, A. Fort, and M. Barzoukas. Large optical nonlinearities with conjugated ferrocene and ruthenocene derivatives. *Synthetic Metals*, 81(2–3):133 – 136, 1996.

[24] S. Barlow, H. E. Bunting, C. Ringham, J. C. Green, G.U. Bublitz, S. G. Boxer, J. W. Perry, and S. R. Marder. Studies of the electronic structure of metallocene-based second-order nonlinear optical dyes. *Journal of the American Chemical Society*, 121(15):3715–3723, 1999.

[25] G. G. A. Balavoine, J. Daran, G. Iftime, P. G. Lacroix, E. Manoury, J. A. Delaire, I. Maltey-Fanton, K. Nakatani, and S. Di Bella. Synthesis, crystal structures, and second-order nonlinear optical properties of new chiral ferrocenyl materials. *Organometallics*, 18(1):21–29, 1999.

[26] J. Chiffre, F. Averseng, G. G. A. Balavoine, J. Daran, G. Iftime, P. G. Lacroix, E. Manoury, and K. Nakatani. A novel and perfectly aligned crystal of a ferrocenyl chromophore displaying high quadratic nonlinear optical bulk efficiency. *European Journal of Inorganic Chemistry*, 2001(9):2221–2226, 2001.

[27] E. Peris. From long-chain conjugated oligomers to dendrimers: synthesis and physical properties of phenyl-ethenyl-ferrocenyl containing one- and two-dimensional complexes. *Coordination Chemistry Reviews*, 248(3–4):279 – 297, 2004.

[28] K. N. Jayaprakash, P. C. Ray, I. Matsuoka, M. M. Bhadbhade, V. G. Puranik, P. K. Das, H. Nishihara, and A. Sarkar. Ferrocene in conjugation with a fischer carbene: synthesis, NLO, and electrochemical behavior of a novel organometallic *Push-Pull* system. *Organometallics*, 18(19):3851–3858, 1999.

[29] I. Janowska, J. Zakrzewski, K. Nakatani, J. A. Delaire, M. Palusiak, M. Walak, and H. Scholl. Ferrocenyl D-π-A chromophores containing 3-dicyanomethylidene-1-indanone and 1,3-bis(dicyanomethylidene)indane acceptor groups. *Journal of Organometallic Chemistry*, 675(1–2):35 – 41, 2003.

[30] I. Janowska, J. Zakrzewski, K. Nakatani, M. Palusiak, M. Walak, and H. Scholl. Ferrocenyl da conjugated polyenes with 3-dicyanomethylidene-1-indanone and 1,3-bis(dicyanomethylidene)indane acceptor groups: Synthesis, linear and second-order nonlinear optical properties and electrochemistry. *Journal of Organometallic Chemistry*, 691(3):323 – 330, 2006.

[31] C. Arbez-Gindre, B. R. Steele, G. A. Heropoulos, C. G. Screttas, J. Communal, Werner J. Blau, and I. Ledoux-Rak. A facile organolithium route to ferrocene-based triarylmethyl dyes with substantial near IR and NLO properties. *Journal of Organometallic Chemistry*, 690(6):1620 – 1626, 2005.

[32] D.A Davies, J Silver, G Cross, and P Thomas. Synthesis and nonlinear optical properties of a range of 1-ferrocenyl(2-(4-alkyl)pyridiniumyl)ethylene iodides. *Journal of Organometallic Chemistry*, 631(1-2):59–66, 2001.

[33] J. A. Mata, E. Peris, I. Asselberghs, R. Van Boxel, and A. Persoons. Large second-order NLO properties of new conjugated oligomers with a pendant ferrocenyl and an end-capped pyridine. *New J. Chem.*, 25:1043–1046, 2001.

[34] B. J. Coe, R. J. Docherty, S. P. Foxon, E. C. Harper, M. Helliwell, J. Raftery, K. Clays, E. Franz, and B. S. Brunschwig. Syntheses and properties of salts of chromophores with ferrocenyl electron donor groups and quaternary nitrogen acceptors. *Organometallics*, 28(24):6880–6892, 2009.

[35] Santo D. B. Second-order nonlinear optical properties of transition metal complexes. *Chem. Soc. Rev.*, 30:355–366, 2001.

[36] E. Cariati, M. Pizzotti, D. Roberto, F. Tessore, and R. Ugo. Coordination and organometallic compounds and inorganic-organic hybrid crystalline materials for second-order non-linear optics. *Coordination Chemistry Reviews*, 250(11-12):1210–1233, 2006. Inorganic Chemistry in Italy.

[37] K. A. Green, M. P. Cifuentes, M. Samoc, and M. G. Humphrey. Syntheses and {NLO} properties of metal alkynyl dendrimers. *Coordination Chemistry Reviews*, 255(17–18):2025 – 2038, 2011. Special Issue: 39th International Conference on Coordination Chemistry.

[38] G. Grelaud, M. P. Cifuentes, F. Paul, and M. G. Humphrey. Group 8 metal alkynyl complexes for nonlinear optics. *Journal of Organometallic Chemistry*, 751(0):181 – 200, 2014.

[39] D.M. Roundhill and J.P. Fackler. *Optoelectronic Properties of Inorganic Compounds*. Modern Inorganic Chemistry. Springer, 1999.

[40] H.F. Chin. *Organometallic Compounds: Preparation, Structure and Properties*. Materials science and technologies series. Nova Science Publishers, 2010.

[41] A-R. Dias, M. H. Garcia, J. C. Rodrigues, J. C. Petersen, T. Bjornholm, and Tommy Geisler. Third-harmonic generation in organometallic ruthenium(II) derivatives containing coordinated p-substituted benzonitriles. *Journal of Materials Chemistry*, 5:1861–1865, 1995.

[42] W. Wenseleers, A. W. Gerbrandij, E. Goovaerts, M. H. Garcia, M. P. Robalo, P. J. Mendes, J. C. Rodrigues, and A. R. Dias. Hyper-Rayleigh scattering study of η^5-monocyclopentadienyl-metal complexes for second order non-linear optical materials. *Journal of Materials Chemistry*, 8:925–930, 1998.

[43] M. H. Garcia, P. F., M. F. M. Piedade, M. T. Duarte, M. P. Robalo, J. Heck, C. Wittenburg, J. Holtmann, and E. Licandro. Synthesis of organometallic Ru(II) and Fe(II) complexes containing fused rings hemi-helical ligands as chromophores. Evaluation of non-linear optical properties by HRS. *Journal of Organometallic Chemistry*, 693(18):2987 – 2999, 2008.

[44] A. Valente, S. Royer, M. Narendra, T. J.L. Silva, P. J.G. Mendes, M. P. Robalo, M. Abreu, J. Heck, and M. H. Garcia. Synthesis of new Fe(II) and Ru(II) η^5-monocyclopentadienyl compounds showing

significant second order NLO properties. *Journal of Organometallic Chemistry*, 736(0):42 – 49, 2013.

[45] M. H. Garcia, S. Royer, M. P. Robalo, A. Romão Dias, J. Tranchier, R. Chavignon, D. Prim, A. Auffrant, F. Rose-Munch, E. Rose, J. Vaissermann, A. Persoons, and I. Asselberghs. Synthesis, characterisation of (arene)tricarbonylchromium complexes linked to cationic Fe and Ru derivatives and studies of first hyperpolarisabilities by Hyper-Rayleigh Scattering. *European Journal of Inorganic Chemistry*, 2003(21):3895–3904, 2003.

[46] S. Houbrechts, K. J. Clays, A. P. Persoons, V. Cadierno, M. P. Gamasa, J. Gimeno, I. R. Whittall, and M. G. Humphrey. New organometallic materials for nonlinear optics: metal σ-arylacetylides. *Proceedings of SPIE*, 2852:98–108, 1996.

[47] I. R. Whittall, M. G. Humphrey, A. Persoons, and S. Houbrechts. Organometallic complexes for nonlinear optics. 3.1 molecular quadratic hyperpolarizabilities of ene-, imine-, and azo-linked ruthenium σ-acetylides: x-ray crystal structure of Ru((E)-4,4‘-C$\equiv$CC_6H_4CHCHC$_6H_4NO_2$)(PPh_3)$_2$(η^5-C_5H_5). *Organometallics*, 15(7):1935–1941, 1996.

[48] M. H. Garcia, P. J. Mendes, M. P. Robalo, A. R. Dias, J. Campo, W. Wenseleers, and E. Goovaerts. Compromise between conjugation length and charge-transfer in nonlinear optical η^5-monocyclopentadienyliron(II) complexes with substituted oligo-thiophene nitrile ligands: Synthesis, electrochemical studies and first hyperpolarizabilities. *Journal of Organometallic Chemistry*, 692(14):3027 – 3041, 2007.

[49] T. J. L. Silva, P. J. Mendes, A. M. Santos, M. H. Garcia, M. P. Robalo, J. P. P. Ramalho, A. J. P. Carvalho, M. Büchert, C. Wittenburg, and J. Heck. Mono(η^5-cyclopentadienyl)metal(II) complexes with thienyl acetylide chromophores: Synthesis, electrochemical studies, and first hyperpolarizabilities. *Organometallics*, 33(18):4655–4671, 2014.

[50] S. K. Hurst, M. P. Cifuentes, J. P. L. Morrall, N. T. Lucas, I. R. Whittall, M. G. Humphrey, I. Asselberghs, A Persoons, M. Samoc, B. Luther-Davies, and A. C. Willis. Organometallic complexes for nonlinear optics. 22.1 Quadratic and cubic hyperpolarizabilities of trans-bis(bidentate phosphine)ruthenium σ-arylvinylidene and σ-arylalkynyl complexes. *Organometallics*, 20(22):4664–4675, 2001.

[51] S. R. Marder, L. Cheng, and B. G. Tiemann. The first molecular electronic hyperpolarizabilities of highly polarizable organic molecules: 2,6-di-tert-butylindoanilines. *Chemical Communications*, pages 672–674, 1992.

[52] A. M. McDonagh, M. P. Cifuentes, N. T. Lucas, M. G. Humphrey, S. Houbrechts, and A. Persoons. Organometallic complexes for nonlinear optics: Part 19. syntheses and molecular quadratic hyperpolarizabilities of indoanilino–alkynyl–ruthenium complexes. *Journal of Organometallic Chemistry*, 605(2):184 – 192, 2000.

[53] M. P. Cifuentes, C. E. Powell, M. G. Humphrey, G. A. Heath, M. Samoc, and B. Luther-Davies. Organometallic complexes for nonlinear optics. Reversible electrochemical switching of nonlinear absorption. *The Journal of Physical Chemistry A*, 105(42):9625–9627, 2001.

[54] C. E. Powell, M. P. Cifuentes, J. P. Morrall, R. Stranger, M. G. Humphrey, M. Samoc, B. Luther-Davies, and G. A. Heath. Organometallic complexes for nonlinear optics. 30.1 Electrochromic linear and nonlinear optical properties of alkynylbis(diphosphine)ruthenium complexes. *Journal of the American Chemical Society*, 125(2):602–610, 2003.

[55] D. R. Kanis, M. A. Ratner, and T. J. Marks. Design and construction of molecular assemblies with large second-order optical nonlinearities. quantum chemical aspects. *Chemical Reviews*, 94(1):195–242, 1994.

[56] A. M. McDonagh, M. P. Cifuentes, M. G. Humphrey, S. Houbrechts, J. Maes, A. Persoons, M. Samoc, and B. Luther-Davies. Organometallic complexes for nonlinear optics: Part 21. syntheses and quadratic hyperpolarizabilities of alkynyl complexes containing optically active 1,2-bis(methylphenylphosphino)benzene ligands. *Journal of Organometallic Chemistry*, 610(1–2):71 – 79, 2000.

[57] B. J. Coe, J. A. Harris, L. J. Harrington, J. C. Jeffery, L. H. Rees, S. Houbrechts, and A. Persoons. Enhancement of molecular quadratic hyperpolarizabilities in ruthenium(II) 4,4‘-bipyridinium complexes by N-phenylation. *Inorganic Chemistry*, 37(13):3391–3399, 1998.

[58] B. J. Coe. Molecular materials possessing switchable quadratic nonlinear optical properties. *Chemistry - A European Journal*, 5(9):2464–2471, 1999.

[59] B. J. COE and N. R. M. CURATI. Metal complexes for molecular electronics and photonics. *Comments on Inorganic Chemistry*, 25(5-6):147–184, 2004.

[60] B. J. Coe, A. Avramopoulos, M. G. Papadopoulos, K. Pierloot, S. Vancoillie, and H. Reis. Theoretical modelling of photoswitching of hyperpolarisabilities in ruthenium complexes. *Chemistry - A European Journal*, 19(47):15955–15963, 2013.

[61] B. J. Coe, L. A. Jones, J. A. Harris, B. S. Brunschwig, I. Asselberghs, K. Clays, and A. Persoons. Highly unusual effects of π-conjugation extension on the molecular linear and quadratic nonlinear optical properties of ruthenium(II) ammine complexes). *Journal of the American Chemical Society*, 125(4):862–863, 2003. PMID: 12537472.

[62] B. J. Coe, J. A. Harris, K. Clays, A. Persoons, K. Wostyn, and B. S. Brunschwig. A comparison of the pentaammine(pyridyl)ruthenium(II) and 4-(dimethylamino)phenyl groups as electron donors for quadratic nonlinear optics. *Chem. Commun.*, pages 1548–1549, 2001.

[63] B. J. Coe, J. A. Harris, and B. S. Brunschwig. Determination of the molecular quadratic non-linear optical responses of V-shaped metallochromophores by using stark spectroscopy. *Dalton Trans.*, pages 2384–2386, 2003.

[64] B. J. Coe, J. A. Harris, L. A. Jones, B. S. Brunschwig, K. Song, K. Clays, J. Garín, J. Orduna, S. J. Coles, and M. B. Hursthouse. Syntheses and properties of two-dimensional charged nonlinear optical chromophores incorporating redox-switchable cis-tetraammineruthenium(II) centers. *Journal of the American Chemical Society*, 127(13):4845–4859, 2005. PMID: 15796549.

[65] B. J. Coe, S. Houbrechts, I. Asselberghs, and A. Persoons. Efficient, reversible redox-switching of molecular first hyperpolarizabilities in ruthenium(II) complexes possessing large quadratic optical nonlinearities. *Angewandte Chemie International Edition*, 38(3):366–369, 1999.

[66] L. Boubekeur-Lecaque, B. J. Coe, K. Clays, S. Foerier, T. Verbiest, and I. Asselberghs. Redox-switching of nonlinear optical behavior in LangmuirBlodgett thin films containing a Ruthenium(II) ammine complex. *Journal of the American Chemical Society*, 130(11):3286–3287, 2008.

[67] M. Malaun, Z. R. Reeves, R. L. Paul, J. C. Jeffery, J. A. McCleverty, M. D. Ward, Inge A., K. Clays, and A. Persoons. Reversible switching of the first hyperpolarisability of an nlo-active donor-acceptor molecule based on redox interconversion of the octamethylferrocene donor unit. *Chemical Communications*, pages 49–50, 2001.

[68] T. Weyland, I. Ledoux, S. Brasselet, J. Zyss, and C. Lapinte. Nonlinear optical properties of redox-active mono-, bi-, and trimetallic σ-acetylide complexes connected through a phenyl ring in the Cp*(dppe)Fe series. an example of electro-switchable nlo response. *Organometallics*, 19(24):5235–5237, 2000.

[69] F. Paul, K. Costuas, I. Ledoux, S. Deveau, J. Zyss, J. Halet, and C. Lapinte. Redox-switchable second-order molecular polarizabilities with electron-rich iron -aryl acetylides. *Organometallics*, 21(24):5229–5235, 2002.

[70] M. Samoc, N. Gauthier, M. P. Cifuentes, F. Paul, C. Lapinte, and M. G. Humphrey. Electrochemical switching of the cubic nonlinear optical properties of an aryldiethynyl-linked heterobimetallic complex between three distinct states. *Angewandte Chemie International Edition*, 45(44):7376–7379, 2006.

[71] N. Gauthier, G. Argouarch, F. Paul, L. Toupet, A. Ladjarafi, K. Costuas, J. Halet, M. Samoc, M. P. Cifuentes, T. C. Corkery, and M. G. Humphrey. Electron-rich iron/ruthenium arylalkynyl complexes for third-order nonlinear optics: Redox-switching between three states. *Chemistry – A European Journal*, 17(20):5561–5577, 2011.

[72] H. Le Bozec and V. Guerchais. Photochromic bipyridyl metal complexes: Photoregulation of the nonlinear optical and/or luminescent properties. *Comptes Rendus Chimie*, 16(12):1172 – 1182, 2013.

[73] M. Irie. Diarylethenes for memories and switches. *Chemical Reviews*, 100(5):1685–1716, 2000.

[74] K. J. Chen, A. D. Laurent, and Denis J. Strategies for designing diarylethenes as efficient nonlinear optical switches. *The Journal of Physical Chemistry C*, 118(8):4334–4345, 2014.

[75] G. Berkovic, V. Krongauz, and V. Weiss. Spiropyrans and spirooxazines for memories and switches. *Chemical Reviews*, 100(5):1741–1754, 2000.

[76] Y. Yokoyama. Fulgides for memories and switches. *Chemical Reviews*, 100(5):1717–1740, 2000.

[77] B. L. Feringa, R. A. van Delden, N. Koumura, and E. M. Geertsema. Chiroptical molecular switches. *Chemical Reviews*, 100(5):1789–1816, 2000.

[78] B. L. Feringa. *Molecular Switches*. Wiley-VCH Verlag GmbH, 2001.

[79] P. M. Beaujuge and J. R. Reynolds. Color control in π-conjugated organic polymers for use in electrochromic devices. *Chemical Reviews*, 110(1):268–320, 2010.

[80] F. Castet, V. Rodriguez, J. Pozzo, L. Ducasse, A. Plaquet, and B. Champagne. Design and characterization of molecular nonlinear optical switches. *Accounts of Chemical Research*, 46(11):2656–2665, 2013.

[81] V. Guerchais, L. Ordronneau, and H. Le Bozec. Recent developments in the field of metal complexes containing photochromic ligands: Modulation of linear and nonlinear optical properties. *Coordination Chemistry Reviews*, 254(21–22):2533 – 2545, 2010.

[82] L. Ordronneau, H. Nitadori, I. Ledoux, A. Singh, J. A. G. Williams, M. Akita, and H. Guerchais Le Bozec. Photochromic metal complexes: Photoregulation of both the nonlinear optical and luminescent properties. *Inorganic Chemistry*, 51(10):5627–5636, 2012.

[83] S. K. Hurst, M. G. Humphrey, J. P. Morrall, M. P. C., M. Samoc, B. Luther-Davies, G. A. Heath, and A. C. Willis. Organometallic complexes for nonlinear optics: Part 31. Cubic hyperpolarizabilities of ferrocenyl-linked gold and ruthenium complexes. *Journal of Organometallic Chemistry*, 670(1–2):56 – 65, 2003.

[84] L. Gobbi, P. Seiler, and F. Diederich. A novel three-way chromophoric molecular switch: ph and light controllable switching cycles. *Angewandte Chemie International Edition*, 38(5):674–678, 1999.

[85] K. Green, M. Cifuentes, T. Corkery, M. Samoc, and M. Humphrey. Switching the cubic nonlinear optical properties of an electro-, halo-, and photochromic ruthenium alkynyl complex across six states. *Angewandte Chemie International Edition*, 48(42):7867–7870, 2009.

[86] L. H. Thomas. The calculation of atomic fields. *Mathematical Proceedings of the Cambridge Philosophical Society*, 23:542–548, 1 1927.

[87] E. Fermi. Eine statistische methode zur bestimmung einiger eigenschaften des atoms und ihre anwendung auf die theorie des periodischen systems der elemente. *Zeitschrift für Physik*, 48(1-2):73–79, 1928.

[88] P. Hohenberg and W. Kohn. Inhomogeneous electron gas. *Physical Review B*, 136:B864–B871, Nov 1964.

[89] J. Perdew and S. Kurth. Density functionals for non-relativistic coulomb systems in the new century. In Carlos Fiolhais, Fernando Nogueira, and MiguelA.L. Marques, editors, *A Primer in Density Functional Theory*, volume 620 of *Lecture Notes in Physics*, pages 1–55. Springer Berlin Heidelberg, 2003.

[90] W. Koch and M.C. Holthausen. *A chemist's guide to density functional theory.* Wiley-VCH, 2000.

[91] M. J. Frisch, G. W. Trucks, H. B. Schlegel, G. E. Scuseria, M. A. Robb, J. R. Cheeseman, G. Scalmani, V. Barone, B. Mennucci, G. A. Petersson, H. Nakatsuji, M. Caricato, X. Li, H. P. Hratchian, A. F. Izmaylov, J. Bloino, G. Zheng, J. L. Sonnenberg, M. Hada, M. Ehara, K. Toyota, R. Fukuda, J. Hasegawa, M. Ishida, T. Nakajima, Y. Honda, O. Kitao, H. Nakai, T. Vreven, J. A. Montgomery, Jr., J. E. Peralta, F. Ogliaro, M. Bearpark, J. J. Heyd, E. Brothers, K. N. Kudin, V. N. Staroverov, R. Kobayashi, J. Normand, K. Raghavachari, A. Rendell, J. C. Burant, S. S. Iyengar, J. Tomasi, M. Cossi, N. Rega, J. M. Millam, M. Klene, J. E. Knox, J. B. Cross, V. Bakken, C. Adamo, J. Jaramillo, R. Gomperts, R. E. Stratmann, O. Yazyev, A. J. Austin, R. Cammi, C. Pomelli, J. W. Ochterski, R. L. Martin, K. Morokuma, V. G. Zakrzewski, G. A. Voth, P. Salvador, J. J. Dannenberg, S. Dapprich, A. D. Daniels, Ö. Farkas, J. B. Foresman, J. V. Ortiz, J. Cioslowski, and D. J. Fox. Gaussian 09 Revision C.01. Gaussian Inc. Wallingford CT 2009.

[92] S.J.A. van Gisbergen, J.G. Snijders, and E.J. Baerends. Implementation of time-dependent density functional response equations. *Computer Physics Communications*, 118(2–3):119 – 138, 1999.

[93] V. Monev. Density functional theory calculations of molecular hyperpolarizabilities. *Molecular Engineering*, 8(3):217–234, 1998.

[94] *Quantum Mechanical Methods for Predicting Nonlinear Optical Properties*, pages 241–279. John Wiley & Sons, Inc., 2007.

[95] H. Wu, A. Chaudhari, and S. Lee. Theoretical studies on nonlinear optical properties of formaldehyde oligomers by ab initio and density functional theory methods. *Journal of Computational Chemistry*, 26(15):1543–1564, 2005.

[96] G. J. B. Hurst, M. Dupuis, and E. Clementi. *Ab initio* analytic polarizability, first and second hyperpolarizabilities of large conjugated organic molecules: Applications to polyenes C_4H_6 to C_2H_24. *The Journal of Chemical Physics*, 89(1):385–395, 1988.

[97] B. Champagne, E. Botek, M.000 Nakano, T. Nitta, and K. Yamaguchi. Basis set and electron correlation effects on the polarizability and second hyperpolarizability of model open-shell π-conjugated systems. *The Journal of Chemical Physics*, 122(11):–, 2005.

[98] D. A. Dixon and N. Matsuzawa. Density functional study of the structures and nonlinear optical properties of urea. *The Journal of Physical Chemistry*, 98(15):3967–3977, 1994.

[99] P. R. T. Schipper, O. V. Gritsenko, S. J. A. van Gisbergen, and E. J. Baerends. Molecular calculations of excitation energies and (hyper)polarizabilities with a statistical average of orbital model exchange-correlation potentials. *The Journal of Chemical Physics*, 112(3):1344–1352, 2000.

[100] M. de Wergifosse and B. Champagne. Electron correlation effects on the first hyperpolarizability of *Push-Pull* π-conjugated systems. *The Journal of Chemical Physics*, 134(7):074113–074125, 2011.

[101] T. Yanai, D. P. Tew, and N. C. Handy. A new hybrid exchange–correlation functional using the coulomb-attenuating method (cam-b3lyp). *Chemical Physics Letters*, 393(1–3):51 – 57, 2004.

[102] C. Liu, X. Guan, and Z. Su. Computational study on redox-switchable 2D second-order nonlinear optical properties of pushpull mono-tetrathiafulvalene-bis(salicylaldiminato) zn(II) schiff base complexes. *The Journal of Physical Chemistry C*, 115(13):6024–6032, 2011.

[103] B. Kirtman, S. Bonness, A. Ramirez-Solis, B. Champagne, H. Matsumoto, and H. Sekino. Calculation of electric dipole (hyper)polarizabilities by long-range-correction scheme in density functional theory: A systematic assessment for polydiacetylene and polybutatriene oligomers. *The Journal of Chemical Physics*, 128(11):–, 2008.

[104] J. R. Hammond and K. Kowalski. Parallel computation of coupled-cluster hyperpolarizabilities. *The Journal of Chemical Physics*, 130(19):–, 2009.

[105] F. Castet and B. Champagne. Assessment of DFT Exchange–Correlation functionals for evaluating the multipolar contributions to the quadratic nonlinear optical responses of small reference molecules. *Journal of Chemical Theory and Computation*, 8(6):2044–2052, 2012.

[106] J. Tomasi, B. Mennucci, and R. Cammi. Quantum mechanical continuum solvation models. *Chemical Reviews*, 105(8):2999–3094, 2005.

[107] M. Cossi, V. Barone, R. Cammi, and J. Tomasi. *Ab initio* study of solvated molecules: a new implementation of the polarizable continuum model. *Chemical Physics Letters*, 255(4-6):327–335, 1996.

[108] G. Scalmani and M. J. Frisch. Continuous surface charge polarizable continuum models of solvation. I – general formalism. *The Journal of Chemical Physics*, 132(11):–, 2010.

[109] A. Willetts, J. E. Rice, D. M. Burland, and D. P. Shelton. Problems in the comparison of theoretical and experimental hyperpolarizabilities. *The Journal of Chemical Physics*, 97(10):7590–7599, 1992.

[110] M. G. Kuzyk, C. W. Dirk, and Inc NetLibrary. *Characterization Techniques And Tabulations For Organic Nonlinear Optical Materials*. Optical Engineering. Marcel Dekker, New York, 1998.

Chapter 2

Organometallic Compounds Containing Benzo[*c*]thiophene Derivatives

2.1 Introduction

Since the discovery in the late 1970's of metal-like conductivity by linear polyaromatic systems such as polyacetylene, polypyrrole and polythiophene, the research on functional π-conjugated systems has grown rapidly, enclosing many multidisciplinary fields such as organic, inorganic and organometallic chemistry, electrochemistry, photophysics and material sciences.[1,2] Later, in 1990, the work of Friend *et. al* revealed that polyaromatic compounds could be used as electroluminescent compounds, resulting in the burst of a new era for aromatic π-conjugated polymers and oligomers that found new applications in the fields of liquid crystals, nonlinear optics, electroluminescence and photochromic materials, among others.[3]

Thiophene-based materials (polythiophenes, oligothiophenes and fused thiophenes) and its derivatives are by far the most used compounds for such purposes.[4–6] There are two main reasons for this fact. First, thiophene chemistry is very well established, and probably alongside with benzene chemistry, is one of the most well developed - there are numerous methodologies for customize the core unit. These structural variations allow the fine tuning of the electronic and solid state properties, and hence it is possible to easily achieve stable materials and control their optical and electric properties. Secondly, it is the

presence of an highly polarizable sulphur heteroatom in the five membered aromatic ring of thiophene that gives these materials their interesting and still surprising properties. Hence, it is unquestionable why their synthetic versatility, unique aromaticity, relative chemical stability and polarizability constitute the key features made them so attractive for the scientific community.

In 1993 it was showed experimentally that the replacement of benzene rings with thiophene rings in donor-acceptor chromophores lead to significant enhances of the second-order nonlinear optical (SONLO) hyperpolarizability.[7] This work lead to a burst in thiophene-based materials for NLO applications and other optical applications, and a myriad of papers appeared since then. The synthesis, properties and optical applications have been subject of several reviews and books. For examples please see refs.[4–6,8–13]

Optimizing the NLO properties of thiophene-based and, in general, any other π-conjugated organic material relies on a fundamental understanding of the relationships between the chemical structure and the molecular optical nonlinearities. As previously mentioned in Section 1.3.4, the development of new, highly SONLO-active chromophores was initially based on the assumptions of the Two-level Model (TLM), that states that high NLO responses are obtained in end-capped chromophores with strong electron-donor and electron-accepting groups at both ends of a π-conjugated bridge.[14] In the case of thienyl-based π-conjugated bridges, several combinations of electron-donors/acceptors were tested so far. In addition to the usual organic end-groups, transition metal moieties have been also extensively studied in combination with thienyl chromophores in order to maximize their NLO properties. Several molecular geometries were developed.[15–23] In particular, mono(η^5-cyclopentadienyl)metal complexes bearing several thienyl chromophores showed that the combination of these organometallic fragments with thienyl based chromophores present very good nonlinear optical properties when couple with strong acceptor groups, like a nitro group (-NO_2).[24–31]

However, it is long known that the *push-pull* strategy is not always effective.[32] Other factors can directly affect the structural and electronic properties of the chromophores, such as the position of the substituent in the π-conjugated system, aromatic resonance energies, conjugation length, planarity and intermolecular interactions, making the fine tuning of the NLO properties very challenging for chemists. For example, it has been observed that the nonlinear optical response saturates as the π-conjugated bridge length is increased in *push-pull* systems like oligo(phenyleneethynylene) ruthenium complexes.

The reasons for this saturation remain unclear, but it is hypothesized that, once the critical length of the ligand is achieved, a breakdown in the interaction between the donor and the acceptor groups occurs.[24,33] Therefore, alternatives to the usual linear dipolar *push-pull* molecular geometries were developed. The use of ring-fused aromatic fragments are a different approach for the enhancement of the NLO properties of organic fragments. By combining the typical end-capped donor-acceptor architectures with the presence of pendant cyclic proto-aromatic groups, also known as pro-quinoidal groups, ring-fused systems allow to promote and conserve the charge separation that is usually achieved by the use of *push-pull* systems, without the need of explicit donor or acceptor groups. Additionally, when compared with "normal" thiophenes, ring-fused thiophenes exhibit an extended conjugation and a more rigid structure, hence improving its charge transfer processes and potentially enhancing their NLO activity. The strong quinoidal structure of ring-fused thiophenes has been recently proven.[34] These facts were the motivation for working with the fused-thiophene systems.

The scope of these chapter is limited to the benzo[*c*]thiophene family. For the synthesis of other ring-fused thiophene families, like benzo[b]thiophene or thienoacenes, several reviews can be consulted.[5,35–37] In the next sections, a short introduction to benzo[*c*]thiophene based compounds will be adressed, followed by the synthetic methodologies for obtaining the benzo[*c*]thiophene core. Its reactivity and main applications together with uses in organometallic chemistry will be discussed. Finally, the syntheses, characterization and NLO properties of a new family of iron(II) and ruthenium(II) complexes of general formula $[M(\eta^5\text{-}C_5H_5)(PP)(L)][PF_6]$ (M=Fe, PP=κ^2-dppe; M=Ru, PP=κ^2-dppe or $2Ph_3$: L = benzo[*c*]thiophene based ligand) will be made.

2.2 The Benzo[*c*]thiophene core

Ring-fused thiophenes are bicyclic or polycyclic aromatic compounds presenting, at least, one thiophene ring. Depending on the location and type of the fused ring on the thiophene core there can be several types of ring-fused thiophenes. **Figure 2.1** depicts some examples of their structures.

Benzo[*c*]thiophene, also called isothianaphtalene (ITN), is a bicyclic compound formed by a 1,3-cyclohexadiene system fused to the C3-C4 bond of a thiophene ring, resulting in competing aromaticity between the two rings. Depending on the substituents at the C1

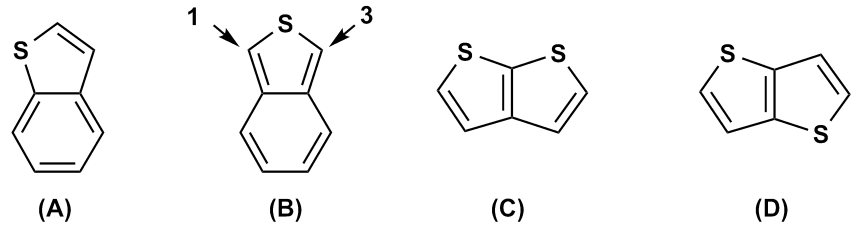

Figure 2.1: Structures of some fused-thiophene compounds

: (A) Benzo[*b*]thiophene; (B) Benzo[*c*]thiophene; (C) thieno[2,3-*b*]thiophene; (D) thieno[3,2-*b*]thiophene

and C3 positions, benzo[*c*]thiophene can be stabilized in either the aromatic or quinoidal form. These two forms are depicted in **Figure 2.2**. It was recently estimated that, in polymeric poly(ITN), the quinoidal form is 2.4 kcal/mol lower in energy than the aromatic form. This difference can be explained by the aromatic stabilization of the benzene ring vs. the thiophene ring (36 kcal/mol vs. 29 kcal/mol, respectively). In fact, benzo[*c*]thiophene is one of the polymers with lowest band gap nowadays, 1.0 eV.

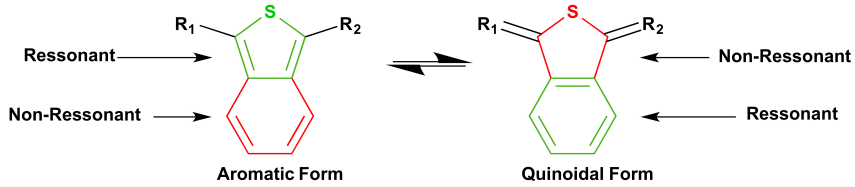

Figure 2.2: Aromatic and Quinoidal Structures of benzo[*c*]thiophene

The synthesis of benzo[*c*]thiophene skeleton was first reported by Mayer *et al.*[38] In the following years, this compound, and some of it's derivatives, were thoroughly studied by Cava *et. al*[39–41]. However, benzo[*c*]thiophene is only moderately stable in its unsubstituted form. The tendency of the fused ring to complete its aromaticity makes the C1 and C3 positions highly reactive towards, for example, Diels-Alder reactions, even at low temperatures. These reactions were already described in the first papers by Mayer and Cava.[38,39] Hence, in order to obtain fairly stable compounds, the majority of synthesized benzo[*c*]thiophenes are obtained in the 1,3-disubstituted form.

The synthesis of 1,3-dichloro-benzo[*c*]thiophene in a 60% yield, as well as the use of this compound to achieve other disubstituted derivatives, namely, the asymmetric

1-chloro-3-methoxycarbonyl (75% yield), dissilylated derivatives (85% yield) and the diformylated and dicyanovynilated derivatives (63% and 85%, respectively) has already been reported.[40] Attempts to synthesize 1,3-diiodo-benzo[*c*]thiophene starting from the disilylated compounds afforded only the dimer, trimer and tetramer of the initial starting material, showing the reactivity of the 1,3-dihalogenated-benzo[*c*]thiophenes towards oxidative polymerization.[41]

In order to increase the stability of the benzo[*c*]thiophene cores, the inclusion of aromatic substituents was studied by several groups.[42–45] The presence of these aromatic groups allowed a greater electronic delocalization that resulted in the enhancement of the stability of the compounds. Among these 1,3-diaryl-benzo[*c*]thiophenes, the thienyl-benzo[*c*]thiophene derivatives are the most studied.

2.2.1 1,3-Thienyl-benzo[*c*]thiophene Synthesis

The synthesis of 1,3-dithienyl-benzo[*c*]thiophene was reported by four independent groups. The first two methods appeared simultaneously and were proposed by Lorcy *et al.* and Bauerle *et al.*[42,43] **Scheme 2.1** depicts these methods. They were both based on a Friedel-Crafts acylation of thiophene, or a thiophene derivative, with phtalic anhydride in the presence of aluminium trichloride, affording acylated ortho-(2-thienoyl)benzoic acids. These compounds were then treated with a reducing agent, typically sodium borohydride, to give the cyclic lactone 3-thienyl-3H-isobenzofuran-1-one. In its turn, the lactone was reacted with a Grignard reagent (Bauerle's method) or a lithiated thiophene (Lorcy's method) to afford ortho-aryldiketones, the key intermediate for the obtention of benzo[*c*]thiophene skeleton. After cyclization with Lawesson's reagent, 1,3-dithienyl-benzo[*c*]thiophene was obtained. These methods presented a straightforward way for obtaining both symmetrical and unsymmetrical benzo[*c*]thiophenes, depending on the selected nucleophile in the second step.

Later, in 1993, Musmanni *et. al* proposed a slightly different method, in which benzene-1,2-dicarbaldehyde was treated with 2-thienylmagnesium bromide to give a diol intermediate.[44] This intermediate was then oxidized to the 1,2-di-(2-thenoyl)benzene with a CrO_3:H_2SO_4 mixture and finally cyclized with Lawesson's reagent to afford the desired compound in only 32% yield.

The major drawbacks of these three methods were their low yield and the formation on undesired products in moderate yields, such as 3,3-dithienylisobenzofuran-1(3H)-one.

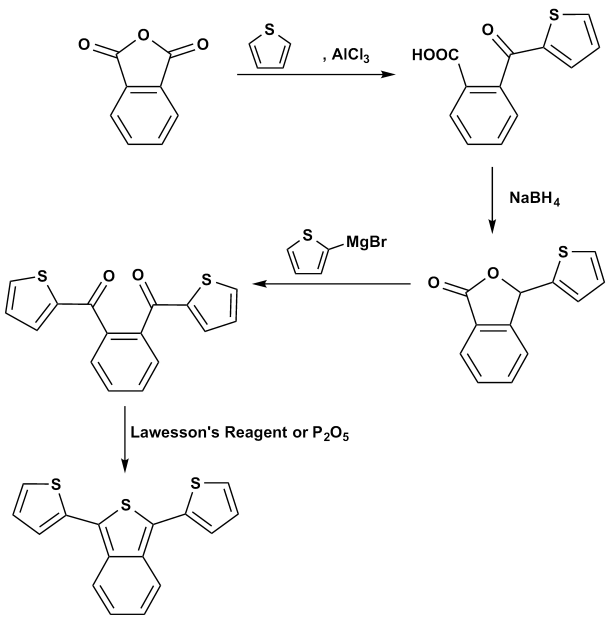

42,43

Scheme 2.1: Synthesis of 1,3-dithienylbenzo[*c*]thiophene by the methods of Lorcy *et al.* and Bauerle *et al.*

The synthesis of asymmetric thienyl-benzo[*c*]thiophenes has also been achieved by Mohanakrishnan *et al.*[46–53] Based on the methods by Lorcy and Bauerle, this author treated phthalic anhydride with several thiophene derivatives such as 2-bromothiophene and bithiophene in order to obtain the respective ortho-thienoyl-benzoic acids. Afterwards, the reduction of these benzoic acid derivatives provided the 3-thienyl-3H-isobenzofuran-1-ones, that were finally reacted with several arylmagnesium reagents, in a typical Grignard procedure, affording asymmetric diketones. Cyclization with Lawesson's reagent provided the asymmetric benzo[*c*]thiophene derivatives.

In 1997, Kiebooms *et. al* proposed an improvement to the methods of Lorcy and Musmanni.[45] He correctly identified that the bottleneck in the synthesis of 1,3-dithienylbenzo[*c*]-thiophene was the preparation of the precursor ortho-aryldiketone. He proposed the use of 2-mercaptopyridine in the initial modification of phthaloyl dichloride to afford S,S-di(pyridin-2-yl)benzene-1,2-bis(carbothioate). When treated with thienylmagnesium bromide, this compound afforded only the disubstituted 1,2-phenylenebis(thiophen-2-yl)methanone. After cyclization with Lawesson's reagent, the final product is obtained with high yield. The Kieboom's method is depicted in **Scheme 2.3**. Using this method,

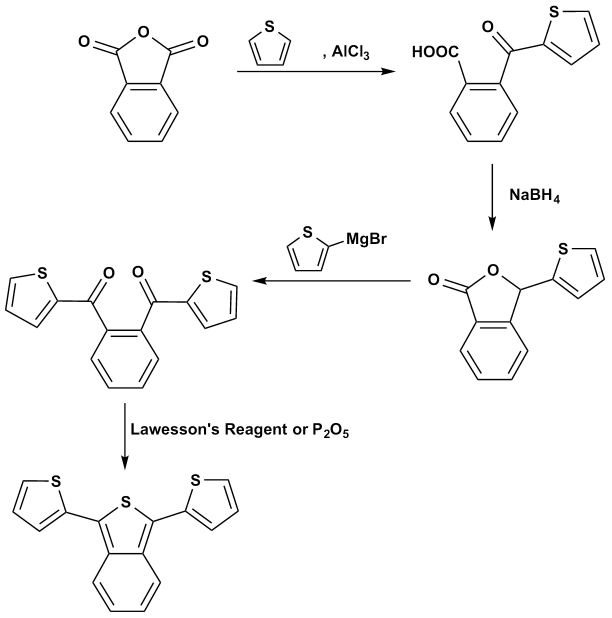

52

Scheme 2.2: Synthesis of 1,3-dithienylbenzo[*c*]thiophene by the method of Mohanakrishnan *et al.*

the synthesis of 5,6-disubstituted-1,3-dithienylbenzo[*c*]thiophenes starting from 4,5-dichlorophthalic acid was also reported.[54]

In a different approach, Meek *et. al* synthesized thienylbenzo[**c**]thiophenes via acid-mediated condensation of 2-carboxybenzaldehyde and substituted benzenes to give the initial cyclic lactone.[55] This intermediate was then reacted with a thienyllithium reagent to afford 1-aryl-3-thienylbenzo[*c*]furans, that could easily be transformed in benzo[*c*]thiophenes through treatment with Lawesson's reagent. This method is depicted in **Scheme 2.4**.

2.2.2 Organometallic Complexes Containing Benzo[*c*]Thiophene based Chromophores

As aforementioned in Section 2.1, oligothiophene-based materials are used in a wide range of applications, where their optimal electronic properties make them adequate for use in optoelectronics, molecular electronics and nonlinear optical applications. Concerning the later, work has been done in the development of not only purely organic thiophene-based chromophores, but also in new organometallic compounds containing a thiophene

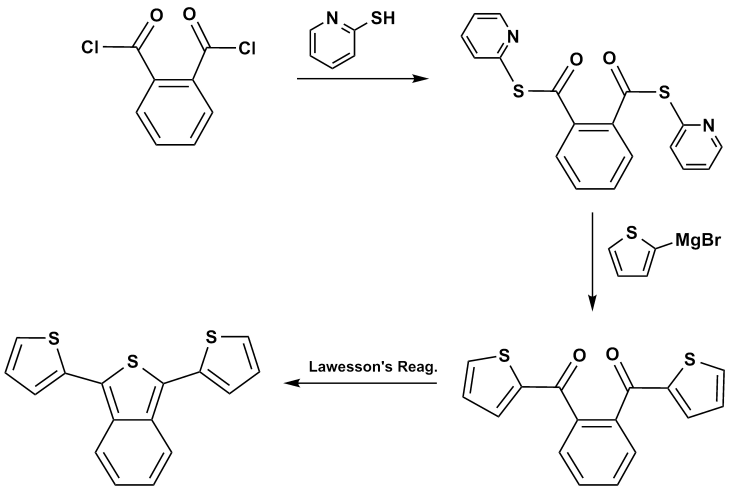

45

Scheme 2.3: Synthesis of 1,3-dithienylbenzo[*c*]thiophene by the method of Kiebooms *et al.*

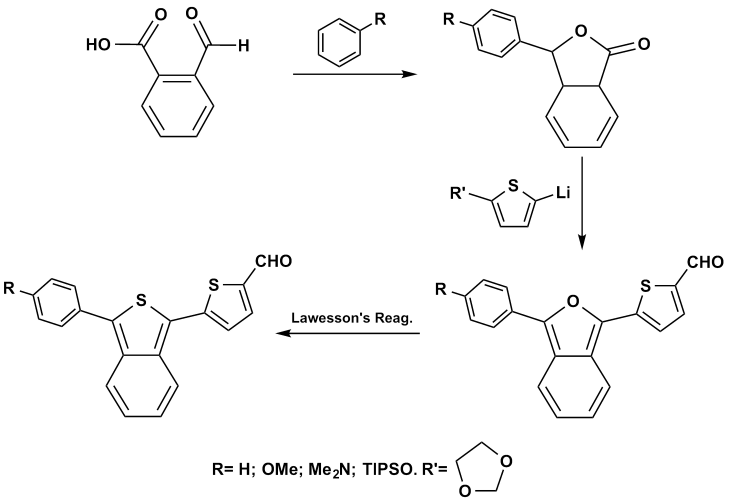

55

Scheme 2.4: Synthesis of 1-aryl-3-thienylbenzo[*c*]thiophenes by the method of Meek *et al.*

backbone which is linked directly to the metal center or through a linkage group. However, organometallic compounds containing benzo[*c*]thiophene or 1,3-diaryl-benzo[*c*]thiophenes are scarce.

The development of new mono- and biferrocenyl acetylides complexes with poly(3,4-ethylenedioxythiophene) (PEDOT) monomer has been reported.[56] The complexes presented reversible electrochemical behaviour and strong and intense absorption bands in their neutral and oxidized states, with maxima located around 450 and 1200 nm respectively. A similar bisferrocenyl complex with a benzo[*c*]thiophene unit linked directly to the cyclopentadienyl moiety of ferrocene has also been synthesized.[57] This complex also presented well-defined electrochemical reversibility. The synthesis and photovoltaic properties of a heteroleptic cis-di(isothiocyanato)(2,2'-dicarboxylic acid-2,2'-bipyridyl) ruthenium(II) complex containing two 1,3-dithienylbenzo[*c*]thiophene units was reported.[58] This complex presented very broad and intense absorption bands over almost the entire UV-Vis. region, along with an exceptional photovoltaic performance comparing to the other complexes presented in his work. Finally, derivatives of $[Fe_2(\eta^5\text{-}C_5H_5)_2(CO)_2(\mu\text{-}CO)(\mu\text{-}CCH_3)]^+$ containing dithienylbenzo[c]thiophene have been synthesized, and their nonlinear optical properties were obtained.[17] The ring-fused thiophene have shown to act as good donor end-groups but presented lower second-order hyperpolarizablity than its parent linear thienyl analogue.

It is then quite surprising that, to date, only the four aforementioned organometallic complexes containing benzo[*c*]thiophene units are found in the literature, specially taking into account the fact that they present good optical properties alongside electrochemical reversibility. This fact motivated the idea that benzo[*c*]thiophene would be good candidates for SONLO applications, specially if combined with the $(\eta^5\text{-}C_5H_5)$iron(II)/ruthenium (II) fragments, that already proven to be an adequate organometallic fragments for NLO applications. In fact, organometallic fragments with a different family of ring-fused thiophenes, namely hemi-helical thiophenes has already been reported.[28,29] The results suggested that, despite the low hyperpolarizabilities found, the good electrochemical properties of the complexes make them promising candidates for NLO-switching applications. In the next sections, the synthesis and full characterization of a new family of $(\eta^5\text{-}C_5H_5)$iron(II)/ruthenium(II) complexes is reported.

2.3 Results

2.3.1 Synthesis and Spectroscopic Studies of the Ligands

The reactivity of 1,3-dithienyl-benzo[*c*]thiophenes resembles the reactivity of other thiophene oligomers, such as terthiophene. The most active positions are the 2- and the 5'-positions, and hence electrophilic aromatic substitutions occur mainly at these positions. However, the presence of the fused aromatic ring increases drastically the 1,3-dithienyl-benzo[*c*]thiophene reactivity towards electrophiles, when compared with terthiophene. For this reason, when whenever is possible, the functionalization of the 1,3-dithienyl-benzo[*c*]thiophene skeleton should be done prior to cyclization. For this reason the methodology of Mohanakrishnan *et al.* was adopted as the initial strategy.[46,47]

The first attempts to synthesize 1,3-dithienyl-benzo[*c*]thiophene derivatives were made by reacting 2-bromothiophene, 2-thiophenecarbonitrile, 2-nitrothiophene and benzenecarbonitrile with phthalic anhydride, in dried dichloromethane (DCM), in the presence of aluminium trichloride at room temperature. **Scheme 2.5** summarizes these reactions.

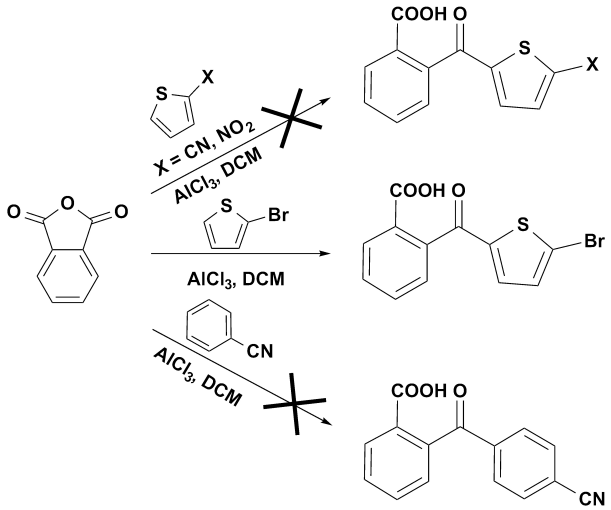

Scheme 2.5: Attempted Friedel-Crafts reaction for the synthesis of thienylbenzo[*c*]thiophenes.

It is well known that: i) Friedel-Crafts acylations require the use of, at least, stoichiometric amounts of the Lewis acid; ii) the nucleophile is usually an electron rich aromatic compound; iii) aromatic compounds substituted with electron-withdrawing groups tend

to be inert.[59] For these reasons, no reaction was obtained using 2-thiophene carbonitrile, 2-nitrothiophene and benzenecarbonitrile, since all of them possess mild or strong electron-withdrawing groups. 2-(5-bromo-2-thenoyl)benzoic acid was obtained as a very impure mixture and in moderate yield (56%). Several attempts to purify this compound (recrystallization and column chromatography) were unsuccessful. In order to improve both the yield and the pureness of the product, other reaction conditions were also tried, namely the reaction temperature and the addiction rate of the acylating agent. In the case of the first, the temperature of the reaction was lowered in the initial stage of the reaction to minimize the formation of secondary products. No significant improvements were achieved. Addition of aluminium trichloride in two portions of 1 mole equivalent each, instead of adding 2 mole equivalents at once, was also tried but again no improvement of the reaction yield was achieved. Nonetheless, the resulting impure fractions of 2-(5-Bromo-2-thienoyl)-benzoic acid were combined and used in the subsequent reduction reaction with $NaBH_4$. Several conditions were tested following the procedures by Lorcy, Bauerle and Mohanakrishnan.[42,43,46] Addition of 15 mole equivalents of $NaBH_4$ to a hot alkaline solution of NaOH or $NaHCO_3$ resulted in only traces of product due to the low solubility of the starting material. To improve this result, the reduction was tested in 1:1 mixture of ethanol and water, but still only traces of the lactone were obtained.

It is surprising that the direct synthesis of 2-(5-bromo-2-thienoyl)-benzoic acid was reported by Mohanakrishnan *et al.* with high yields (84%), and that no other electron-withdrawing substituted 2-thienoyl-benzoic acids were published using this author's methodology.[46] Furthermore, in his following papers, this author used a completely different methodology for obtaining asymmetric 1,3-diaryl-benzo[*c*]thiophenes bearing electron-withdrawing groups. This new methodology was based on the papers by Kato *et. al* and Jensen *et. al* for synthesis of lactones through metalation of 2-bromobenzoic acid using a combination of Bu_2Mg and n-BuLi under noncryogenic conditions. The lactones were then reacted in a subsequent Grignard reaction with a second arylmagnesium reagent to afford the asymmetric 1,3-diaryl-benzo[*c*]thiophenes.[60,61] Hence, for all the above stated reasons, the methodology was abandoned.

The method proposed by Kiebooms has shown to be a much more straightforward method for the obtention of the 1,3-dithienylbenzo[*c*]thiophene skeleton and was used by several other authors to obtain different derivatives of this compound.[54,57,62,63] These method was then used to synthesize the chromophore's core.

The initial reaction of phthaloyl dichloride with 2-mercaptopyridine afforded the S-(2-pyridinyl) thioester **(1)** in almost quantitative yields. This first step is crucial for the remaining steps, since it prevents the formation of the unwanted 3,3-dithienylisobenzofuran-1(3H)-one, which is observed in significant yields from the reaction of both Friedel-Craft-type and Grignard reactions between phthaloyl dichloride, phthalic anhydride or thiophthalic anhydride with thienyl nucleophiles. Compound **(2)** was then treated with freshly prepared thiophen-2-yl-magnesium bromide to afford 1,2-phenylenebis(thiophen-2-yl-methanone) **(3)** in very good yields. Finally cyclization of **(3)** with the Lawesson Reagent (LR) gave the desired 1,3-dithienyl-benzo[*c*]thiophene **(4)** in good yields. This compound was synthesized at a 3-gram scale and involved a single purification step.

The reactivity of **(3)** towards several functionalization reactions was tested, namelly nitration with Claycop, brominations with N-bromosuccinimide (NBS) and finally formylation by the Vielsmeyer-Haack reaction. To date, there are no reports of nitro compounds of 1,3-dithienyl-benzo[*c*]thiophene. Nitration with Claycop at low temperatures resulted in a complex mixture of compounds, which separation was not achievable. The complex mixture of reaction products is easily explain by the enhance reactivity of 1,3-dithienyl-benzo[*c*]thiophene towards highly active electrophiles, such as the nitronium cation, NO_2^+.

The synthesis of 1,3-bis(5-bromothiophen-2-yl)benzo[*c*]thiophene by reacting 1,3-dithienylbenzo[*c*]thiophene with NBS at bellow in DMF or a mixture of chloroform:acetic acid as solvent was recently published.[64,65] Attempts to reproduce the synthesis of monobrominated 1,3-dithienyl-benzo[*c*]thiophene were made according to this established procedure. Treatment of **(4)** with 1 mole equivalent of NBS in DMF, $CHCl_3$ or a mixture of chloroform:acetic acid at room temperature resulted in the formation of two main secondary products, alongside a significant amount of unreacted starting material. The crude mixture was chromatographed is a silica gel column using hexane as eluent but the difference in Rf did not allowed the complete separation of the main three components. Lowering the reaction temperature to bellow 0 °C resulted in longer reaction times, but no improvement of reaction result was obtained. Reaction of **(4)** with NBS in the presence of yellow mercury (II) oxide resulted in the appearing of a black solid which shown to be unable to further treatments. This product is probably due to oxidative polymerization of the starting material and was not characterized. The oxidative polymerization of benzo[*c*]thiophenes has already been observed for other derivatives.[66]

Finally, a typical Wielsmeyer-Haack procedure using DMF and phosphoryl chloride

($POCl_3$) was tested, and 1,3-di(thiophen-2-yl)benzo[*c*]thiophenecarboxaldehyde **(5)** was obtained in very good yield. Noteworthy, is the fact that only the monosubstituted compound was obtained, even when a great excess of the formylating agent was used (<2.5 mole equivalents).

Reaction of **(5)** with hydroxylammonium chloride in pyridine and dehydration with acetic anhydride afforded 5-(3-(thiophen-2-yl)benzo[c]thiophen-1-yl)thiophene-2-carbonitrile, **L1**, in good yield. Malononitrile is known to react with ring-fused heteroaromatic aldehydes affording dicyanovinylic compounds.[67] In this sense, the aldehyde **(5)** was thought as a good precursor for the synthesis unprecedent dicyanovinylic compound based in the 1,3-dithienyl-benzo[*c*]thiophene core. Hence, treatment of compound **(5)** with malononitrile in DCM with a catalytic amount of triethylamine afforded ligand **L2** in good yield. The syntheses of **L1** and **L2** is depicted on **Scheme 2.6**.

The new ligands were fully characterized by FT-IR, ^{1}H and ^{13}C-NMR and UV-Vis. spectroscopies.

The solid state FT-IR spectrum of **L1** showed the characteristic stretching vibration of the nitrile functional group at 2203 cm^{-1}. This value is in the same range of that found for parent 2,2':5',2"-terthiophene-5-carbonitrile (2216 cm^{-1}) or for typical *push-pull* 5"-nitro-2,2':5',2"-terthiophene-5-carbonitrile (2190 cm^{-1}).[24,68] The spectrum of **L2** presents two assymmetrical signals for the dicyanovynil group at 2201 cm^{-1} and 2212 cm^{-1}, being the latter of higher intensity. Although other dicyanovynil-benzo[*c*]thiophenes have already been reported by Meek *et. al* and Mohanakrishnan *et al.*, no information about the FT-IR of the compounds is found in the literature.[46,55] However, other parent thienyl-based compounds possessing the dicyanovynil functional group were reported, allowing to conclude that the stretching modes of **L2** are again in the typical range for dicyanovynil substituted oligothiophenes.[69]

The detailed NMR data for both ligands are given in Section 2.6. The obtained ^{1}H-NMR spectra for the ligands and respective atom numbering are showed in **Figure 2.3**.

The ^{1}H-NMR of spectrum of **L1** revealed the typical doublets for the disubstituted T1 ring, with proton H3 appearing downfielded relatively to proton H4 due to the proximity of the electron acceptor group. The usual signals for monosubstituted thiophene ring (T3) are also present, that is, two doublet of doublets assigned to protons H15 and H17 and third doublet of doublets for H16. The fused-benzene ring (B) presents the typical signals for this structure, *i. e.*, two doublets assigned to H8 and H11 and two superimposed

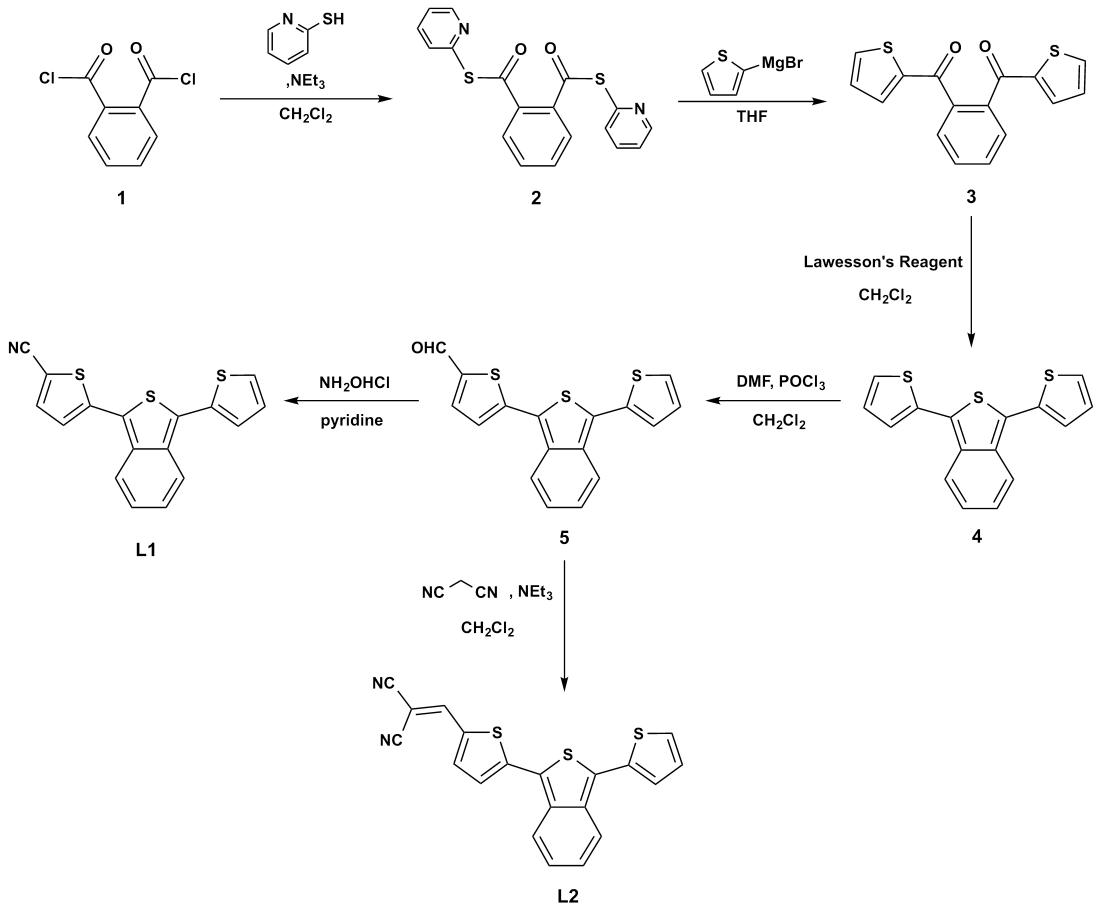

Scheme 2.6: Reaction scheme for the synthesis of **L1** and **L2**

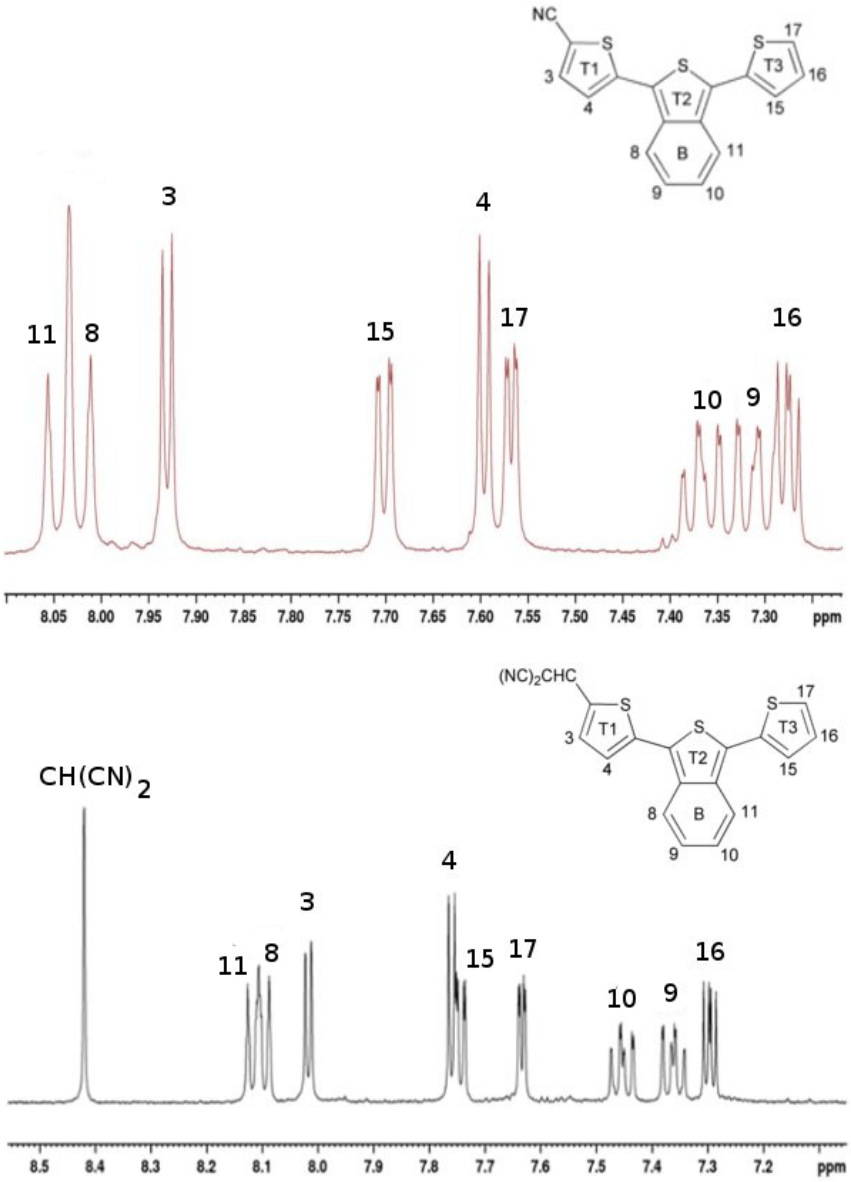

Figure 2.3: ^{1}H-RMN spectra for **L1** and **L2**

triplets of doublets at 7.30 and 7.37 ppm assigned to H9 and H10, respectively. Concerning ring B, it is noteworthy the fact that protons H8 and H11 appear downfielded when compared with other alkyl or halogenated disubstituted benzo[*c*]thiophenes. For example, in 1,3-dichloro-benzo[*c*]thiophene and other related derivatives, the H8 and H11 protons present a resonance bellow 7.50 ppm.[40] Hence, it is hypothesized that this deshielding

effect arises from two causes: first, the ring current anisotropy effect from the heteroaryl T1 and T3 rings; secondly, the spacial proximity of the electronegative sulphur atom, that seems originate weak hydrogen bonding. These two interactions are depicted in **Figure 2.4**.

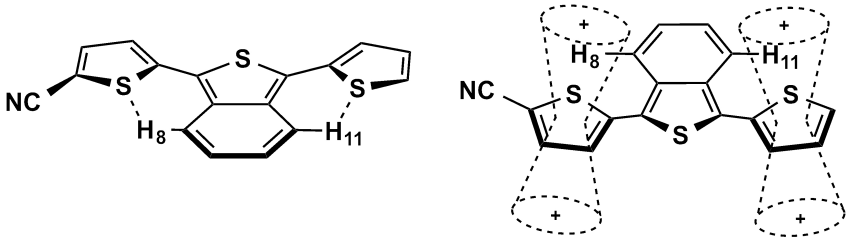

Figure 2.4: Hypothisized interactions occouring in the benzo[*c*]thiophene ligands

The current anisotropy effect is also present for other 1,3-diaryl-benzo[*c*]thiophenes, for which the H8 and H11 protons appear in the same range for the present ligands. The weak hydrogen bonding effect was tested by measuring the ^{1}H-NMR of **L1** in deuterated chloroform. The results show that the signals for the two protons (H8 and H11) appear deshielded by *ca.* 0.1 ppm in this solvent. Hence, it is hypothesized that the acidic proton of chloroform can interact with the sulphur atoms of the T1 and T3 rings, cancelling the weak hydrogen interaction of this electronegative atom with the H8 and H11 protons and resulting, therefore, in the upfielded observed shift.

Comparatively to **L1**, the ^{1}H-NMR spectrum of **L2** is characterized by an additional deshielded sharp singlet characteristic of the dicyanovynil functional group. The relative pattern of the benzo[*c*]thiophene skeleton is slightly changed when compared to **L1** ligand, in particular the signals for H9 and H10 that now appear as two perfectly distinct triplet of doublets. The overall deshielding in the ^{1}H-NMR of **L2** in comparison with **L1** is consistent with the change in the electronic behaviour of the functional group, from a moderate electron acceptor group (N≡C) to a strong acceptor C=C(CN)$_2$ group.

The ^{13}C-NMR spectrum of **L1** revealed the typical signals for the aromatic skeleton as well as for the nitrile functional group at a resonance of 114 ppm. This value is in the same range found for parent terthiophene compounds.[24,68] For **L2** the carbon spectra show a signal at 115.44 ppm corresponding to both the (N≡C) groups, along with two signals at 75.54 and 135.10 corresponding to the vynilidene carbons of the dicyanovynil group. In accordance with the ^{1}H-NMR spectra, **L2** presents a dishielding for all the

Table 2.1: Uv-Vis absorption maxima for the ligands

λ /nm($\epsilon \times 10^4$(mol^{-1}cm^{-1}))		
Compound	Chloroform	DMF
L1	452 (2.1)	443 (1.9)
L2	563 (4.1)	567 (3.7)

carbons due to the presence of a stronger electron acceptor group.

The UV-Vis. spectra of both **L1** and **L2** are characterized by two absorption bands: one in the UV region and a second strong and broad absorption band in the visible region. Since it is the lowest energy band that might be correlated with the NLO properties of the chromophores, the following discussion will be based solely on this band. The lowest-energy band of **L1** is within the range of that found for benzo[**c**]thiophene derivatives, whereas the lowest energy band of **L2** is strongly red shifted by *c.a.* 100 nm compared to **L1**.[50,70] This fact can be justified by a strong stabilization of the LUMO orbital of this compound due to the presence of a stronger acceptor group. According to DFT calculations performed on ligand **L1** both bands were assigned to $\pi - \pi^\star$ electronic transitions (*vide infra*).

The solvatochromic behaviour of both ligands was tested in chloroform and DMF and are summarized in **Table 2.1**.

The solvatochromic behaviour of the lowest energy band of ligand **L1** is characterized by a blue shift of the maximum of absorption accompanied by an hypochromic shift of the intensity. The negative solvathocromism behaviour for **L1** is attributed to a stabilization of the HOMO orbital accompanied by a destabilization of the LUMO with the increasing polarity of the solvent. Conversely, **L2** presents the opposite behaviour, that is, a slight positive solvatochromism effect, attributed mainly to the stabilization of the LUMO orbital due to the presence of the dicyanovynil electron acceptor.

2.3.2 Electrochemical studies on the Ligands

In order to evaluate the electronic richness and the reversibility of the oxidation/reduction processes, the redox behaviour of the ligands was studied by cyclic voltammetry in dichloromethane and acetonitrile, between the limits imposed by the solvents. The elec-

trochemical behaviour of **L1** is depicted in **Figure 2.5** as an example of the typical behaviour of these ligands. The electrochemical data of both ligands is summarized in **Table 2.2**.

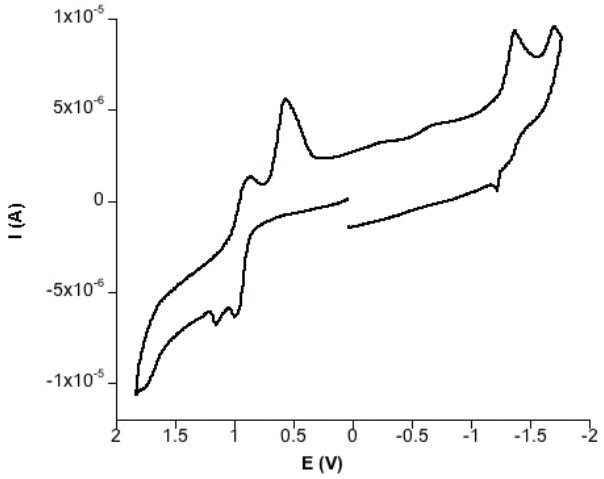

Figure 2.5: Cyclic Voltammetry of ligand **L1** in acetonitrile (200mV/s)

The electrochemistry of the ligand **L1** is characterized by an irreversible oxidative process and two reductive processes at negative potentials in dichloromethane, and by two irreversible oxidative processes and two reductive processes in acetonitrile. The reductive processes are irreversible in dichloromethane but the first one becomes quasi-reversible in acetonitrile ($E_{1/2}$=-1.36V). The oxidative waves are attributed to one-electron oxidations on the thiophene moieties, affording the radical and cationic species, $\mathbf{L1}^{+\bullet}$ and $\mathbf{L1}^{+}$ respectively. The presence of the radical species in solution results in the polymerization of the ligand, as shown by the high intensity cathodic counterpart of first oxidative process, also indicating that the polymer is conductive. The polymerization of 1,3-dithienylbenzo[c] thiophene derivatives is a very well known phenomenon and it is well reported by several authors.[42,44] The presence of the electrogenerated polymer was also confirmed by a deposition of a dark purple film at the electrode surface.

Considering the reduction processes of ligand **L1**, the first reduction wave affords the radical $L1^{-\bullet}$. The lack of the anodic counterpart indicates that these species are rather unstable in solution, and decompose prior to re-oxidation. A similar electrochemical behaviour was found for other nitrile substituted oligothiophenes.[24,28,71] However, the

Table 2.2: Cyclic Voltammetry data for ligands **L1** and **L2**

Comp.	Solvent	Ep_a (V)	Ep_c (V)	$E_{1/2}$ (V)	ΔE (mV)	$\frac{ipc}{ipa}$
L1	**DCM**	1.00	-	-	-	-
		-	-1.38	-	-	-
		-	-1.58	-	-	-
	ACN	1.13	-	-	-	-
		0.98	0.89	0.94	90	0.4
		-1.32	-1.39	-1.36	70	0.8
		-	-1.71	-	-	-
L2	**DCM**	1.81	-	-	-	-
		0.97	0.79	0.88	180	-
		-	-1.03	-	-	-
	ACN	2.03	-	-	-	-
		1.86	-	-	-	-
		1.10	1.01	1.08	90	-
		-0.65	-0.68	-0.72	-	-

synthesized ligands present lower redox potentials than the published derivatives due to their electron-donating inductive effect of the fused cyclohexene.[41,50,64]

The electrochemical behaviour of **L2** is characterized by two oxidative processes and one reductive process in dichloromethane, and by three oxidative processes and one reductive process in acetonitrile. All processes are irreversible. The first oxidative process occurs at $E_{1/2}$=0.88 V in dichloromethane and $E_{1/2}$=1.08 V in acetonitrile, whereas the second oxidative process occurs at Epa=1.81 V in dichloromethane and Epa=1.86 V in acetonitrile. The reductive process, in its turn, occur at Epc=-1.03 V in dichloromethane and $E_{1/2}$=-0.72 V in acetonitrile. This reduction process is facilitated by the presence of the dicyanovynil functional group, that stabilizes the radical anion of **L2**. As expected, the reductive process is found at lower potentials (*ca.* 150mV) when compared to the first reduction process of **L1** due to the better electron acceptor properties of dicyanovynil group. Noteworthy is also the fact that, compared to the behaviour found for **L1**,**L2** does not electropolymerize at the electrode surface.

2.3.3 Synthesis and Spectroscopic Studies of the Complexes

Complexes of general formula [M(η^5-C_5H_5)(PP)(L1)][PF_6] (PP = κ^2-dppe, 2 PPh_3 when M = Ru and PP = κ^2-dppe when M = Fe) were prepared by halide abstraction with $TlPF_6$ starting from the neutral complexes [M(η^5-C_5H_5)(PP)X] (M=Fe(II), X=I; M=Ru(II), X=Cl), in dichloromethane at room temperature, in the presence of an adequate excess of the corresponding ligand. In a similar fashion, attempts to prepare complexes of general formula [M(η^5-C_5H_5)(PP)(L2)][PF_6] (PP = κ^2-dppe, 2 PPh_3 when M = Ru and PP = κ^2-dppe when M = Fe) were made. However, no complexes bearing ligand **L2** were obtained, despite the several attempts made. For example, using refluxing dichloromethane or DMF at 80 °C resulted in complex mixture of products that were inseparable by recrystallization techniques. Attempts to separate the products by column chromatography resulted also in complete degradation of the product mixtures.

The new compounds are fairly stable towards oxidation in air and to moisture both in the solid state and in solution and were characterized by analytical data, FTIR and ^{1}H, ^{13}C and ^{31}P NMR spectroscopies.

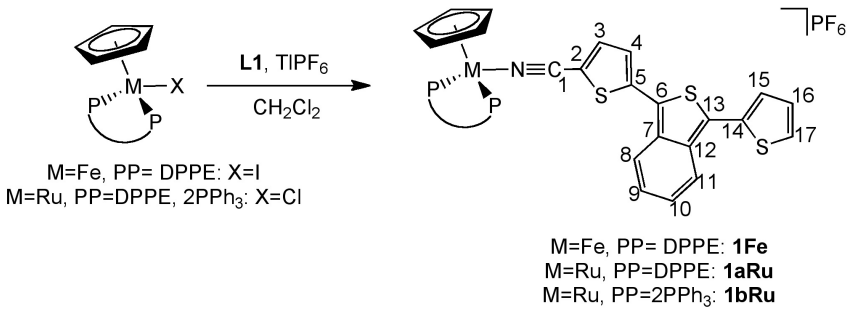

Scheme 2.7: Reaction scheme for the synthesis of benzo[*c*]thiophene Fe/Ru derived complexes and numbering scheme for NMR spectral assignments.

The analysis of FTIR spectra of organometallic compounds provides a essential tool for analysing the coordination modes of new ligands to the metal center, as well as their influence in its electronic properties. Typical FTIR bands confirm the presence of the cyclopentadienyl coligand (ca. 3000 - 3100 cm^{-1}) and the PF_6^- counter anion (838 cm^{-1} and 557 cm^{-1}). The coordinated nitrile ligand appears as a medium intensity band in the 2196-2213 cm^{-1} range for all the complexes. Comparison of (N≡C) stretching frequency upon coordination of the ligand reveals a negative shift of -7 cm^{-1} for **1Fe**

and a positive shift of +8 and +10 cm^{-1} for **1aRu** and **1bRu**, respectively. In the case of the present compounds, the nitrile functional group is coordinated in a linear fashion to the iron (II) or ruthenium (II) metal centres. The bonding of the nitrile group can be explained by a synergetic effect resulted from: σ-donation from the ligand to the metal and π-backdonation from the metal to the ligand. The σ-donation consists in the donation of the lone pair of the nitrogen orbital to vacant metal orbital. The π-backdonation, in its turn, results from the overlap between the filled metal orbitals with the low lying π-antibonding orbitals of the nitrile group. The balance between these two effects results in the increasing or decreasing of the stretching frequency of the nitrile group, and is well established that high π-backdonations lead to a negative shift in the stretching modes of linearly coordinated ligands, such as nitriles, acetylides or even CO. The negative or positive shifts observed for the complexes are therefore related with the magnitude of the σdonation/ π-backdonation effects. The magnitude of this π-backdonation interaction is expected to be higher for the iron(II) complex considering the better π-donor ability of the Iron(II) moiety. The benzo[*c*]thiophene derivatives seems to have a more effective π-backdonation interaction compared to the ones possessing terthiophene units with an acceptor nitro end group on related oligothiophene iron(II) and ruthenium(II) complexes.[24,27] Moreover, a less effective π-backdonation interaction was found in comparison with parent 1,2-di-(2-thienyl)-ethene iron(II) and ruthenium(II) complexes which possesses one vinylidene unit between the two thiophene rings.[29]

The detailed NMR data for all the complexes are given in experimental section. **Figure 2.6** shows the ^{1}H NMR spectra for **L1**, **1Fe** and **1aRu**, whereas **Table 2.3** show the relevant data for the ligand and for the three synthesized complexes.

The ^{1}H NMR resonances for the singlet of the η^5-C_5H_5 (Cp) ring are in the range usually observed for other oligothiophene monocationic Fe(II) and Ru(II) complexes and also for 1,2-di-(2-thienyl)-etheneiron(II) and ruthenium(II) related complexes.[24,27,72] The Cp signal depends on the metal centre and, for the Ru (II) complexes, the phosphane co-ligand. The effect of coordination on the nitrile ligand is mainly observed on T1 ring (protons H3 and H4) and B ring (protons H8 to H11). In the case of H3 and H4, the resonances shift upfield upon coordination to the organometallic moieties, as a result of the π-backdonation from the metal. The higher shielding effect observed for **1Fe** is consistent with a higher degree of π-backdonation for this compound, in accordance with the FTIR data. Comparing the two ruthenium complexes, a higher degree of π-

Table 2.3: Selected ^{1}H-NMR data for the ligand and the complexes

	^{1}**H RMN** δ /ppm [a]									
Comp.	$\mathbf{H}_{Cp}$	$\mathbf{H}_3$	$\mathbf{H}_4$	$\mathbf{H}_8$	$\mathbf{H}_9$	$\mathbf{H}_{10}$	$\mathbf{H}_{11}$	$\mathbf{H}_{15}$	$\mathbf{H}_{16}$	$\mathbf{H}_{17}$
L1		7.94	7.60	8.02	7.30	7.37	8.05	7.71	7.27	7.56
1Fe	4.71	6.88 (-1.06)	7.30 (-0.30)	7.81 (-0.24)	7.42 (0.12)	7.33 (-0.04)	8.04 (0.02)	7.72 (0.01)	7.28 (0.01)	7.55 (-0.01)
1aRu	5.06	6.93 (-1.01)	7.32 (-0.28)	7.82 (-0.20)	7.43 (0.13)	7.33 (-0.04)	8.05 (0.00)	7.73 (0.02)	7.28 (0.01)	7.55 (-0.01)
1bRu	4.79	7.56 (-0.27)	7.67 (-0.04)	7.94 (-0.08)	7.44 (0.14)	7.35 (-0.02)	8.07 (0.02)	7.73 (0.02)	7.20 (-0.07)	7.59 (0.03)

[a] in parenthesis the difference between the coordinated and the free ligand resonances $\delta_{(coord)} - \delta_{(free)}$

backdonation is observed for **1aRu** due to the presence of the better κ^2-dppe σ-donor. In the case of H8-H11 protons, the coordination to the metal centre suggests a change in the electronic properties of the B ring. It is observed that proton H8 is slightly shielded upon coordination, whereas proton H9 present a deshielding effect. In the case of protons H10 and H11 only a minor effect is observe but the general trend is a shielding of proton H10 and a deshielding effect on proton H11. The behaviour of proton H8 and H11 can be justified by the π-backdonation from the metal centre. Also, the stronger shielding of H8, compared with the magnitude of the deshielding of proton H9 for example, can be also attributed to some effect of the anisotropic ring currents from the phosphane co-ligand, due to their proximity. Thus, in conclusion, it appears clear that the π-backdonation effect is extended to the H8 and H9 protons of the B ring. Comparatively to the free ligand signals , the protons resonances on T3 ring (H15-H17) remain almost unchanged for all complexes.

In **Table 3.6** are showed the selected ^{13}C RMN data for both the ligand and the complexes. In general, the ^{13}C signals are more sensible to the presence of the metal center than the ^{1}H RMN signals. The major changes on the carbon resonances upon coordination were observed in the nitrile group (C1), the T1 ring and in the B ring, in agreement with the trend observed in ^{1}H RMN spectra. A significant deshielding effect on the C1 carbon of the ligand was observed upon coordination due to the σ-coordination through this functional group. Not surprisingly, the carbons of the B ring (C7-C12) present some deviation to the free ligand signals, suggesting a change in the

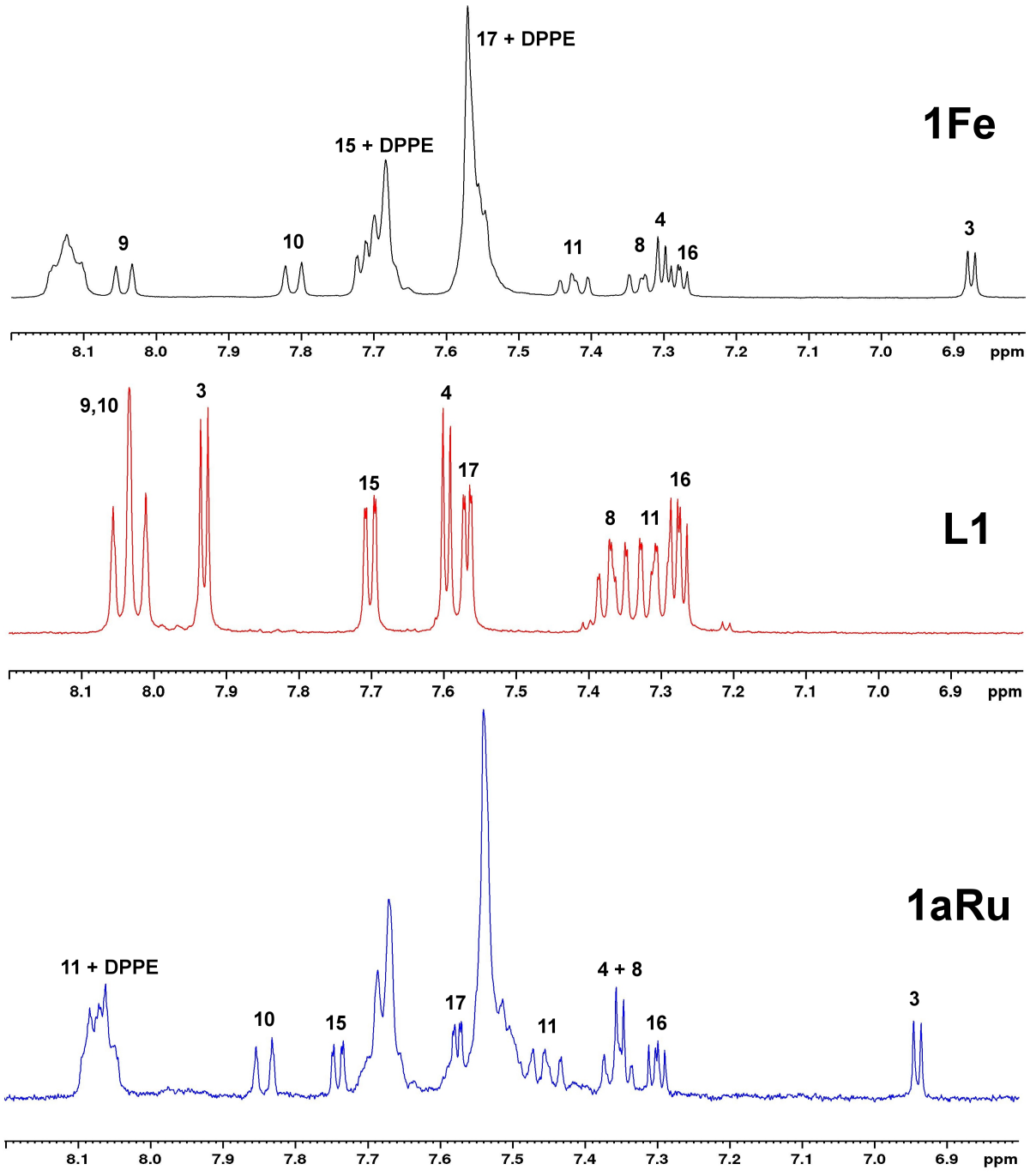

Figure 2.6: ^{1}H-RMN spectra for **1Fe**, **L1** and **1aRu**

Table 2.4: Selected ^{13}C-NMR data for the ligand and the complexes

	^{13}**C RMN** δ /ppm [a]							
Comp.	$\mathbf{C_1}$	$\mathbf{C_2}$	$\mathbf{C_3}$	$\mathbf{C_4}$	$\mathbf{C_5}$	$\mathbf{C_6}$	$\mathbf{C_7}$	$\mathbf{C_8}$
L1	114.56	108.09	139.93	126.33	143.34	123.86	136.09	121.76
1Fe	128.37	108.32	139.82	125.39	143.49	123.78	136.08	121.57
	(13.81)	(0.23)	(-0.11)	(-0.94)	(0.15)	(-0.08)	(-0.01)	(-0.19)
1aRu	121.60	107.14	141.08	125.49	144.77	123.63	136.01	121.53
	(7.04)	(-0.95)	(1.15)	(-0.84)	(1.43)	(-0.23)	(-0.08)	(-0.23)
1bRu	125.70	107.48	141.11	126.01	144.08	123.70	136.14	121.64
	(11.14)	(-0.61)	(1.18)	(-0.32)	(0.74)	(-0.16)	(0.05)	(-0.12)

[a] in parenthesis the difference between the coordinated and the free ligand resonances $\delta_{(coord)} - \delta_{(free)}$

electronic features of this ring. The same behaviour was already found in the ^{1}H NMR of the complexes. The deviation are particularly noticeable for carbons C9-C13, where an alternate behaviour is found on every other carbon. In particular, C10 and C11 present deviation of 5.27 to 5.48 ppm and -3.56 to -4.89 ppm, respectively. The fact that carbon C8 is not strongly affected corroborate the hypothesis that ring current effects from the phosphane co-ligand affected H8. The behaviour of the resonance of these carbons can be justified by an increase of the aromatic character of the B ring motivated by the π-backdonation from the organometallic fragments. In fact, both FTIR and NMR spectroscopies suggest a contribution of the quinoidal form of the ligand, especially for **1Fe**.

The ground-state quinoidal character of poly(ITN) was already investigated in model non-aromatic and quinoidal (aromatic) benzo[*c*]thiophene model compounds by means of NMR spectroscopy.[73] Results showed that the chemical shifts of the quinoidal forms are higher by 2-4 ppm than the non-aromatic compounds, in good accordance with the resonances of poly(benzo[*c*]thiophene) that is known for having a strong quinoidal character. Hence, for the synthesized compounds, the differences observed for C7-C12 allows to state that the coordination of ligand **L1** to good organometallic electron donors, such as the $[M(\eta^5\text{-}C_5H_5)(\kappa^2\text{-dppe})]^+$ (M=Fe, Ru) fragments seems to enhance the degree of aromaticity in the fused benzene ring of the benzo[*c*]thiophene moiety.

^{31}P-NMR data showed the typical singlet signal for the phosphane co-ligands revealing an expected deshielding upon coordination, according to the σ-donor character of these

Table 2.4: Selected ^{13}C-NMR data for the ligand and the complexes (cont.)

Comp.	^{13}C RMN δ /ppm [a]								
	C_9	C_{10}	C_{11}	C_{12}	C_{13}	C_{14}	C_{15}	C_{16}	C_{17}
L1	127.74	122.63	126.46	137.13	130.57	135.10	127.66	129.35	128.08
1Fe	126.53	127.90	122.84	137.04	131.06	134.94	128.32	129.44	127.93
	(-1.21)	(5.27)	(-4.89)	(-0.09)	(0.49)	(-0.16)	(0.66)	(0.09)	(-0.25)
1aRu	126.54	128.00	122.85	137.12	132.30	134.89	127.95	129.52	128.37
	(-1.20)	(5.37)	(-3.61)	(-0.01)	(1.73)	(-0.21)	(0.29)	(0.17)	(0.29)
1bRu	126.59	128.11	122.90	137.28	131.50	134.92	127.99	131.12	127.01
	(-1.15)	(5.48)	(-3.56)	(0.15)	(0.93)	(-0.18)	(0.33)	(1.77)	(-1.07)

[a] in parenthesis the difference between the coordinated and the free ligand resonances $\delta_{(coord)} - \delta_{(free)}$

ligands.

The optical absorption spectra of all complexes were recorded using 1.0×10^{-5}M solutions in chloroform, acetone and DMF. **Figure 2.7** shows the typical behaviour of the synthesized complexes in chloroform and **Table 2.5** shows the optical data in the three solvents.

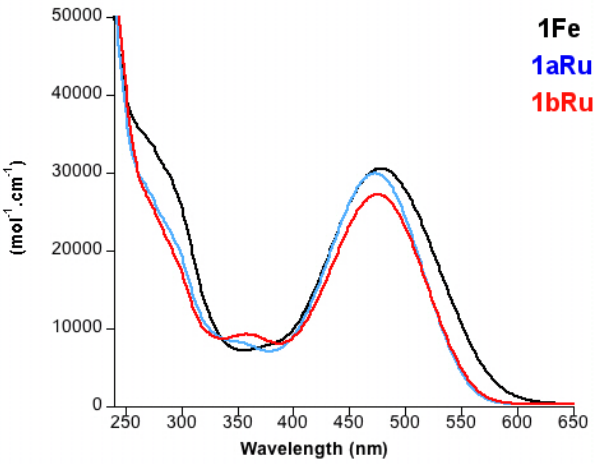

Figure 2.7: UV-Vis. spectra of 1.0×10^{-5}M chloroform solutions of **1Fe**, **1aRu** and **1bRu**

Table 2.5: Solvatochromic behaviour of 1.0×10^{-5}M solutions of **1Fe**, **1aRu** and **1bRu**

	λ /nm ($\epsilon\times10^4$(mol^{-1}cm^{-1}))		
Compound	Chloroform	Acetone	DMF
1Fe	478 (3.0)	457 (2.1)	464 (2.0)
1aRu	473 (3.0)	468 (2.2)	473 (1.8)
1bRu	475 (2.7)	448 (1.7)	452 (1.4)

The electronic spectra of the complexes are characterized by high energetic bands in the range of 280-290 nm, alongside with intense low energy bands in the range of 452 to 478 nm. The maxima of the low energy absorption bands depend on the organometallic fragment and resembles the free ligand band, both in shape and intensity, leading to the assumption that it has strong intraligand charge transfer (ILCT) character. As it will be shown later in Section 2.4.1, the DFT calculations on the Fe(II) and Ru(II) complexes, will in fact support this attribution.

When compared to the free ligand, the low-energy band of the complexes appear red-shifted by 21 to 26 nm depending on the metal centre. This fact is consistent with the increasing length of the π-conjugated system. Also, the biggest shift observed for the Fe (II) complex is consistent with the higher π-backdonation for this complex. Comparison with similar Fe (II) and Ru (II) thiophene nitrile complexes presenting a nitro acceptor group show that the present complexes present lower energy transitions by at least *ca.* 30 nm, thus favouring their NLO properties, according to the TLM.[25,27,72]

The solvatochromic behaviour of the complexes was studied in chloroform, acetone and DMF. Results show a similar behaviour found for the free ligand, that is, a blue shift is observed with the increasing of solvent polarity. The shift is more prominent for **1Fe** and **1bRu**, specially when going from chloroform to acetone, where differences of -21 and -27 nm are observed, respectively. The slight increasing of the λ_{max} going from acetone to DMF can be negectable for all cases. The negative solvatochromism of the complexes is then correlated with a decrease of the dipole moment of the compound upon excitation. This type of solvatochromism was also observed for the ligand and in parent Fe(II) and Ru(II) complexes with thienyl nitrile ligands, as well as in ferrocenylethenyl-thienyl-2-

thienylbenzo[c]thiophene.[17]

2.3.4 Electrochemical studies on the Complexes

The study on the reversibility of the redox processes of organometallic complexes gives an insight about the stability of the oxidized and/or reduced species, and its study is of major importance when dealing with the NLO redox-switching ability of these organometallic compounds. In fact, to be used as molecular switches both on and off forms must be stable and the switching process must be reversible. Thus, electrochemical studies are helpful for the screening of molecules able to be used as potential molecular switches. The redox behaviour of the compounds was studied by cyclic voltammetry in dichloromethane and acetonitrile, between the limits imposed by the solvents, to evaluate the electron richness at the active redox centres and the reversibility of the oxidation/reduction processes. As an example, the electrochemical response for **1Fe** in dichloromethane is shown in **Figure 2.8**, and the most relevant data exhibited by all the complexes in dichloromethane and acetonitrile are summarized in **Table 2.6**.

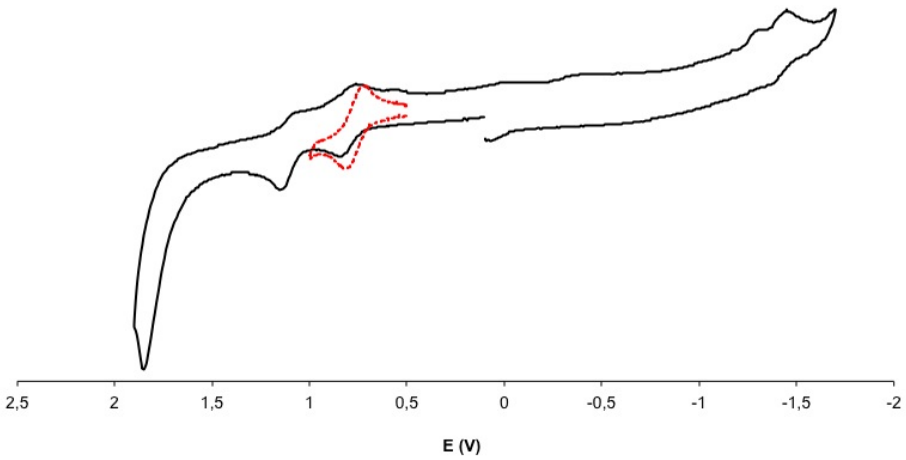

Figure 2.8: Cyclic voltammogram of complex **1Fe** in dichloromethane (200 mV/s). Inset: Isolation of the first oxidative processes

Table 2.6: Electrochemical data for complexes $[M(\eta^5\text{-}C_5H_5)(PP)(L1)]PF_6]$ in CH_2Cl_2 and MeCN

Comp.	Solvent	Ep_a (V)	Ep_c (V)	$E_{1/2}$ (V)	ΔE (mV)	$\frac{ip_c}{ip_a}$ [a]
1Fe	**DCM**	1.07	0.99	1.03	80	0.9
		0.77	0.68	0.73	90	0.9
		-	-1.37	-	-	-
		-	-1.53	-	-	-
	MeCN	1.17	-	-	-	-
		1.09	-	-	-	-
		0.72	0.64	0.68	90	1
		-1.34	-1.42	-1.38	80	0.7[a]
		-	-1.72	-	-	-
1aRu	**DCM**	1.28	-	-	-	-
		0.98	-	-	-	-
		-	-1.36	-	-	-
		-	-1.53	-	-	-
	MeCN	1.09[b]	-	-	-	-
		-	-1.38	-	-	-
		-	-1.70	-	-	-
1bRu	**DCM**	1.29	-	-	-	-
		1.01	-	-	-	-
		-	-1.38	-	-	-
		-	-1.55	-	-	-
	MeCN	1.23	-	-	-	-
		1.10	-	-	-	-
		0.97	-	-	-	-
		-	-1.39	-	-	-
		-	-1.70	-	-	-

[a] $\frac{ip_c}{ip_a}$; [b] very broad wave which contains three oxidative processes

The overall electrochemical behaviour for the organometallic complexes are quite similar of that observed for other iron(II) and ruthenium(II) complexes presenting related substituted thiophene-2-carbonitrile ligands.[27,72] The voltammograms of the complexes are characterized by two oxidative and two reductive processes. The oxidative processes were attributed to an oxidation centered on the ligand and to a $M^{(II)}/M^{(III)}$ oxidation process, whereas the reductive processes were both attributed to reduction of the coordinated ligand, in accordance with the overall behaviour of the free ligand seen previously.

The ligand-centred oxidative processes of the **1Fe** complex is quasi-reversible in dichloromethane ($E_{1/2}$ = 0.73 V) but irreversible in acetonitrile (Ep_a= 0.68 V). The ruthenium complexes present a single ligand-based irreversible oxidation process in dichloromethane (Ep_a= 1.28 V for **1aRu** and Ep_a= 1.29 V for **1bRu**). The potential of these processes are very similar

in acetonitrile: complex **1aRu** present three superimposed anodic waves ($Ep_a \approx 1.09$ V) and complex **1bRu** presents two distinct anodic waves at $Ep_a = 1.23$ and 1.10 V.

Similarly, the first oxidative process is reversible for the iron complex in both solvents (Ep/2 = 0.73 V in dichloro-methane; Ep/2 = 0.68 V in acetonitrile), but irreversible for both the ruthenium complexes (Ep_a= 1.28 V for **1aRu** and Ep_a= 1.29 V for **1bRu** in dichloromethane; $Ep_a \approx 1.09$ V for **1aRu** and Ep_a= 1.23 V for **1bRu** in acetonitrile). Furthermore, the oxidative processes of the ruthenium complexes occur at higher potential than that of the iron complex ($\approx$ +0.21 V), in accordance with the higher electronic density of the iron organometallic moiety.

Finally the two reductive processes are very similar for all complexes, in both solvents ($Ep_c \approx$ -1.38 V and $Ep_c \approx$ -1.55 V for dichloromethane and Ep_c= -1.39 V and $Ep_c \approx$ -1.70 V in acetonitrile). The presence of cathodic waves without the anodic counterpart clear lead to the conclusion that these processes are irreversible and that the formed 19 e^- species are quickly decomposed in solution.

As stated previously, the electrochemical behaviour of the complexes can be correlated to their potential to act as NLO redox-switches. The CV results seem to indicate that only the reversible iron complex is suitable for NLO switching applications. Attempts to synthesize and isolate the Fe(III) complex were tested using silver(I) salts, namely $AgPF_6$ and $AgBF_4$, or the nitrosonium salt $NOBF_4$. In all cases, an incomplete oxidation accompanied by decomposition of the product was obtained, even at low temperatures (-50°C). Nevertheless, oxidation studies were made by UV-Vis. spectroscopy. In these studies, a concentrate dichloromethane solution of the complexes ($\approx 10\times^{-3}$M) was treated with a slight molar excess of $AgPF_6$. **Figure 2.9** show the behaviour found for the ligand and the complexes.

Results show a shift in the low energy bands of all the complexes upon oxidation. The ligand presents a red shift of *ca.* 50 nm that appears after the addition of the oxidizing agent. However, the extinction coefficient of the absorption band clearly indicates that a complete decomposition occurs after approximately 60 minutes. In the case of the organometallic complexes, the absorption band is red-shifted by *ca.* 25 nm and is accompanied by the appearance of a second low lying electronic transition at 768 nm for **1Fe** and 850 nm for **1aRu**. Due to the limits of detection of the Uv-Vis. apparatus, the band for the **1bRu** complex was not determined.

Since the present complexes are Type I switches, the oxidation of the metal centres

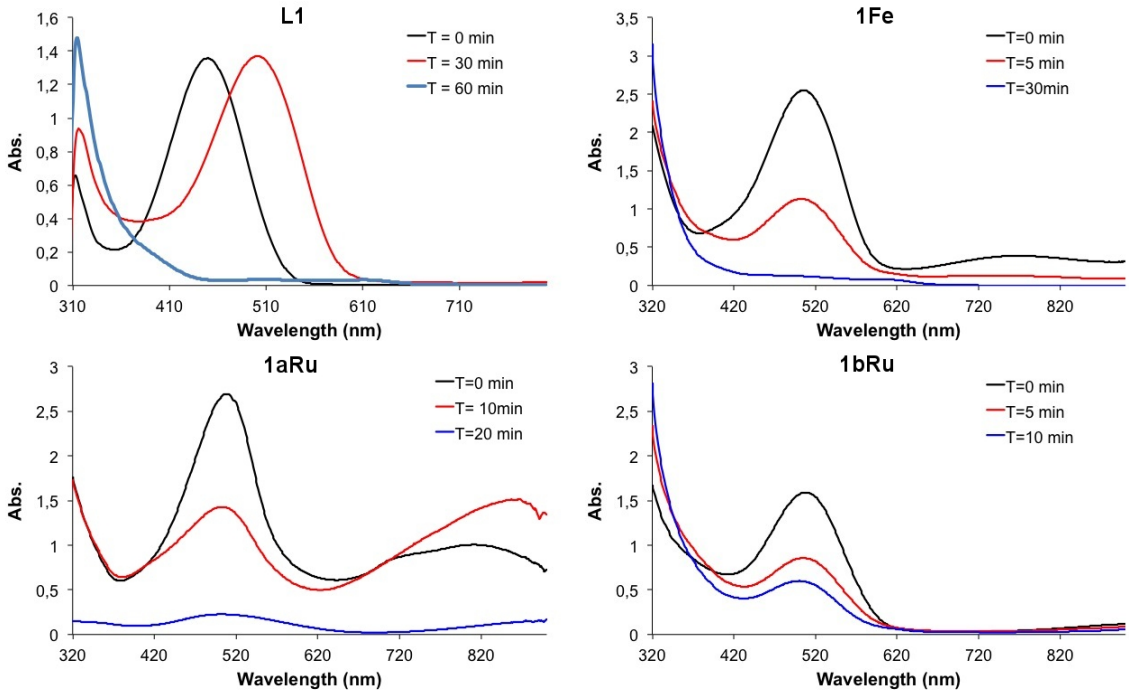

Figure 2.9: UV-Vis spectra of the oxidation tests of **L1**, **1Fe**, **1aRu**, and **1bRu** in dichloromethane

should lead to a decrease in the nonlinear optical properties. However, the appearance of a new electronic transition at lower energy suggests an enhancement of the MLCT in the organometallic complexes, suggesting that the chemical oxidation in solution of the compounds has a high **L1** ligand character, and is not entirely centred at the metal centre as expected. The new electronic transition can, hence, be related to an enhancement of the nonlinear optical properties of the complexes, according to the TLM. As in the case of the free ligand, the stability of the organometallic compounds is very limited, being observed that the complexes undergo fast decomposition in less than 30 minutes. Since it was not possible to achieve the oxidized forms of the complexes, it was not possible to evaluate the molecular switching based on the second-order NLO properties by redox means.

2.3.5 Quadratic Hyperpolarizabilities

Since the complexes present absorption wavelengths in the range of 450-470 nm, measurements by hyper-Rayleigh scattering (HRS) at a 1064 nm fundamental wavelength laser beam should result in the high-resonance enhancement of the measured hyperpolarizabilities.Hence, the nonlinear optical data for the complexes was obtained by made by HRS at a 1500 nm fundamental wavelength laser beam. This laser setup produces a second harmonic-signal at 750 nm, far from the absorption maxima of the complexes, where reasonable results can be expected from the TLM analysis.

It is well known that the TLM is a good approximation for estimating the second-order hyperpolarizabilities of molecules in which only one excited state is strongly coupled with the ground state by the applied electric field and only one component of the β tensor governs the NLO response, *i. e.* for molecules that present an unidirectional charge-transfer transition between the ground state and the first excited state. Equation 2.1 summarizes the TLM assumptions:

$$\beta \propto \frac{\Delta\mu_{eg} f_{eg}}{E_{eg}^3} \tag{2.1}$$

where $\Delta\mu_{eg}$ is the difference between the dipoles moments of the ground state (g) and the excited state (e), f is the oscilator strength of the transition, and E_{eg} is the transition energy. As seen in section 1.3.4, an optimal combination of the factors will provide higher β values. In Section Chap2:DFT, it will be showed that DFT calculations predict a dominant tensor of the molecular hyperpolarizabilities for all complexes. In addition, TD-DFT calculations also predict a single dominant electronic transition in the visible region (attributed to a HOMO→LUMO transition). Thus, an analysis of the results according to the TLM seems to be reasonable for these complexes. In **Table 2.7** the second-order hyperpolarizabilities are presented, together with other spectroscopical data that support the following discussion.

The experimental quadratic hyperpolarizabilities are relatively low. This result is expected considering the molecular feature of these complexes that can be viewed as having a structure of the type D-π-bridge-D', in which the well-known electron donor character of the organometallic fragments was combined with the thienyl-benzo[c]thiophene moiety that behaves mainly as a donor during the lowest energy transition (*vide infra* in Section Chap2:DFT). The results of the TLM suggest some resonant enhancement of the mea-

Table 2.7: Quadratic hyperpolarizabilities and relevant spectroscopic data for the complexes

Comp.	$\nu(\mathbf{cm^{-1}})$[a]	$\lambda_{max}(\mathbf{nm})$	β_{1500}[b]	β_0[c]
1Fe	-7	478	164	87
1aRu	+8	475	147	80
1bRu	+10	473	105	57

[a] Differences on IR upon ligand coordination: $\nu(N \equiv C)_{(complex)}$ - $\nu(N \equiv C)_{(ligand)}$; [b] values $\times 10^{-30}$ esu.
[c] values $\times 10^{-30}$ esu corrected using the TLM with $\beta_0 = \beta_{1500}\left(1 - \left(\frac{2\lambda_{max}}{1500}\right)^2\right)\left(1 - \left(\frac{\lambda_{max}}{1500}\right)^2\right)$

sured hyperpolarizabilities, although the relative orderings were maintained with TLM corrected values: **1Fe** > **1aRu** > **1bRu**. In spite of the magnitude of the experimental quadratic hyperpolarizabilities is relatively similar for all the complexes (the values for **1Fe** and **1aRu** falls within the experimental error of 15%), it is interesting to note that experimental quadratic hyperpolarizabilities follow the trend observed for the relative π-backdonation interaction of the complexes based on spectroscopic FTIR and NMR data. The existence of this interaction was found to play an important role on the second-order NLO response of mono(η^5)cyclopentadienylIron, ruthenium nickel and cobalt complexes with *p*-substituted benzonitrile chromophores where the high values found for Ru(II) and Fe(II) complexes were attributed to the occurrence of π-backdonation.[74] The fact that experimental quadratic hyperpolarizabilities for all complexes are relatively similar is not surprising considering the spectroscopic data discussed above. In fact, for the low-energy band, which is the key for second-order nonlinear optical properties, λ_{max}, is very similar for all the complexes and no significant solvatochromic effect was observed.

2.4 Density Functional Theory Studies

2.4.1 Geometry and optical data

In order to get a better understanding of the structure and the linear optical and second-order nonlinear optical properties in the ligand and in the complexes, DFT studies were

performed using three different functionals.

It is well known that the choice of functionals is crucial to generate reliable and accurate results. The selected functionals belong to two classes: B3LYP[75,76] and CAM-B3LYP[77] belong to the hybrid functional class; and the M06 functional is a meta-hybrid GGA functional.[78] The B3LYP functional is one of the most widely used functionals in computational chemistry because it provides good performance in numerous energy assessments of small molecules and reproduces the geometries of smaller and larger molecules very well. Despite its success, it is well known that this functional can give unreliable results for determination of barriers heights, description of van der Waals interactions, isomer energy differences, and, in the case of organometallic compounds, bond energy trends and spin polarization.[79–82] In spite of these shortcomings, this functional is widely used in calculations of hyperpolarizabilities of organic and organometallic systems[83–88] and was shown to reproduce reasonably well some experimental trends.[86–88] One of the limitations of the DFT methods is the so-called "short-sightedness" of the functionals because they are based in local terms. For instance, TD-DFT calculations using popular density functionals, such as B3LYP, often underestimates long-range CT excitation energies, in particular for donor-acceptor substituted push-pull molecules.[89] Underestimation of long-range CT energetics is a consequence of incorrect asymptotic behaviour on the part of the exchange-correlation potential. This fact led to the development of the range separated functionals, where short-range HF exchange is treated using regular local functionals, like in the conventional hybrid B3LYP functional, whereas at higher interelectronic distances the long-range HF exchange is increased. The CAM-B3LYP[77] functional is one of the most recent versions of range-separated functionals, and it uses variable short-range HF exchange correlation in order to improve long-range interactions. It was found that this functional, in many cases, provides reliable results in the prediction of molecular structures, excitation energies, and hyperpolarizabilities of π-conjugated systems.[90–96] M06 is a hybrid functional for general-purpose applications and is very suitable for applications in transition metal chemistry, giving better performance than B3LYP for main-group thermochemistry, barrier heights, and noncovalent interactions.[82,97,98] Compared to B3LYP, the hybrid M06 functional presents a higher percentage of HF exchange. So far, no systematic study was executed in the performance of M06 functional for organometallic compounds, particularly in view of NLO applications, this pioneering the present study in the use of this functional

It was recently shown that the use of model complexes, in which the phenyl rings in the phosphane co-ligands are substituded by hydrogen atoms, provide a much more computationally affordable method for the estimation of optical and nonlinear optical properties of η^5-cyclopentadienyl iron(II), ruthenium(II) and nickel(II) complexes.[99] This simplified method has proven to give similar results than those using phenylated phosphane co-ligands.[99–101] Hence, in an initial stage, as a compromise between accuracy and computational effort, three simplifications were used in the calculations: (i) dephenylated phosphanes were used, *i. e.*, $H_2PCH_2CH_2PH_2$ instead of κ^2-dppe and PH_3 instead of PPh_3; (ii) only the first 24 lower excitation states were computed in TD-DFT studies; and (iii) isolated molecules in the gas phase were used (i.e., no solvent corrections were employed). Later, the adequacy of the simplifications (ii) and (iii) was checked by a comparison between the calculated optical data obtained for the model complexes and "real" complexes and with experimental data. The adequacy of simplification (i) was checked by the use of 120 excited states for simulating the electronic spectra, and the results were compared to those obtained with 24 excited states.

The optimized structures of ligand **L1** and the model organometallic complexes ^{M}**1Fe**, ^{M}**1aRu** and ^{M}**1bRu** in gas-phase using B3LYP as functional are shown in **Figure 2.10**. No significative differences were observed for the other functionals. **Table 2.8** shows the selected bond distances and bond angles for all the compounds.

The iron and ruthenium complexes adopt a pseudo-octahedral geometry around the metal centre, where the 1,2-bis(dihydrophosphine)-ethane and thienyl ligand occupy three coordinating positions and the η^5-cyclopentadienyl ring occupies the remaining three positions. The angles and bond lengths around the metal centers and within the thienyl system for both ligand and organometallic complexes are consistent with experimental crystal data for parent iron(II) and ruthenium(II) thiophene derivatives[102,103] and other η^5-monocyclopentadienylmetal nitriles.[96–98]

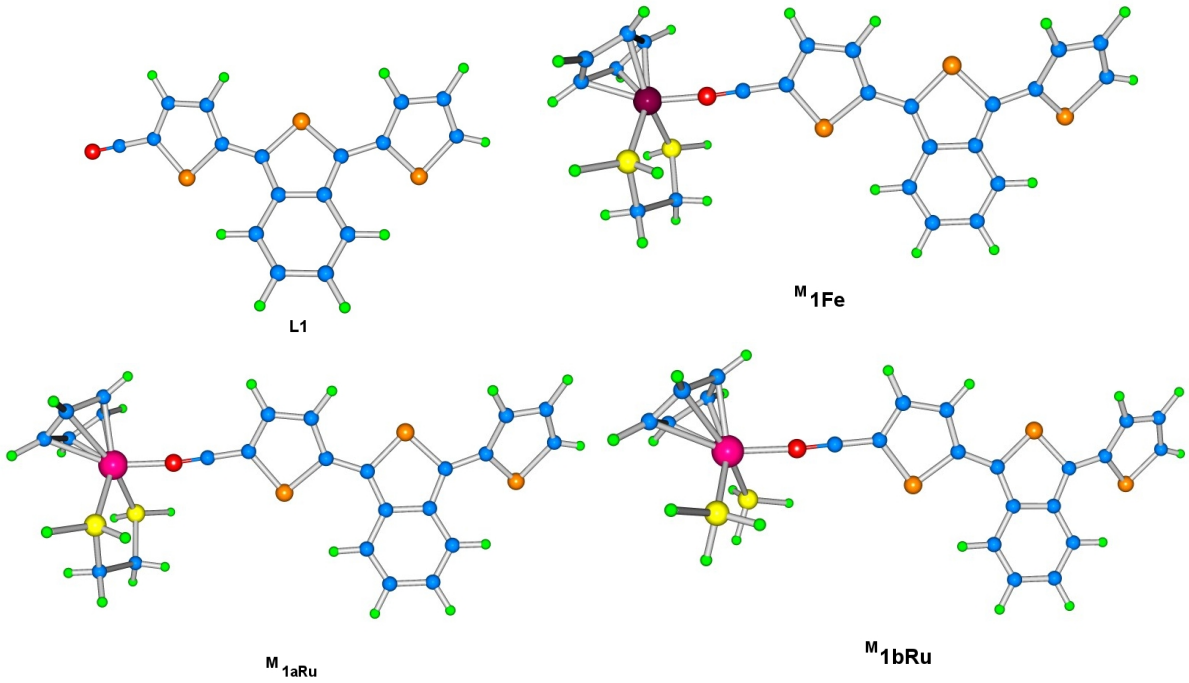

Figure 2.10: DFT optimized structures for ligand **L1** and the monocationic ^{M}**1Fe**, ^{M}**1aRu** and ^{M}**1bRu** complexes

Table 2.8: Selected Bond Distances and Bond Angles for **L1**, ^{M}**1Fe**, ^{M}**1aRu** and ^{M}**1bRu**.

	B3LYP				CAM-B3LYP				M06			
	L1	^{M}**1Fe**	^{M}**1aRu**	^{M}**1bRu**	**L1**	^{M}**1Fe**	^{M}**1aRu**	^{M}**1bRu**	**L1**	^{M}**1Fe**	^{M}**1aRu**	^{M}**1bRu**
Bond Distances (Å)												
M-Cp[a]	-	1.763	1.892	1.886	-	1.738	1.867	1.863	-	1.673	1.845	1.839
M-N	-	1.925	2.069	2.070	-	1.933	2.076	2.078	-	1.899	2.087	2.087
M-P[b]	-	2.334	2.423	2.438	-	2.325	2.415	2.428	-	2.279	2,418	2.431
N-C1	1.166	1.170	1.170	1.170	1.158	1.160	1.160	1.160	1.166	1.170	1.169	1.169
C1-C2	1.410	1.392	1.393	1.392	1.415	1.399	1.400	1.399	1.409	1.391	1.392	1.390
BLA[c]	0.050	0.036	0.038	0.037	0.065	0.052	0.053	0.052	0.050	0.038	0.038	0.036
Bond Angles(°)												
Cp-M-N[a]	-	125.3	125.8	126.2	-	124.5	125.9	126.3	-	126.5	128.7	127.6
P1-M-P2	-	85.2	82.6	93.2	-	85.2	82.6	93.4	-	85.9	82.2	91.7
M-N-C1	-	175.9	173.5	175.9	-	176.3	174.1	176.3	-	178.4	177.0	175.8
N-C1-C2	179.8	179.7	179.8	179.2	179.9	179.7	179.8	179.3	179.9	178.4	178.8	178.7
Dh1[d]	156.7	169.2	168.2	168.5	149.8	163.8	162.4	163.3	158.2	167.4	166.5	173.8
Dh2[e]	-150.4	-152.0	-151.9	-152.2	-144.8	-146.3	-146.2	-146.4	-151.1	-152.9	-152.6	-152.9

[a] M = Fe(II) or Ru(II); Values refer to the centroid of the cyclopentadienyl ring; [b] Avarage M-P bond distance; [c] Bond Length Alternation;
[d] Dh1 refers to the C4-C5-C6-C7 dihedral angle; [e] Dh2 refers to the C12-C13-C14-C15 dihedral angle

In general, results show that the bond lengths within the thienyl nitrile ligand are consistent with an increase of π-conjugation upon metal coordination. As expected, the major effect is observed in chemical bonds close to the metal centre. For instance, larger differences in the bond lengths upon coordination are observed for C1-C2 to C5-C6 (0.012-0.018 Å) than for the remaining bonds (0.001-0.008 Å). The small increase of 0.002-0.005 Å in the N≡C1 bond length upon coordination is consistent with metal-to-ligand π-backdonation interaction. This interaction is consistent with the previously discussed FTIR and HNM data.

The well-known bond-length-alternation (BLA) parameter is defined as the difference between the average carbon-carbon adjacent bond lengths along a conjugated backbone. BLA is closely related to the degree of mixing between the ground-state and charge-separated resonant structures of a molecule, and hence, BLA can be also related to the linear and nonlinear optical properties of molecules. A positive BLA value is associated with non conjugated π-systems or with systems that present weak donor-acceptor groups. A lowering of the BLA parameter is observed with the increasing strength of the donor-acceptor groups (and hence, of that of the polarization state). A null value of BLA is obtained for a complete mixing of the ground and charge-separated states. Finally, negative BLA values are also possible, such as in the case of some zwitterionic species, where the charge-separated structure is, in fact, the main contributor to the ground-state. The BLA values for the ligand and organometallic complexes was calculated. Results show that a lowering of BLA is observed upon coordination of the ligand to the organometallic fragment, allowing to conclude that an increased contribution of the quinoidal resonance form in the ground state upon ligand coordination is observed (**Figure 2.11**).

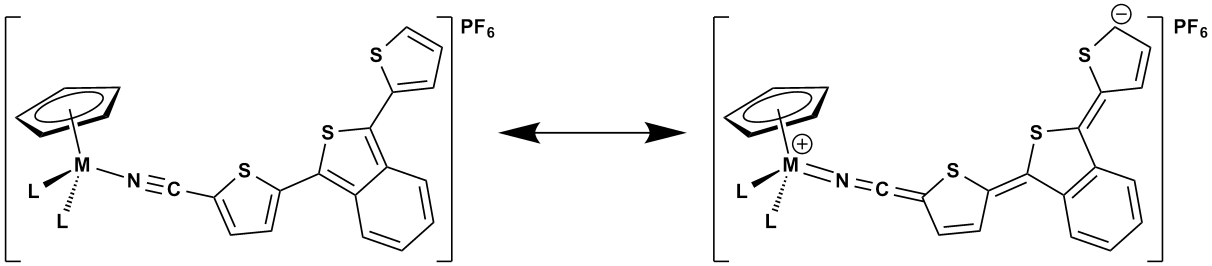

Figure 2.11: Ground-state resonance structures for the studied organometallic complexes

However, some differences were observed when the results of the different functionals

were analysed. The use of B3LYP and M06 functionals originates relatively similar bond lengths and angles, in particular within the conjugate thienyl nitrile framework. CAM-B3LYP, in its turn, provides shorter bond lengths in case of multiple bonds and stretched bond lengths for single bonds. Hence, larger BLAs are observed with CAM-B3LYP functional. However, compared these BLA values to the other two functionals, the variation upon coordination is very similar.

Considering the overall calculated data for the all the complexes, the CAM-B3LYP functional reproduces more successfully and with better accuracy the experimental structural data reported for the parent iron(II) and ruthenium(II) thiophene derivatives.[102,103]

In order to obtain the linear optical data of the ligand, gas-phase TD-DFT calculations were performed in the model complexes. The data is summarized in **Table 2.9**. **Figure 2.12** shows the obtained spectra for all the compounds, using CAM-B3LYP.

TD-DFT calculations predicts a red shift in the electronic transitions upon ligand coordination to the metal centres. These electronic transitions have low energy and substantial oscillator strength, and are in good agreement with the overall shape of the obtained experimental electronic spectra for all complexes. In particular, CAM-B3LYP functional gives optical transition energies very close to the experimental values, especially for ^{M}**1Fe**, with a difference of only +11 nm. The largest deviation was found for the ligand where a difference of -21 nm was obtained. B3LYP and M06 functionals underestimate the low lying electronic transition energies for all compounds, being the major differences obtained for B3LYP with an difference of 90 nm for the complexes and 56 nm for the ligand. Thus, the inclusion of the long range corrected assymptotic behaviour by CAM-B3LYP is of major importance when dealing with extended π-conjugated systems.

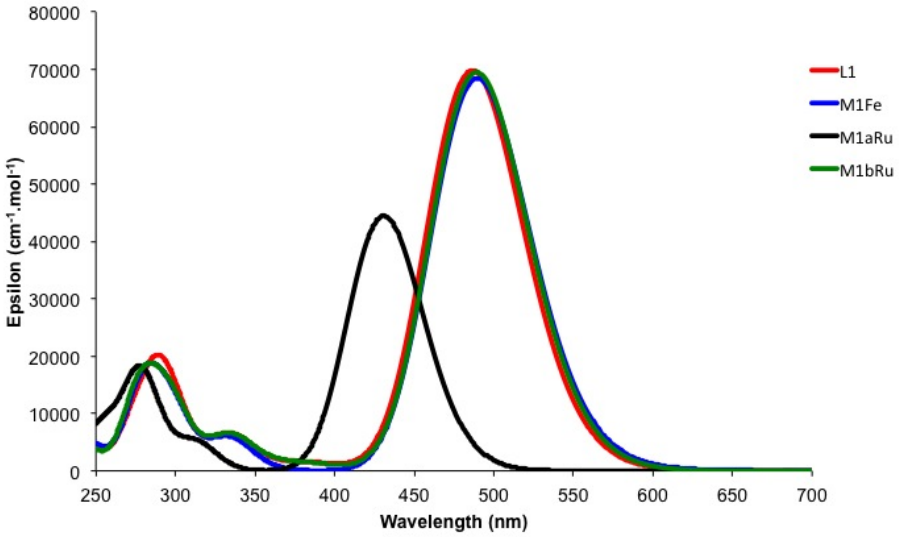

Figure 2.12: CAM-B3LYP TD-DFT spectra of **L1**, ^{M}**1Fe**, ^{M}**1aRu** and ^{M}**1bRu** in gas-phase.

Table 2.9: Relevant TD-DFT results for L, FeL and RuL

Compound	Functional	λ_{max}[a](nm)	E_{eg}(eV)[b]	f[c]	Major Contributions	Character of the CT[d]
	B3LYP	512	2.426	0.6021	HOMO→LUMO (100%)	BcT(50), T3(50) → NC-T1 (100)
L1	CAM-B3LYP	431	2.883	0.6132	HOMO→LUMO (97%)	B(55), T3(45) → NC-T1 (100)
	M06	508	2.445	0.5764	HOMO→LUMO (100%)	B(56), T3(44) → NC-T1 (100)
	B3LYP	565	2.196	0.9501	HOMO→LUMO (98%)	BcT(33), T3(47), OM(20) → NC-T1 (100)
^{M}**1Fe**	CAM-B3LYP	487	2.499	0.7089	HOMO→LUMO (77%)	BcT(52), T3(43), OM(5) → NC-T1 (100)
	M06	558	2.225	0.9268	HOMO→LUMO (100%)	BcT(33), T3(44), OM(23) → NC-T1 (100)
	B3LYP	565	2.196	0.9867	HOMO→LUMO (100%)	BcT(35), T3(47), OM(18) → NC-T1 (100)
^{M}**1aRu**	CAM-B3LYP	486	2.553	0.9636	HOMO→LUMO (96%)	BcT(56), T3(41), OM(3) → NC-T1 (100)
	M06	557	2.231	0.9402	HOMO→LUMO (99%)	BcT(39), T3(44), OM(17) → NC-T1 (100)
	B3LYP	565	2.196	0.9669	HOMO→LUMO (100%)	BcT(45), T3(55)→ NC-T1 (100)
^{M}**1bRu**	CAM-B3LYP	489	2.5406	0.9590	HOMO→LUMO (96%)	BcT(50), T3(50)→ NC-T1(96), Cp(4)
	M06	558	2.225	0.9295	HOMO→LUMO (99%)	BcT(50), T3(50)→ NC-T1(95), Cp(5)

[a] Absorption wavelength of the main transitions;
[b] Energy of the transitions; [c] Oscillator strength; [d] Based on the represented molecule fragments (overall % of the charge transfer is given in parentheses). OM = Organometallic fragment (Metal+Phosphane+cyclopentadienyl ring), P = phosphane co-ligands, NC = nitrile group, BcT = benzo[*c*]thiophene (T2 ring + B ring).

The low lying electronic transitions are attributed to HOMO → LUMO charge transfers. The frontier molecular orbitals for ^{M}**L1**, ^{M}**1Fe**, ^{M}**1aRu** and ^{M}**1bRu**, obtained using CAM-B3LYP, are depicted in **Figure 2.13** (no significant differences were found for the same orbitals using B3LYP and M06 functionals).

The HOMO and LUMO orbitals for all molecules are relatively spread over the ligand with only a small contribution of the metal atom in the case of organometallic complexes. An analysis of the electronic transitions in terms of the contribution of groups atoms involved show that for **L1** the charge transfer mainly arises from the donor thienyl T3 and benzo[*c*]thiophene (BcT) rings to the acceptor thienyl-nitrile unit (T1). The character of the main electronic transitions for ^{M}**1Fe**, ^{M}**1aRu** and ^{M}**1bRu** are very similar, with fairly the same contribution percentage of the metal centre to the transition. Thus, the HOMO→LUMO excitation of organometallic complexes generates a charge transfer mainly within the ligand fragment (ILCT) with some contribution of metal-to-ligand charge transfer (MLCT). CAM-B3LYP predicts only small contributions of a MLCT character to the overall electronic transition (5% for 1Fe, 3% for1aRu and 3% for1bRu), whereas B3LYP and M06 functionals predicts larger contributions (20-23% for 1Fe and 17-18% for both Ru complexes). The overall results allow to state that the T3 ring, alongside with the BcT ring, can behave as an electron donor group in this π-conjugated systems.[104] Considering the well-known electron donor character of the organometallic fragments, these molecules can be viewed as having a structure of the type D-(π-conjugated system)-D', as previously mentioned. Because a red-shift of this electronic transition is observed upon ligand coordination, an increase of the corresponding hyperpolarizabilities is expected, according to the TLM. In fact, it is well known that organometallic fragments play an important role in nonlinear optical properties of benzene and thiophene based nitrile derivatives.[105,106] Low-energy MLCT optical transitions were found clearly to contribute to the experimental molecular hyperpolarizabilities.

The static first hyperpolarizabilities for **L1**, ^{M}**1Fe**, ^{M}**1aRu** and ^{M}**1bRu** were calculated and relevant results are shown in **Table 2.10**. The β_{tot} and β_{HRS} hyperpolarizabilities were estimated using equation 5.2 and equation 1.22.

The β_{tot} values of the all molecules are functional-dependent, in particular for the organometallic complexes. Except for B3LYP, coordination of the ligand to organometallic moieties enhances the second-order NLO properties, particularly using CAM-B3LYP. M06 functional give only moderate changes on hyperpolarizabilities upon ligand coordina-

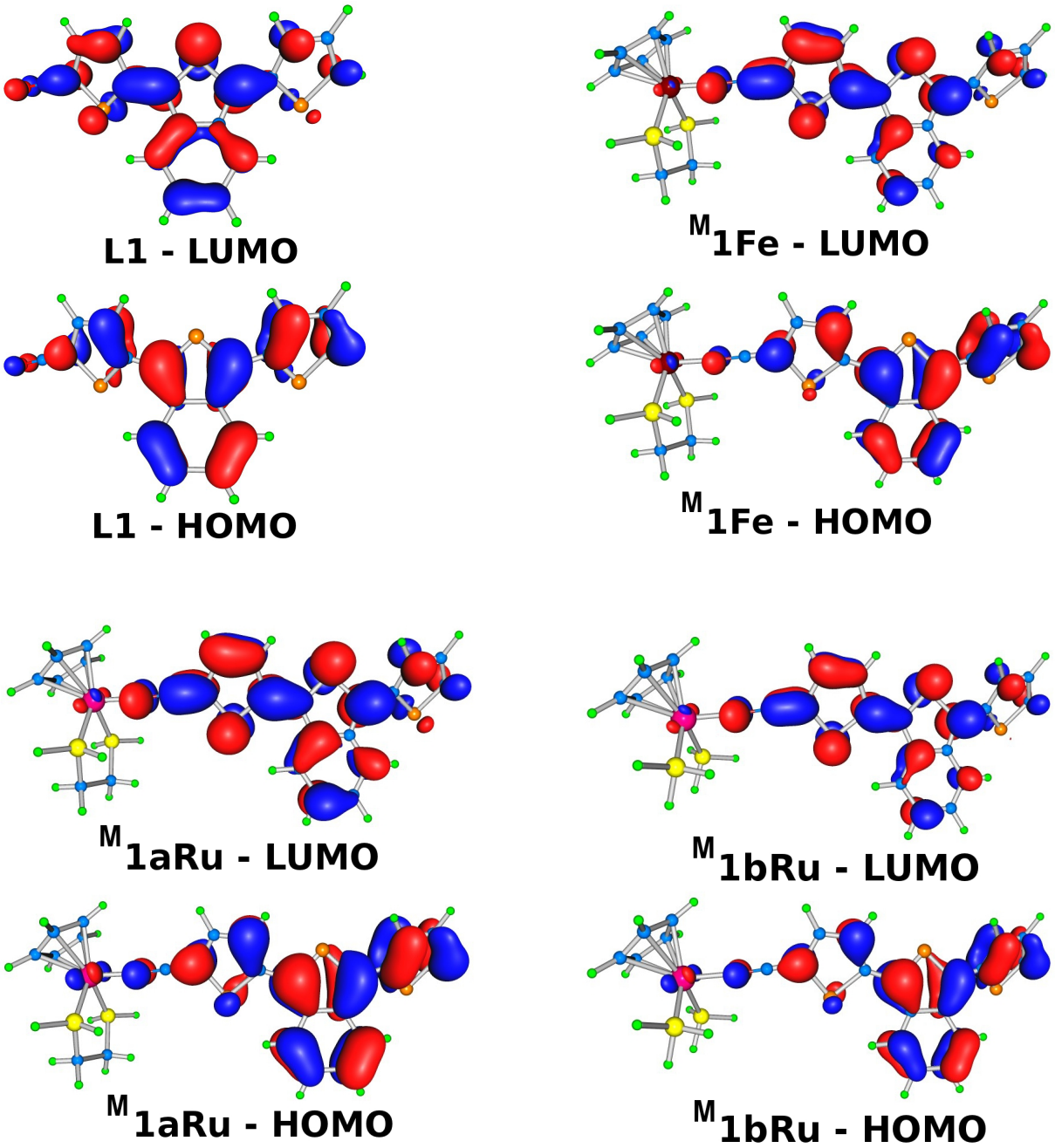

Figure 2.13: Gas-phase HOMO and LUMO molecular orbitals of **L1**, ^{M}**1Fe**, ^{M}**1aRu** and ^{M}**1bRu** using CAM-B3LYP (contour: 0.03 au).

Table 2.10: Gas-phase β_{tot} and β_{HRS} for **L1**, ^{M}**1Fe**, ^{M}**1aRu** and ^{M}**1bRu**.

Comp.	β_{tot} ($\times 10^{-30}$esu)			β_{HRS}($\times 10^{-30}$esu)[a]			β_0^{Exp}[a]
	B3LYP	CAM-B3LYP	M06	B3LYP	CAM-B3LYP	M06	
L1	39.94	30.06	36.79	8.65	6.50	8.03	
^{M}**1Fe**	33.54	113.64	49.43	7.51	23.53	10.39	87
^{M}**1aRu**	31.52	105.78	57.07	7.13	21.99	12.01	80
^{M}**1bRu**	62.07	94.60	71.33	14.17	25.39	14.63	57

[a] values $\times 10^{-30}$ esu

tion. When compared to the experimental TLM corrected values, the overall results show a clear underestimation of the predicted static hyperpolarizabilities using B3LYP and M06 functionals. The only exception is observed in the ^{M}**1bRu** complexe where a overestimation in *ca.* 9% and 25% is obtained with both functionals, respectively. An average overestimation of 30% is observed using the CAM-B3LYP functional for all complexes.

The β_{HRS}, in their turn, are also functional-dependent and are much lower than β_{tot}. The coordination of the ligand to organometallic moieties enhances the second-order NLO properties in approximately a three-fold factor, in accordance with the previously structural and TD-DFT results. CAM-B3LYP provides a greater enhancement upon coordination of **L1** of the hyperpolarizabilities compared to B3LYP and M06 functionals. However, the best result using CAM-B3LYP is still 2.2 times lower than the experimental TLM corrected values.

The difference in calculated values for β_{tot} and β_{HRS} are due to not only the difference in the expression used to the calculation of β but also to the difference in the calculation method, since β_{HRS} are obtained by frequency depedent CPHF method. When compared to the experimental data, β_{tot} provides a lower error than β_{HRS} but the unrealistic physical meaning of the β_{tot} values exclude the possibility of a reliable comparison with the experimental results. However, β_{tot} is still used in the majority of the published works by other authors when dealing with DFT calculation of the nonlinear optical properties of organometallic complexes.[107]

Recently, the influence on the percentage of HF exchange incorporated in different functionals into the excitation energies and the estimated hyperpolarizabilities was adressed.[108] It was shown that, functionals with low HF exchange energy (less than 50%, such as B3LYP and M06) perform poorly in the prediction of hyperpolarizabilities, whereas functionals with more than 50% HF exchange, as well as functionals incorporat-

ing distance-dependent HF exchange (such as CAM-B3LYP) exhibit good performance in the estimation of the hyperpolarizabilities, at the expenses of blue-shifted excitation energies. The same behaviour of the three functionals was observed in the study of the present complexes – a blue-shifted optical excitations and higher hyperpolarizabilities were found for CAM-B3LYP in comparison with B3LYP and M06. However, as stated above, the estimated hyperpolarizabilities are still relatively low in comparison with the experimental TLM corrected results.

It is well known that solvation interactions are, in some cases, critical for obtaining quantitatively satisfactory results of the calculated electronic excitations in comparison with experimental data. Thus, theoretical studies taking into account solvation effects were performed on the ^{M}**1Fe**, ^{M}**1aRu** and ^{M}**1bRu** complexes using CAM-B3LYP as functional. The polarizable continuum model (PCM)[109] was used to simulate the interaction between the complexes with chloroform. Also, to evaluate if the use of model phosphanes describe the behaviour found with real phosphanes, calculations in solvated media were extended to the "real" synthesized ruthenium complexes (here denoted ^{R}**1aRu** and ^{R}**1bRu**). The iron complex containing the κ^2-dppe phosphane was not calculated due a systematic convergence failure in the geometry optimization.

The solvated CAM-B3LYP optimized structures of model organometallic complexes ^{M}**1aRu** and ^{M}**1bRu** resemble the previously optimized structures in the gas-phase, and present only minor differences in the bond distances and bond angles, which are shown in **Table 2.11**. The optimized structures for complexes ^{R}**1aRu** and ^{R}**1bRu** are shown in **Figure 2.14** and present a difference positioning of the **L1** ligand in comparison with the model complexes. The reason for this new positioning is justified by the presence of the more bulky phenyl rings of the phosphane co-ligands. Selected bond angles and bond distances are also shown in **Table 2.11**.

Comparatively to the gas-phase model geometries, the solvated geometries of the model complexes present slightly longer M-Cp and M-P bond lengths and sligth shortening of the M-N≡C bond distance. The cumulative effect of these minor structural differences results in an increase of the BLA parameter for both the solvated and "real" complexes in the range of 0.001 to 0.007.

These results are consistent with the increased bulky nature and donor abilities of the "real" phosphanes comparatively to the model phosphanes.

The β_{HRS} obtained for this set of complexes in presented in **Table 2.12**.

Table 2.11: Bond Distances and Bond Angles for the solvated **L1**, ^{M}**1Fe**, ^{M}**1aRu** and ^{M}**1bRu**.

Compound	^{M}**1Fe**	^{M}**1aRu**	^{M}**1bRu**	^{R}**1aRu**	^{R}**1bRu**
			Bond Distances (Å)		
M-Cp[a]	1.745	1.867	1.863	1.879	1.877
M-N	1.918	2.076	2.068	2.059	2.062
M-P[b]	2.256	2.415	2.427	2.422	2.484
N-C1	1.158	1.160	1.158	1.159	1.159
C1-C2	1.409	1.400	1.404	1.404	1.403
BLA[c]	0.053	0.053	0.059	0.060	0.057
			Bond Angles(°)		
M-N-C1[a]	177.3	174.2	177.0	175.5	174.8
P-M-N	91.8	89.3	88.5	87.3	88.8
P1-M-P2	85.4	82.7	92.6	83.6	103.1
P-M-Cp[a,d]	125.9	128.0	124.7	129.0	121.7
N-C1-C2	179.6	179.8	179.4	179.5	179.3
Dh1[d]	125.9	128.0	124.7	129.0	121.7
Dh2[e]	-138.2	-146.2	-145.5	-144.8	-145.4

[a] M = Fe(II) or Ru(II); Values refer to the centroid of the cyclopentadienyl ring; [b] Avarage M-P bond distance; [c] Bond Length Alternation;
[d] Dh1 refers to the C4-C5-C6-C7 dihedral angle;
[e] Dh2 refers to the C12-C13-C14-C15 dihedral angle

Table 2.12: Relevant TD-DFT results and β_{HRS} for solvated ^{M}**1Fe**, ^{M}**1aRu**, ^{M}**1bRu**, ^{R}**1aRu** and ^{R}**1bRu**

Comp.	λ_{max}	f	Attribution	Major Contributions	β_{HRS}	Ratio
			Model Complexes			
^{M}**1Fe**	447	0.852	HOMO→LUMO (93%)	B(93), Fe+Cp(7)→NC-T1(96),P(4)	20.06	0.85
^{M}**1aRu**	477	1.042	HOMO→LUMO (96%)	B(92), Ru+Cp(8)→NC-T1(96),P(4)	24.72	1.12
^{M}**1bRu**	477	0.936	HOMO→LUMO (96%)	B(95), Ru(5)→NC-T1(100)	26.36	1.04
			"Real" Complexes			
^{R}**1aRu**	465	0.952	HOMO→LUMO (96%)	B(90), Ru+P(10)→NC-T1(100)	24.73	1.12
^{R}**1bRu**	475	1.008	HOMO→LUMO (96%)	B(75), Ru+Cp(25)→NC-T1(100)	29.43	1.16

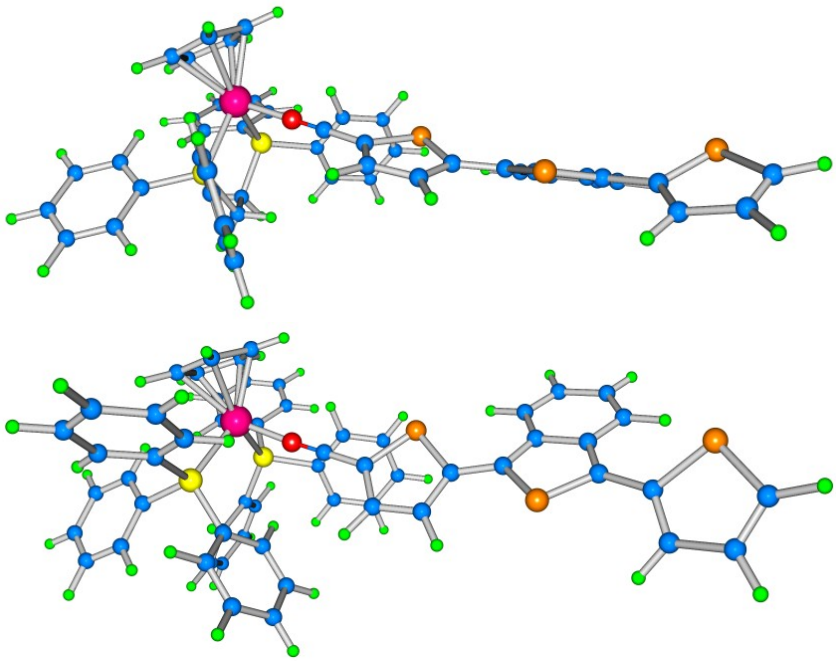

Figure 2.14: CAM-B3LYP chloroform solvated optimized structures of ^{R}**1aRu** (top) and ^{R}**1bRu**(bottom).

It is noticeable that DFT calculations results show that the inclusion of solvent effects lead to an increase of the electronic transition energy for both the model and the "real" complexes. In fact, the solvatochromic behaviour of these complexes showed that an increase of the polarity medium lead to a increase of the energy of the transition. Hence, the DFT results indirectly confirm the solvatochromic behaviour for this complexes.

The inclusion of solvation for these compounds also show an underestimation of the DFT calculated hyperpolarizability values when compared with the experimental two-level model corrected values. Different reasons for these discrepancies can be conjectured. For example, the use of averaged configurations of the complexes for the calculations instead of the minimum energy alone and the inclusion of solvated media with a more detailed model than PCM could probably lead to more realistic results. These issues have been discussed, for example, by Jensen and van Duijnen for the case of the widely studied *p* -nitroaniline.[110] It is also clear that the substitution of the model phosphanes by "real" κ^2-dppe and PPh_3 originates small differences (up to *ca.* 10%) in the corresponding calculated β_{HRS}, thus proving the adequacy of the model complexes to describe, at least

qualitatively, the present system.

The use of κ^2-dppe and PPh_3 instead of the model $H_2P(CH_2)2PH_2$ and PH_3 phosphanes in DFT calculations can give an additional insight relating to the differences on the experimental quadratic hyperpolarizabilities of the ruthenium complexes. DFT calculations on ^{R}**1bRu** predicts an enhanced contribution of the MLCT to the overall excitation (*ca.* 25%). For ^{R}**1aRu**, the contribution of the MLCT is lower (*ca.* 10%). The ILCT arises from a charge transfer from the T3 and the T2 and B rings to the thienyl-nitrile unit whereas the MLCT arises from the organometallic moiety also to the thienyl-nitrile unit. Thus, ILCT and MLCT have opposite directions of the charge transfer. This might result in less charge transfer efficiency during the electronic excitation for ^{R}**1bRu** (which has large MLCT contribution) and an expected hampering effect on the experimental quadratic hyperpolarizability.

2.4.2 Redox switching of the second-order NLO responses

The second-order NLO redox switching abilities of **L1**, ^{M}**1Fe**, ^{M}**1aRu** and ^{M}**1bRu** were evaluated. Unrestricted calculations of the one-electron-oxidized **L1**^{ox}, and model ^{M}**1Fe**^{ox}, ^{M}**1aRu**^{ox} and ^{M}**1bRu**^{ox} and one-electron-reduced **L1**^{red}, and model ^{M}**1Fe**^{red}, ^{M}**1aRu**^{red} and ^{M}**1bRu**^{red} species were performed. Geometries were optimized in gas-phase followed by TD-DFT and hyperpolarizabilities calculations. **Tables 2.13** and **2.14** show the structural features of all species upon oxidation and reduction, respectively.

Table 2.13: Selected DFT structural data for $\mathbf{L1}^{ox}$, $^{M}\mathbf{1Fe}^{ox}$, $^{M}\mathbf{1aRu}^{ox}$ and $^{M}\mathbf{1bRu}^{ox}$.

	B3LYP				CAM-B3LYP				M06			
	$\mathbf{L1}^{ox}$	$\mathbf{1Fe}^{ox}$	$\mathbf{1aRu}^{ox}$	$\mathbf{1bRu}^{ox}$	$\mathbf{L1}^{ox}$	$\mathbf{1Fe}^{ox}$	$\mathbf{1aRu}^{ox}$	$\mathbf{1bRu}^{ox}$	**L1**	$\mathbf{1Fe}^{ox}$	$\mathbf{1aRu}^{ox}$	$\mathbf{1bRu}^{ox}$
Bond Distances (Å)												
M-Cp[a]	-	1.767	1.907	1.901	-	1.741	1.875	1.870	-	1.688	1.865	1.855
M-N	-	1.878	2.028	2.126	-	1.909	2.053	2.058	-	1.853	2.043	2.051
M-P[b]	-	2.347	2.437	2.451	-	2.331	2.422	2.435	-	2.289	2.423	2.440
N-C1	1.165	1.173	1.173	1.193	1.158	1.159	1.160	1.160	1.165	1.174	1.172	1.170
C1-C2	1.410	1.394	1.395	1.359	1.414	1.409	1.408	1.409	1.410	1.391	1.394	1.400
BLA[c]	0.015	0.009	0.010	0.005	0.020	0.016	0.016	0.013	0.015	0.009	0.010	0.006
Bond Angles(°)												
Cp-M-N[a]	-	124.0	125.7	126.4	-	123.6	125.3	126.1	-	125.7	127.9	127.7
P1-M-P2	-	84.6	81.8	92.3	-	84.8	82.2	92.9	-	85.2	81.8	91.6
M-N-C1	-	173.4	172.5	174.5	-	173.4	172.3	174.4	-	175.2	174.2	175.0
N-C1-C2	179.8	178.3	178.6	179.2	179.8	178.1	178.2	178.9	179.8	179.2	179.6	179.8
Dh1[d]	171.0	172.8	173.7	172.2	172.7	171.6	172.7	169.9	171.5	177.5	177.7	172.4
Dh2[e]	169.1	169.7	169.5	-169.7	171.3	174.2	174.2	-173.2	169.6	170.1	170.7	-173.2

[a] M = Fe(II) or Ru(II); Values refer to the centroid of the cyclopentadienyl ring; [b] Avarage M-P bond distance; [c] Bond Length Alternation;
[d] Dh1 refers to the C4-C5-C6-C7 dihedral angle; [e] Dh2 refers to the C12-C13-C14-C15 dihedral angle

Table 2.14: Selected DFT structural data for $\mathbf{L1}^{red}$, ${}^{M}\mathbf{1Fe}^{red}$, ${}^{M}\mathbf{1aRu}^{red}$ and ${}^{M}\mathbf{1bRu}^{red}$.

	B3LYP				**CAM-B3LYP**				**M06**			
	$\mathbf{L1}^{red}$	${}^{M}\mathbf{1Fe}^{red}$	${}^{M}\mathbf{1aRu}^{red}$	${}^{M}\mathbf{1bRu}^{red}$	$\mathbf{L1}^{red}$	${}^{M}\mathbf{1Fe}^{red}$	${}^{M}\mathbf{1aRu}^{red}$	${}^{M}\mathbf{1bRu}^{red}$	$\mathbf{L1}^{red}$	${}^{M}\mathbf{1Fe}^{red}$	${}^{M}\mathbf{1aRu}^{red}$	${}^{M}\mathbf{1bRu}^{red}$
					Bond Distances (Å)							
M-Cp[a]	-	1.771	1.903	1.891	-	1.741	1.870	1.861	-	1.674	1.849	1.838
M-N	-	1.957	2.120	2.126	-	1.951	2.109	2.111	-	1.967	2.156	2.141
M-P[b]	-	2.319	2.403	2.420	-	2.316	2.401	2.416	-	2.267	2.401	2.419
N-C1	1.173	1.191	1.193	1.193	1.165	1.183	1.185	1.186	1.175	1.192	1.194	1.193
C1-C2	1.397	1.361	1.360	1.359	1.400	1.357	1.356	1.353	1.396	1.356	1.356	1.356
BLA[c]	0.016	0.003	0.003	-0.007	0.020	0.000	0.000	-0.012	0.016	0.001	0.001	-0.008
					Bond Angles(°)							
Cp-M-N[a]	-	124.2	124.6	125.0	-	124.9	125.5	125.6	-	124.8	125.6	126.3
P1-M-P2	-	85.8	82.9	93.5	-	85.7	82.8	93.6	-	86.2	82.2	92.1
M-N-C1	-	147.8	140.7	137.9	-	149.2	141.9	138.2	-	136.5	129.7	132.8
N-C1-C2	179.8	178.3	178.6	177.4	179.8	178.1	178.2	177.7	179.8	179.2	179.6	176.6
Dh1[d]	180.0	179.0	179.5	179.1	180.0	179.5	179.6	179.6	180.0	178.8	179.4	178.9
Dh2[e]	180.0	170.3	171.3	-168.7	180.0	173.2	172.9	-172.4	180.0	171.9	176.3	-169.3

[a] M = Fe(II) or Ru(II); Values refer to the centroid of the cyclopentadienyl ring; [b] Avarage M-P bond distance; [c] Bond Length Alternation;
[d] Dh1 refers to the C4-C5-C6-C7 dihedral angle; [e] Dh2 refers to the C12-C13-C14-C15 dihedral angle

Comparison of **Tables 2.8** and **2.13** show the following general trends upon oxidation: (i) slight lengthening of the Cp-M and M-P bonds; (ii) strong shortening of the M-NC bond (the only exception is compound ^{M}**1bRu**^{ox} using B3LYP as functional for which a lengthening of the M-NC bond is observed); (iii) minimal changes on N≡C bond length for ligands and complexes; (iv) decrease in angles around the metal centre, in particular for M-N≡C1; (v) decrease in the N≡C1-C2 bond angle (except for complexes with M06 functionals); and (vi) increased planarity within the conjugated thienyl system, in particular for organometallic complexes. The lengthening of the Cp-M and M-P bonds upon oxidation are consistent with crystal data of piano-stool Fe(III) and Ru(III) complexes.[111–113] The improved planarity within the conjugated thienyl system upon oxidation (dihedral angles between thienyl rings for oxidized species close to 180 °, in comparison with nonoxidized species) is accompanied by the expected decrease in BLA parameter (Table 4). Thus, an enhanced contribution of the quinoidal resonance forms (*cf.* **Figure 2.11**) in the ground state upon oxidation is observed (some deviation of N≡C1-C2 from linearity is consistent with this observation). The major changes in the bond lengths within the conjugated thienyl system, responsible for this behaviour, are observed in the two thienyl rings farthest from the metal center. Thus, a more effective conjugation length is observed upon oxidation, in particular for ^{M}**1bRu**^{ox} that presents a BLA value very close to zero.

For the reduced species, comparing **Tables 2.8** and **2.14**, a different behaviour is observed. The general trend is the shortening of M-P bonds lengths and the lengthening of Cp-M bond, accompanied by a strong lengthening of M-NC bond. Also, an increase in N≡C bond length, in particular for organometallic complexes, accompanied with strong decrease of M-N≡C1 angles is observed. This effect is most denoted in the Ru complexes. However, an increased planarity within the conjugated thienyl system is observed, in particular for organometallic complexes. As was observed upon oxidation, the improved planarity within the conjugated thienyl system upon reduction is accompanied by the expected decrease on BLA parameter. The effect is, now, strongly enhanced. In fact, the dihedral angles between thienyl rings for reduced species are even closer to 180°, in comparison with oxidized species, and, for the case of ^{M}**1bRu**^{red}, the BLA parameter is negative proving that a strong charge separation is obtained upon reduction. Similarly, for ^{M}**1Fe**^{red} and ^{M}**1aRu**^{red} almost an equal contribution of the aromatic/quinoidal resonance forms are achieved in ground state.

Summarizing, the major differences between oxidation vs reduction are observed on: i) M-NC bond length: oxidation originates strong shortening whereas reduction provides strong lengthening; ii) N≡C bond: both increase bond length but reduction process results in an enhanced effect; iii) M-N≡C1 angle: both decrease the bond angle but reduction process originates a stronger effect; iv) planarity within the conjugated thienyl system: both originate enhanced planarity but an improved effect is observed upon reduction. Also, the overall results show that most significant structural changes upon oxidation/reduction process are observed on organometallic complexes, in particular upon reduction.

Considering the different studied functionals, the same general observations as those obtained in the non-oxidized/reduced species are observed in the oxidized/reduced counterparts. Thus, B3LYP and M06 functionals gives similar bond lengths and angles within the thienyl nitrile framework. In addition, CAM-B3LYP provides somewhat larger BLA's than those produced by B3LYP and M06, with the exception of the organometallic reduced species. In the case of chemical bonds involving metal atoms, the same general trends are also observed: 1) major differences are obtained for iron complex; 2) B3LYP and CAM-B3LYP predict closer bond lengths and angles values and; 3) M06 gives higher angles and shorter bond lengths when compared to the B3LYP and CAM-B3LYP functionals.

The molecular electrostatic potential (MEP) maps are highly informative concerning the nuclear and electronic charge distribution of a given molecule. To further investigate the influence of the redox stimulus on the electronic charge distribution, the molecular electrostatic potential maps were obtained for all complexes. As an example, the MEP maps of ^{M}**1Fe**, ^{M}**1Fe**^{ox} and ^{M}**1Fe**^{red} are given in **Figure 2.15**. Similar results are obtained for the other complexes.

The MEP results show that ^{M}**1Fe** has less positive charge densities (blue region) mainly located in the T3 and B rings of thienyl ligand and more positive charge densities (red regions) in the organometallic fragment, in particular on metal and phosphorous atoms. Upon one-electron oxidation, the organometallic fragment retains its positive potential, with exception of the Cp ring that becomes more negatively charged. In the case of the ligand, the negative charge seems to appear more delocalized between the B and the T3 rings, indicating a possible enhanced delocalization of the π-conjugated system. Upon one-electron reduction, the major difference to the ^{M}**1Fe**^{red} compound is that the entire ligand becomes less positive, indicating a greatly enhanced π-delocalization. Thus,

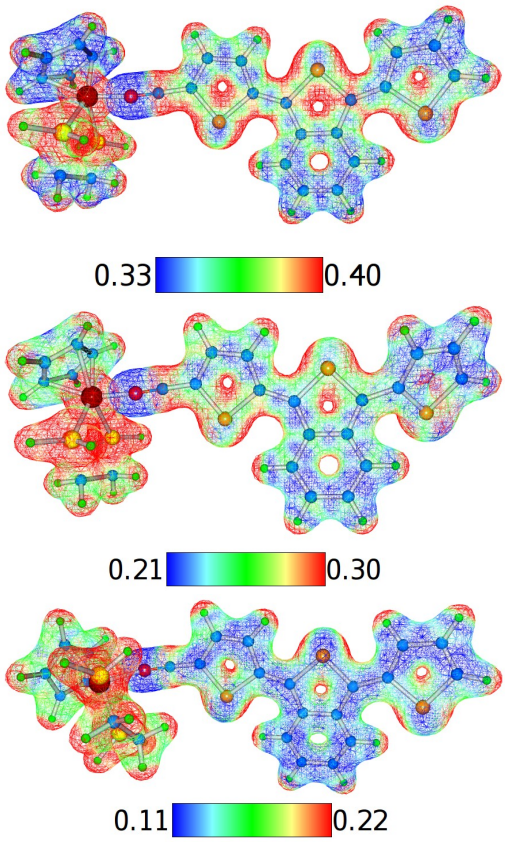

Figure 2.15: Molecular Electrostatic Potential (MEP) map distribution for ^{M}**1Fe** (top), ^{M}**1Fe**^{ox} (middle) and ^{M}**1Fe**^{red} (bottom) using CAM-B3LYP. (contour: 0.045 au)

both oxidation and reduction appear to lead to a more homogeneous charge density distribution within the molecule, which agree with the enhanced conjugation length discussed previously, and clearly seen in the BLA analysis.

The static first hyperpolarizabilities were determined and TD-DFT calculations were performed in the gas-phase to give further insight of the electronic transitions responsible for the hyperpolarizabilities of the complexes. No solvatated calculations were performed since the complexes were not enough stable in solution in order to measure their hyperpolarizabilites. For the same reason, β_{HRS} was not calculated. The presented results will be discussed simply as trends, and relevant experimental results will be addressed for comparison only when necessary.

The relevant results of the TD-DFT calculations for the oxidized species have been listed in **Table 2.15**. The estimated hyperpolarizabilities were also included.

Table 2.15: β_{tot} and relevant TD-DFT results for **L1**^{ox}, ^{M}**1Fe**^{ox}, ^{M}**1aRu**^{ox} and ^{M}**1bRu**^{ox}

Compound	Functional	λ_{max} (nm)	E$_{eg}$(eV)	f	Major Contributions	β_{tot} ($\times 10^{-30}$ esu)	$\frac{\beta^{ox}_{tot}}{\beta_{tot}}$
L1^{ox}	B3LYP	582	2.13	0.2218	βH-1→βL (47%);βH→βL (26%)	41.93	1.04
		581	2.18	0.2218	βH-1→βL (46%); βH→βL (26%)		
		568	2.18	0.3603	βH-1→βL (33%); βH→βL (33%)		
	CAM-B3LYP	547	2.27	0.6261	βH→βL(63%); αH→αL (14%)	53.38	1.77
	M06	575	2.16	0.3836	βH→βL (46%);βH-1→βL (20%)	44.32	1.20
		562	2.18	0.1735	βH-2→βL (25%); βH-1→βL (46%)		
^{M}**1Fe**^{ox}	B3LYP	1492	0.83	0.3207	β→βL (91%)	7268.15	216.70
		863	1.44	0.2410	βH→βL (72%)		
		582	1.44	0.1776	βH-4→βL (51%); βH-2→βL (16%)		
		509	1.44	0.1555	βH-6→βL (21%); βH-5→βL (48%)		
	CAM-B3LYP	633	1.96	0.6068	β→βL (57%)	622.67	5.47
		546	2.28	0.2651	βH-2→βL (48%)		
	M06	1365	0.91	0.2801	β→βL (85%)	4090.95	82.76
		842	1.48	0.2811	αH→αL (62%)		
		699	1.48	0.1200	βH-1→βL+4 (25%); βH→βL (19%)		
		583	2.13	0.2955	βH-3→βL (27%);αH→αL (17%)		
^{M}**1aRu**^{ox}	B3LYP	1222	1.02	0.2121	βH→βL (86%)	2120.27	67.27
		852	1.46	0.3876	αH→αL (63%)		
		618	2.01	0.2203	αH-1→αL (63%);βH-3→βL (21%)		
		518	2.01	0.1025	βH-4→βL (51%);βH→βL+1 (24%)		
	CAM-B3LYP	675	1.84	0.6324	βH→βL (61%)	874.41	8.27
		546	2.28	0.3040	βH-3→βL (53%)		
	M06	1202	1.03	0.2114	βH→βL (87%)	2134.89	37.41
		850	1.46	0.3401	αH→αL (53%)		
		615	2.02	0.2423	αH→αL (29%);βH-3→βL (22%)		
		572	2.02	0.1151	βH-3→βL (25%); βH→βL (35%)		
^{M}**1bRu**^{ox}	B3LYP	1105	2.13	0.1511	βH→βL (82%)	1695.16	27.31
		839	2.18	0.3460	αH→αL (60%)		
		613	2.18	0.2447	βH-3→βL (52%)		
	CAM-B3LYP	609	2.27	0.6711	βH→βL(59%)	508.77	5.38
		546	2.27	0.2147	βH-3→βL(52%)		
	M06	1074	2.13	0.1341	βH→βL (84%)	1538.20	21.56
		827	2.18	0.1177	βH-1→βL (63%)		
		762	2.18	0.1006	βH-2→βL (85%)		
		605	2.18	0.2073	βH-3→βL (45%); βH-4→βL (28%)		

The main optical feature for all oxidized molecules is the presence of low energy electronic transitions attributed to HOMO→LUMO charge transfers. The significant molecular orbitals for ^{M}**L1**^{ox}, ^{M}**1Fe**^{ox}, ^{M}**1aRu**^{ox} and ^{M}**1bRu**^{ox}, obtained using CAM-B3LYP, are depicted in **Figure 2.16**. No significant differences were found for the same orbitals using B3LYP and M06 functionals.

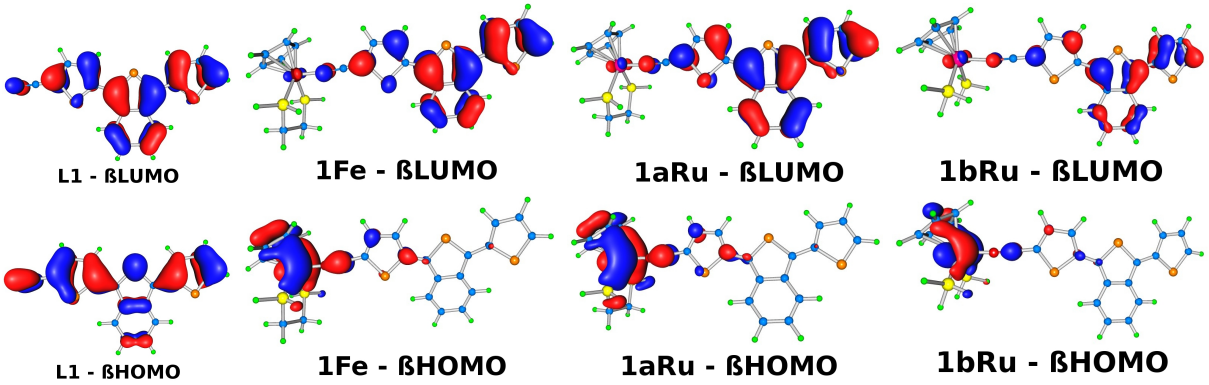

Figure 2.16: βHOMO and βLUMO molecular orbitals involved in the dominant optical transitions of **L1**^{ox}, ^{M}**1Fe**^{ox}, **1aRuL1**^{ox} and **1bRuL1**^{ox} using CAM-B3LYP. (contour: 0.03 au)

For **L1**^{ox}, the charge transfer associated to the βHOMO→ βLUMO transition mainly arises from the side thienyl rings (T1 and T3) to the benzo[c]thiophene group. For oxidized organometallic complexes, it is clearly seen that βHOMO orbitals are located in the organometallic moiety and βLUMO orbitals are spread over the ligand. Therefore, βHOMO→βLUMO transitions can be assigned to MLCT. As discussed above, HOMO→LUMO excitations of ^{M}**1Fe**, ^{M}**1aRu** and ^{M}**1bRu** were assigned as an ILCT since both HOMO and LUMO clearly have ligand character. Consequently, the βHOMO→ βLUMO transition of the oxidized organometallic complexes lead to an effective charge transfer from the organometallic moiety to the ligand. This feature is supported by the almost linear M-N≡C1-C2 geometry, which favours metal-to-ligand π-backdonation interaction, and a more effective conjugation length observed upon oxidation. In fact, the most significant optical changes upon one-electron oxidation are a strong red shift of the main electronic transitions and a decrease of the corresponding oscillator strength, as clearly seen in **Figure 2.17** that depicts the TD-DFT spectra for all the oxidized molecules .

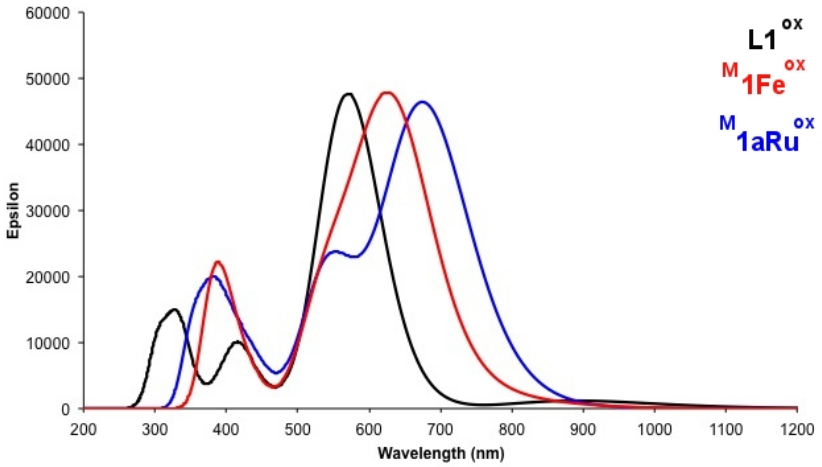

Figure 2.17: Calculated optical spectra for $\mathbf{L1}^{ox}$ and ${}^{M}\mathbf{1Fe}^{ox}$ and ${}^{M}\mathbf{1aRu}^{ox}$ using CAM-B3LYP.

The red shift of the lowest energy band upon oxidation was also observed experimentally, as discussed above. In fact, the TD-DFT results clearly predicts the overall trend for both the ligand and the organometallic complexes, in particular using the B3LYP and M06 functionals, for which the NIR transitions are observed with modestly accurate results. CAM-B3LYP, in its turn, predicts these NIR transitions with almost neglegible oscillator strength, and for that reason they were not included in the previous **Table 2.15**.

According to the TLM, the overall effect of the optical data should lead to an increase of the NLO response upon oxidation for all molecules, in particular for organometallic complexes. The calculated β_{tot} are, in fact, in agreement with those expected trends (*cf* **Table 2.15**). For instance, using CAM-B3LYP, the transition energies of major molecular orbital transitions decrease in the following order: $\mathbf{L1}^{ox} > {}^{M}\mathbf{1bRu}^{ox} > {}^{M}\mathbf{1Fe}^{ox} > {}^{M}\mathbf{1aRu}^{ox}$ and no significant differences on the corresponding oscillator strength is observed. Thus, β_{tot} increases as follows: $\mathbf{L1}^{ox} <<< {}^{M}\mathbf{1bRu}^{ox} < {}^{M}\mathbf{1Fe}^{ox} < {}^{M}\mathbf{1aRu}^{ox}$. According to CAM-B3LYP results, the ${}^{M}\mathbf{1aRu}^{ox}$ complex seems to be the better candidate for NLO switching through an oxidation stimulus. In fact, β_{tot} of ${}^{M}\mathbf{1aRu}^{ox}$ enhances 8.27 times relatively to ${}^{M}\mathbf{1aRu}$ whereas β_{tot} of ${}^{M}\mathbf{1Fe}^{ox}$ and ${}^{M}\mathbf{1bRu}^{ox}$ increase 5.47 and 5.38 times relatively to ${}^{M}\mathbf{1Fe}$ and ${}^{M}\mathbf{1bRu}$, respectively. Nevertheless, B3LYP and M06 give opposite results, in the sense that the iron complex seems to be the better candi-

date for NLO switching through an oxidation stimulus. In addition, these functionals predict a much larger enhancement of β_{tot} upon oxidation comparing with that obtained with CAM-B3LYP. As mentioned above, these values seem to be overestimated since they arise from the unexpected very low energies of βHOMO→βLUMO transition, in the NIR region. It is well known that the B3LYP functional, with low percentage of HF orbital exchange, can overestimate molecular hyperpolarizabilities, in particular for large conjugated molecules. The reason is related to the self-interaction error in the exchange part of the density functional[114–116], which is responsible for over-delocalization of the electron density. This result in incorrect screening of the external electric field[117] and incorrect description of the charge transfer processes[118] often leading to an underestimation of the energies of excitations with a long-range spatial extent.[89,119] The M06 functional, more suitable for applications in transition metal chemistry, has a fixed percentage of HF exchange (as B3LYP) and similar deviations than the observed using B3LYP functional could be observed. In the case of oxidized complexes, βHOMO→βLUMO transitions can be clearly assigned to MLCT. Thus, a charge transfer from a low energy occupied orbital (centred in the organometallic fragment) to a virtual unoccupied orbital located in another part of the molecule (thienyl moiety) result in a charge separation. Therefore, a coulombic interaction within this charge separated excited stated should be taken into account, in terms of an attractive 1/R dependence. CAM-B3LYP, which contains long-range corrected eects using the Coulomb-attenuating method, can overcome (at least partially) this problem since corrects the potential energy curves of the charge transfer state along the orbital separation coordinate, resulting in a better description of the mentioned excited state, and hence a better estimation of the charge transfer energy. Thus, the hyperpolarizabilities obtained with B3LYP and M06 functionals are consistent with the underestimation of the charge transfer energies, and are by far an overestimation of such property for the organometallic oxidized molecules.

The fact that oxidation leads to improved hyperpolarizabilities should be commented here. Most of the metal-organic compounds studied for SONLO switching are typically *push-pull* systems in which the metal centre acts as an electron-donor group in a dipolar D-π-A structure. According to the well-known Type I switching mechanism, upon oxidation the donor becomes a competing acceptor moiety thus leading to lower hyperpolarizability. In the case of the present molecules, with a more likely less studied D-π-D' feature, the oxidation leads to the achievement of a D-π-A structure and, hence, an expected

increase on the corresponding quadratic hyperpolarizability. The electronic behaviour of the thiophene ring farthest from the N≡C group, and benzo[c]thiophene moiety is reversed upon oxidation, behaving as a donor in non-oxidized species and electron-acceptor in the oxidized form. Thus, the charge transfer in the oxidized molecules resembles the behavior found in the classic picture of the metal as donor and a ligand with an acceptor moiety. Some examples of improved hyperpolarizabilities upon oxidation are found in the literature.[120]

DFT calculations in the reduced forms of the present complexes were also performed. The β_{tot} static first hyperpolarizabilities for the reduced species were determined and TD-DFT calculations were performed in the gas-phase in order to evaluate the electronic properties of the reduced compounds. The relevant TD-DFT results and the estimated first hyperpolarizabilities for all the compounds are listed in **Table 2.16**.

Table 2.16: β_{tot} and relevant TD-DFT results for $\mathbf{L}^{red}$, $^{M}\mathbf{1Fe}^{red}$, $^{M}\mathbf{1aRu}^{red}$ and $^{M}\mathbf{1bRu}^{red}$

Compound	Functional	λ_{max} (nm)	E_{eg}(eV)	f	Major Contributions	β_{tot}	$\frac{\beta^{red}_{tot}}{\beta_{tot}}$
$\mathbf{L1}^{red}$	B3LYP	957	—	0.0321	αH→αL (26%);βH→βL (73%)	45.78	1.15
		663	—-	0.4306	αH→αL (62%); β→βL (21%)		
		576	—-	0.1769	αH→αL (73%)		
	CAM-B3LYP	870	—	0.0815	αH→αL (18%);βH→βL (82%)	92.69	3.08
		635	—-	0.4883	αH→αL (67%); β→βL (12%)		
		521	—-	0.1357	αH→αL (50%); β→βL+2 (15%)		
	M06	954	—	0.0379	αH→αL+2 (23%);βH→βL (75%)	58.18	1.50
		666	—-	0.4321	αH→αL+2 (66%); β→βL (19%)		
		570	—-	0.1472	αH→αL+6 (71%)		
$^{M}\mathbf{1Fe}^{red}$	B3LYP	815	1.52	0.1988	αH→αL+1 (22%); βH→βL (36%)	582.14	17.36
		656	—	0.421	αH-9→αL+1 (11%); βH-8→βL+2 (16%)		
		634	—	0.2449	αH→αL+3 (38%); βH→βL (17%)		
		547	2.27	0.1903	αH-1→αL+1 (21%); βH→βL+2 (11%); βH→βL+4 (11%)		
	CAM-B3LYP	608	2.04	0.5655	αH→αL+2 (17%); βH→βL (33%)	99.11	0.87
		583	2.59	0.1481	αH-5→αL+1 (10%); βH-5→βL+2 (11%); βH→βL (14%)		
		479	2.59	0.2827	αH-1→αL+2 (10%); βH→βL+2 (15%); βH→βL+3 (11%)		
	M06	693	2.04	0.1974	αH→αL+2 (54%); βH→βL (19%)	336.85	6.81
		612	2.59	0.1561	αH→αL+3 (28%); αH→αL+5 (18%); βH→βL (11%)		
		538	2.59	0.1015	αH-4→αL (11%); αH-1→αL (14%)		
$^{M}\mathbf{1aRu}^{red}$	B3LYP	785	1.58	0.3333	αH→αL (19%); βH→βL (49%)	499.44	15.85
		631	1.97	0.2114	αH→αL+2 (64%); βH→βL (13%)		
		606	2.05	0.3009	αH→αL+3 (28%);βH→βL (14%)		
	CAM-B3LYP	617	1.03	0.7021	αH→αL (21%); βH→βL (54%)	45.06	0.42
		529	1.46	0.1001	αH-2→αL (11%); αH→αL+4 (11%)		
		482	2.02	0.1378	αH→αL (15%)		
	M06	755	1.03	0.2580	αH→αL (26%); αH→αL+5 (21%); βH→βL (42%)	278.87	4.89
		665	1.46	0.1301	αH→αL+2 (76%); βH→βL (10%)		
		606	2.02	0.2181	αH→αL+5 (51%);βH→βL (15%)		
		573	2.02	0.1502	αH-1→αL (14%);βH→βL+1 (38%)		
$^{M}\mathbf{1bRu}^{red}$	B3LYP	1173	—	0.1109	αH→αL (78%);βH→βL (14%)	887.85	14.3
		802	—-	0.3040	αH→αL+2 (19%); αH→αL (10%); βH→βL (52%)		
		628	—-	0.4830	αH→αL+2 (48%); βH→βL (26%)		
	CAM-B3LYP	1104	....	0.0841	αH→αL (70%); βH→βL (17%)	83.00	0.88
		784	—-	0.3277	αH→αL+2 (11%); αH→αL (12%); βH→βL (53%)		
		616	—-	0.4835	αH→αL+2 (30%); αH→αL+3 (20%); βH→βL (25%)		
	M06	1004	—	0.0589	αH→αL (66%); βH→βL(21%)	278.68	3.91
		755	—-	0.2582	αH→αL (26%); αH→αL+5 (14%); βH→βL (42%)		
		665	—-	0.1301	αH→αL+2 (76%); βH→βL (10%)		
		607	—-	0.2179	αH→αL+5 (51%); βH→βL (15%)		
		573	—-	0.1507	αH-1→αL (14%); βH→βL+1 (30%)		

Like in the case of the former discussed oxidized species, the main optical feature for all the reduced molecules is the presence of low energy electronic transitions attributed to HOMO→LUMO charge transfers. In **Figure2.18** are depicted the TD-DFT spectra obtained with CAM-B3LYP for $\mathbf{L1}^{red}$, ${}^{M}\mathbf{1Fe}^{red}$, ${}^{M}\mathbf{1aRu}^{red}$ and ${}^{M}\mathbf{1bRu}^{red}$.

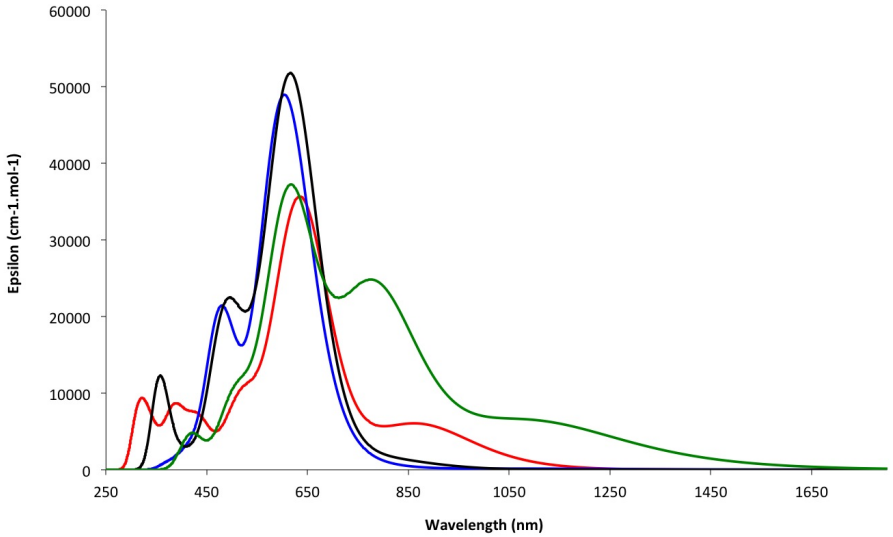

Figure 2.18: Calculated optical spectra for ${}^{M}\mathbf{L1}^{red}$ (-), ${}^{M}\mathbf{1Fe}^{red}$ (-), ${}^{M}\mathbf{1aRu}^{red}$ (-) and ${}^{M}\mathbf{1bRu}^{red}$ (-)

Compared to the parent non-oxidized/reduced compounds, and similarly to the oxidized species, a red-shift of the main optical transitions and a decrease in the corresponding oscillator strength is observed. It is also clear that two distinct behaviours are obtained. On one side, the ligand $\mathbf{L}^{red}$ and the ${}^{M}\mathbf{1bRu}^{red}$ complex are characterized by two low lying electronic transitions, one occurring in the NIR region and the second in the visible region. Both of these transitions are associated to a βHOMO→ βLUMO transition for the case of the ligand and αHOMO→ αLUMO transition for the case of the ${}^{M}\mathbf{1bRu}^{red}$ complex . The CAM-B3LYP molecular orbitals involved in these transitions are shown in **Figure 2.19**. No significant differences were found for the same orbitals using B3LYP and M06 functionals.

The lowest energy transfer for the $\mathbf{L}^{red}$ is, hence, attributed to a $\pi - \pi^{\star}$ transition that is fully delocalized over the entire molecule, whereas the lower transition of the ${}^{M}\mathbf{1bRu}^{red}$ complex is attributed to LMCT, mainly arising from the B and T1 rings to the organometallic fragment. For the second transition, the molecular orbitals show

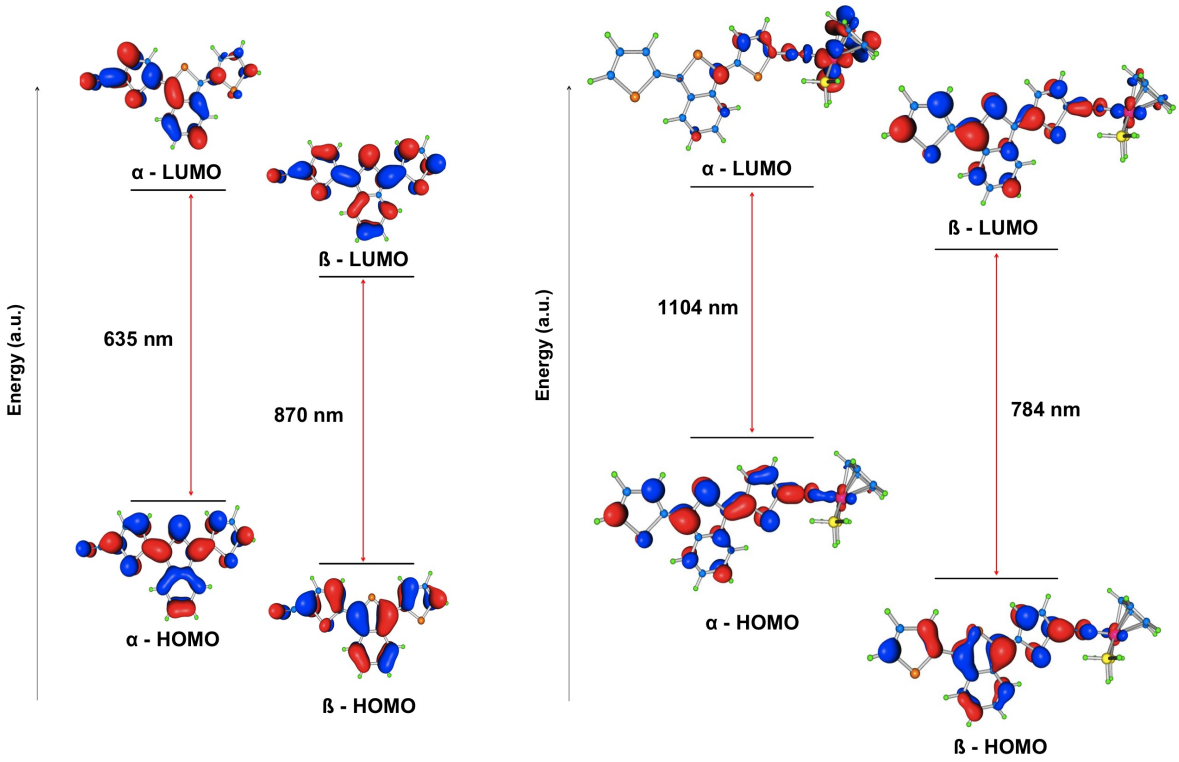

Figure 2.19: CAM-B3LYP molecular orbital for $\mathbf{L1}^{red}$ and ${}^{M}\mathbf{1bRu}^{red}$ involved in the two lower energy transitions. (contour: 0.03 au)

that, in the case of the ligand, the transition results mainly of a charge transfer to the T1 and acceptor group (N≡C). In the case of the ruthenium complex, this transition is mainly attributed to a $\pi - \pi^{\star}$ ILCT with some contribution of the organometallic fragment (LMCT). In accordance with the TLM, the presence of this low lying LMCT should increase the hyperpolarizability of this complex.

On the other hand, the ${}^{M}\mathbf{1Fe}^{red}$ and ${}^{M}\mathbf{1aRu}^{red}$ complexes present a single low energy transition that is also attributed to HOMO → LUMO transitions. However, for ${}^{M}\mathbf{1Fe}^{red}$, additional contribution of a αHOMO→αL+1 or αHOMO→$\alpha-$L+2 (depending on the used functional) is also observed. The relevant CAM-B3LYP molecular orbitals for this transition for these two complexes are shown in **Figure 2.20**. No significant differences were found for the same orbitals using B3LYP and M06 functionals.

According to the orbital densities, the lower-energy electronic transition of the ${}^{M}\mathbf{1Fe}^{red}$ and ${}^{M}\mathbf{1aRu}^{red}$ organometallic complexes can be mainly assigned to an ILCT with a

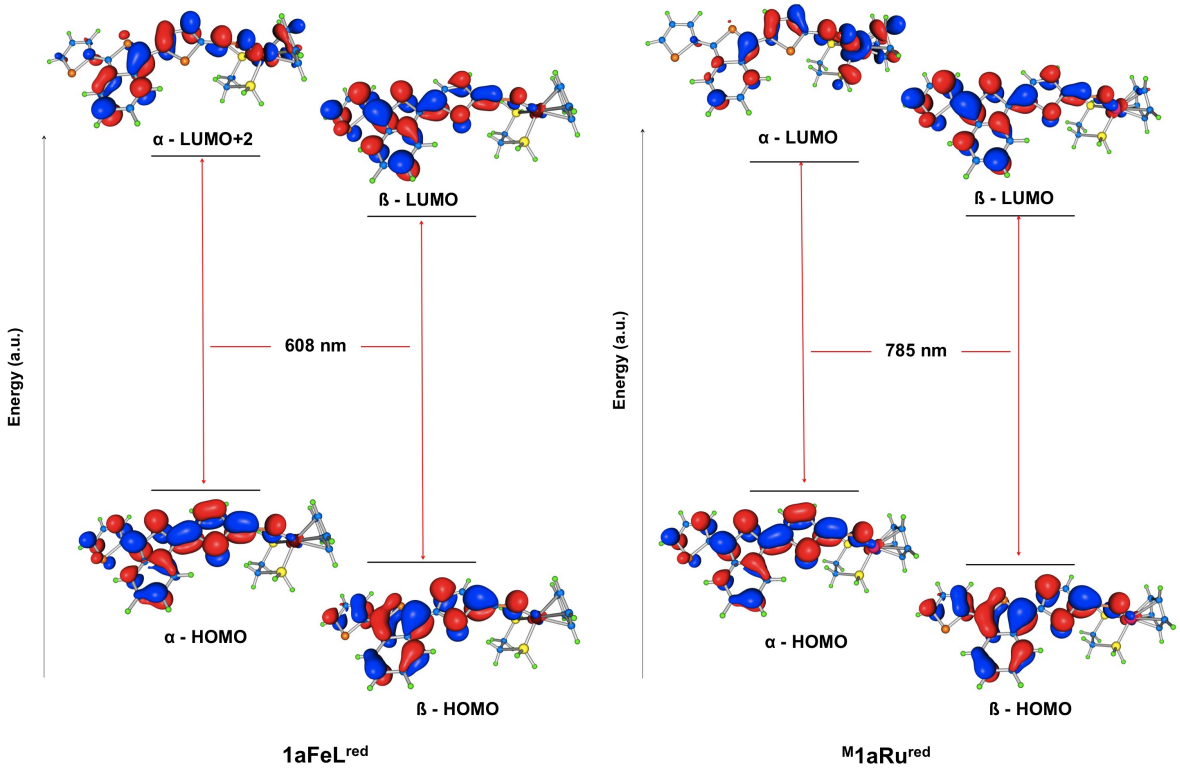

Figure 2.20: CAM-B3LYP molecular orbital for ^{M}**L1**^{red} and ^{M}**1bRu**^{red} involved in the two lower energy transitions.(contour: 0.03 au)

contribution of LMCT. Contrariwise to the case of **L1**^{red} and ^{M}**1bRu**^{red}, where, each βHOMO$\rightarrow$ βLUMO and αHOMO$\rightarrow$ αLUMO transitions gave rise to a discrete transition, the lowest energy transition for ^{M}**1Fe**^{red} and ^{M}**1aRu**^{red} result of a superposition in the α and β transitions.

The behaviour of the estimated hyperpolarizabilities for the organometallic complexes is somewhat similar to that found for the oxidation stimulus, that is, a strong enhancement of the estimated hyperpolarizabilities are observed when the molecules are reduced. When considering the results obtained with B3LYP and M06 functionals, β_{tot} clearly increases upon reduction, in particular for organometallic complexes. However, for the CAM-B3LYP β_{tot} functional the first hyperpolarizabilities diminish upon reduction, contrary to what occurred for the oxidative counterpart. For this functional, the role played by the organometallic moiety on the first hyperpolarizability is less significant than the observed for oxidized species. In fact, the main optical transition was clearly assigned

to MLCT with a favourable geometry for metal-ligand interaction for all the oxidized species. However, only some contribution of a LMCT is observed for ^{M}**1Fe**^{red}, ^{M}**1aRu**^{red} and ^{M}**1bRu**^{red}. Indeed, the character and energies of these transitions are close to those found for **L**^{red}. Also, the M-N≡C1 angle largely deviates from linearity, which does not lead to a favourable metal-ligand -interaction in ground state. As a result, the values of first hyperpolarizabilities of the reduced organometallic complexes are lower than the first hyperpolarizabilities of the ligand, using CAM-B3LYP.

Comparing the CAM-B3LYP functional to B3LYP and M06 functionals, it is show that the latter predict a transition energy of 1.52 eV and 1.79 eV, respectively, for ^{M}**1Fe**^{red}, whereas the first predicts an energy of 2.04 eV. The main reason seems to be the underestimation of the main optical transition energies when B3LYP and M06 functional were used, as was discussed for the oxidized molecules. Furthermore, the character of the optical transition seems also to play a role, and the differences in the optical transition involving α orbitals can justify the huge difference in the hyperpolarizability results. Using B3LYP, the αL+1 orbital has a higher contribution of the organometallic moiety when compared to the αL+2 obtained with CAM-B3LYP. Thus, an enhanced contribution of LMCT is observed with B3LYP, which could lead to higher hyperpolarizabilities. The predicted energies of the main electronic transition using B3LYP and M06 for reduced species, in the range of 1.52-1.79 eV, are significantly higher than those obtained in oxidized molecules (0.83-1.03 eV) and, consequently, closer to the values found when using CAM-B3LYP functional. As mentioned above, for reduced species, the main electronic transitions can be assigned to ILCT with some contribution of LMCT. Therefore, when compared to the oxidized species, lower charge separation results from the excitations. Thus, it is expected that B3LYP and M06 functionals could give less unrealistic results.

Summarizing, the results for the hyperpolarizabilities show that β_{tot}: a) are dominated by β_{xxx} tensor; b) are functional-dependent and; c) indicate a clear dependence on NLO responses from the redox stimulus. In particular, the oxidation of organometallic complexes significantly enhances second-order hyperpolarizabilities: β_{tot} of ^{M}**1Fe**^{ox} enhances up to 217 times relatively to ^{M}**1Fe**, β_{tot} of ^{M}**1aRu**^{ox} enhances up to 67 times relatively to ^{M}**1aRu** and β_{tot} for ^{M}**1bRu**^{ox} enhances up to 27 times comparatively to ^{M}**1bRu**, depending on the used functional. Instead, the oxidation of **L** gives only moderate enhancing effect on β_{tot}. Reduction of the studied molecules originates some subtle results. As in the oxidation process, the reduction of **L** leads to a moderate enhancing effect on

β_{tot}, although the increase of β_{tot} is now slightly higher. For organometallic complexes, the use of different functionals originates contradictory results. By using B3LYP and M06 functionals, an increase on β_{tot} is observed, although more moderate than observed with the oxidation process: β_{tot} of $^{M}\mathbf{1Fe}^{red}$, $^{M}\mathbf{1aRu}^{red}$ and $^{M}\mathbf{1bRu}^{red}$ enhances up to 14 - 17 times relatively to the corresponding non-reduced counterparts, depending on the functional used. However, by using CAM-B3LYP, β_{tot} decreases upon reduction, in particular for the$^{M}\mathbf{1aRu}^{red}$ complex. The β_{tot} of oxidized and reduced species, in particular for organometallic complexes, using B3LYP and M06 functionals seem to be not reasonably. In fact, these values appear to be largely overestimated since they arise from the unexpected and unrealistic low-energy charge transfer transitions, especially for oxidized species.

2.5 Conclusion

This chapter dealt with the syntesis and DFT studies of new (η^5-C_5H_5)-iron(II) and ruthenium(II) complexes containing the 5-(3-(thiophen-2-yl)benzo[c] thiophen-1-yl) thiophene-2-carbonitrile ligand. Three new complexes have been synthesized and fully characterized, and their quadratic hyperpolarizabilities have been determined by HRS measurements at 1500 nm. Density Functional Theory and Time-Dependent Density Functional Theory calculations were employed to achieve a deeper knowledge of the relevant structural and electronic transitions involved, which was helpful in the discussion of the experimental quadratic hyperpolarizabilities.

The organometallic complexes presented resonant enhanced hyperpolarizabilities values in the range of 105 - 164 $\times 10^{-30}$ esu. Application of the two-level-model, allowed to obtain corrected values in the range of 57 - 87 $\times 10^{-30}$ esu. The nonlinear optical properties were also computed using DFT calculations. The calculation results, together with TD-DFT data, showed that TLM could be applied in the rationalization of the experimental NLO properties of the studied complexes. The observed quadratic hyperpolarizabilities, almost similar for all complexes, could be explained due to the very similar energies and intensities of the lowest-energy electronic transition that show to have mainly an ILCT character. The use of real and model phosphanes to simulate electronic spectra of the complexes using DFT calculations shows no significant differences on the calculated energies when compared to experimental data. Therefore, the use of model phosphanes, with

the obvious gain in computational cost, proves to be a good compromise between accuracy on the predicted excitation energies and the computational effort. However, the results show that the use of real phosphanes in DFT calculations can be important to give an additional understanding of the experimental values of the quadratic hyperpolarizabilities.

Concerning the NLO switching abilities of the complexes, the overall DFT and TD-DFT results show that organometallic moieties play an important role in the NLO response with respect to the redox stimulus. The calculated data using B3LYP and M06 functionals shows, in general, similar results and/or trends, in particular on structural and optical data. These functionals predicts (in an unrealistic manner) significant enhancement of second-order hyperpolarizabilities of the studied organometallic complexes through one-electron oxidation/reduction processes. CAM-B3LYP functional, however, points to a more moderate effect and opposite effects on NLO response upon oxidation and reduction. For the most of metal-containing compounds that have been studied for redox NLO switching, the changing on hyperpolarizability properties is, in fact, moderate: the largest experimental second-order NLO response (on form) is approximately 2 to 20-fold greater than the off form. Also, as indicated above, this functional seems to predict more reliable structural and optical data for the studied molecules in this work and better reproduces experimental hyperpolarizability trends upon ligand coordination in parent compounds. Thus, it is reasonable to assume that NLO response trends upon redox stimulus obtained with CAM-B3LYP functional could be more realistic. Therefore, the studied complexes can be viewed as acting as redox NLO switchable, both using oxidative or reductive stimulus. However, the NLO switching is more effective using oxidation stimulus since larger differences on $\beta_t ot$ are observed between non-oxidized and oxidized species. However, attempts to synthesize and isolate the oxidized complexes were unsucessfull and it is not possible to confirm the assumptions made by the DFT modelling studies.

2.6 Experimental

Synthesis of the ligands were performed in standard conditions, unless otherwise stated. Commercial reagents were used as received and without further purification. Compounds 1 - 3 were prepared following published procedures with some modifications (see details below).[45] 5-(3-Thiophen-2-yl-benzo[c]thiophen-1-yl)thiophene-2-carbaldehyde (4) was pre-

pared following a published procedure with a different purification method.[58] All synthesis involving organometallic complexes, including the Grignard reactions, were carried out under nitrogen atmosphere using current Schlenk techniques. The details of the synthesis of the starting organometallic complexes and the characterization methods are described in **Chapter 5**.

2.6.1 Synthesis

2.6.1.1 Attemps of synthesis of *o*-aryl-benzoic acids

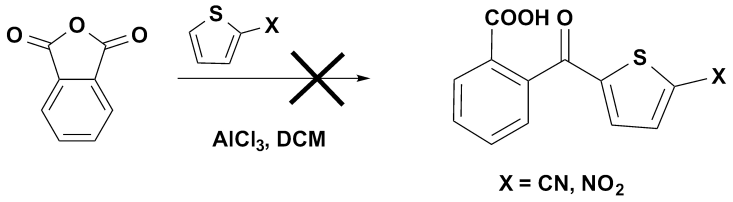

In a typical procedure, a suspension of anhydrous aluminium chloride (1.8 g, 1.35 mmol) and phthalic anhydride (1 g, 0.67 mmol) in dry CH_2Cl_2 (50 mL) was stirred for 0.5 hrs at room temperature. A dichloromethane solution of the corresponding thiophene derivative (0.74 mmol in 10 mL) was then slowly added dropwise (10 minutes). The resulting dark brown coloured reaction mixture was stirred for 4 h at room temperature, then poured into ice water containing a 20 % hydrochloric acid solution. The organic layer was separated and dried over anhydrous magnesium sulphate. Removal of the solvent in vacuum afforded brownish yellow powders that were analized by NMR spectroscopy. Results revealed a complex mixture of products with a considerable amount of the desired product. Attempts to purify the products by column chromatography (silica gel, dichloromethane:petroleum spirit (1:1) and recrystalization techniques were not successful.

2.6.1.2 Attemps of synthesis of lactones

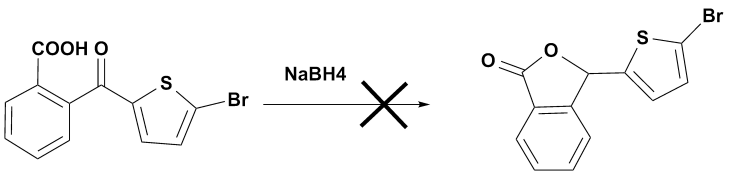

A hot solution of 2-bromothenoylbenzoic acid was added to an aqueous solution of sodium bicarbonate (15.9 g in 2 L of H_2O) and was treated with $NaBH_4$ (15 eqs.) in portions. After standing overnight, it was heated for 1 hr and was allowed to cool to room temperature. A 12% aqueous hydrochloric acid solution was added cautiously until the pH reach 2. The mixture was then stirred for 2 h at room temperature, and the precipitated solid was filtered and analysed by NMR spectroscopy showing only traces of the desired product. In a different attempts, the bicarbonate solution was substituted by a THF-MeOH (2:5) solution or by a aqueous sodium hydroxide solution at pH=9. No improvements were achieved.

2.6.2 S,S-Di(pyridin-2-yl)benzene-1,2-bis(carbothioate) (1)

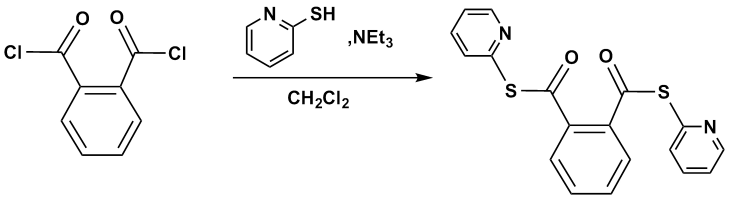

To 50 mL of freshly dried THF were added 5 mL of triethylamine and 3.3 g of 2-mercaptopyridine (30 mmol). After stirring for 10 minutes full dissolution of the 2-mercaptopyridine was observed, the mixture was placed in an iced cold bath and stirred at 0 °C for further 15 min. A solution of phthalic acid chloride (2.2 mL, 15 mmol) in dried THF (50 mL) was added at once and with vigorous stirring. The reaction was quenched immediately with 200 mL of 2 % HCl (aq) solution and extracted with chloroform. The combined organic fractions were washed with 10% NaOH (aq.) and water until neutrality,

dried over anhydrous $MgSO_4$, and the solvent was evaporated in vacuum. Crystallization from $CHCl_3$/diethyl ether afforded the desired product as white crystal needles in 80% yield. ^{1}H NMR (400 MHz, $CHCl_3$, 25 °C): 7.24 (dt, 2H, Hpy), 7.59 (m, 2H, Hbenz), 7.71 (m, 4H, Hpy), 7.82 (m, 2H, Hbenz), 8.57 (d, 2H, Hpy) ppm.

2.6.2.1 1,2-Phenylenebis(thiophen-2-yl)methanone (2)

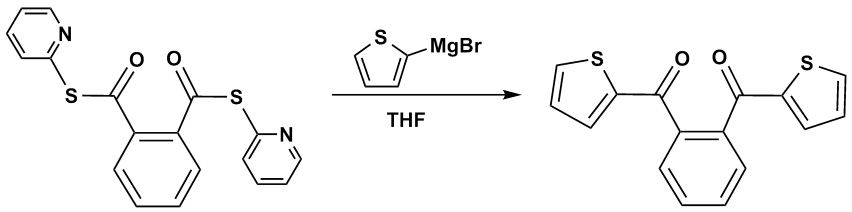

In a Schlenk flask containing THF (100 mL), activated magnesium turnings (1.2 g, 46 mmol) and a catalytic amount of iodine were added followed by 2-bromothiophene (4.5 mL, 46 mmol). The mixture was heated to a gentle reflux for 3 hrs. until complete reaction of the magnesium and then left to cool at room temperature. The Grignard solution was added dropwise through a Teflon cannula to a stirred solution of **1** (7.95 g, 23 mmol) in THF (150 mL) at 0 °C. The resulting mixture was stirred for additional 30 min. and quenched with 200 mL of 5% hydrochloric acid aqueous solution. After extraction with several portions of chloroform, the combined organic extract were washed with a 10% sodium hydroxide aqueous solution, followed by a saturated $NaHCO_3$ solution and, finally, water. After drying with anhydrous $MgSO_4$, the solvent was removed in vacuum. Crystallization from $CHCl_3$/petroleum ether 40-60 afforded a brownish orange solid in 90% yield. ^{1}H NMR (400 MHz, $(CD_3)_2CO$, 25 °C): 7.19 (dt, 2H, Hth), 7.59 (dd, 2H, Hth), 7.78 (m, 2H, Hbenz), 7.83 (m, 2H, Hbenz), 7.97 (dd, 2H, Hth) ppm.

2.6.3 1,3-Di(thiophen-2-yl)benzo[*c*]thiophene (3)

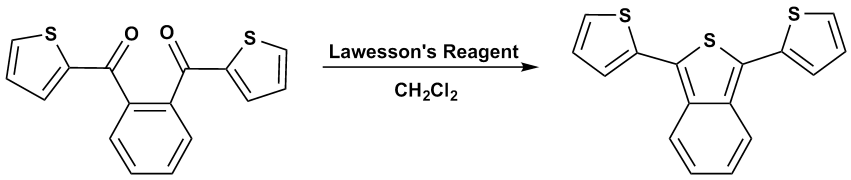

Lawessons reagent (8.13 g, 20.1 mmol) was added in two portions to a solution of **2** (6.0 g, 20.1 mmol) in 100 mL of dichloromethane. After stirring overnight, the solvent was removed under vacuum, and 100 mL of ethanol was added. This new solution was stirred with heating for 30 min. The solvent was removed and the brown residue was added to dichloromethane, washed with 10 % sodium hydroxide aqueous solution and several times with water. After drying with anhydrous $MgSO_4$ and filtered, the solvent was evaporated in vacuum and the resultant brownish orange solid was then chromatographed on silica gel. Elution with petroleum spirit (40-60) afforded the desired product as orange crystals in 55% yield. ^{1}H NMR (400 MHz, $(CD_3)_2CO$, 25 °C): 7.26 (m, 2H, Hth), 7.51 (dd, 2H, Hth), 7.64 (dd, 2H, Hth), 8.00 (m, 2H, Hbenz) ppm.

2.6.3.1 5-(3-(Thiophen-2-yl)benzo[c]thiophen-1-yl)thiophene-2- carbaldehyde (4)

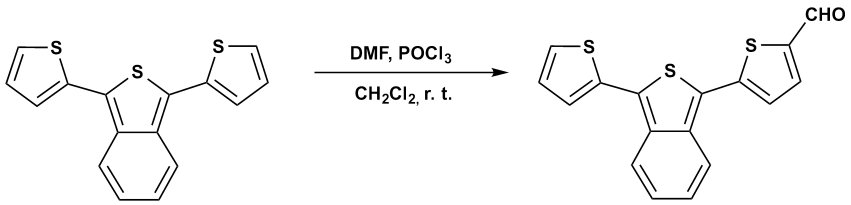

A mixture of phosphorus oxychloride (2.42 mL, 26 mmol) and DMF (2 mL, 26 mmol) in dichloromethane (10 mL) was added to a solution of **3** (1.55 g, 5.2 mmol) in dichloromethane (50 mL) at room temperature. After stirring overnight, a saturated solution of sodium acetate (100 mL) was added and stirred for 1 hr. to complete the hydrolysis. The suspension formed was extracted with dichloromethane. The combined organic layers were

washed with water, dried over anhydrous magnesium sulphate and the solvent was removed in vacuum. The red solid obtained was chromatographed on silica gel. Elution with petroleum ether 40-60/diethyl ether 7:3 to petroleum ether 40-60/diethyl ether 1:1 afforded the desired product as red crystals in 80% yield. ^{1}H NMR (400 MHz, $(CD_3)_2CO$, 25 °C): 7.26 (m, 2H, H2), 7.51 (dd, 2H, H3), 7.64 (dd, 2H, H1), 8.00 (m, 2H, H4, H5) ppm.

2.6.4 5-(3-(Thiophen-2-yl)benzo[c]thiophen-1-yl)thiophene-2- carbonitrile (L1)

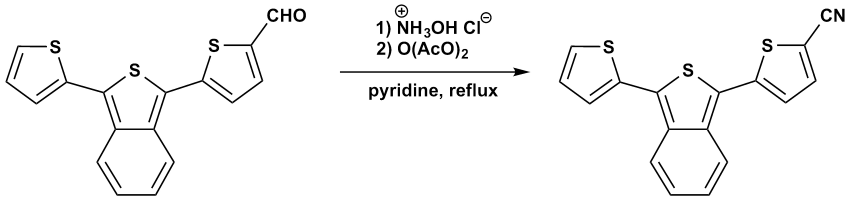

A solution of H_2NOH-HCl (2.13 g, 30.7 mmol) in pyridine (10 mL) was added to a stirred solution of **4** (2.0 g, 6.13 mmol) in pyridine (30 mL) at 0°C. The reaction was allowed to reach the room temperature. After stirring for 1 hr., acetic anhydride (5 mL) was added dropwise and the mixture was refluxed for 2 hr.. After cooling to room temperature, the mixture was poured into a mixture of ice containing 10 % of an aqueous hydrochloric acid solution. The obtained orange precipitate was dissolved in dichloromethane, washed with water and dried over anhydrous magnesium sulphate. The solvent was removed in vacuum and the crude product was purified by column chromatography on silica gel. Elution with solvent gradient from petroleum ether 40-60/diethyl ether 7:3 to petroleum ether 40-60/diethyl ether 1:1 afforded the desired product as an orange solid in 72 % yield.

FTIR: ν(KBr)/cm^{-1}: 2203 (N≡C).

^{1}H-NMR (400 MHz, $(CD_3)_2CO$, 25 °C): 7.27 (dd, $^3J_{H,H}$=3.7 and 5.3 Hz, 1H, H16), 7.30 (ddd, $^3J_{H,H}$=1.0, 6.7 and 8.8 Hz, 1H, H9), 7.37 (ddt,$^3J_{H,H}$=1.2, 6.7 and 9.0 Hz, 1H, H10), 7.56 (dd, $^3J_{H,H}$=1.0 and 5.7 Hz, 1H, H17), 7.60 (d, $^3J_{H,H}$=4.1 Hz, 1H, H4), 7.71 (dd, $^3J_{H,H}$=1.0 and 3.7 Hz, 1H, H15), 7.94 (d, $^3J_{H,H}$=4.1 Hz, 1H, H3), 8.02 (d, $^3J_{H,H}$=9.0 Hz, 1H, H8), 8.05 (d, $^3J_{H,H}$=8.9 Hz, 1H, H11) ppm.

^{13}C-NMR (100 MHz, $(CD_3)_2CO$, 25 °C): 108.09 (C2), 114.56 (C1), 121.76 (C8),122.63 (C10),123.87 (C6), 126.33 (C4), 126.46 (C11), 127.66 (C15), 127.74 (C9), 128.07 (C17), 129.35 (C16), 130.57 (C13), 135.10 (C14), 136.09 (C7), 137.13 (C12), 139.93 (C3), 143.34 (C5) ppm.

UV-Vis.: ($CHCl_3$): λ_{max}/nm ($\epsilon \times 10^4$/ $M^{-1}cm^{-1}$): 452 (2.1).

Anal. calc. for L1•0.1CH_2Cl_2: C, 61.87; H, 2.79; N, 4.22; S, 28.98. Found for L1•0.1CH_2Cl_2: C, 61.81; H, 3.01; N, 3.96; S, 27.75.

2.6.5 2-((5-(3-(Thiophen-2-yl)benzo[c]thiophen-1-yl)thiophene-2-yl) methylene)malononitrile carbonitrile (L2)

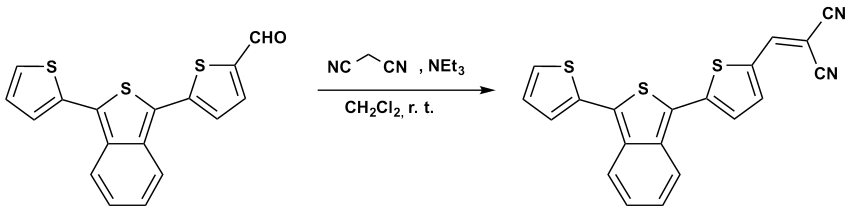

To a solution of **4** (2.13 g, 30.7 mmol) in dried dichloromethane (10 mL) was added malononitrile (2.0 g, 6.13 mmol) followed by 3 drops of dried triethylamine. The reaction was stirred at room temperature for two hours. After stirring, the mixture was poured into a mixture of ice and 10 % HCl (aq). The obtained purple precipitate was purified by column chromatography on silica gel. Elution with solvent gradient from petroleum ether 40-60/diethyl ether 7:3 to petroleum ether 40-60/diethyl ether 1:1 afforded the desired product as dark purple solid in 90 % yield.

FTIR: ν(KBr)/cm^{-1}: 2201 and 2212 (N≡C).

^{1}H-NMR (400 MHz, $(CD_3)_2CO$, 25 °C): 7.30 (dd, $^3J_{H,H}$=3.6 and 5.2 Hz, 1H, H16), 7.36 (ddd, $^3J_{H,H}$=1.0, 6.5 and 9.1 Hz, 1H, H11), 7.45 (dt, $^3J_{H,H}$=1.0, 6.5 and 8.9 Hz, 1H, H8), 7.63 (dd, $^3J_{H,H}$=1.0 and 3.6 Hz, 1H, H17), 7.74 (dd, $^3J_{H,H}$=1.1 and 5.2 Hz, 1H, H15), 7.76 (d, $^3J_{H,H}$=4.2 Hz, 1H, H4), 8.02 (d, $^3J_{H,H}$=4.3 Hz, 1H, H3), 8.10 (t, $^3J_{H,H}$=7.5 Hz, 1H, H8), 8.12 (t, $^3J_{H,H}$=7.8 Hz, 1H, H11), 8.42 (s, 1H, H_b) ppm.

^{13}C NMR (100 MHz,$(CD_3)_2CO$, 25 °C): not attributed (C6, C13), 75.54 (C_a), 115.44 (C1), 122.14 (C10),123.09 (C8), 126.85 (C4), 126.76 (C11), 128.20 (C17), 128.43 (C15), 128.61 (C9), 129.51 (C16), 131.01 (C2),134.86 (C14),136.40 (C12), 137.58 (C7), 142.25 (C3), 147.74 (C5), 151.83 (C_B) ppm.

UV-Vis.: ($CHCl_3$): λ_{max}/nm ($\epsilon\times10^4$/ $M^{-1}cm^{-1}$): 563 (4.1).

2.6.6 General procedure for the $[(\eta^5\text{-}C_5H_5)M(LL)L1]PF_6$ complexes

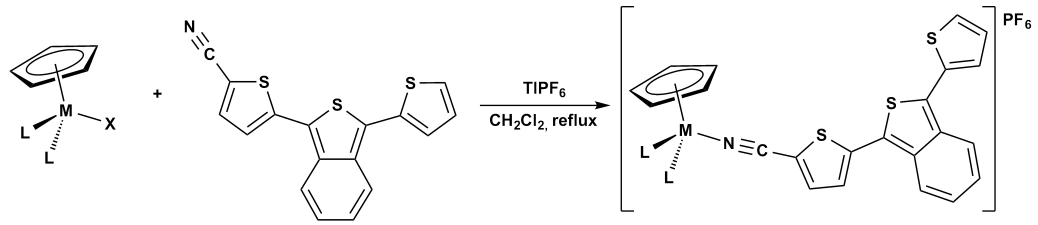

M= Fe, LL= DPPE, X= I
M=Ru, LL= DPPE or 2 PPh_3, X= Cl

The complexes were synthesized by halogen abstraction of the organometallic precursors in a Schlenk tube. A mixture of $[M(\eta^5\text{-}C_5H_5)(LL)X]$ (0.5 mmol), $TlPF_6$ (1.5 eq.) and **L1** (1.1 eq.) in freshly dried dichloromethane (30 mL) was refluxed overnight under nitrogen atmosphere. After filtration to remove TlX formed during the reaction, the solvent was evaporated under vacuum and the solid residues were recrystallized twice from dichloromethane/hexane mixture to afford the desired compounds as reddish solids.

2.6.7 $[(\eta^5\text{-}C_5H_5)Fe(\kappa^2\text{-dppe})L1]PF_6$ (1Fe)

Dark red. 360 mg, 73% yield.

FTIR; ν(KBr)/cm^{-1}: 2196 (N≡C), 838 and 557 (PF_6^-);

^{1}H NMR (400 MHz, $(CD_3)_2CO$, 25 °C): 2.67 (m, 2H, CH_2), 2.84 (m, 2H, CH_2), 4.71 (s, 5H, η^5-C_5H_5), 6.88 (d, $^3J_{H,H}$= 4.1 Hz, 1H, H3),7.28 (dd, $^3J_{H,H}$=3.7 and 5.2 Hz, 1H, H16), 7.30 (d, $^3J_{H,H}$=4.1 Hz, 1H, H4), 7.33 (ddd, $^3J_{H,H}$=1.0, 6.8 and 8.8 Hz, 1H, H10), 7.42 (ddd, $^3J_{H,H}$=1.0, 6.5 and 9.1 Hz, 1H, H9), 7.55 (dd, $^3J_{H,H}$=1.0 and 3.7 Hz, 1H, H17), 7.57 (m, 8H, H $_{ortho}$-Ph), 7.68 (m, 8H, H_{meta}-Ph), 7.72 (dd, $^3J_{H,H}$=1.0 and 5.1 Hz,

1H, H15), 7.81 (d, $^{3}J_{H,H}$=9.0 Hz, 1H, H8),8.04 (d, $^{3}J_{H,H}$=8.9 Hz, 1H, H11), 8.12 (m, 4H, H_{para}-Ph) ppm;

^{13}C NMR (100 MHz, $(CD_3)_2CO$, 25 °C): 28.51 (t, $^{1}J_{CP}$=42.0 Hz, CH2-κ^2-dppe), 81.12 (η^5-C_5H_5), 108.32 (C2), 121.57 (C8), 122.84 (C11),123.78 (C6), 125.39 (C4), 126.53 (C9), 127.90 (C10), 127.93 (C17), 128.32 (C15), 128.37 (C1), 129.44 (C16), 130.05 and 130.26 (t, $^{3}J_{C,P}$= 10.0 Hz, C_{meta}-Ph), 131.06 (C13), 131.40 and 131.84 (s, C_{para}-Ph), 132.40 and 134.02 (t,$^{2}J_{C,P}$= 10.0 Hz, C_{ortho}-Ph), 134.94 (C14), 136.08 (C7), 137.04 (C12), 137.60 (t, $^{1}J_{C,P}$= 41.0 Hz, C_{ipso}-Ph), 139.82 (C3), 143.49 (C5) ppm;

^{31}P NMR (161 MHz, $(CD_3)_2CO$, 25 °C): 96.98 (s, κ^2-dppe), 144.25 (sept, PF_6) ppm;

UV-Vis.: ($CHCl_3$): λ_{max}/nm ($\epsilon\times10^4$/$M^{-1}cm^{-1}$): 478 (3.0);

Anal. Calc. for 1Fe•1/3CH_2Cl_2: Calc.: C 57.13, H 3.84, N 1.38, S 9.47. Found: C 57.25, H 3.66, N 1.42, S 9.34;

2.6.8 [(η^5-C_5H_5)Ru(κ^2-dppe)L1]PF_6 (1aRu)

Light Red. 284 mg, 55% yield.

FTIR: ν(KBr)/cm^{-1}: 2211 (N≡C), 838 and 557 (PF_6^-);

^{1}H NMR (400 MHz, $(CD_3)_2CO$, 25 °C): 1.89 (m, 2H, CH_2), 2.20 (m, 2H, CH_2), 5.06 (s, 5 H, η^5-C_5H_5), 6.93 (d, $^{3}J_{H,H}$= 4.2 Hz, 1H, H3), 7.28 (d, $^{3}J_{H,H}$=3.5 and 5.2 Hz, 1H, H16), 7.33 (ddd, overlaped, H10), 7.33 (d, $^{3}J_{H,H}$=4.2 Hz, 1H, H4), 7.43 (ddd, $^{3}J_{H,H}$= 1.0, 6.6 and 8.7 Hz, 1H, H9), 7.52 (m, 8H, H_{ortho}-Ph), 7.55 (dd, $^{3}J_{H,H}$=1.0 and 3.6, H17), 7.65 (m, 8H, H_{meta}-Ph), 7.73 (dd, $^{3}J_{H,H}$=1.0 and 5.2, H15), 7.81 (d, $^{3}J_{H,H}$=8.9 Hz, 1H, H8), 8.05 (d, $^{3}J_{H,H}$=8.9 Hz, 1H, H11), 8.05 (m, 8H, H_{para}-Ph) ppm;

^{13}C NMR (100 MHz, $(CD_3)_2CO$, 25 °C): 28.53 (t, $^{1}J_{C,P}$=46 Hz, CH_2-κ^2-dppe), 81.12 (η^5-C_5H_5), 107.14 (C2), 121.53 (C8), 121.60 (C1), 122.85 (C11), 123.63 (C6), 125.49 (C4), 126.54 (C9), 127.95 (C15), 128.00 (C10), 128.37 (C17), 129.52 (C16), 129.86 and 130.09 (t, $^{3}J_{C,P}$= 9.00 Hz, C_{meta}-Ph), 131.29 and 131.79 (s, C_{para}-Ph), 131.97 and 134.27 (t, $^{2}J_{C,P}$= 22.0 Hz, C_{ortho}-Ph), 132.30 (C13), 134.89 (C14), 136.01 (C7), 136.48 (t, $^{1}J_{C,P}$= 57.0 Hz, C_{ipso}-Ph), 137.12 (C12), 141.08 (C3), 144.77 (C5) ppm;

^{31}P NMR (161 MHz, $(CD_3)_2CO$, 25 °C): = 79.08 (s, κ^2-dppe), 144.26 (sept, PF_6) ppm;

UV-Vis.: ($CHCl_3$): λ_{max}/nm ($\epsilon\times10^4$/$M^{-1}cm^{-1}$): 475 (3.0);

Anal. Calc. for 1aRu•2CH_2Cl_2: Calc.: C 49.93, H 3.52, N 1.16, S 8.00 Found: C 50.40, H 3.60, N 1.20, S 8.00.

2.6.9 $[(\eta^5\text{-}C_5H_5)Ru(PPh_3)_2L1]PF_6$ (1bRu)

Dark red. 361 mg, 62 % yield.

FTIR: ν(KBr)/cm^{-1}: 2213 (N≡C), 838 and 557 (PF_6^-).

^{1}H NMR (400 MHz, $(CD_3)_2CO$, 25 °C): 4.79 (s, 5H, η^5-C_5H_5), 7.20 (dd, overlaped, H16), 7.35 (ddd, overlaped, H10), 7.44 (ddd, overlaped, H9), 7.52 (m, 12H, H_{ortho}-Ph), 7.56 (d, $^3J_{H,H}$=4.1 Hz, 1H, H3), 7.59 (dd, $^3J_{H,H}$=3.8 Hz, 1H, H17), 7.65 (m, 12H, H_{meta}-Ph), 7.67 (dd, $^3J_{H,H}$= 3.8 Hz, 1H, H4), 7.73 (dd, $^3J_{H,H}$=1.0 and 5.0 Hz, 1H, H15), 7.94 (1H, $^3J_{H,H}$=8.9 Hz, H11), 8.04 (m, 6H, H_{para}-Ph), 8.07 (d, $^3J_{H,H}$=8.9 Hz, 1H, H8) ppm.

^{13}C NMR (100 MHz, $(CD_3)_2CO$, 25 °C): 85.33 (η^5-C_5H_5), 107.48 (C2), 121.60 (C8), 122.90 (C11), 123.70 (C6), 125.70 (C1), 126.01 (C4), 126.59 (C9), 127.99 (C15),127.01 (C17), 128.11 (C10), 128.42 (C15), 129.43 (t, $^3J_{C,P}$ = 9.0 Hz, C_{meta}-Ph), 129.43 (t, $^2J_{C,P}$= 11.0 Hz, C_{ortho}-Ph), 131.12 (C16), 131.50 (C13), 134.27 (t, $^4J_{C,P}$= 10.0 Hz, C_{para}-Ph), 134.92 (C14), 136.14 (C7), 136.49 (t, $^1J_{C,P}$= 44.0 Hz, C_{ipso}-Ph), 137.28 (C12), 141.11 (C3), 144.80 (C5) ppm.

^{31}P NMR (161 MHz, $(CD_3)_2CO$, 25 °C): 41.72 (s, κ^2-dppe), 144.06 (sept, PF_6) ppm.

UV-Vis. ($CHCl_3$): λ_{max}/nm ($\epsilon\times10^4$/ M^{-1}cm^{-1}): 473 (2.7).

Anal. calc. for 1bRu•1/4CH_2Cl_2: C 59.27, H 3.80, N 1.19, S 8.15. Found: C 59.27, H 4.12, N 1.19, S 7.82.

References

[1] Paras N. Prasad and Bruce A. Reinhardt. Is there a role for organic materials chemistry in nonlinear optics and photonics? *Chemistry of Materials*, 2(6):660–669, 1990.

[2] 3,4-ethylenedioxythiophene (EDOT) as a versatile building block for advanced functional π-conjugated systems. *Journal Material Chemistry*, 15:1589–1610, 2005.

[3] J. H. Burroughes, D. D. C. Bradley, A. R. Brown, R. N. Marks, K. Mackay, R. H. Friend, P. L. Burns, and A. B. Holmes. Light-emitting diodes based on conjugated polymers. *Nature*, 347:539–541, 1990.

[4] Klaus Müllen and G. Wegner. *Electronic materials: the oligomer approach.* Wiley-VCH, 1998.

[5] D.F. Perepichka and I.F. Perepichka. *Handbook of Thiophene-based Materials: Applications in Organic Electronics and Photonics. Synthesis and theory.* Number 1. Wiley, 2009.

[6] Felix Sunjoo Kim, Guoqiang Ren, and Samson A. Jenekhe. One-dimensional nanostructures of π-conjugated molecular systems: Assembly, properties, and applications from photovoltaics, sensors, and nanophotonics to nanoelectronics. *Chemistry of Materials*, 23(3):682–732, 2011.

[7] A. K-Y. Jen, V. P. Rao, K. Y. Wong, and K. J. Drost. Functionalized thiophenes: second-order nonlinear optical materials. *Journal of the Chemical Society, Chemical Communications*, pages 90–92, 1993.

[8] J. Roncali. Conjugated poly(thiophenes): synthesis, functionalization, and applications. *Chemical Reviews*, 92(4):711–738, 1992.

[9] S. Gronowitz and A-B. Hörnfeldt. In A. Katritzky, O. Meth-Cohn, and C.W. Rees, editors, *Thiophenes, Best Synthetic Methods.* Academic Press, Oxford, 2004.

[10] A. Mishra, C.-Q. Ma, and P. Bauerle. Functional oligothiophenes: Molecular design for multidimensional nanoarchitectures and their applications. *Chemical Reviews*, 109(3):1141–1276, 2009.

[11] S.C. Rasmussen. In I.F. Perepichka and D.F. Perepichka, editors, *Handbook of Thiophene-Based Materials. Applications in Organic Electronics and Photonics.* Wiley-VCH Verlag, Oxford, 2004.

[12] A. Mishra and P. Bauerle. Small molecule organic semiconductors on the move: Promises for future solar energy technology. *Angewandte Chemie International Edition*, 51(9):2020–2067, 2012.

[13] P-L. T. Boudreault, A. Najari, and M. Leclerc. Processable low-bandgap polymers for photovoltaic applications. *Chemistry of Materials*, 23(3):456–469, 2011.

[14] Seth R. Marder and Joseph W. Perry. Molecular materials for second-order nonlinear optical applications. *Advanced Materials*, 5(11):804–815, 1993.

[15] Iuan-Yuan Wu, Jiann T. Lin, Jimmy Luo, Chyi-Shiun Li, Chiitang Tsai, Yuh S. Wen, Chia-Chen Hsu, Fen-Fen Yeh, and Sean Liou. Syntheses and second-order optical nonlinearity of ruthenium -acetylides with an end-capping organic electron acceptor and thienyl entity in the conjugation chain. *Organometallics*, 17(11):2188–2198, 1998.

[16] In Su Lee, Hwimin Seo, and Young Keun Chung. Preparation of (thiophene)manganese tricarbonyl cations for nonlinear optics. *Organometallics*, 18(6):1091–1096, 1999.

[17] Richard D.A. Hudson, Inge Asselberghs, Koen Clays, Laurence P. Cuffe, John F. Gallagher, Anthony R. Manning, André Persoons, and Kurt Wostyn. The linear and nonlinear optical properties of organometallic chromophores derived from ferrocene, $[fe_2(\eta^5\text{-}C_5H_5)_2(CO)_2(\mu\text{-}CO)(\mu\text{-}CCH_3)]^+[BF_4]$ and terthienyl spacers. crystal structure of 2-[(e)-2-ferrocenylethenyl]-5-(2-thienyl)thiophene. *Journal of Organometallic Chemistry*, 637–639(0):435 – 444, 2001.

[18] In Su Lee, Dae Seung Choi, Dong Mok Shin, Young Keun Chung, and Cheol Ho Choi. Preparation of thiophene-coordinated ruthenium complexes for nonlinear optics. *Organometallics*, 23(8):1875–1879, 2004.

[19] Jean-Luc Fillaut, Johann Perruchon, Philippe Blanchard, Jean Roncali, Stéphane Golhen, Magali Allain, Anna Migalsaka-Zalas, Ivan V. Kityk, and Bouchta Sahraoui. Design and synthesis of ruthenium oligothienylacetylide complexes. New materials for acoustically induced nonlinear optics. *Organometallics*, 24(4):687–695, 2005.

[20] Tian-Gao Zhang, Yuxia Zhao, Inge Asselberghs, André Persoons, Koen Clays, and Michael J. Therien. Design, synthesis, linear, and nonlinear optical properties of conjugated (porphinato)zinc(II)-based donor-acceptor chromophores featuring nitrothiophenyl and nitrooligothiophenyl electron-accepting moieties. *Journal of the American Chemical Society*, 127(27):9710–9720, 2005.

[21] R. Dustan Myrex, Gary M. Gray, Amelia G. VanEngen Spivey, and Christopher M. Lawson. Synthesis and characterization of transition metal systems containing phosphino-oligothiophene ligands for nonlinear optical materials. *Organometallics*, 25(21):5045–5050, 2006.

[22] Joseph P. Morrall, Gulliver T. Dalton, Mark G. Humphrey, and Marek Samoc. Organotransition metal complexes for nonlinear optics. volume 55 of *Advances in Organometallic Chemistry*, pages 61 – 136. Academic Press, 2007.

[23] António M. Fonseca, Michael Belsley, Etelvina Matos Gomes, M. Cidália R. Castro, and M. Manuela M. Raposo. Molybdenum complexes bearing (bi)thienyl- or arylthienyl-substituted -conjugated spacers: Synthesis, electrochemical, spectroscopic and nonlinear optical properties. *European Journal of Inorganic Chemistry*, 2010(19):2998–3004, 2010.

[24] M. H. Garcia, P. J. Mendes, M. P. Robalo, A. R. Dias, J. Campo, W. Wenseleers, and E. Goovaerts. Compromise between conjugation length and charge-transfer in nonlinear optical 5-monocyclopentadienyliron(ii) complexes with substituted oligo-thiophene nitrile ligands: Synthesis, electrochemical studies and first hyperpolarizabilities. *Journal of Organometallic Chemistry*, 692(14):3027 – 3041, 2007.

[25] M. Helena Garcia, M. Paula Robalo, Alberto R. Dias, M. Teresa Duarte, Wim Wenseleers, G. Aerts, Etienne Goovaerts, Marie P. Cifuentes, Steph Hurst, Mark G. Humphrey, Marek Samoc, and Barry Luther-Davies. Synthesis and nonlinear optical properties of η^5-monocyclopentadienyliron(ii) acetylide derivatives. X-ray crystal structures of [Fe(η^5-C_5H_5)(DPPE)(p-C$\equiv$C$C_6H_4NO_2$)] and [Fe(η^5-C_5H_5)(DPPE)((E)-p-C$\equiv$CC_6H_4C(H)C(H)$C_6H_4NO_2$)]. *Organometallics*, 21(10):2107–2118, 2002.

[26] M. Helena Garcia, João C. Rodrigues, A. Romão Dias, M.Fátima M. Piedade, M. Teresa Duarte, M. Paula Robalo, and Nelson Lopes. Second harmonic generation of 5-monocyclopentadienyl ruthenium p-benzonitrile derivatives by kurtz powder technique. crystal and molecular structure determinations of [ru(η^5-C_5H_5)((+)-diop)(p-ncc6h4no2)][x], x=pf6, cf3so3 and [ru(η^5-C_5H_5)((+)-diop)(ncch3)][pf6]. *Journal of Organometallic Chemistry*, 632(1–2):133 – 144, 2001.

[27] M. H. Garcia, P. J. Mendes, M. P. Robalo, M. T. Duarte, and N. Lopes. Synthesis and electrochemical studies of η^5-monocyclopentadienylruthenium(II) complexes with substituted thiophene nitrile ligands. crystal structure of [Ru(η^5-C_5H_5)(dppe)(NC{SC_4H_2}$_2$$NO_2$)][$PF_6$]. *Journal of Organometallic Chemistry*, 694(18):2888 – 2897, 2009.

[28] M. Helena Garcia, Pedro Florindo, M. Fátima M. Piedade, M. Teresa Duarte, M. Paula Robalo, Etienne Goovaerts, and Wim Wenseleers. Synthesis and structural characterization of ruthenium(ii) and iron(ii) complexes containing 1,2-di-(2-thienyl)-ethene derived ligands as chromophores. *Journal of Organometallic Chemistry*, 694(3):433 – 445, 2009.

[29] Maria Helena Garcia, Pedro Florindo, Maria de Fátima M. Piedade, Stefano Maiorana, and Emanuela Licandro. New organometallic Ru(II) and Fe(II) complexes with tetrathia-[7]-helicene derivative ligands. *Polyhedron*, 28(3):621 – 629, 2009.

[30] Wim Wenseleers, Etienne Goovaerts, Pascale Hepp, M. Helena Garcia, M. Paula Robalo, A.R. Dias, M.Fátima M. Piedade, and M. Teresa Duarte. High first hyperpolarizability and perfectly aligned crystal packing for an organometallic compound [fe(5-c5h5)((r)–prophos)(p-ncc6h4no2)][pf6]ch2cl2. *Chemical Physics Letters*, 367(3–4):390 – 397, 2003.

[31] Andreia Valente, Sophie Royer, Milan Narendra, Tiago J.L. Silva, Paulo J.G. Mendes, M. Paula Robalo, Manuel Abreu, Jürgen Heck, and M. Helena Garcia. Synthesis of new Fe(II) and Ru(II) η^5-monocyclopentadienyl compounds showing significant second order NLO properties. *Journal of Organometallic Chemistry*, 736(0):42 – 49, 2013.

[32] Seth R. Marder, Christopher B. Gorman, Bruce G. Tiemann, and Lap Tak Cheng. Stronger acceptors can diminish nonlinear optical response in simple donor-acceptor polyenes. *Journal of the American Chemical Society*, 115(7):3006–3007, 1993.

[33] Guillaume Grelaud, Marie P. Cifuentes, Frédéric Paul, and Mark G. Humphrey. Group 8 metal alkynyl complexes for nonlinear optics. *Journal of Organometallic Chemistry*, 751(0):181 – 200, 2014.

[34] Miklos Kertesz, Cheol Ho Choi, and Shujiang Yang. Conjugated polymers and aromaticity. *Chemical Reviews*, 105(10):3448–3481, 2005.

[35] Mehmet Emin Cinar and Turan Ozturk. Thienothiophenes, dithienothiophenes, and thienoacenes: Syntheses, oligomers, polymers, and properties. *Chemical Reviews*, 0(0):null, 0. PMID: 25831021.

[36] Kazuo Takimiya, Shoji Shinamura, Itaru Osaka, and Eigo Miyazaki. Thienoacene-based organic semiconductors. *Advanced Materials*, 23(38):4347–4370, 2011.

[37] Aiko Fukazawa, Daisuke Kishi, Yuki Tanaka, Shu Seki, and Shigehiro Yamaguchi. Diarylated bi(thieno[2,3-c]thiophene)s: A ring-fusing strategy for controlling the molecular alignment of oligoarenes. *Angewandte Chemie International Edition*, 52(46):12091–12095, 2013.

[38] R. Mayer, H. Kleinert, S. Richter, and K. Gewald. Synthesis of isothicnaphthene. *Angewandte Chemie International Edition in English*, 1(2):115–115, 1962.

[39] M. P. Cava, N. M. Pollack, O. A. Mamer, and M. J. Mitchell. Synthetic route to benzo[c]thiophene and the naphtho[c]thiophenes. *The Journal of Organic Chemistry*, 36(25):3932–3937, 1971.

[40] Y. Okuda, M. V. Lakshmikantham, and M. P. Cava. A new route to 1,3-disubstituted benzo[c]thiophenes. *The Journal of Organic Chemistry*, 56(21):6024–6026, 1991.

[41] D. Lorcy, K. D. Robinson, Y. Okuda, J. L. Atwood, and M. P. Cava. Novel electron acceptors derived from isothianaphthene. *J. Chem. Soc., Chem. Commun.*, pages 345–347, 1993.

[42] D. Lorcy and Michael P. Cava. Poly(isothianaphthene–bithiophefe): A new regularly structured polythiophene analogue. *Advanced Materials*, 4(9):562–564, 1992.

[43] P. Bauerle, G. Götz, P. Emerle, and H. Port. Synthesis and characterization of new annelated terheterocycles. *Advanced Materials*, 4(9):564–568, 1992.

[44] S. Musmanni and J. P. Ferraris. Preparation and characterization of conducting polymers based on 1,3-di(2-thienyl)benzo [c]thiophene. *Journal of the Chemical Society, Chemical Communications*, pages 172–174, 1993.

[45] R. H. L. Kiebooms, P. J. A. Adriaensens, D. J. M. Vanderzande, and J. M. J. V. Gelan. Grignard reactions on ortho dicarboxylic arene derivatives. synthesis of 1,3-dithienylisothianaphthene compounds. *The Journal of Organic Chemistry*, 62(5):1473–1480, 1997.

[46] A. K. Mohanakrishnan, M. V. Lakshmikantham, C. McDougal, M. P. Cava, J. W. Baldwin, and R. M. Metzger. Studies in the dithienylbenzo[c]thiophene series. *The Journal of Organic Chemistry*, 63(9):3105–3112, 1998.

[47] A. K. Mohanakrishnan, P. Amaladass, and J. A. Clement. Synthesis of end-blocked thienyl oligomers incorporating benzo[c]thiophene. *Tetrahedron Letters*, 48(5):779 – 784, 2007.

[48] A. K. Mohanakrishnan, J. A. Clement, P. Amaladass, and V.S. Thirunavukkarasu. Synthesis of 1,3-disubstituted benzo[c]thiophene analogs containing benzo[b]thiophene/benzo[b]pyrrole. *Tetrahedron Letters*, 48(49):8715 – 8720, 2007.

[49] A. K. Mohanakrishnan, N. S. Kumar, and P. Amaladass. Synthesis and characterization of 9,9-dialkylfluorene capped benzo[c]thiophene/benzo[c]selenophene analogs as potential oleds. *Tetrahedron Letters*, 49(32):4792 – 4795, 2008.

[50] Pitchamuthu Amaladass, J. Arul Clement, and Arasambattu K. Mohanakrishnan. Synthesis and characterization of benzannelated thienyl oligomers. *European Journal of Organic Chemistry*, 2008(22):3798–3810, 2008.

[51] J. . Clement, P. Gunasekaran, and A. K. Mohanakrishnan. Synthesis of benzo[c]thiophene analogs containing benzimidazole, benzothiazole, and oxazole. *Synthetic Communications*, 39(18):3324–3337, 2009.

[52] J. A. Clement and A. K. Mohanakrishnan. Synthesis and characterization of naphth-annelated thiophene analogs. *Tetrahedron*, 66(13):2340 – 2350, 2010.

[53] N. S. Kumar and A. K. Mohanakrishnan. Synthesis and characterization of fluorene tethered benzo[c]thiophene/benzo[c]selenophene analogs. *Tetrahedron*, 66(30):5660 – 5670, 2010.

[54] D. L. Vangeneugden, D. J. M. Vanderzande, J. Salbeck, P. A. van Hal, R. A. J. Janssen, J. C. Hummelen, C. J. Brabec, S. E. Shaheen, and N. S. Sariciftci. Synthesis and characterization of a poly(1,3-dithienylisothianaphthene) derivative for bulk heterojunction photovoltaic cells. *The Journal of Physical Chemistry B*, 105(45):11106–11113, 2001.

[55] S. T. Meek, E. E. Nesterov, and T. M. Swager. Near-infrared fluorophores containing benzo[c]heterocycle subunits. *Organic Letters*, 10(14):2991–2993, 2008.

[56] Y. Zhu and M. O. Wolf. Charge transfer and delocalization in conjugated (ferrocenylethynyl)oligothiophene complexes. *Journal of the American Chemical Society*, 122(41):10121–10125, 2000.

[57] S. Ogawa, H. Muraoka, K. Kikuta, F. Saito, and R. Sato. Design of reversible multi-electron redox systems using benzochalcogenophenes containing aryl and/or ferrocenyl fragments. *Journal of Organometallic Chemistry*, 692(1–3):60 – 69, 2007.

[58] K. Willinger, K. Fischer, R. Kisselev, and M. Thelakkat. Synthesis, spectral, electrochemical and photovoltaic properties of novel heteroleptic polypyridyl ruthenium(ii) donor-antenna dyes. *Journal Material Chemistry*, 19:5364–5376, 2009.

[59] R. Bruckner and M. Harmata. *Organic Mechanisms Reactions, Stereochemistry and Synthesis*. Spektrum Akademischer Verlag, Berlin Heidelberg, 2010.

[60] Shinji Kato, Nobuaki Nonoyama, Koji Tomimoto, and Toshiaki Mase. Non-cryogenic metalation of aryl bromides bearing proton donating groups: formation of a stable magnesio-intermediate. *Tetrahedron Letters*, 43(41):7315 – 7317, 2002.

[61] Anne Eeg Jensen, Wolfgang Dohle, Ioannis Sapountzis, David M. Lindsay, Viet Anh Vu, and Paul Knochel. Preparation and reactions of functionalized arylmagnesium reagents. *Synthesis*, 2002(04):0565–0569, 2002.

[62] D.L. Vangeneugden, R.H.L. Kiebooms, D.J.M. Vanderzande, and J.M.J.V. Gelan. A general synthetic route towards soluble poly(1,3-dithienylisothianaphthene) derivatives. *Synthetic Metals*, 101(1–3):120 – 121, 1999.

[63] Jean-Manuel Raimundo, Philippe Blanchard, Hugues Brisset, Said Akoudad, and Jean Roncali. Proquinoid acceptors as building blocks for the design of efficient [small pi]-conjugated fluorophores with high electron affinity. *Chem. Commun.*, pages 939–940, 2000.

[64] U. Mitschke and P. Bauerle. Synthesis, characterization, and electrogenerated chemiluminescence of phenyl-substituted, phenyl-annulated, and spirofluorenyl-bridged oligothiophenes. *J. Chem. Soc., Perkin Trans. 1*, pages 740–753, 2001.

[65] Roman Kisselev and Mukundan Thelakkat. Synthesis of novel 1,3-bis(5-diarylaminothiophen-2-yl)isothianaphthenes. *Chem. Commun.*, pages 1530–1531, 2002.

[66] Yang Qin, Jung Yong Kim, C. Daniel Frisbie, and Marc A. Hillmyer. Distannylated isothianaphthene: A versatile building block for low bandgap conjugated polymers. *Macromolecules*, 41(15):5563–5570, 2008.

[67] Chunyan Du, Jianming Chen, Yunlong Guo, Kun Lu, Shanghui Ye, Jian Zheng, Yunqi Liu, Zhigang Shuai, and Gui Yu. Dicyanovinyl heterotetracenes: Synthesis, solid-state structures, and photophysical properties. *The Journal of Organic Chemistry*, 74(19):7322–7327, 2009. PMID: 19711948.

[68] T. M. Barclay, A. W. Cordes, C. D. MacKinnon, R. T. Oakley, and R. W. Reed. Oligothiophenes end-capped by nitriles. preparation and crystal structures of dicyanooligothiophenes. *Chemistry of Materials*, 9(4):981–990, 1997.

[69] M. Manuela M Raposo, A. M. C. Fonseca, and G. Kirsch. Synthesis of donor–acceptor substituted oligothiophenes by stille coupling. *Tetrahedron*, 60(18):4071 – 4078, 2004.

[70] A. K. Mohanakrishnan and P. Amaladass. Synthesis of 1,3-diarylbenzo[c]selenophenes. *Tetrahedron Letters*, 46(42):7201 – 7204, 2005.

[71] Philippe Hapiot, Frédéric Demanze, Abderrahim Yassar, and Francis Garnier. Molecular engineering of band level energies in oligothiophenes, through cyano-substitutions. *The Journal of Physical Chemistry*, 100(20):8397–8401, 1996.

[72] M. Helena Garcia, Paulo J. Mendes, M. Paula Robalo, M. Teresa Duarte, and Nelson Lopes. Synthesis and electrochemical studies of 5-monocyclopentadienylruthenium(ii) complexes with substituted thiophene nitrile ligands. crystal structure of [ru(5-c5h5)(dppe)(ncSC4H22no2)][pf6]. *Journal of Organometallic Chemistry*, 694(18):2888 – 2897, 2009.

[73] R. Kiebooms, I. Hoogmartens, P. Adriaensens, D. Vanderzande, and J. Gelan. Low-band-gap conjugated polymers. Improved model compounds for the structural analysis of poly(isothianaphthene). *Macromolecules*, 28(14):4961–4969, 1995.

[74] Wim Wenseleers, Abraham W. Gerbrandij, Etienne Goovaerts, M. Helena Garcia, M. Paula Robalo, Paulo J. Mendes, Joao C. Rodrigues, and Alberto R. Dias. Hyper-rayleigh scattering study of [small eta]5-monocyclopentadienyl-metal complexes for second order non-linear optical materials. *J. Mater. Chem.*, 8:925–930, 1998.

[75] Axel D. Becke. Densityfunctional thermochemistry. iii. the role of exact exchange. *The Journal of Chemical Physics*, 98(7):5648–5652, 1993.

[76] Chengteh Lee, Weitao Yang, and Robert G. Parr. Development of the colle-salvetti correlation-energy formula into a functional of the electron density. *Phys. Rev. B*, 37:785–789, Jan 1988.

[77] Takeshi Yanai, David P Tew, and Nicholas C Handy. A new hybrid exchange–correlation functional using the coulomb-attenuating method (cam-b3lyp). *Chemical Physics Letters*, 393(1–3):51 – 57, 2004.

[78] Yan Zhao and DonaldG. Truhlar. The m06 suite of density functionals for main group thermochemistry, thermochemical kinetics, noncovalent interactions, excited states, and transition elements: two new functionals and systematic testing of four m06-class functionals and 12 other functionals. *Theoretical Chemistry Accounts*, 120(1-3):215–241, 2008.

[79] Yan Zhao and Donald G. Truhlar. Attractive noncovalent interactions in the mechanism of grubbs second-generation ru catalysts for olefin metathesis. *Organic Letters*, 9(10):1967–1970, 2007.

[80] Nathan E. Schultz, Yan Zhao, and Donald G. Truhlar. Density functionals for inorganometallic and organometallic chemistry. *The Journal of Physical Chemistry A*, 109(49):11127–11143, 2005.

[81] Jeremy N. Harvey. On the accuracy of density functional theory in transition metal chemistry. *Annu. Rep. Prog. Chem., Sect. C: Phys. Chem.*, 102:203–226, 2006.

[82] Yan Zhao and Donald G. Truhlar. Density functionals with broad applicability in chemistry. *Accounts of Chemical Research*, 41(2):157–167, 2008.

[83] Chun-Guang Liu, Xiao-Hui Guan, and Zhong-Min Su. Computational study on redox-switchable 2d second-order nonlinear optical properties of pushpull mono-tetrathiafulvalene-bis(salicylaldiminato) zn(ii) schiff base complexes. *The Journal of Physical Chemistry C*, 115(13):6024–6032, 2011.

[84] Shabbir Muhammad, Hongliang Xu, Muhammad Ramzan Saeed Ashraf Janjua, Zhongmin Su, and Muhammad Nadeem. Quantum chemical study of benzimidazole derivatives to tune the second-order nonlinear optical molecular switching by proton abstraction. *Phys. Chem. Chem. Phys.*, 12:4791–4799, 2010.

[85] Hai-Bo Zhao, Yong-Qing Qiu, Chun-Guang Liu, Shi-Ling Sun, Yan Liu, and Rong-Shun Wang. Redox-switchable second-order nonlinear optical responses of tempo-dithiolate ligand and (tempodt)m complexes (m = pt, pd). *Journal of Organometallic Chemistry*, 695(19–20):2251 – 2257, 2010.

[86] P.L. Franzen, S.C. Zilio, A.E.H. Machado, J.M. Madurro, A.G. Brito-Madurro, L.T. Ueno, R.N. Sampaio, and N.M. Barbosa Neto. Experimental and theoretical investigation of first hyperpolarizability in aminophenols. *Journal of Molecular Structure*, 892(1–3):254 – 260, 2008.

[87] Chaoyong Mang and Kechen Wu. First hyperpolarizabilities of vinylogue organometallic sesquifulvalene chromophores: A dft study. *International Journal of Quantum Chemistry*, 106(12):2529–2535, 2006.

[88] C. Cardoso, P. E. Abreu, and F. Nogueira. Structure dependence of hyperpolarizability in octopolar molecules. *Journal of Chemical Theory and Computation*, 5(4):850–858, 2009.

[89] R. J. Magyar and S. Tretiak. Dependence of spurious charge-transfer excited states on orbital exchange in tddft: large molecules and clusters. *Journal of Chemical Theory and Computation*, 3(3):976–987, 2007.

[90] Lara Ferrighi, Luca Frediani, Chiara Cappelli, Paweł Sałek, Hans Ågren, Trygve Helgaker, and Kenneth Ruud. Density-functional-theory study of the electric-field-induced second harmonic generation (efishg) of push–pull phenylpolyenes in solution. *Chemical Physics Letters*, 425(4–6):267 – 272, 2006.

[91] Michael J. G. Peach, Trygve Helgaker, Pawel Salek, Thomas W. Keal, Ola B. Lutnaes, David J. Tozer, and Nicholas C. Handy. Assessment of a coulomb-attenuated exchange-correlation energy functional. *Phys. Chem. Chem. Phys.*, 8:558–562, 2006.

[92] Denis Jacquemin, Eric A. Perpète, Giovanni Scalmani, Michael J. Frisch, Rika Kobayashi, and Carlo Adamo. Assessment of the efficiency of long-range corrected functionals for some properties of large compounds. *The Journal of Chemical Physics*, 126(14):–, 2007.

[93] Denis Jacquemin, Eric A. Perpète, Miroslav Medved', Giovanni Scalmani, Michael J. Frisch, Rika Kobayashi, and Carlo Adamo. First hyperpolarizability of polymethineimine with long-range corrected functionals. *The Journal of Chemical Physics*, 126(19):–, 2007.

[94] Denis Jacquemin, Eric A. Perpète, Gustavo E. Scuseria, Ilaria Ciofini, and Carlo Adamo. Td-dft performance for the visible absorption spectra of organic dyes: conventional versus long-range hybrids. *Journal of Chemical Theory and Computation*, 4(1):123–135, 2008.

[95] Peter A. Limacher, Kurt V. Mikkelsen, and Hans Peter Lüthi. On the accurate calculation of polarizabilities and second hyperpolarizabilities of polyacetylene oligomer chains using the cam-b3lyp density functional. *The Journal of Chemical Physics*, 130(19):–, 2009.

[96] Alessandro Corozzi, Benedetta Mennucci, Roberto Cammi, and Jacopo Tomasi. Structure versus solvent effects on nonlinear optical properties of pushpull systems: A quantum-mechanical study based on a polarizable continuum model. *The Journal of Physical Chemistry A*, 113:14774–14784, 2009.

[97] Rosendo Valero, Ramon Costa, Ibério de P. R. Moreira, Donald G. Truhlar, and Francesc Illas. Performance of the m06 family of exchange-correlation functionals for predicting magnetic coupling in organic and inorganic molecules. *The Journal of Chemical Physics*, 128(11):–, 2008.

[98] Denis Jacquemin, Eric A. Perpète, Ilaria Ciofini, Carlo Adamo, Rosendo Valero, Yan Zhao, and Donald G. Truhlar. On the performances of the m06 family of density functionals for electronic excitation energies. *Journal of Chemical Theory and Computation*, 6(7):2071–2085, 2010.

[99] Tiago J. L. Silva, Paulo J. Mendes, Ana M. Santos, M. Helena Garcia, M. Paula Robalo, J. P. Prates Ramalho, A. J. Palace Carvalho, Marina Büchert, Christian Wittenburg, and Jürgen Heck. Mono(5-cyclopentadienyl)metal(ii) complexes with thienyl acetylide chromophores: Synthesis, electrochemical studies, and first hyperpolarizabilities. *Organometallics*, 33(18):4655–4671, 2014.

[100] Paulo J. Mendes, A.J. Palace Carvalho, and J.P. Prates Ramalho. Role played by the organometallic fragment on the first hyperpolarizability of iron–acetylide complexes: A td-dft study. *Journal of Molecular Structure: {THEOCHEM}*, 900(1–3):110 – 117, 2009.

[101] Paulo J. Mendes, Tiago J.L. Silva, A.J. Palace Carvalho, and J.P. Prates Ramalho. {DFT} studies on thiophene acetylide ru(ii) complexes for nonlinear optics: Structure–function relationships and

solvent effects. *Journal of Molecular Structure: {THEOCHEM}*, 946(1–3):33 – 42, 2010. Achievements and Challenges of Computational Chemistry in Portugal Selection of Papers Presented at the Portuguese Society Conference of Physical Chemistry 9ENQF-Portuguese Society Conference of Physical Chemistry.

[102] Shang-Shing P. Chou, Der-Jen Sun, Hong-Cheu Lin, and Pao-Keng Yang. Second-order nonlinearities and crystal structures of methylsulfonyl- and phenylsulfonyl-substituted thiophene imino dyes. *Chem. Commun.*, pages 1045–1046, 1996.

[103] Maria Helena Garcia, Sophie Royer, Maria Paula Robalo, Alberto Romão Dias, Jean-Philippe Tranchier, René Chavignon, Damien Prim, Audrey Auffrant, Françoise Rose-Munch, Eric Rose, Jacqueline Vaissermann, André Persoons, and Inge Asselberghs. Synthesis, characterisation of (arene)tricarbonylchromium complexes linked to cationic Fe and Ru derivatives and studies of first hyperpolarisabilities by hyper-Rayleigh scattering. *European Journal of Inorganic Chemistry*, 2003(21):3895–3904, 2003.

[104] J. Roncali. Molecular engineering of the band gap of -conjugated systems: Facing technological applications. *Macromolecular Rapid Communications*, 28(17):1761–1775, 2007.

[105] Catherine Branger, Minh Lequan, Rose Marie Lequan, Marguerite Barzoukas, and Alain Fort. Boron derivatives containing a bithiophene bridge as new materials for non-linear optics. *J. Mater. Chem.*, 6:555–558, 1996.

[106] Denis Jacquemin and Carlo Adamo. Bond length alternation of conjugated oligomers: Wave function and dft benchmarks. *Journal of Chemical Theory and Computation*, 7(2):369–376, 2011.

[107] Frédéric Castet, Vincent Rodriguez, Jean-Luc Pozzo, Laurent Ducasse, Aurélie Plaquet, and Benoît Champagne. Design and characterization of molecular nonlinear optical switches. *Accounts of Chemical Research*, 46(11):2656–2665, 2013.

[108] Lewis E. Johnson, Larry R. Dalton, and Bruce H. Robinson. Optimizing calculations of electronic excitations and relative hyperpolarizabilities of electrooptic chromophores. *Accounts of Chemical Research*, 0(0):null, 0. PMID: 24967617.

[109] Jacopo Tomasi, Benedetta Mennucci, and Roberto Cammi. Quantum mechanical continuum solvation models. *Chemical Reviews*, 105(8):2999–3094, 2005. PMID: 16092826.

[110] Lasse Jensen and Piet Th. van Duijnen. The first hyperpolarizability of p-nitroaniline in 1,4-dioxane: A quantum mechanical/molecular mechanics study. *The Journal of Chemical Physics*, 123(7):–, 2005.

[111] Raphaël Denis, Loïc Toupet, Frédéric Paul, and Claude Lapinte. Electron-rich piano-stool iron -acetylides bearing a functional aryl group. synthesis and characterization of iron(ii) and iron(iii) complexes. *Organometallics*, 19(21):4240–4251, 2000.

[112] Michael I. Bruce, Benjamin G. Ellis, Paul J. Low, Brian W. Skelton, and Allan H. White. Syntheses, structures, and spectro-electrochemistry of Cp*(PP)RuccccRu(PP)Cp* (pp = dppm, dppe) and their mono- and dications. *Organometallics*, 22(16):3184–3198, 2003.

[113] Frédéric Paul, Loic Toupet, Jean-Yves Thépot, Karine Costuas, Jean-François Halet, and Claude Lapinte. Electron-rich piano-stool iron -acetylides. electronic structures of arylalkynyl iron(iii) radical cations. *Organometallics*, 24(22):5464–5478, 2005.

[114] Adrienn Ruzsinszky, John P. Perdew, Gábor I. Csonka, Oleg A. Vydrov, and Gustavo E. Scuseria. Density functionals that are one- and two- are not always many-electron self-interaction-free, as shown for h2+, he2+, lih+, and ne2+. *The Journal of Chemical Physics*, 126(10):–, 2007.

[115] Adrienn Ruzsinszky, John Perdew, Gábor Csonka, Gustavo Scuseria, and Oleg Vydrov. Understanding and correcting the self-interaction error in the electrical response of hydrogen chains. *Phys. Rev. A*, 77:060502, Jun 2008.

[116] Oleg A. Vydrov, Gustavo E. Scuseria, John P. Perdew, Adrienn Ruzsinszky, and Gábor I. Csonka. Scaling down the perdew-zunger self-interaction correction in many-electron regions. *The Journal of Chemical Physics*, 124(9):–, 2006.

[117] Benoît Champagne, Eric A. Perpète, Denis Jacquemin, Stan J. A. van Gisbergen, Evert-Jan Baerends, Chirine Soubra-Ghaoui, Kathleen A. Robins, and Bernard Kirtman. Assessment of conventional density functional schemes for computing the dipole moment and (hyper)polarizabilities of pushpull -conjugated systems. *The Journal of Physical Chemistry A*, 104(20):4755–4763, 2000.

[118] Andreas Dreuw and Martin Head-Gordon. Failure of time-dependent density functional theory for long-range charge-transfer excited states: the zincbacteriochlorinbacteriochlorin and bacteriochlorophyllspheroidene complexes. *Journal of the American Chemical Society*, 126(12):4007–4016, 2004.

[119] Andreas Dreuw and Martin Head-Gordon. Single-reference ab initio methods for the calculation of excited states of large molecules. *Chemical Reviews*, 105(11):4009–4037, 2005. PMID: 16277369.

[120] T. Weyland, I. Ledoux, S. Brasselet, J. Zyss, and C. Lapinte. Nonlinear optical properties of redox-active mono-, bi-, and trimetallic σ-acetylide complexes connected through a phenyl ring in the Cp*(dppe)Fe series. an example of electro-switchable nlo response. *Organometallics*, 19(24):5235–5237, 2000.

Chapter 3

Organometallic Compounds containing *s*-Tetrazine Derivatives

3.1 Introduction

Tetrazine refers to a general class of compounds formed by a six-member aromatic ring possessing four nitrogen atoms and two carbon atoms. There are three known isomers for the tetrazine ring, the 1,2,3,4-, 1,2,3,5- and 1,2,4,5-tetrazine, whose structures are depicted in **Figure 3.1**. The latter, also named *s*-tetrazine or *sym*-tetrazine, due to the symmetric position of the nitrogen atoms, is the most studied and stable of the three isomers and it will be the focus of this work.

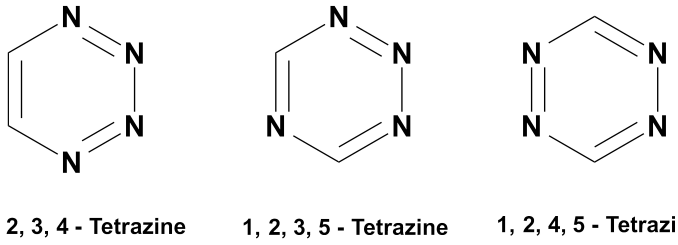

Figure 3.1: Structures of the three known tetrazine isomers.

Tetrazines are found various applications, ranging from pyrotechnics[1–5] and material sciences[6–10] to biological and biochemical sciences.[11–14] The versatility of the *s*-tetrazine ring is due to several factors. On one hand, the tetrazine ring is the electron-poorest aro-

matic system of the N-heterocyclic family, and its strong electron-acceptor ability, comparable with tetranitrobenzene, together with its electrochemical reversibility (tetrazines are easily reduced to their radical anions) and tunable fluorescent properties, makes them suitable for many applications in the field of fluorescent sensors or displays and, of course, NLO materials. On the other hand, their stability depends strongly on the ring substituents, and therefore the tetrazines are frequently used in the development of high energetic materials, namely explosives and other pyrotechnic compounds.

Although several substituents of the *s*-tetrazine are known, which include alkyl, alkynyl, aryl, heteroaryl, alkoxyl and alkylmercapto groups, 3,6-dihydro-*s*-tetrazine and 3,6-dialkyl-*s*-tetrazines are rather unstable. Halogenated, aromatic or heterocyclic aromatic 3,6-diaryl-*s*-tetrazines are stable and can be stored for long periods, and for this reason, these compounds are more commonly found as 3,6-diaryl-substituted compounds.

The lack of convenient synthetic methodologies has been considered a roadblock to the use of tetrazine-based compounds. This fact is easily seen by the dispersion of the synthetic works.[15] For example, only a small number of molecules, such as bis-(pyridyl)-*s*-tetrazine family, are found in organometallic chemistry or in metal-organic frameworks (MOF's).[7,16]

3.1.1 Synthesis of 3,6-diaryl-*s*-tetrazines

Synthetic methods prior to 1995 have been extensively reviewed by Neunhoeffe[17] and by Sauer[15] and will not be discussed in this work. The only exception will be made for the Pinner synthetic method, for which modified procedures were recently proposed. Furthermore, this method is still one of the most efficient methods for the synthesis of 3,6-diaryl-*s*-tetrazines.

There are several different procedures for preparing 3,6-diaryl-*s*-tetrazines, but most of them results in low yields and its applicability is scarce. Still, the majority of the methods share a common step - the obtention of a hydro-*s*-tetrazine ring followed by its oxidation. In fact, it is this bottleneck step that governs the overall yield of reaction. The most commonly used method for the preparation of hydro-*s*-tetrazines ring is by cyclocondensation of nitrile imines, obtained from the reaction of a nitrile with hydrazine or hydrazones. Since they can be quite unstable, hydro-*s*-tetrazines are not often isolated and its oxidation to the aromatic *s*-tetrazines is performed immediately without purification. Typical mild oxidizing agents can be used in the oxidation step, being the most

common nitrites, bromine, ferric chloride, hydrogen peroxide, chromic oxide or even air. The choice of the oxidizing agent depends mostly of the substituent on *s*-tetrazine ring, but the formation of sub-products that are hard to separate from the reaction mixture is also an important factor of choice.

The first report of the *s*-tetrazine ring synthesis was by Pinner, in 1893.[18] In his work, Pinner reacted several aryl nitriles with hydrazine in aqueous potassium hydroxide solution and, after oxidation, he obtained red compounds that were identified as *s*-tetrazines. Since Pinner's synthesis there were two main variations of the methodology, which improved the overall yield of the reactions. The first modification was made by Wiley *et al.*, who carried the reaction in anhydrous methanol and triethylamine which lead to a small enhancement of the reaction yield.[19] The second was based on the fact that sulphur reacts very rapidly with hydrazine, originating an addition product H_2N-NH-SH. This addition product reacts more efficiently with the aryl nitrile originating, after oxidation, the 3,6-diaryl-*s*-tetrazine ring in moderate to good yields. Also, this new method prevented the usage of harsh conditions as well as a high excess of hydrazine, and allow more mild conditions to be used. **Scheme 3.1** shows the currently accepted mechanism for the sulphur catalysed Pinner method.

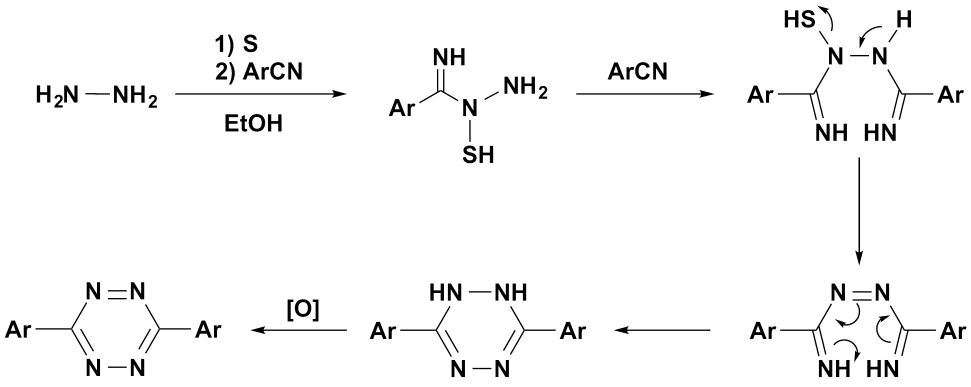

Scheme 3.1: Mechanism of the sulfur catalysed Pinner method

Pinner's method, and its variations, have the major drawback that are only useful for the synthesis of aromatic *s*-tetrazines.[20] Further improvement allowed the extension of the Pinner method for the obtention of aliphatic *s*-tetrazines simply by replacing the initial nitrile for an aldehyde. Nevertheless, two oxidation steps are needed, which affords low overall reaction yields.

The synthesis of bis-alkyl and bis-aryl *s*-tetrazines was recently developed.[21] The method is still based on the Pinner methodology but it involves a transition metal (Ni or Zn) as co-catalyst. This extremely versatile methodology allowed also the synthesis in moderate yields of asymmetric aryl-aryl, alkyl-alkyl and aryl-alkyl 3,6-disubstituted-*s*-tetrazines, which were obtained mainly as trace products in other methodologies. The overall reaction yields are dependent on the nature of the starting materials, and are lower in the case of the aryl derivatives.

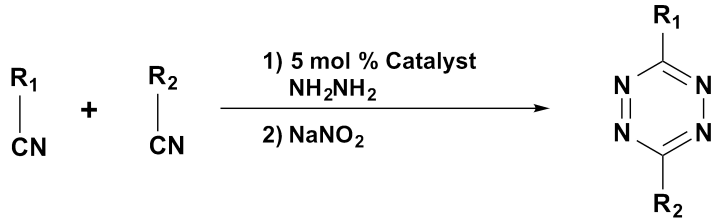

Catalyst = $Ni(Otf)_2$ or $Zn(Otf)_2$

R_1, R_2 = alkyl, 24 - 90%; R_1 = aryl and R_2 = alkyl, 40 - 70%; R_1, R_2 = aryl, 10 - 20%

Scheme 3.2: Synthesis of *s*-tetrazines by Neat's methodology

Thermal methods have also been seldom used for the synthesis of 3,6-diaryl-*s*-tetrazines. The thermal transformation of tetrazoles into symmetrical 3,6-diaryl-*s*-tetrazines in benzonitrile has been reported (**Scheme 3.3**).[22] Recently, a series of 3,6-bis(3,4-dialkoxyphenyl)-*s*-tetrazines and 3,6-bis(4-alkoxy-phenyl)-*s*-tetrazines were synthesized by heating an adequate trityltetrazole derivative in benzonitrile at high temperature, albeit no improvement of the yields was observed.[23] The major drawbacks of the thermal methods is their harsh conditions and the multiple-step procedures, make them less straightforward than the previous discussed synthetic methods.

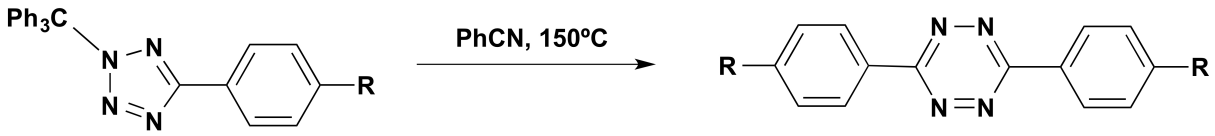

R = H, 65%; R = Cl, 77%; R = OMe, 41%

Scheme 3.3: Thermal method for the synthesis of tetrazines

Organometallic reagents also shown to be useful in the synthesis of 3,6-diaryl-*s*-tetrazines. According to Zielinsky procedure, the treatment of N'-(benzylidene)benzohydrazonoyl chlorides with titanium tetrachloride in chloroform, followed by oxidation with nitrous acid afforded the correspondent 3,6-diaryl-*s*-tetrazines in 32 to 56% yield (**Scheme 3.4**).[24] Also 3,6-bis(styryl)-*s*-tetrazines have been prepared by treatment of cinnamoylhydrazines with Appel reagent (a mixture of triphenylphosphane with a tetrahalogenated carbon) followed by oxidation with N-bromosuccinimide under air conditions. The yields of these reactions were again low, 9 to 13%.[25]

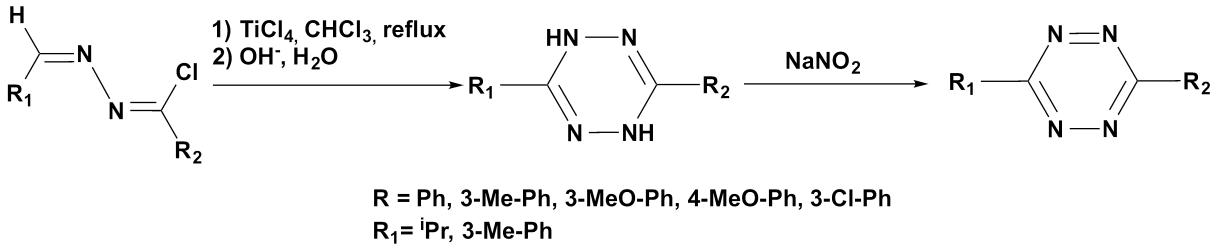

Scheme 3.4: Synthesis of tetrazines according to Zielinsky

Diaryl and dialkyl *s*-tetrazines were also obtained in high yields by Liu's methodology starting from *p*-toluenesulfonyl hydrazones, mediated by [hydroxyl-(tosyloxy)iodo]benzene (HTIB) as oxidizing agent in the presence of pyridine (**Scheme 3.5**).[26]

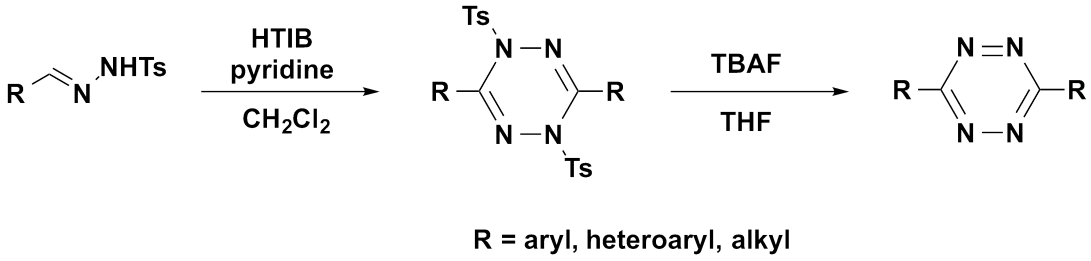

Scheme 3.5: Synthesis of 3,6-bis(styryl)-*s*-tetrazines by Liu's methodology

It is easily seen that all these recent methodologies are not straightforward nor even would be the first choice of a synthetic chemist for the synthesis of *s*-tetrazines. Except for Liu's methodology, one could even say that they were lucky strikes, and the low yields seem to prove that the obtained tetrazines are actually sub-products of the reactions.

This are some of the reasons why Pinner's method is still the most effective and used method for the synthesis of *s*-tetrazines.

3.1.2 Tetrazine Reactivity

Tetrazine reactivity is quite different from the other heterocyclic aromatic systems due to its unique electronic properties. In this section only reactions with retention of the *s*-tetrazine ring will be discussed. Exception is made for the [4+2] cycloaddition that will be briefly presented in the following paragraphs. Other ring contraction or expansion, thermal and photochemical reactions are well described elsewhere.[15]

The most important reaction of the *s*-tetrazine ring is, by far, the Aromatic Nucleophilic Substitution (ArSN - **Scheme 3.6**) at the 3 and 6-positions. This reaction provides alternative routes to new *s*-tetrazine-based compounds.[27] The starting *s*-tetrazines used in the ArSN reactions are usually 3,6-dichloro-*s*-tetrazines, 3,6-bis(methylthio)-*s*-tetrazines or 3,6-bis(3,5-dimethylpyrazolyl)-*s*-tetrazines. Thus, since the initial substituents are good leaving groups, such as halogens, thiolates, sulphonates or azolyl groups, a nucleophilic attack at the 3- and 6- positions by C, N, O or S- nucleophiles can occur, leading to the formation of new symmetrical or unsymmetrical *s*-tetrazines, depending on the used experimental conditions. For example, recently 3,6-dichloro-*s*-tetrazine was used as precursor in the synthesis of the symmetrical 3,6-dimethoxy-*s*-tetrazine and the asymmetrical 3-chloro-6-methoxy-*s*-tetrazine. The first was prepared simply by stirring 3,6-dichloro-*s*-tetrazine in methanol at room temperature, whereas the latter was obtained by treating the same precursor in refluxing methanol overnight.[28] In a similar fashion, 3-methoxy-6-methylthio-*s*-tetrazine and 3,6-dimethoxy-*s*-tetrazine were prepared starting from 3,6-bis(methylthio)-*s*-tetrazine using different experimental conditions.[29]

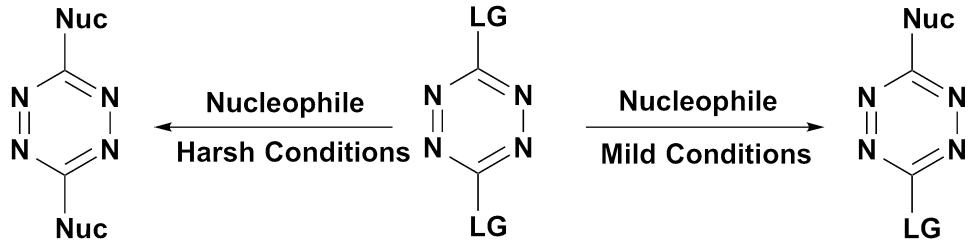

Scheme 3.6: Aromatic Nucleophilic Substitution on the *s*-tetrazine ring

The reaction of *s*-tetrazines derivatives with stronger nucleophiles was also investigated. Reaction of alkyllithium and Grignard reagents with different dialkylthio-*s*-tetrazines afforded addition products to the tetrazine nitrogen – N-alkyl-3,6-dialkylthio-*s*-tetrazines.[30] This result was quite surprising since a ArSN of the alkylthio substituents was expected. Other organometallic reagents, like zinc reagents, proved that the affinity towards the nitrogen atoms by strong C-nucleophiles is due to the highest nucleophilicity of the carbanions. Depending on the nature of the alkylmetal reagent, a reduction of the *s*-tetrazine ring or a simple complex formation were observed.[31]. In fact, the incorporation of C-nucleophiles is less trivial than N- or S-nucleophiles.[32,33] However, tetrazine derivatives bearing an N-heterocyclic carbene (NHC) in the 3-position and a keto in the 6-position, and thus having a quinoidal-like structure, are readily and easily obtained.[34]

Despite the fact that reactions of tetrazines with organometallic compounds can be troublesome, cross coupling reactions of nonsymmetrical chloro-tetrazines under Sonogashira and Negishi conditions were investigated.[35] The reactions yield of Sonogashira couplings ranged from 29 to 65%, whereas the highest yield for the Negishi couplings was only 30%. In either coupling reaction, the higher yields were obtained when a tertiary amine was present at 6-position of the tetrazine. All other substituents (chloro, methoxy and pyrrolyl groups) lead to decomposition or acetylyde homocoupling reaction products, showing that the cross coupling is strongly dependent on the 6-position substituent, and is apparently limited to electron-donating groups. Stille cross coupling reactions between either 3,6-dichloro-*s*-tetrazine and bis(2-picolyl)amine-*s*-tetrazine with 4-(trimethylstannyl)-tetrathiafulvalene (TTF) have been recently presented.[36] Reaction yields were moderate to low (49% and 28%, respectively) and clearly show that in this case, electron withdrawing groups provide the best substracts for palladium cross coupling reactions.

Oxidation reactions on the tetrazine ring leading to N-oxides can be performed by the standard oxidizing agents such as peroxymonosulfuric acid, peroxytrifluoroacetic acid and hypofluorous acid. Complex mixtures are usually obtained since there are several N-oxidation sites. For example, Chavez *et al.* reported that the oxidation reaction of 3,6-diamino-*s*-tetrazine and 3,6-azobis(6-amino)-*s*-tetrazine originate mixtures of bis-N-oxides and poly-N-oxides, respectively (**Scheme 3.7**).[37,38]

Finally, reduction reactions at the *s*-tetrazine ring are also possible. For example, reduction of the heterocyclic N=N bond of 3,6-diphenyl-*s*-tetrazine by hydride transfer

reactions promoted by scandium triflate were recently performed.[39]

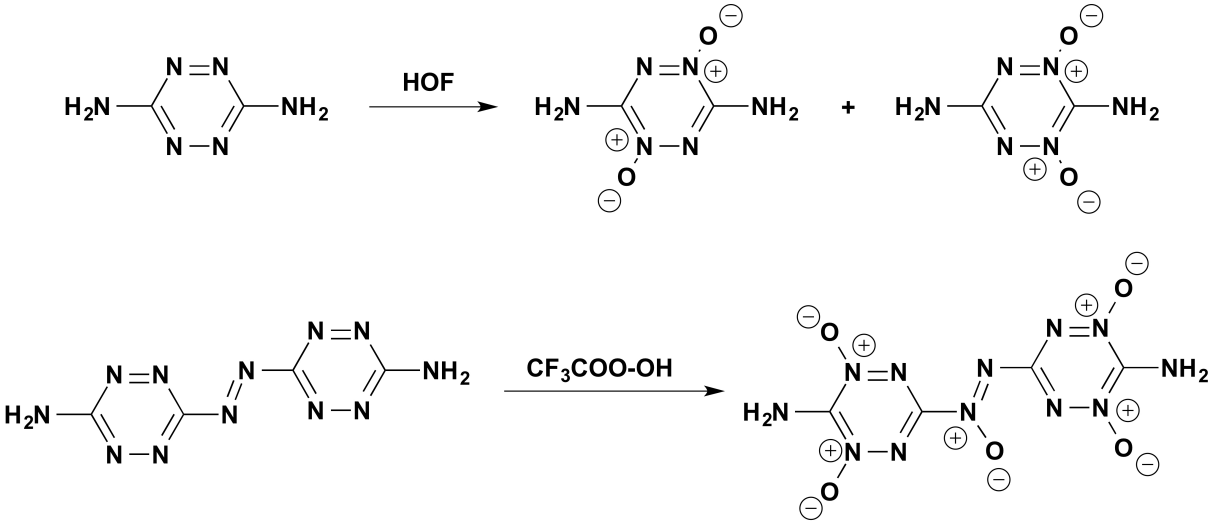

Scheme 3.7: Oxidations of the tetrazine ring performed by Chavez

3.1.3 Tetrazine Applications

Tetrazine chemistry had always a relatively fair interest to chemists, but this interest has grown in the past two decades. This recent grown interest was probably due to novel applications related not only with material chemistry but also, and by far more importantly, medicinal and pharmaceutical chemistry. Nowadays, tetrazine find application in four main research areas: High Energetic Density Materials (HEDM's), Coordination Chemistry, Pharmaceutical Chemistry and Material Chemistry.

High Energetic Density Materials (HEDM's) are organic compounds that possess a large number of N-N and C-N bonds and a low percentage of carbon and hydrogen. Therefore, the term HEDM's is mainly a posh name for a class of explosives and pyrotechnic compounds, and its derived from the two main features of such compounds: very high positive values of heats of formation and high crystal densities. These materials can be surprisingly insensitive towards friction, impact and electrostatic discharges. Their reduced stability makes them suitable for explosive and propellant applications. In fact, tetrazines are one of the best performing family of compounds for this application.

The development of HEDM compounds based on tetrazine has been enormously de-

veloped by Hiskey *et al.*, which purposed the majority of the known tetrazine-based compounds in this area.[37,38,40] **Figure 3.2** shows some structures of compounds synthesized by this author. Heats of formation of a series of *s*-tetrazine derivatives have also been studied by quantum methods.[5,41]

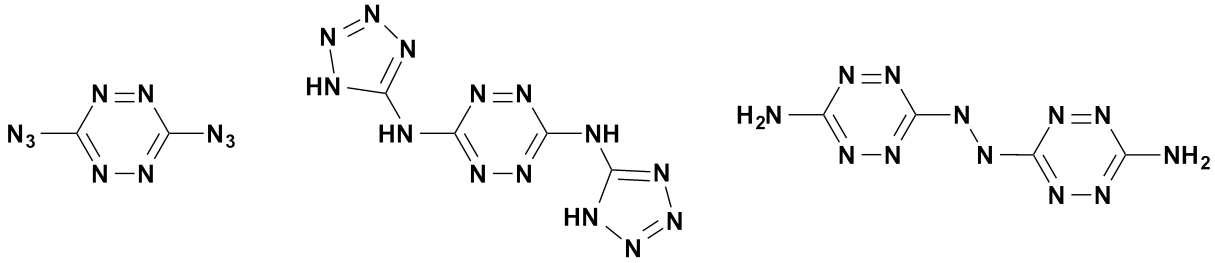

Figure 3.2: Some examples of HDEM's based on tetrazine derivatives and their heat's of formation.

In the past decade, the exploitation of the electronic properties of tetrazine-based compounds, as well as the advances in their synthetic methodologies, brought them to light in the scientific community, in particular to the organometallic chemistry area. In general, the *s*-tetrazine coordination chemistry is characterized by the ability of these heteroatom-rich ligands to bridge metal centres in various ways, depending on its substituents. The complexes usually present highly efficient electron and charge transfer phenomena, low-energy absorptions, electrical conductivity and stability of paramagnetic radical or mixed-valence intermediates. The coordination chemistry of tetrazines was recently revised.[42] The most frequent tetrazine ligands used in coordination chemistry are the 3,6-bis(pyridyl)- and the 3,6-bis(pyrimydil)-*s*-tetrazine families, whose structures are depicted in **Figure 3.3**.[43,44]

The 3,6-bis(pyridyl) family presents two pyridyl rings that makes the chelation of metal centres easily achieved. From the three possible isomers, the 3,6-bis(2-pyridyl)-*s*-tetrazine ligand is the most studied and there are several reports of ($\mu^2 : \mu^2$)-complexes containing this ligand. Several monomeric or heterodinuclear complexes of this ligand are known.[45] It can act as a transoid symmetrically bis-chelating ligand, coordinating two metal centres per tetrazine unit (**Figure 3.4**). The 3,6-bis(3-pyridyl)-*s*-tetrazine, in its turn, originates both cisoid and transoid structures, providing different coordination

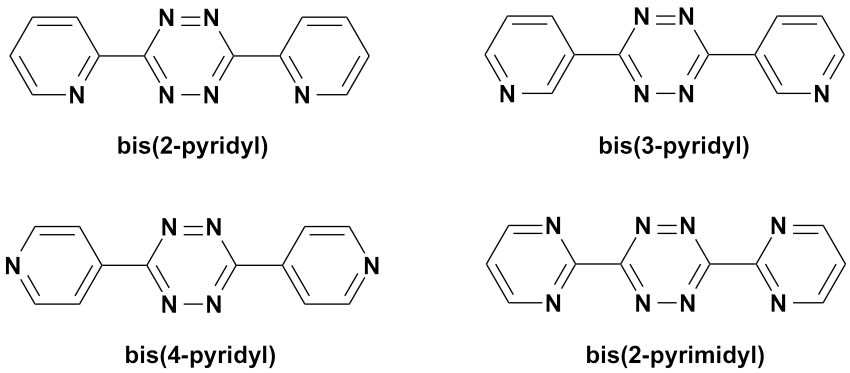

Figure 3.3: Structures of the 3,6-bis(pyridil)-*s*-tetrazine and 3,6-bis(pyrimydil)-*s*-tetrazine families.

fashions like zig-zag chains or non-interpenetrated ladder structures. Both structures can be controlled by choosing the adequate synthetic method, in particular the solvent used in the reaction.[44] The counter anion also plays a crucial role in the crystalographic structure of the final product.[46] The 3,6-bis(4-pyridyl)-*s*-tetrazine is the only linearly binding ligand of the three isomers and it can coordinate to metal centres in the same fashion as pyrazyne and 4,4'-bipyridine. It is appropriate to form dinuclear complexes, but the formation of coordination oligomers or polymers is the most frequent product of reaction. There are known polymeric complexes of tungsten, iron, ruthenium, osmium, silver, copper and cadmium with the 3,6-bis(4-pyridyl)-*s*-tetrazine isomer.[42,47]

The stability of the formed metal complexes is also dependent on the metal centre. For example, although dinuclear ruthenium (II) containing bridging 3,6-bis(2-pyridyl)-*s*-tetrazine complexes are well known and characterized, their iron (II) analogues quickly decompose and attempts to grow single crystals were not successful.[48–50].

Coordination to pentaamine-ruthenium$^{(II)}$ through only the *s*-tetrazine nitrogens has been observed.[51,52] Both the mononuclear $[Ru(NH_3)_5(tetrazine)]^{2+}$ and the dinuclear $[Ru(NH_3)_5(tetrazine)Ru(NH_3)_5]^{4+}$ were successfully synthesized (**Figure 3.5**). The acetonitrile electronic spectrum of the dinuclear complexe presented a very low-energy charge transfer band (750 nm) assigned to a MLCT, revealing the high coupling between the metal centre and the tetrazine-based ligand.

Octahedral mononuclear $[Ru(acac)_2(tetrazine)]^{2+}$ and $[Ru(bpy)_n(tetrazine)_m]^{2+}$ (acac = acetylacetonate, bpy = 2,2-bipyridine and tetrazine = 3-amino-6-(3,5-dimethylpyrazol-

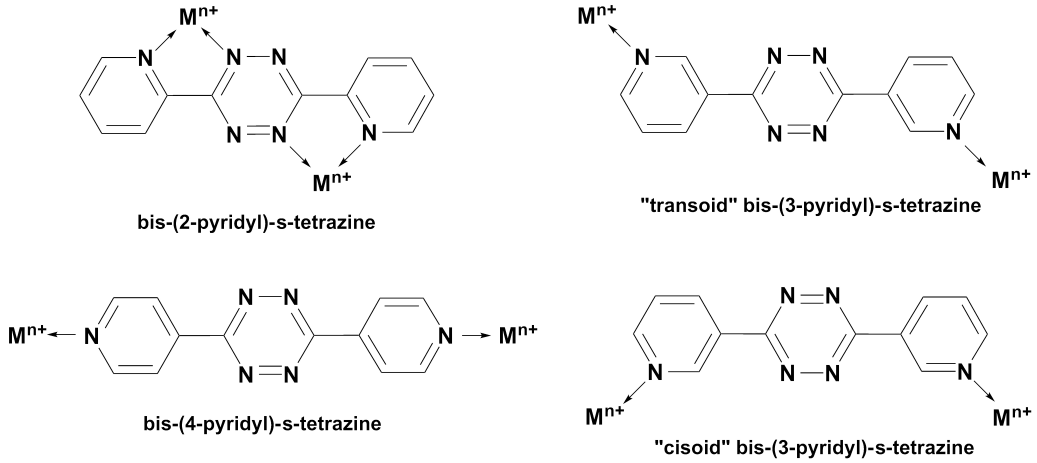

Figure 3.4: Coordination modes of the 3,6-bis(pyridil)-*s*-tetrazine isomers.

1-yl)-1,2,4,5-tetrazine; n=2 when m=1 and n=1 when m=2) were also synthesized.[53] Structural studies reveal that the good electron donor acac co-ligands provided better π-backdonation to the metal centre than the bispyridyl analogues, resulting in lower energy MLCT transitions and lower redox potentials.

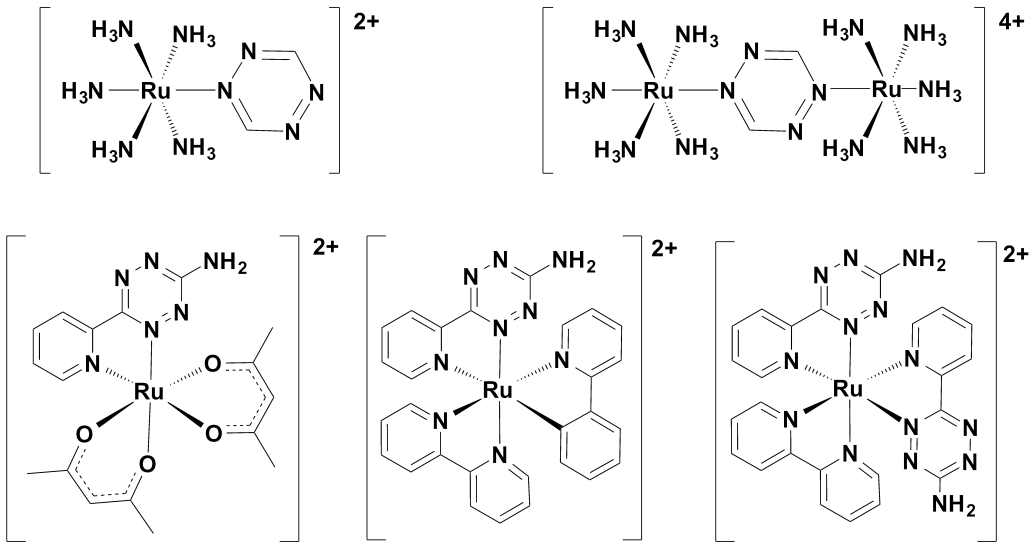

Figure 3.5: Coordination modes of the 3,6-bis(pyridil)-*s*-tetrazine isomers.

The usage of *s*-tetrazines, and specially their hydro derivatives, in medicinal and phar-

maceutical chemistry have also been evaluated. In fact, *s*-tetrazines had already showed high potential for biological activity, namely antimalarial activity.[54] Since then, other diarylamino-*s*-tetrazines with significative antimalarial activity were reported.[55] Also, it was recently demonstrated that the simple 3,6-dimethyl-*s*-tetrazine and its carboxamide derivatives showed the good efficacy on the treatment of tumours.[11,56–58]

More recently, *s*-tetrazines have been widely used in bioorthogonal reactions through a [4+2] Diels-Alder addition reaction with biomarkers, fluorogenic compounds like boron-dipyrromethene (BODIPY) derivatives, nanoparticles or simple strained dienophiles such as norbornene and cyclooctyne (**Scheme 3.8**). These reactions are catalyst free and have high kinetic constants both in aqueous solutions or serum.[12,14]

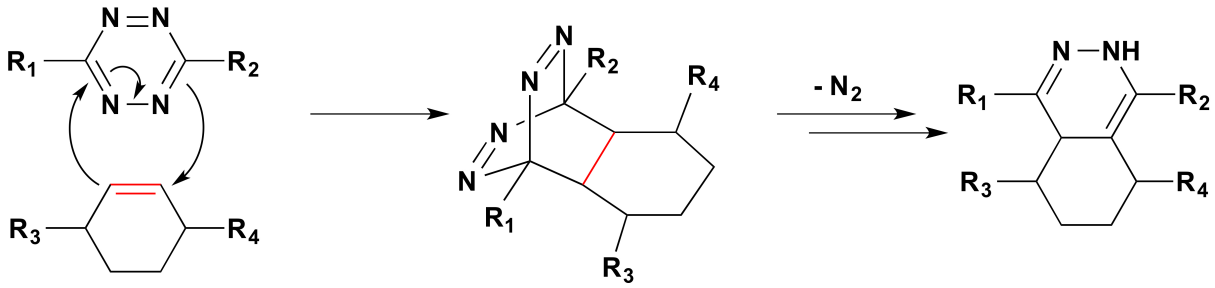

Scheme 3.8: Schematic representation of the [4+2] cycloaddition reaction between *s*-tetrazines and a diene.

Over the past two decades there was a enormous burst in the field of molecular materials, especial in the tailoring of molecular properties for applications such as conducting polymers, photovoltaic devices or Organic Light-Emitting Diodes (OLED's) and of course NLO materials. Over this period several aromatic systems were tested but is quite surprising that only in the past few years *s*-tetrazines has been tested for such applications.

Due to their unique electronic characteristics, one of the most frequent application of tetrazine-based compounds is the preparation of *n*-dopable conducting polymers. Although Soloducho *et al.* presented one of the first synthetic methodology of *s*-tetrazine building blocks for polymerization applications he never synthesized any polymer, and he only studied the properties of the polymers theoretically. These building blocks were based on 2-pyrrolyl and 2-thienyl-*s*-tetrazine.[6] The first report of an electroconducting polymer was made by Audbert *et al.* a few years ago, where he took the building blocks prepared by Soloducho *et al.* and performed the electrochemical polymerization of bis[5-

(2,2-bithienyl)]-*s*-tetrazine.[59]The interesting result found by this author is that dipyrrol-*s*-tetrazine does not polymerize, and that this feature is common for all *s*-tetrazines singly substituted with a heterocyclic ring, like dithiophene-*s*-tetrazine. However, it is still not clear why some singly substituted *s*-tetrazine do polymerize, like difluoropyrrole-*s*-tetrazine, di(trifluoromethyl)thiophene-*s*-tetrazine or di(3,4 -Ethylenedioxythiophene)-*s*-tetrazine.[7]

Being a very strong electron acceptor, the *s*-tetrazine ring has great potential to make part of a classical *push-pull* system for NLO applications. It was also proposed that, besides this dipolar *push-pull* systems, *s*-tetrazine can contribute to the formation of an octupole linear system. Also, the tetrazine ring can be the attractive centre of symmetrical quadrupolar molecules, for enhanced third-order hyperpolarizabilities, γ.

This synthesis of 1,3-bis(ferrocenyl)-*s*-tetrazine and 1,3-bis(4-ferrocenphenyl)-*s* -tetrazine, whose structures are presented in **Figure 3.6**, have been recently reported and their third-order nonlinear optical properties were evaluated.[60] It was shown that these compounds present a intramolecular charge transfer interaction between the metal centres, especially for the shorter molecule. Their third order NLO properties are moderate and show that the ferrocenyl group does not play a highly important role in the γ values. A possible explanation for the γ values could be the fact that ferrocene is not a strong electron donor.

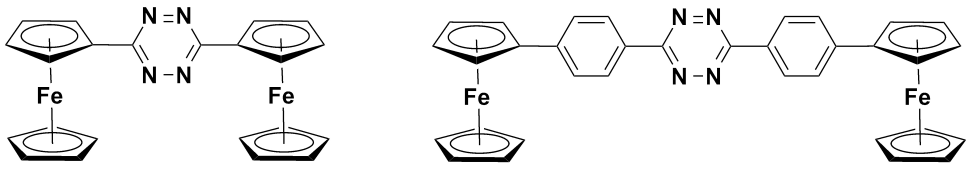

Figure 3.6: Structures of ferrocenyl tetrazine derivatives.

Finally, it was recently shown that simple tetrazine compounds like 3-chloro-6-metoxy-*s*-tetrazine or 3,6-bis-(bithienyl)-*s*-tetrazine can act as electrofluorescent molecular switches.[61,62] These compounds featured both highly stable reduced anion-radicals and fluorescence in the neutral state. The fact that the fluorescence of the tetrazine fluorophores can be switched "on" and "off" reversibly makes a perfect example that *s*-tetrazines are suitable candidates for electroswitchable NLO devices.

3.2 Results

3.2.1 Synthesis and Spectroscopic Studies of the Ligands

Syntheses of the tetrazine ligands were based in two different methodologies, both of them involving the formation of the *s*-tetrazine ring. The structures of the synthesized ligands are showed in **Figure 3.7**.

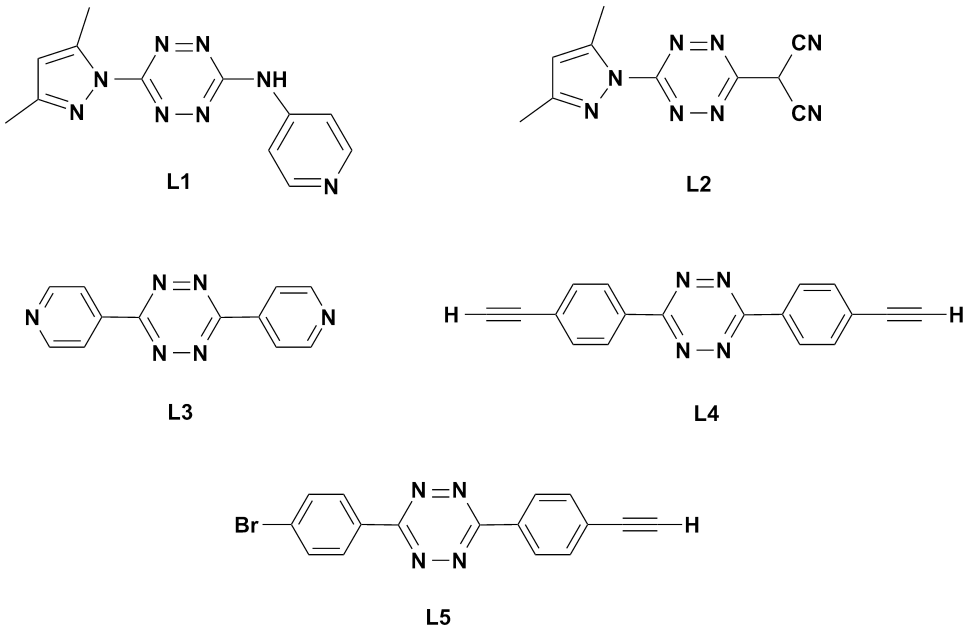

Figure 3.7: Structure of the synthesized *s*-tetrazine-based ligands

The first method, applied to ligands **L1** and **L2**, was based on nucleophilic aromatic substitution (ArSN) reactions involving 3,6-bis(3,5-dimethylpyra-zol-1-yl)-*s*-tetrazine (**3**), that, in its turn, was synthesized based on a published procedure with some modifications.[63,64] The second method, applied in the synthesis of ligands **L3** and the precursor of ligands **L4** and **L5**, was based in Pinner's synthetic method as described previously. Finally, ligands **L4** and **L5** were synthesized by an unprecedented Sonogashira reaction, starting from 3,6-bis(4-bromophenyl)-*s*-tetrazine (**6**).

Ligands **L1** and **L2** were both synthesized starting from 3,6-bis(3,5-dimethylpyra-zol-1-yl)-*s*-tetrazine (**3**). This precursor was synthesized according to **Scheme 3.9**. Initially, guanidine hydrochloride was refluxed in 1,4-dioxane with a 80% hydrazine hydrate solution

in water to afford triaminoguanidine (**1**) in quantitative yield. The obtained white solid was then condensed with 2,4-pentanedione to afford 3,6-bis(3,5-dimethylpyrazol-1-yl)-1,2-dihydro-*s*-tetrazine (**2**) as a stable orange solid. The procedure by Coburn then purposed the use of a sodium nitrite/acetic acid mixture to promote the oxidation of the 1,2-dihydro-tetrazine to its fully aromatic analogue.[63,64] However, it was found that the reaction occurred smoothly in just 4 hours, with no lost in yield, if the 1,2-dihydro-*s*-tetrazine (**2**) was treated with isoamyl nitrite in dichloromethane. Work-up of this reaction was made by simply washing the dark red solution of the product with water. At this point the product is good enough for usage in further reactions. Nonetheless, a more pure product was obtained by performing column chromatography in silica-gel using dichloromethane as eluent. The final product was obtained in good yield as a dark-red, needle-shaped crystalline solid.

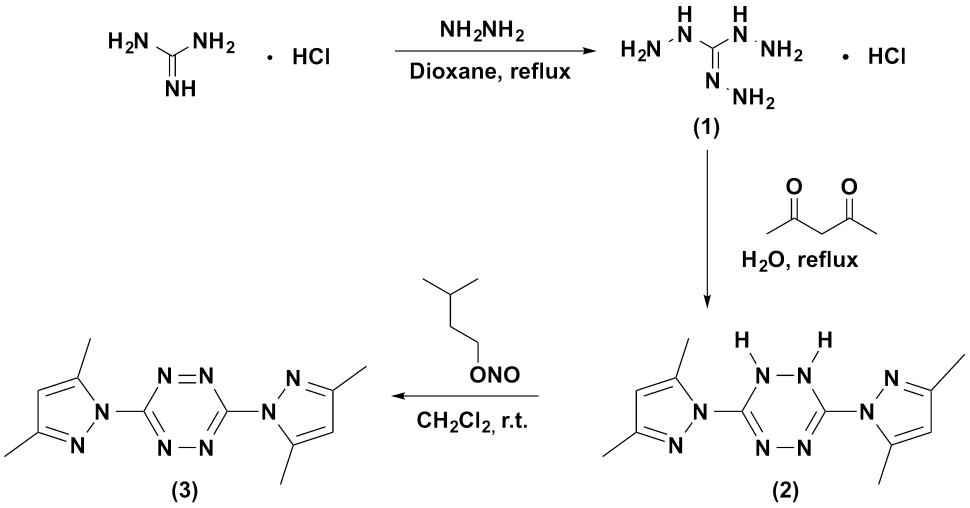

Scheme 3.9: Synthesis of 3,6-bis(3,5-dimethylpyrazol-1-yl)-*s*-tetrazine.

The 3,5-dimethylpyrazolyl group is a good leaving group in the synthesis of several symmetric and asymmetric tetrazines by ArSn reactions.[65] Ligands **L1** and **L2** were hence prepared by ArSn with the adequate nucleophiles as depicted in **Scheme 3.10**. The overnight reaction of (**3**) with one equivalent of 4-aminopyridine in dried acetonitrile and in the presence of an excess of triethylamine, followed by column chromatography (silica-gel/DCM/EtOH (9:1)), afforded **L1** in a moderate yield as a bright orange compound. Reaction of (**3**) with one equivalent of malononitrile in the presence of 1.2 equivalents of

triethylamine has already been described.[66] The reaction was performed in dry toluene from which the product precipitates as a dark purple solid. After evaporation of the solvent and washing of the resulting solid with a 10% hydrochloric acid solution in water, **L2** is obtained in good yield (**Scheme 3.10**).

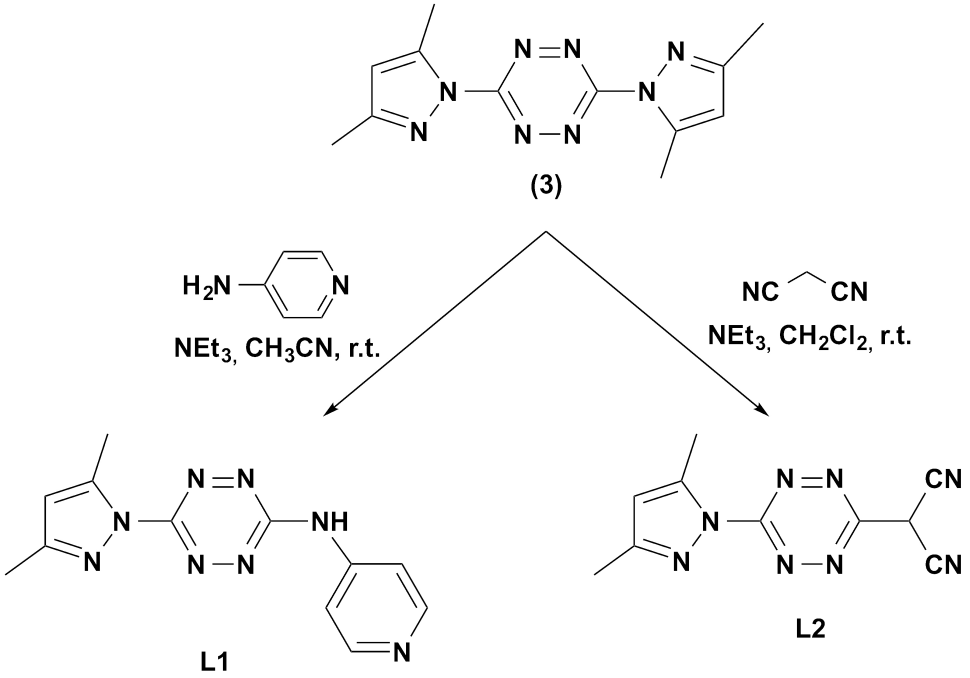

Scheme 3.10: Synthesis of ligands **L1** and **L2**.

Ligand **L3** and the precursor of ligands **L4** and **L5**, in their turn, were synthesized by Pinner's method. In the case of **L3**, refluxing 4-cyanopyridine with an 80% water solution of hydrazine hydrate, in the presence of a catalytic amount of sulphur, afforded the 3,6-di(pyridin-4-yl)-1,2-dihydro-*s*-tetrazine (**4**) as a quickly air-oxidizable orange compound. Due to its quick oxidation, compound (**4**) was immediately treated with isoamyl nitrite in dichloromethane, as described previously for the synthesis of tetrazine (**3**), to afford ligand **L3** in good yield (**Scheme 3.11**). In a similar fashion, the precursor of ligands **L4** and **L5** was also obtained by refluxing the adequate nitrile (4-bromo-benzonitrile) with an 80% water solution of hydrazine hydrate, in the presence of a catalytic amount of sulphur, affording 3,6-bis(4-bromophenyl)-1,2-dihydro-*s*-tetrazine (**5**) as a yellow solid, in good yield. Oxidation was then performed by dissolving (**5**) in dichloromethane containing 10% acetic acid followed by addition of sodium nitrite (**Scheme 3.12**). The resulting 3,6-bis-

(4-bromophenyl)-*s*-tetrazine **(6)** was obtained as a purple solid, insoluble in most solvents. Due to its low solubility, ranging from common halogenated organic solvents, alcohols, DMF and even DMSO, this product was only characterized by FTIR spectroscopy and was used without further purification.

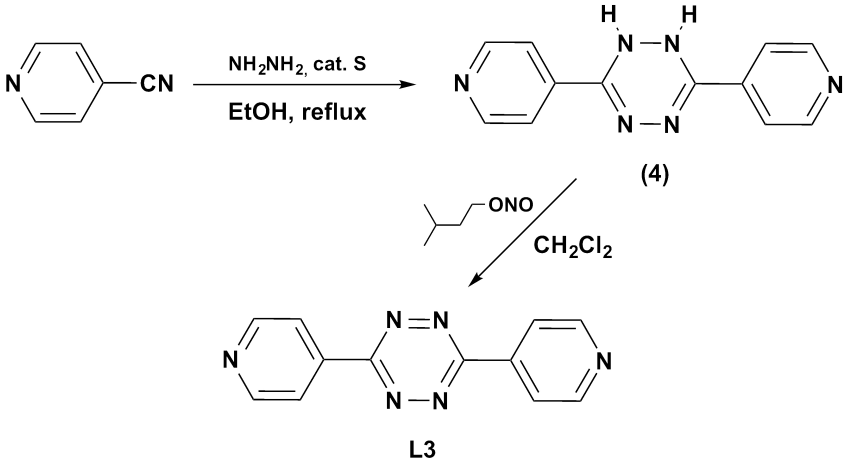

Scheme 3.11: Synthesis of ligand **L3**

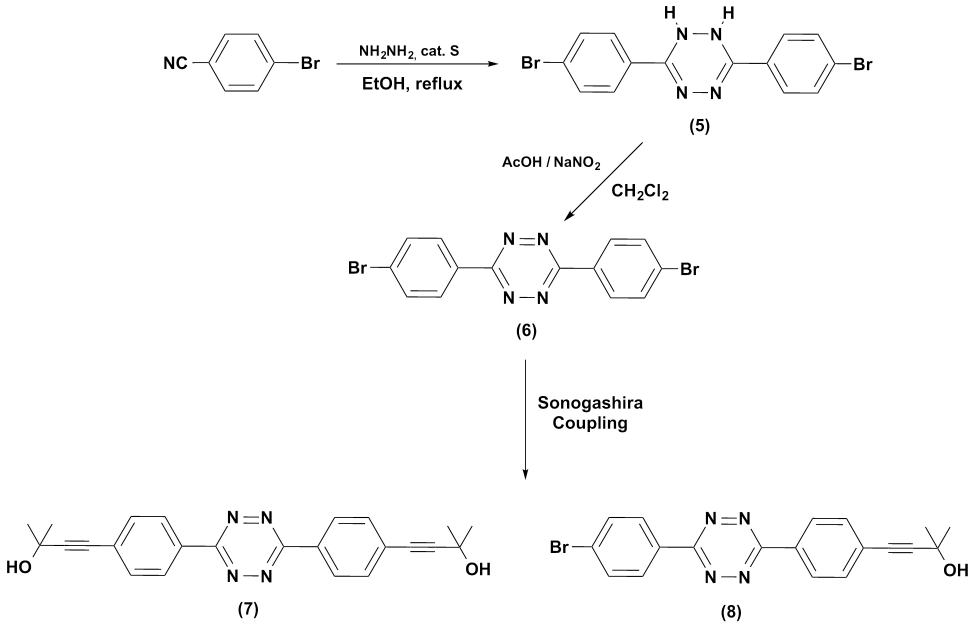

Scheme 3.12: Synthesis of the precursor of ligands **L4** and **L5**

The synthesis of the novel symmetric 3,6-bis(4-ethynylphenyl)-*s*-tetrazine was envisaged by Sonogashira reactions starting from compound (**6**), as showed also in **Scheme 3.12**. In fact, Palladium cross-coupling reactions, namely Negishi and Sonogashira coupling reactions were already described using tetrazine derivatives.[35] Sonogashira couplings have proven to be very limited since only morpholino-substituted tetrazines were found to be stable in the typical Sonogashira conditions. Furthermore, the initial acetylene had also huge influence on the outcome of the reaction. More recently, Sonogashira cross-couplings with 3-(4-iodophenyl)-6-methyl-*s*-tetrazine using trimethylsylilacetylene were found to afford 3-(4-ethynyl)phenyl-6-methyl-*s*-tetrazine in 74% yield.[67] As far as this work is concern, this is the only ethynylaryl-*s*-tetrazine derivative in the literature, and therefore a great opportunity was forecasted.

It is well known that Sonogashira cross coupling can be performed in a huge variety of organic solvents, aqueous mixtures containing organic solvents, water or even in solventless conditions. Furthermore there are several examples in the literature for which arylhalides bearing strong electron withdrawing groups provide low reaction yields. For these cases, it was shown that, depending on the arylhalide substracte, the usage of diisopropylamine (DIPA) as base or solvent can outperform the typical triethylamine.[68–70] Therefore, the optimization of the reaction conditions for the synthesis of novel ethynylaryl-*s*-tetrazines in terms of solvent, base and temperature was mandatory. Due to the strong electron acceptor characteristics of the tetrazine-based ligands, the palladium catalyst and the copper co-catalyst loadings were increased from the typical 5–10 mmol% to 20 mmol%. Also, the solvent-to-base proportion was kept constant in all reactions so that the yields could be rationalized considering solely the properties of the chosen acetylene, base and solvent.

The typical conditions for the cross-couplings Sonogashira reaction used in the synthesis of several other heteroaromatic NLO-phores was initially tested.[71] Treatment of compound (**6**) with two equivalents of trimethylsilylacetylene (TMSA) in THF and in the presence of triethylamine (TEA) at room temperature did not afforded any reaction product. The fact that TMSA is very volatile prevented the usage of higher temperatures in the reaction, and therefore, 2-methyl-3-butyn-2-ol (MEBYNOL) was tested. This reagent presents several advantages in comparison with TMSA since, not only allows higher reaction temperatures, but also because the coupling products can be easier purified by column chromatography due to the huge different chromatographic polarities between

Table 3.1: Conditions[a] and Yields for the Sonogashira Coupling reactions with tetrazine (**4**)

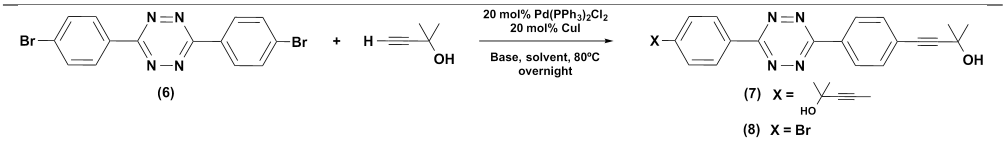

Entry	Solvent	Base	Isolated Yields (%)	
			Comp. (7)	Comp. (8)
1	THF	TEA	0	11
2	DMF	DIPA	15	28
3	DMF	TEA	0	14
4	DMF	DIPA	12	48
5[b]	DMF	DIPA	76	3

[a] - 1 mmol tetrazine; 2 eqs. acetylene; 10 mL solvent; 3 mL base; 20 mol% Pd catalyst; 20 mol% CuI. [b] - 1 mmol tetrazine; 4 eqs. acetylene; 10 mL solvent; 3 mL base; 20 mol% Pd catalyst; 20 mol% CuI.

the products and the starting arylhalides.[72] Results are summarized in **Table 3.1**.

Increasing the temperature of the reaction to 80 °C maintaining the previous conditions (solvent and base) resulted in a low yield of the monoacetylenic compound (**8**) (Entry 1). Performing the reaction at 80 °C in THF in the presence of the less basic diisopropylamine (DIPA) lead to the formation of both the di- and monoacetylenic compounds (**7**) and (**8**) in a 1:2 proportion, albeit low yields were obtained (Entry 2). The influence of the solvent polarity was then investigated. Increasing the polarity of the solvent, going from THF to DMF, maintaining the reaction temperature at 80 °C and using TEA as base afforded only product (**8**) in low yield (Entry 3). Comparatively to the results of Entry 1, minimal changes of the reaction yield are observed, and thereby it is clear that the selected base has great influence in the reaction mechanism. Combining the usage of DMF and DIPA as solvent and base, respectively, an improvement of the reaction yield was observed, in particular for compound (**8**) which yield is now 4 times higher than the yield obtained for compound (**7**) (Entry 4). It is then clearly noticeable performing the reaction at 80 °C in a DMF/DIPA mixture are more adequate conditions for this particular reaction. Finally, doubling the loading of the acetylene under the previous conditions resulted in a high increase of the formation of compound (**7**) (Entry 5). Therefore, the mono- or di-ethynyltetrazine compounds (**7**) and (**8**) can be obtained in moderate to good yields

choosing the adequate conditions.

Deprotection of the synthesized protected acetylides to afford ligands **L4** and **L5** was made by the method purposed elsewhere.[73] Refluxing compounds (**7**) and (**8**) with sodium hydroxide in the presence of sodium triphosphate resulted in a complete removal of the 2-methyl-3-butyn-2-ol group, affording the symmetrical 3,6-bis(4-ethynylphenyl)-*s*-tetrazine (**L4**) and asymmetric 3-bromo-6-(4-ethynylphenyl)-*s*-tetrazine (**L5**) in good yield (**Scheme 3.13**).

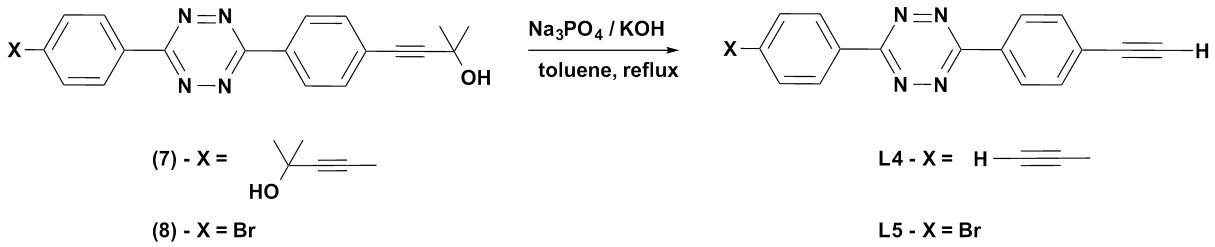

Scheme 3.13: Deprotection reaction of compounds (**7**) and (**8**) to afford ligands **L4** and **L5**

The five synthesized ligands were fully characterized by FTIR, NMR and Uv-Vis. spectroscopies.

The FTIR spectra of all the ligands, as well as the spectra for the ligand precursors (**3**) and (**6**), present the characteristic peaks attributed to the *s*-tetrazine C=C and N=C ring vibrations in the 1600−1350 cm^{-1} and 1000−1200 cm^{-1} regions, respectively.[74] The ligands present other characteristic signals, correlated with their functional groups. In particular, ligand **L1** presents a band at 3236 cm^{-1} characteristic for the ν_{NH} vibration. Concerning ligand **L2**, it presents two sharp signals of equal intensity at 2207 and 2176 cm^{-1} assigned to the symmetric stretching of the dicyanovinyl group. These values are in the typical range observed for other NLO chromophores containing dicyanovinyl groups.[75,76]

Ligand precursors (**7**) and (**8**) present the characteristic hydroxyl stretching signal at 3438 and 3285 cm^{-1}, respectively. The differences both in signal position and intensity ((**7**) shows a broader and higher intensity band than (**8**)) reflects the presence of one or two hydroxyl groups, respectively. Noteworthy is the fact that the typical C≡C stretching band is not present or has very low intensity.

The successful deprotection of the 3-methylbut-3-yn-2-ol group in the synthesis of ligands **L4** and **L5** was confirmed by the absence of the previously mentioned hydroxyl stretching band, and by the presence of the characteristic band for a terminal C≡C–H, at 3286 and 3270 cm^{-1}, respectively. Like in the case of compounds (**7**) and (**8**) the typical C≡C stretching band is not observed.

The detailed ^{1}H-NMR and ^{13}C-NMR chemical shifts and integral of resonance signals for the **L1**-**L5** ligands are given in Section 3.5. **Figure 3.8** shows the structures and the numbering used in the NMR attributions, whereas **Tables 3.2** and **3.3** summarize the collected ^{1}H-NMR and ^{13}C-NMR data. The ligands present only moderate solubility in $CDCl_3$ or $(CD_3)_2CO$, and for the sake of comparison between them DMSO-d^6 was chosen as the NMR solvent. Also, ligand **L5** presents poor solubility in most deuterated solvents and hence only ^{1}H-NMR is presented.

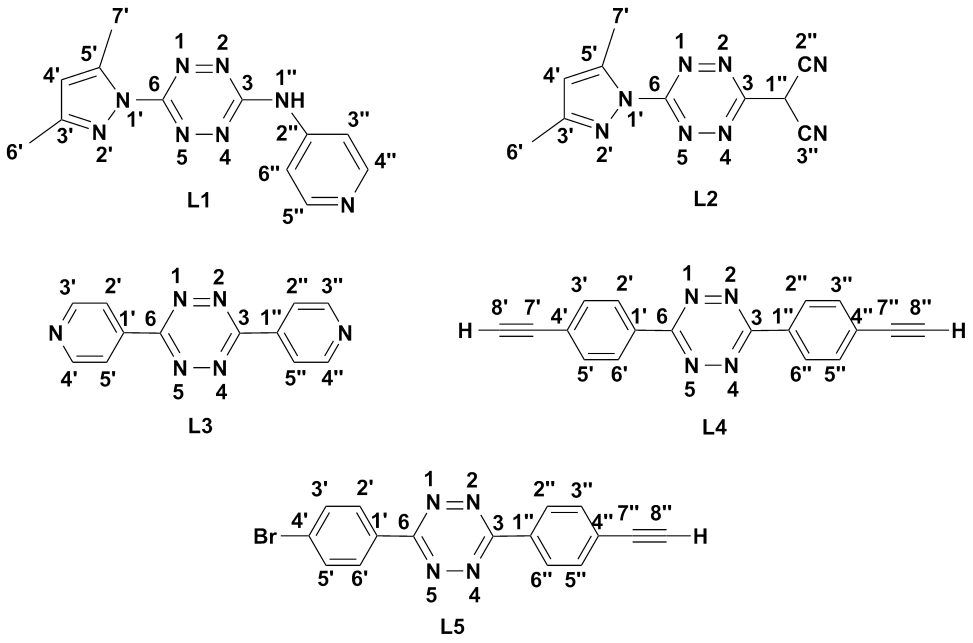

Figure 3.8: Structures and atom numbering used in the NMR characterization of the tetrazine ligands

The ^{1}H-RMN spectra of compound (**3**) and ligands **L1** and **L2** present the characteristic singlets attributed to the 3,6-bis(3,5-dimethylpyrazolyl) groups. Comparison of the resonances for protons $H_{4'}$, $H_{6'}$ and $H_{7'}$ of compound (**3**) with the analogous protons for ligands **L1** and **L2** suggest that the substitution of one of the 3,6-bis(3,5-dimethylpyrazolyl)

Table 3.2: ^{1}H-NMR data for compounds (**3**), (**7**) and (**8**) and for ligands **L1**-**L5**

	^{1}**H-RMN** δ /ppm [a]							
Comp.	(**3**)	**L1**	**L2**	**L3**	(**7**)	**L4**	(**8**)	**L5**
$\mathbf{H}_{2'}$				8.46	8.55	8.55	8.46	8.47
$\mathbf{H}_{3'}$				8.96	7.70	7.80	7.91	7.92
$\mathbf{H}_{4'}$	6.37	6.27	6.15					
$\mathbf{H}_{5'}$				8.96	7.70	7.80	7.91	7.92
$\mathbf{H}_{6'}$	2.28	2.25	2.21	8.46	8.55	78.55	8.46	8.47
$\mathbf{H}_{7'}$	2.60	2.50	2.37					
$\mathbf{H}_{8'}$						4.52		
$\mathbf{H}_{10'}$					1.51			
$\mathbf{H}_{11'}$					1.51			
$\mathbf{H}_{1''}$		11.45						
$\mathbf{H}_{2''}$				8.46	8.55	8.55	8.52	8.55
$\mathbf{H}_{3''}$			8.50	8.96	7.70	7.80	7.69	7.80
$\mathbf{H}_{4''}$				7.75				
$\mathbf{H}_{5''}$			7.75	8.96	7.70	7.80	7.69	7.80
$\mathbf{H}_{6''}$			8.50	8.46	8.55	8.55	8.52	8.55
$\mathbf{H}_{8'}$						4.52		4.54
$\mathbf{H}_{10''}$					1.51		1.51	
$\mathbf{H}_{11''}$					1.51		1.51	

[a] all ^{1}H NMR values in DMSO-d ^{6}.

groups leads to a slight change in the electronic properties of the molecules. In particular, a slight shielding of these protons is observed in both ligands comparatively to compound (**3**), indicating a lower electronic donation from this group to the *s*-tetrazine ring. In fact, the presence of a very downfield shifted singlet at 11.45 ppm, attributed to the $H_{1''}$ proton, suggests a greater electronic coupling between the *s*-tetrazine ring and the nitrogen atom of the 4-aminopyridine ring. For **L2**, the absence of the $H_{1''}$ signal had already been described.[66]

Due to its C_{2v} symmetry, the ^{1}H-RMN spectra of ligand **L3** presents only two doublets at 8.46 and 8.96 ppm assigned to the aromatic protons of both pyridyne rings. However, after being stored for some time, the spectra of this ligand becomes different, now presenting four doublets as shown in **Figure 3.9**, indicating a breaking in the symmetry of the molecule. It is hence hypothesized that, upon long period of storage in air, a reaction with moisture should occur, protonating one of the nitrogen atoms of one of the pyri-

dine rings or the *s*-tetrazine ring. This assumption is confirmed in the correlation in the Heteronuclear Multiple Quantum Coherence (HMQC) and Heteronuclear Multiple Bond Correlation (HMBC) spectra, where $^{1}J_{C\text{-}H}$ and $^{3}J_{C\text{-}H}$ correlations are observed (also shown in **Figure 3.9**). In fact, it is clearly observed from the 2D correlation spectra that the quaternary carbons are much more affected than the remaining aromatic carbon atoms, suggesting that an interaction with the *s*-tetrazine ring is present. In order to confirm that the observed NMR behaviour is an interaction and not a formal *s*-tetrazine ring reduction, a second spectrum of the same sample tube, to which approximately 1μL of triethylamine was added, was acquired (**Figure 3.10**). The diminishing of the intensity, and therefore the integration area, of two of the doublets suggests that, indeed, protonation without ring reduction had occurred. Noteworthy is the fact that the water present in the deutarated DMSO prevented the complete disappearance of the mentioned signals.

Like the case of **L3** and due to symmetry reasons, compound (**7**) and ligand **L4** present only two doublets in the aromatic region. Conversely, compound (**8**) and ligand **L5** present four doublets in the aromatic region confirming the single substitution of a bromine atom by the alkyne in the previously described Sonogashira conditions. The similarity in the obtained chemical shifts in the spectra of the compounds bearing either protect of free acetylide groups allows to state that the presence of different substituents in the aromatic rings does not have significative influence on the electronic properties of the different compounds. However, comparatively to other terminal acetylenes, both ligands present resonances slightly shifted to upfiled, showing the strong electron withdrawing effect of the tetrazine ring.[71] Also, comparison of the aromatic protons of **L3** with both **L4** and **L5** shows a significative deshielding of the signals for **L3**, reflecting the presence of the more electronegative pyridine rings.

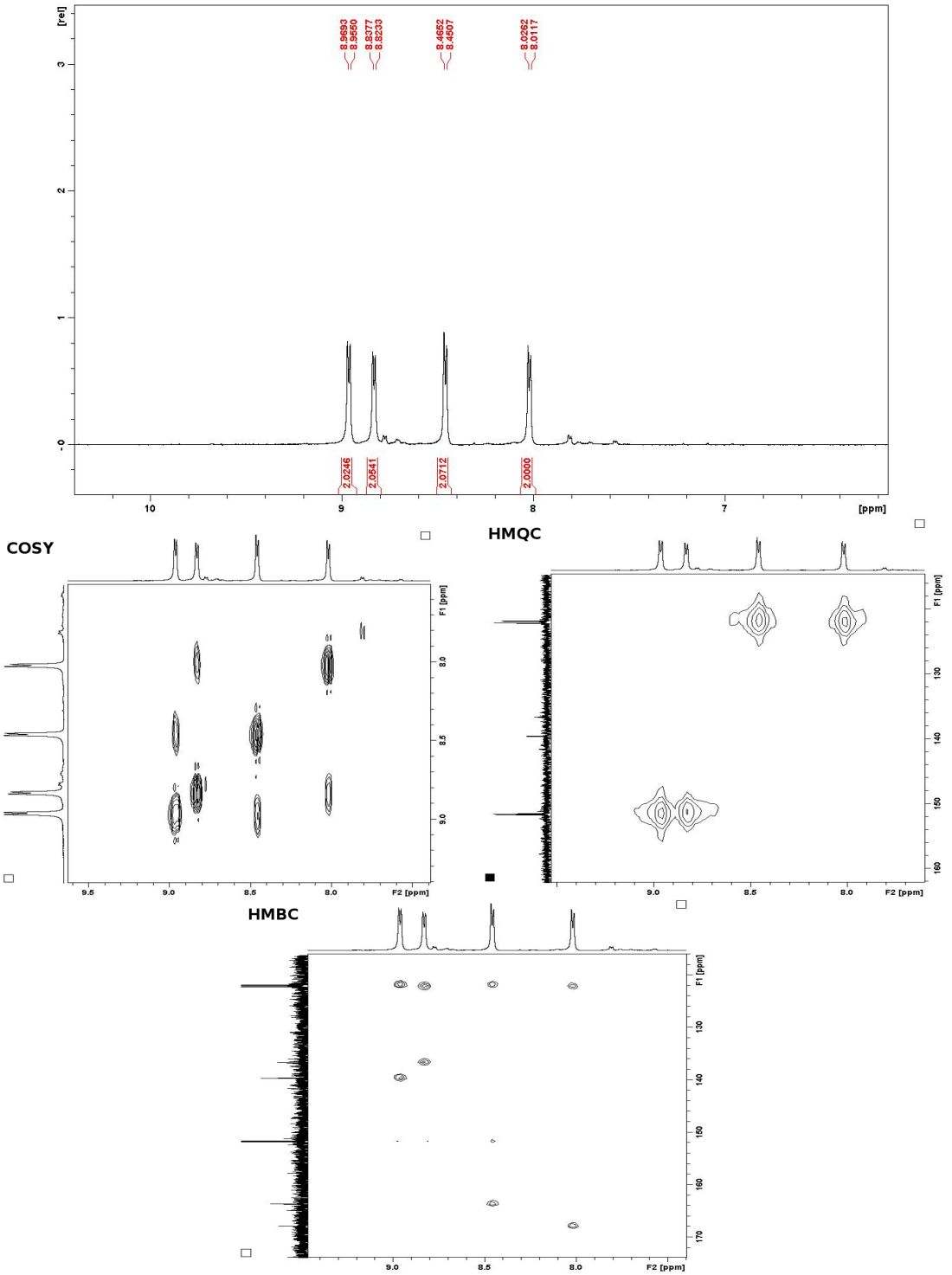

Figure 3.9: Proton and 2D correlation spectra for the protonated adduct of **L3**

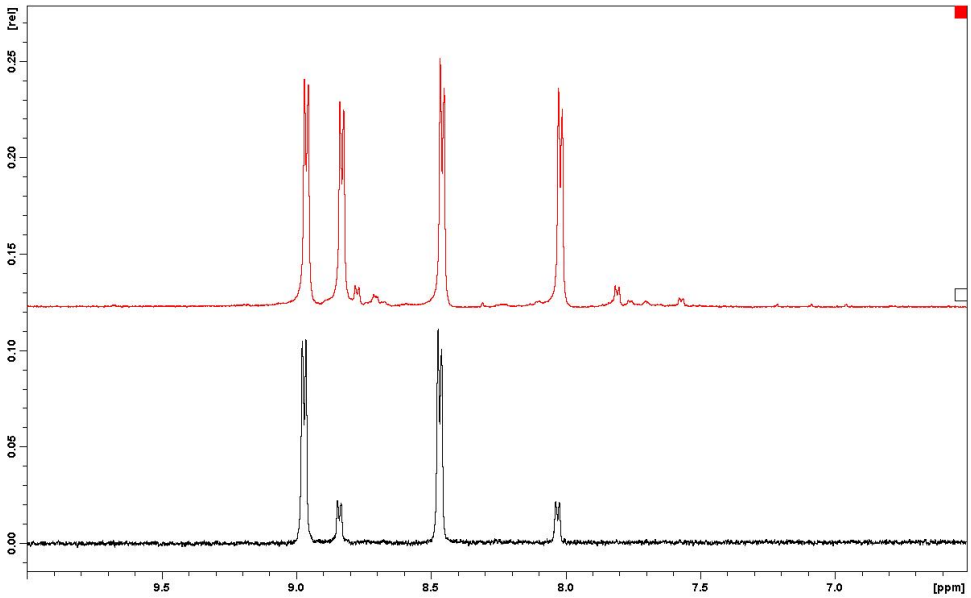

Figure 3.10: DMSO-d^6 ^{1}H-NMR spectrum of **L3** treated with $\approx 1\mu$L of triethylamine

Conversely to the ^{1}H-RMN spectra where only a few correlations of the protons of different ligands can be made, the analysis of C_3 and C_6 carbons in the ^{13}C-RMN for each ligand can give some insight on the electronic character of the tetrazine ring, since all the ligands share a common central tetrazine ring. This correlation is important since the ligands have different donor/acceptor properties, and hence one can infer about the substituent electronic effects on the tetrazine ring.

Carbons C_3 and C_6 appear as the most deshielded signals of the carbon spectra of all the ligands, at *ca.* 160 ppm, clearly reflecting the presence of the four nitrogen atoms in the tetrazine ring. The presence of different substituents, with different electronic properties, does not linearly correlate with the C_3 and C_6 resonance signals. For example, compound (**3**), bearing only electron donating groups, shows a lower resonance than **L3** that possess only electron withdrawing groups. However, compound (**7**) and **L4**, both presenting electron donor groups, have resonances closer to **L3**. It is hence noticeable that the linkage of the tetrazine ring to its substituents has also great influence in the overall electronic properties of the compounds. Tetrazines linked to their substituents through C–C bonds present more downfield resonances for C_3 and C_6 when compared to tetrazines linked with C–N bonds. This fact is clearly shown by the signals of **L2**, presenting both types of bonds, for which C_3 (involved in a C–C bond) has a resonance of 169.93 ppm

whereas C_6 (involved in a C–N bond) has a resonance of 156.39 ppm. The high resonance for C_3 in **L2**, in comparison with other ligands, is obviously due to the presence of the good electron acceptor dycianovynyl group.

Table 3.3: ^{13}C-NMR data for compounds (**3**), (**7**) and (**8**) and for ligands **L1**-**L4**

	^{13}**C-RMN** δ /ppm [a]						
Comp.	**3**	**L1**	**L2**	**L3**	**7**	**L4**	**8**
$\mathbf{C_3}$	159.16	160.58	169.93	163.45	163.00	163.17	162.94
$\mathbf{C_6}$	159.16	157.21	156.39	163.45	163.00	163.17	162.72
$\mathbf{C_{1'}}$				139.45	126.80	126.27	131.12
$\mathbf{C_{2'}}$				121.69	127.75	128.17	129.51
$\mathbf{C_{3'}}$	152.97	151.09	149.70	151.58	132.29	132.19	132.66
$\mathbf{C_{4'}}$	111.37	109.59	108.27		131.32	132.41	126.83
$\mathbf{C_{5'}}$	143.49	142.04	141.19	151.58	132.29	132.41	132.66
$\mathbf{C_{6'}}$	14.05	13.44	13.35	121.69	127.75	132.19	129.51
$\mathbf{C_{7'}}$	13.85	12.92	12.21		79.96		
$\mathbf{C_{8'}}$					99.47	55.31	
$\mathbf{C_{9'}}$					63.74		
$\mathbf{C_{10'}}$					31.48		
$\mathbf{C_{11'}}$					31.48		
$\mathbf{C_{1''}}$			139.45	139.45	126.80	126.80	131.29
$\mathbf{C_{2''}}$		145.35	119.90	121.69	127.75	128.18	127.76
$\mathbf{C_{3''}}$	152.97	150.49	119.90	151.58	132.29	132.19	132.30
$\mathbf{C_{4''}}$	111.37	113.17			131.32	132.41	126.75
$\mathbf{C_{5''}}$	143.49	113.17		151.58	132.29	132.19	132.30
$\mathbf{C_{6''}}$	14.05		150.49	121.59	127.75	132.41	127.76
$\mathbf{C_{7''}}$	13.85				79.96		79.95
$\mathbf{C_{8''}}$					99.47	55.31	99.51
$\mathbf{C_{9'}}$					63.74		63.75
$\mathbf{C_{10'}}$					31.48		31.48
$\mathbf{C_{11'}}$					31.48		31.48

[a] all ^{13}C NMR values values in DMSO-d ^{6}.

The ^{13}C-RMN signals of the substituent groups are consistent with the analysis made for ^{1}H-RMN described previously. In the case of compound (**3**) and ligands **L1** and **L2**, the same behaviour found for in $H_{4'}$, $H_{6'}$ and $H_{7'}$ is observed in carbons $C_{3'}$-$C_{7'}$, that is a shielding in every carbon going from compound (**3**) to ligands **L1** and **L2**. Like in the

case of the proton spectra, this behaviour in the carbon signals reflect the donor/acceptor properties of the remaining substituents.

The ^{13}C-RMN spectrum of **L3**, in its turn, presents a reduced number of signals due to the symmetry of the compound. For ligands **L4** and **L5** and their precursors, compounds (**7**) and (**8**) the assignments of the acetylene carbons were made by heteronuclear multiple-bond correlation spectroscopy (HMBC), where a clear correlation between both $C_{5'}$ and $C_{5''}$ with $C_{7'}$ and $C_{7''}$, in the case of **L4** and (**7**), and $C_{5''}$ and $C_{7''}$ in the case of **L5** and (**6**) were observed. The carbon signals from the terminal acetylenes are in the typical region found for other highly delocalized terminal acetylenes.[71]

The UV-Vis. spectra for the ligands were performed in 1.0 $\times 10^{-4}$ M chloroform solutions and the spectra were collected from the 900 nm to the cut-off wavelength of the solvent. **Figure 3.11** depicts the obtained spectra for all the ligands, whereas **Table 3.4** summarizes the collected data.

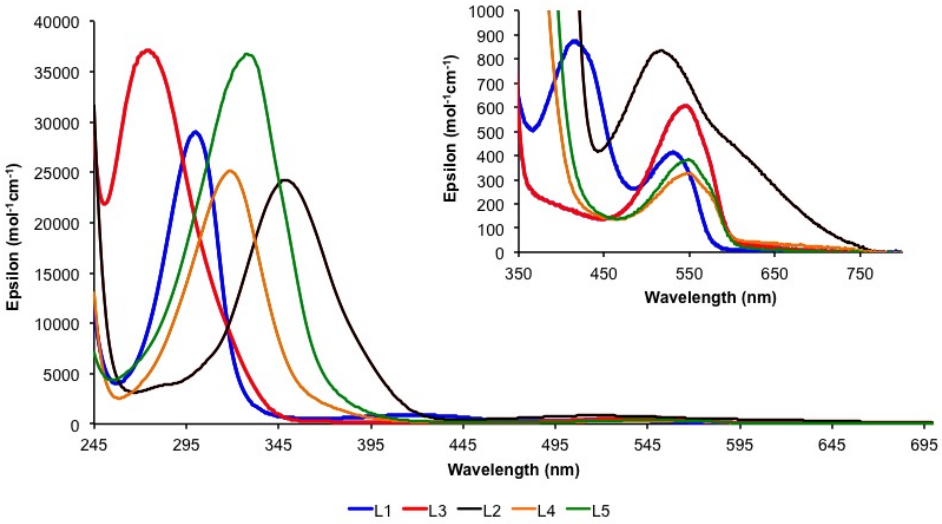

Figure 3.11: UV-Vis. spectra for ligands **L1-L5**

. Inset: Expansion of the 350-700 nm range.

The spectra of the tetrazine-based ligands are characterized by a strong absorption band in the UV region in the 250–370 nm range, attributed to an allowed $\pi \rightarrow \pi^{\star}$ transition, alongside a very weak transition in the visible region (450–560 nm), attributed to a forbidden $n \rightarrow \pi^{\star}$ transition. Ligand **L1** presents an addicional transition centered at 414 nm also attributed to a $\pi \rightarrow \pi^{\star}$ transition. The relative position and intensity of these

Table 3.4: Uv-Vis absorption maxima for the ligands **L1**–**L5**

λ /nm ($\epsilon \times 10^4$(mol^{-1}cm^{-1}))		
Compound	Chloroform	DMF
L1	300 (2.9) 414 (0.09) 530 (0.05)	299 (3.0) 407 (2.1) 523 (0.05)
L2	349 (2.4) 516 (0.09) 638 (sh, 0.04)[a]	339 (3.0) 525 (0.1) [b]
L3	274 (3.7) 544 (0.07)	-[c] 532 (0.06)
L4	319 (2.5) 549 (0.05)	314 (2.4) 543 (0.06)
L5	328 (3.7) 551 (0.04)	325 (3.5) 539 (0.04)

[a] - shoulder; [b] - not observed [c] not observed due to the solvent cut-off

bands can be correlated to the electronic effect of the different *s*-tetrazine substituents. This effect is much more pronounced for the UV band than for the band in the visible region, for which minor differences are observed either in the peak intensity or in the energy of the transition. In fact, the lowest energy transition, attributed to a forbidden $n \rightarrow \pi^\star$, is centred at the tetrazine ring and hence it is not greatly affected by the substituent effects, as shown for other *s*-tetrazine-based compounds and by DFT calculations (*vide infra*).[28,77,78] Concerning this latter transition, it seems, however, that the presence of both two electron donating or two electron accepting groups lead to a slight red shift of this band. Also, a small hyperchromic effect seems to be present. This fact can be justified due to the contribution of both end-groups to the main transition, removing or adding electron density to the tetrazine ring and hence facilitating the transition.

Contrariwise, the UV band, attributed to an allowed $\pi \rightarrow \pi^\star$, transition depends greatly on the type of substituents of the *s*-tetrazine ring. It is clearly shown that electron-donating groups lead to a red shift of this band, accompanied by an hyperchromic effect, whereas electron accepting groups lead to the opposite behaviour, that is a blue shift

accompanied by a hypsochromic effect. For example, ligand **L3**, possessing two electron acceptor pyridyne groups, presents a higher energy transition than both ligands **L1** and **L2**, possessing one electron donating and one electron accepting group. Yet, ligand **L5**, possessing two electron donating groups, is the ligand with lower energy transition in the UV region.

The solvatochromic behaviour of the ligands is also shown in **Table 3.4**. All the ligands present negative solvatochromism, when going from chloroform to DMF, indicating a decrease in their excited state dipole moment upon photo-excitation. In fact, as it will be shown later in Section 3.3, both the forbidden $n \rightarrow \pi^\star$ and allowed the $\pi \rightarrow \pi^\star$ transitions occur with minimum change of the electronic densities or with opposite directions, respectively, leading to an overall net result of a decrease in the dipole moment in the excited state.

3.2.2 Quadratic Hyperpolarizabilities of the Ligands

Although the optical nonlinearity of the ligands were not measured, some considerations based on the obtained spectroscopic data and considering the Two-Level Model (TLM) assumptions can be made. Since ligands **L3** and **L4** have C_{2v} symmetry their hyperpolarizability will be null. In fact, the goal in the synthesis of these ligands its to create asymmetric compounds upon coordination to metal centres in order to break the symmetry of the compounds, hence establishing a quadrupolar architecture.

Due to the nature of the lowest energy transition, it is fair to state that this band will not have significative influence on the measured hyperpolarizabilities of the ligands. For that reason, the nonlinearities for this set of compounds will only be discussed in terms of the higher energy transition. According to the TLM assumptions, low to moderate hyperpolarizabilities are expected for ligands **L1**, **L2** and **L5** for two main reasons: on one side, the energy transition presented by these ligands is relatively high comparatively to other organic or organometallic compounds; on the other side, the change in the dipole moment upon photo-excitation its not expected to be high enough to compensate the previously mentioned electron transition. Another drawback of ligand **L1** is the inadequate positioning of the acceptor group in relation to the donor moiety, diminishing the charge transfer efficiency and hence hampering the hyperpolarizability.

3.2.3 Synthesis and Spectroscopic Studies of the Complexes

Although mononuclear organometallic complexes containing 3,6,-bis(2-pyridyl)-*s*-tetrazine as ligand have been reported (see for example refs.[53,79,80]), there is a single example of a Os (III) mononuclear complex bearing 3,6,-bis(4-pyridyl)-*s*-tetrazine, for which its dymer was also synthesized. Its synthesis involved very harsh conditions (reflux in ethylene glycol for 5 hrs.) and takes advantage of the sterically hindered *cis*-$Os(bpy)_2Cl_2$ organometallic fragment to prevent the formation of polymeric products.[16,81] In this sense, $[(\eta^5\text{-}C_5H_5)M(PP)]^+$ organometallic fragments seemed to be adequate for the synthesis of linear mononuclear *s*-tetrazine-based complexes, since both the monocyclopentadienyl ring and phosphane ligands provide the necessary sterical hindrance to prevent polymer formation.

Complexes of general formula $[(\eta^5\text{-}C_5H_5)M(PP)(TET)[Y]$ (PP = κ^2-dppe when M = Fe(II) and PP = κ^2-dppe or 2 PPh_3 when M = Ru(II); TET = tetrazine ligand; Y = counteranion) were synthesized by halide abstraction starting from the parent neutral complexes $(\eta^5\text{-}C_5H_5)M(PP)X$ (M = Fe(II), PP = κ^2-dppe, X = I; M = Ru(II), PP = κ^2-dppe or 2 PPh_3, X = Cl), in an adequate solvent, in the presence of an excess of the corresponding ligand. In order to establish a working protocol for the new organometallic compounds, the synthesis of the organometallic complexes were initiated by using ligand **L3**. As seen previously, this ligand is easily obtained in a high-yielding two-step synthesis, making it the perfect case study for the unprecedent synthesis with the $[(\eta^5\text{-}C_5H_5)M(PP)]^+$ (M = Fe, Ru; PP = phosphane) organometallic fragment.

The σ-donation strength of a series of azabenzenes was determined by *ab initio* calculations.[82] These calculations showed that the ligand σ-donor strength decreases with the increasing number of nitrogen atoms in the aromatic ring, that is, when going from pyridine to *s*-tetrazine rings. The π-acceptor strength follows the contrary trend, it increases with the increasing nitrogen content of the aromatic rings. Consequently, the coordination of *s*-tetrazines is made by a net result of a small stabilization of empty metal *d* orbitals (ligand σ-donation effect), and by a significative stabilization of the low lying ligand-centred LUMO orbitals by filled *d* orbitals from the metal (ligand π-acceptance effect). Hence, second and third row transition metals are more capable of taking advantage of the $\pi^\star$-orbitals of the ligands, justifying the scarcity of, for example, mononuclear iron-based organometallic tetrazine complexes.

Ligand **L3** can act both as a monodentate or a bidentate ligand. On one hand, if

a single $[(\eta^5\text{-}C_5H_5)M(PP)]^+$ organometallic fragment is coordinated to the ligand, the resulting complex will present the typical Donor-Acceptor (*push-pull*) architecture. On another hand, if two organometallic fragments coordinate to the ligand, the product will present a linear Donor-Acceptor-Donor quadrupolar architecture. This architecture is known for exhibiting different nonlinear optical properties in comparison to those of the *push-pull* architecture.[83] Thus, attempts to synthesize both products were made.

The coordination of **L3** to the Ru(II) metal centre was initially attempted by mixing $(\eta^5\text{-}C_5H_5)Ru(\kappa^2\text{-dppe})Cl$ with the corresponding ligand in dried DCM, at room temperature, in the presence of $TlPF_6$. After *work-up*, the reaction afforded dark purple solids, for which the NMR analysis showed the absence of the characteristic $(\eta^5\text{-}C_5H_5)$ singlet accompained by the appearance of several ^{31}P NMR signals sugestting the decomposition of the initial oraganometallic fragments followed by a possible oligomerization, judging by the amount of intractable solid formed. Mantaining the same conditions and changing the reaction solvent to DMF afforded similar results. Silver (I) salts, namely silver trifluoromethanesulfonate (AgOTf), are long known for being good halogen abstractor agents in the synthesis of $[(\eta^5\text{-}C_5H_5)M(PP)]^+$ (M = Fe, Ru; PP = phosphane) organometallic complexes bearing nitrogen-based ligands.[84,85] However, silver (I) complexes bearing *s*-tetrazine-based ligands, in particular 3,6,-bis(4-pyridyl)-*s*-tetrazine, are long known and for that reason the usage of silver salts as halide abstractor agent is highly unrecommended.[42] Thus, thallium(I) trifluoromethanesulfonate (TlOTf) was selected in the further attempts.

Reaction of ligand **L3** with one equivalent of $(\eta^5\text{-}C_5H_5)Fe(\kappa^2\text{-dppe})I$ afforded a dark purple solution. Attempts to recrystallize the obtained crude dark purple solid resulted in decomposition. However, performing the reaction with the parent ruthenium starting material $(\eta^5\text{-}C_5H_5)Ru(\kappa^2\text{-dppe})Cl$ originated a mixture of the mono and dinuclear complexes together with a considerable of amount unreacted ligand. The excess of the ligand was partially removed by consecutive washings with dried toluene. Selective precipitation afforded the binuclear complex **aRu$_2$L3** in low yield. Further attempts to precipitate the mononuclear **aRuL3** from the remaining supernatant were unsuccessful.

In a similar fashion, reaction of ligand **L3** with one equivalent of $(\eta^5\text{-}C_5H_5)Ru(PPh_3)_2Cl$ originated a mixture of the mono and dinuclear complexes. Separation of the two species was again achieved by selective precipitation of the dinuclear complex **bRu$_2$L3**, as described.

The difference of the ligand solubility in toluene in comparison to the mono and dinuclear complexes suggested that toluene could be an alternative solvent for these reactions, since the formed complexes would precipitate upon formation. Also, in order to prevent the formation of the dinuclear complexes it was hypothesized that an increase of the amount of solvent together with a portionwise addition of the ligand or of the halogen abstractor should be performed. Therefore, ligand **L3** and one equivalent of the initial organometallic ruthenium complexes were reacted in toluene and 10 mol% portions of TlOTf were added every 2 hrs. After completion of the TlOTf addition the mixture was left to stir overnight. The reaction afforded both the mono and dinuclear complexes in a 3:1 proportion (determined by NMR spectroscopy) and a considerable amount of the unreacted ligand. After removal of the ligand by consecutive washing with toluene, selective precipitation afforded again the dinuclear complex. The supernatant was dried and further precipitations were attempted in different solvent mixtures. No pure fractions of either the mono or dinuclear complexes were obtained.

With the successful protocol established for the **L3** ligand, attempts to synthesize organometallic complexes with the remaining ligands were performed.

The organometallic starting complex (η^5-C_5H_5)Ru(κ^2-dppe)Cl was reacted with ligand **L1** in DCM in the presence of TlOTf at room temperature (**Scheme 3.14**). After stirring overnight, a NMR sample of the crude was prepared and analysed showing that no reaction had occurred. The reaction was placed at reflux temperature and was allowed to stir until the following day. Again, NMR results of a crude sample showed that only decomposition of the organometallic starting complex had occurred. The low solubility of the ligand and the long reaction time has been hypothesized as the causes for the unsuccessful reaction. Hence, in order ensure the full dissolution of the ligand, a second attempt was performed using a mixture of dried THF and dichloromethane. Placing the reaction at 50 °C and allowing it to stir overnight afforded only decomposition products. No further attempts were made.

The reaction of the κ^2-dppe-containing organometallic complexes with ligand **L2** was made by the previously developed protocol. Hence, reaction of (η^5-C_5H_5)M(κ^2-dppe)X (M=Fe, X=I; M=Ru, X=Cl) was performed in DCM in the presence of TlOTf. After stirring overnight, aliquots from both reactions were removed and analysed by NMR. The mixture presented the signals derived from the decomposition of the organometallic fragments and the signals from the unreacted ligand.

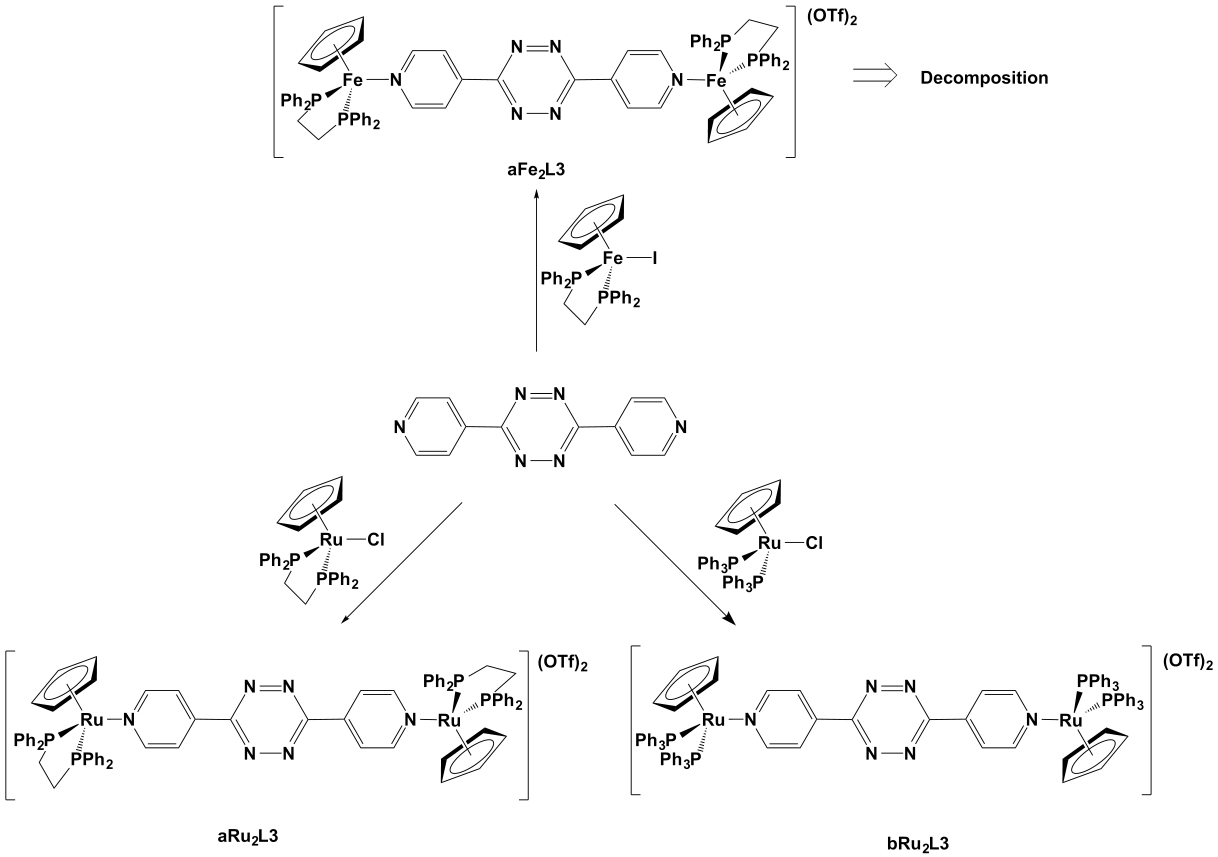

Scheme 3.14: Synthesis of **L3**-based ruthenium complexes

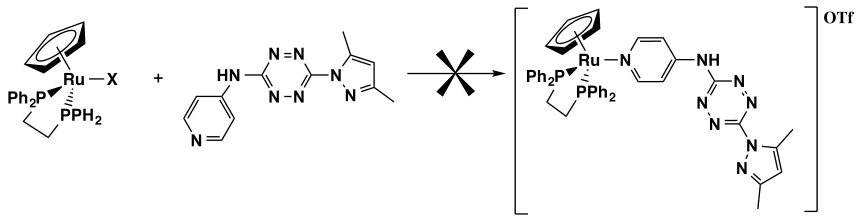

Scheme 3.15: Synthesis of **L1**-based complexes

In a similar fashion, reaction of ligand **L2** with one equivalent of $(\eta^5\text{-}C_5H_5)Ru(PPh_3)_2Cl$ in the presence of TlOTf resulted in the formation of the zwitterionic **bRuL2** complex (**Scheme 3.16**). The zwitterionic character of this complex was confirmed by spectroscopic data (*vide infra*).

Organometallic complexes, in particular η^5-monocyclopentadienylruthenium(II) com-

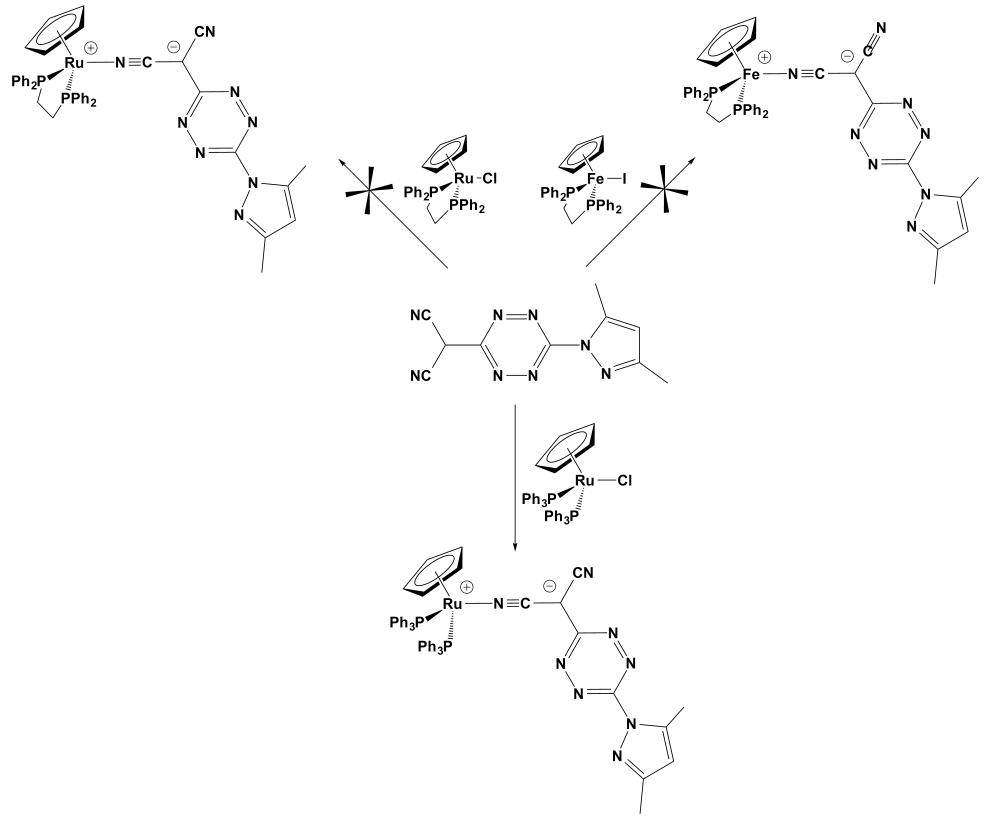

Scheme 3.16: Synthesis of the **bRuL2** complex

plexes, containing C- and N-bound cyanocarbanions have been recently studied.[86] These complexes present a dynamic exchange in the coordination mode, where N-bound complexes can be interconverted to their C-bound analogues as showed in **Scheme 3.17**.

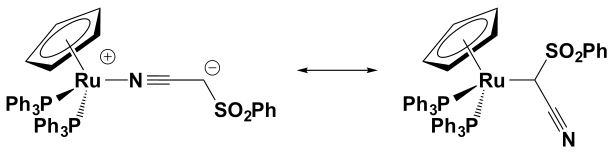

86

Scheme 3.17: Coordination interconversion of organometallic complexes containing cyanocarbanions

It was shown that different phosphanes can favour the N- or the C-bound coordination mode. In particular, PPh_3, $P(^iPr)_3$, dppb and dppf preferentially originate rise to N-

bound isomers, whereas $PMePh_2$, PMe_2Ph, dmpe, dppm, and dppe favour the C-bound coordination mode. Thus, considering the obtained results for the synthesis of complexes bearing **L2**, it is hypothesized that κ^2-dppe-containing organometallic complexes lead to the formation of unstable C-bound isomers than the N-bound isomer formed by the $(\eta^5\text{-}C_5H_5)Ru(PPh_3)_2Cl$ complex.

Coordination of acetylide ligands to $(\eta^5\text{-}C_5H_5)M(PP)X$ organometallic fragment has been previously described using various methods.[71,87,88] Reaction of **L4** with two equivalents of $(\eta^5\text{-}C_5H_5)Ru(\kappa^2\text{-dppe})I$ in the presence of NH_4PF_6 afforded only the starting materials. In a similar fashion, reaction of **L5** with one equivalent of $(\eta^5\text{-}C_5H_5)Fe(\kappa^2\text{-dppe})I$ in the presence of NH_4PF_6 afforded no reaction. It was then hypothesized that deprotonation of the terminal acetylene should be performed prior to the coordination reaction. Both ligands **L4** and **L5** were then treated with potassium *tert*-butoxide in dried THF prior to attempts of the coordination to the metal centre. After stirring overnight at room temperature, no changes in the reaction were observed. The unsuccessful reaction was also confirmed by NMR where only unreacted ligand was observed. Although reaction of tetrazine with alkyllithium are known to afford N-addition products, the deprotonation of ligands **L4** was attempted by the strong *n*-butyl lithium base. Due to the presence of a bromine atom in ligand **L5**, that can suffer substitution reactions, the deprotonation reaction by usage of *n*-butyl lithium was not performed. Hence, treatment of **L4** with *n*-butyl lithium afforded a dark brown solid which was carefully transferred under inert atmosphere conditions to a Schlenk vessel containing a THF solution of 0.5 eqs. of $(\eta^5\text{-}C_5H_5)Ru(\kappa^2\text{-dppe})Cl$ and 0.6 eqs. of TlOTf. After stirring overnight, NMR results of the crude mixture shown only decomposition products (**Scheme 3.18**). No attempts were made with the other organometallic fragments.

It is hypothesized that the unreactivity of ligands **L4** and **L5** towards coordination reactions to the organometallic fragments is due to the strong electron-withdrawing character of the nearby *s*-tetrazine ring. The deprotonation of the terminal acetylene proton should, in fact, lead to an electronic delocalization of the generated carbanion towards the tetrazine ring, hence creating an unreactive anion. The synthesis of organometallic complexes bearing acetylene-based tetrazine were thus abandoned.

The obtained complexes were then characterized by FTIR, NMR and UV-Vis. spectroscopies.

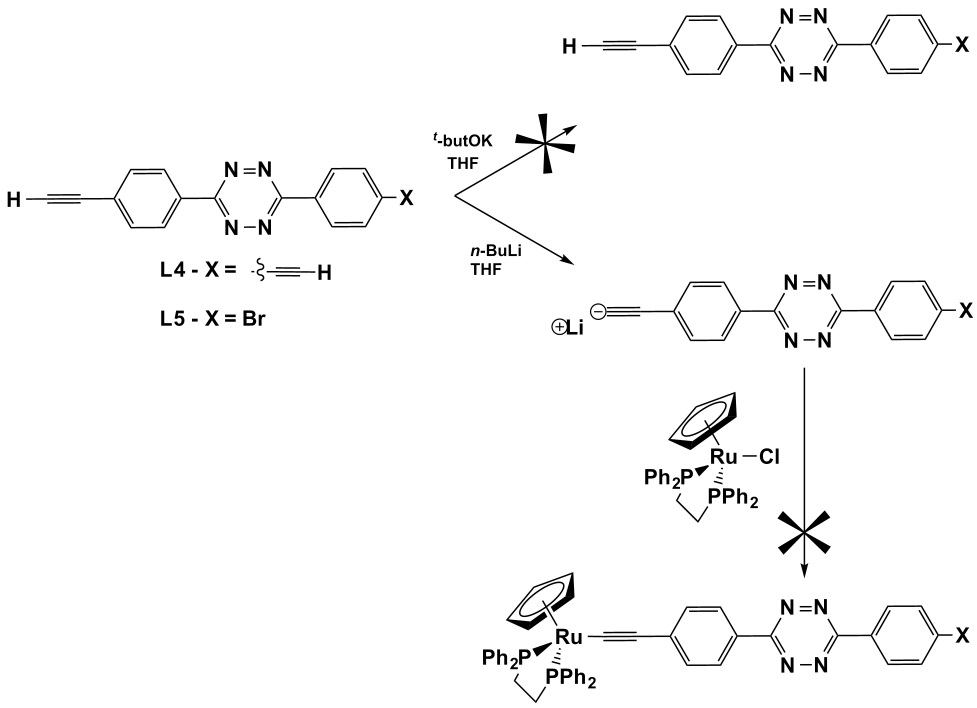

Scheme 3.18: Attempts of syntheses of **L4** and **L5**-based complexes

The analysis of FTIR spectra provides very useful information about electronic properties of the synthesized organometallic compounds, in particular regarding the π-backdonation effect. Typical FTIR bands confirm the presence of the η^5-monocyclopentadienyl coligand (3000 - 3100 cm^{-1}) for all complexes and the OTf^- counter anion (1200 - 1300 cm^{-1}) for complexes $\mathbf{aR_2L3}$ and $\mathbf{bR_2L3}$. The absence of the counter anion band in complex **bRuL2** supports the proposed structure showed in **Scheme 3.16**. All the complexes present the characteristic signals attributed to the *s*-tetrazine C=C and N=C ring vibrations in the 1600−1350 cm^{-1}.

Complex **bRuL2** presents two intense signals at 2209 and 2173 cm^{-1} attributed to the N≡C stretching frequencies of the dycianovynil group. Comparison of N≡C stretching frequency upon coordination reveals a positive shift of 3 cm^{-1} suggesting a very low π-backdonation from the metal centre. In fact, σ-donating/π-accepting ligands, such as the case of the present *s*-tetrazine ligands, are known to lessen the lowering of the N≡C vibration upon coordination.[86] Complexes $\mathbf{aRu_2L3}$ and $\mathbf{bRu_2L3}$, in their turn, do not present significant diferences in the FTIR spectra comparatively to the ligand, suggesting

a weak π-backdonation from the metal centre.

In order to enable the comparison with the free ligands, NMR spectra of the complexes were also obtained in DMSO-d^6. **Figure 3.12** shows the numbering used in the NMR attributions. **Figure 3.13** show the obtained ^{1}H-NMR spectra for **bRuL2**, whereas **Figure 3.14** shows the obtained ^{1}H-NMR spectra for complexes **aR$_2$L3** and **bR$_2$L3**. The spectrum for ligand **L3** was included in the latter mentioned figure for comparison. Selected ^{1}H-NMR data is showed in **Tables 3.5**.

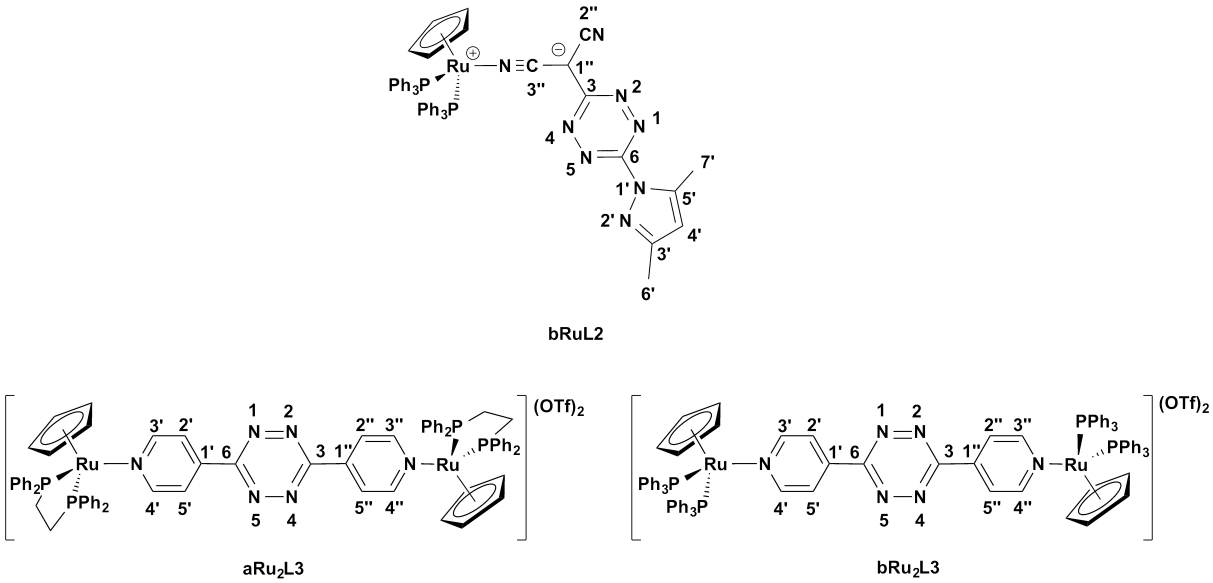

Figure 3.12: Structure and atom numbering for the synthesized complexes

The confirmation of the monodentate coordination mode of complex **bRuL2** was made by the phosphine/Cp integration of the resonance signals, where a 30:5 ratio was obtained. The singlet of the η^5-C_5H_5 (Cp) ring for complex **bRuL2** was used to confirm the zwitterionic structure of the complex. ^{1}H-NMR spectrum for this complex was obtained using $CDCl_3$ as solvent in order to exclude solvent effects in the comparison of this resonance with other published monocationic and neutral complexes presenting the $[(\eta^5\text{-}C_5H_5)Ru(PPh_3)_2]^+$ fragment. Results show a $\delta_{Cp} = 4.37$ ppm resonance for complex **bRuL2**. Comparatively to other nitrile-based monocationic ruthenium (II) complexes, for which the Cp resonance is in the 4.80 -5.10 ppm range, a shielding of the resonance of the Cp ring for complex **bRuL2** is observed. The opposite behavior is observed when comparison with neutral complexes is made (δ_{Cp} for neutral complexes $\approx$ 4.00 - 4.20

ppm), that is complex **bRuL2** presents a shielded Cp resonance. Hence, the Cp resonance suggests that the synthesized complex does not present a "purely" monocationic organometallic fragment, as already suggested by the absence of the counteranion signal in the FTIR spectrum. It is then hypothesized that a zwitterionic structure for this complex is present, either in solution or in solid state. This fact is corroborated with DFT calculations (*vide infra*). Additionally, the ^{1}H-RMN spectra of compound **bRuL2** presents the characteristic singlets attributed to the 3,6-bis(3,5-dimethylpyrazolyl) group, protons $H_{4'}$, $H_{6'}$ and $H_{7'}$, at $\delta = 6.21$, 2.44 and 2.24 ppm, respectively. Comparison of the resonances in the complex and in the free ligand shows a shielding of these protons upon coordination. The results suggest that the coordination of the ligand leads to a dominant electronic delocalization towards the metal centre as a result of the σ-donation. In fact, the previously discussed FTIR data, clearly showed that no significant π-backdonation is observed for this complex.

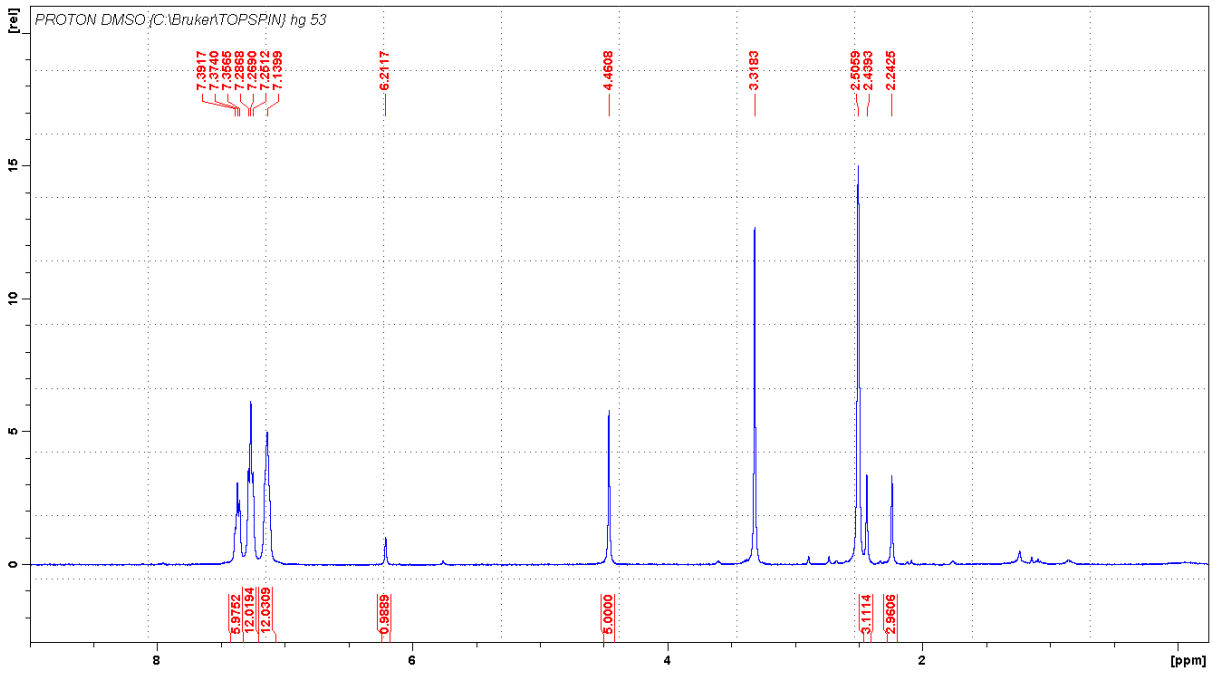

Figure 3.13: ^{1}H-NMR spectra for **bRuL2**

For the case of complexes **aRu$_2$L3** and **bRu$_2$L3** the ^{1}H-RMN resonances for the singlet of the Cp ring depends on the phosphane co-ligand and are in the range usually observed for other dicationic Ru(II) complexes.[76,89–91] The ^{1}H-RMN spectra presents also

the characteristic doublets attributed to the aromatic protons of the pyridine rings of the ligand. In the case of complex **aRu$_2$L3**, a high shielding of these protons is observed. In particular, a deshielding of 1.13 ppm is observed for the protons closer to the metal centres, $H_{3'}$, $H_{5'}$, $H_{3''}$ and $H_{5''}$, as a result from the π-backdonation from the metal centre. Remarkably, complex **bRu$_2$L3** presents no deviation of the aforestated protons. The similarity between the ligand and the complex FTIR spectra already suggested a very weak π-backdonation in these complexes. The difference in the NMR behaviour of the complexes was hypothesized to be related to the presence of the bulky PPh_3 phosphane that lead to weaker M-L bond than complex **aRu$_2$L3**. In fact, the lower stability of the **bRu$_2$L3** complex was observed during the acquisition of the NMR data, where decomposition of the complex was seen after long periods in solution of the deuterated solvent.

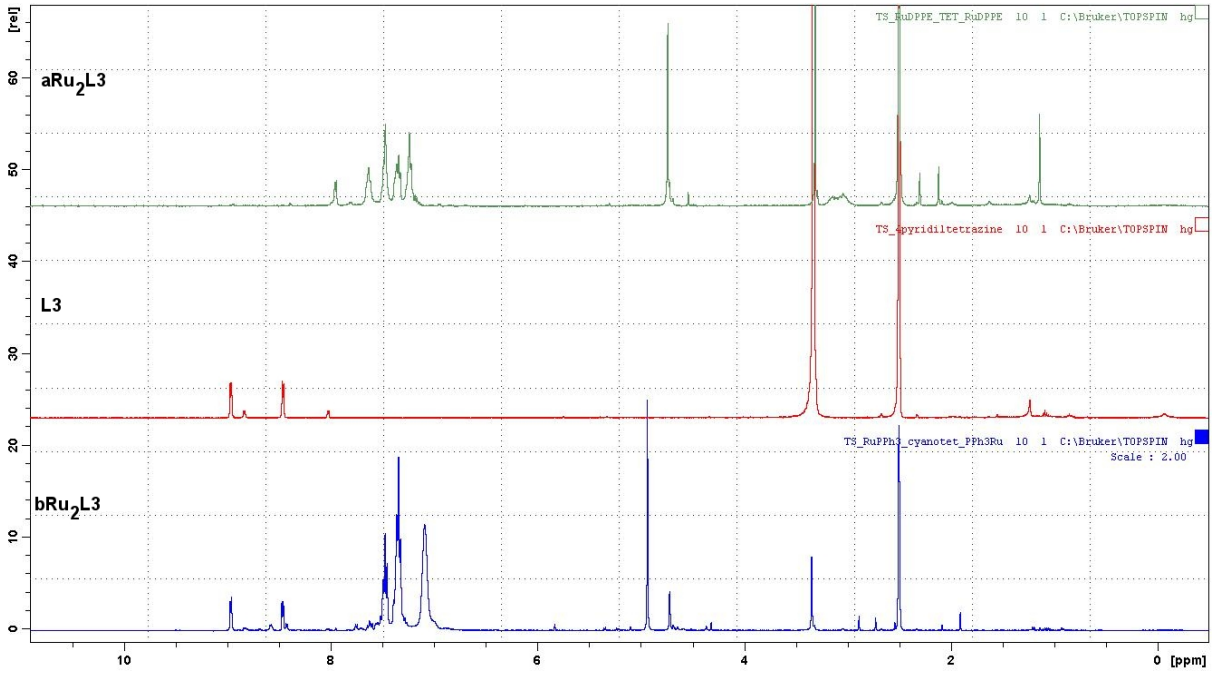

Figure 3.14: ^{1}H-NMR spectra for **aRu$_2$L3** and **bRu$_2$L3**

The spectra of ligand **L3** was included for comparison

Table 3.6 shows the selected ^{13}C-RMN data for the complexes. In accordance with the ^{1}H-RMN data, the major changes on the carbon resonances upon coordination were observed in the carbons closer to the metal centre.

Table 3.5: Selected ^{1}H-NMR data for the *s*-tetrazine complexes

	^{1}**H-RMN** δ /ppm [ab]		
Comp.	**bRuL2**	**aRu$_2$L3**	**bRu$_2$L3**
Cp	4.46	4.74	4.93
$\mathbf{H}_{2'}$		7.95 (-1.01)	8.46 (0.00)
$\mathbf{H}_{3'}$		7.33 (-1.01)	8.96 (0.00)
$\mathbf{H}_{4'}$	6.21 (+0.06)		
$\mathbf{H}_{5'}$		7.33 (-1.01)	8.96 (0.00)
$\mathbf{H}_{6'}$	2.24 (+0.03)	7.95 (-1.01)	8.46 (0.00)
$\mathbf{H}_{7'}$	2.24 (+0.03)		

[a] all ^{1}H NMR values in DMSO-d ^{6};
[b] in parenthesis the difference between the coordinated and the free ligand resonances $\delta_{(coord)} - \delta_{(free)}$

To confirm the aforementioned hypothesis that complex **bRuL2** present a zwitterionic structure, the ^{13}C-RMN spectrum in $CDCl_3$ was also acquired and the resonance for the Cp ring was compared with other manocationic and neutral ruthenium (II) complexes. Results show that the obtained δ_{Cp} resonance for the present compound is in between the typical values for this signal on other monocationic and neutral ruthenium (II) complexes (δ_{Cp}(**bRuL2**) = 83.06 ppm; δ_{Cp}([CpRu(PP)L]$^{+}$) $\approx$ 80 - 82 ppm; δ_{Cp}(CpRu(PP)L) $\approx$ 84 - 86 ppm). Hence, the obtained results are in accordance with the previously discussed ^{1}H-RMN data. For complex **bRuL2** a general shielding of the carbons of the 3,6-bis(3,5-dimethylpyrazolyl) is also observed, alongside a shielding of 13.98 ppm in C6. Also for this complex, both the carbons of the nitrile function of the dicyanomethyl group appear deshielded, in particular $C_{2''}$ where a deshielding of *ca.* 16 ppm is observed. These results are consistent with the coordination of the organometallic fragment to the N$\equiv$C$''_2$ group. Hence, it is also possible to state that the $[(\eta^5\text{-}C_5H_5)Ru(PPh_3)_2]^{+}$ favours the N-bound coordination mode, in accordance with the data for other zwitterionic ruthenium (II) complexes.[86]

Comparison of the obtained spectra for complexes **aRu$_2$L3** and **bRu$_2$L3** revealed subtle changes in the resonance of the carbon signals upon coordination to the metal centre. In general a deshielding effect is observed for all the carbons. For complex **aRu$_2$L3** the highest deshielding is observed for carbons closest to the metal centre ($C_{3'}$, $C_{5'}$ and $C_{3''}$, $C_{5''}$) for which a deshielding of *ca.* 8 ppm is observed. Complex **bRu$_2$L3** in its turn, present very small differences comparatively to the free ligand, as already suggested by the ^{1}H-RMN. The ^{13}C-RMN data is consistent with the electron donating abilities of the phosphane co-ligands.

The optical absorption spectra of the complexes were recorded using 1.0 $\times 10^{-5}$ M solutions in chloroform and DMF. **Figure 3.15** shows the typical behaviour of the synthesized complexes in chloroform and **Table 3.7** shows the optical data in both solvents.

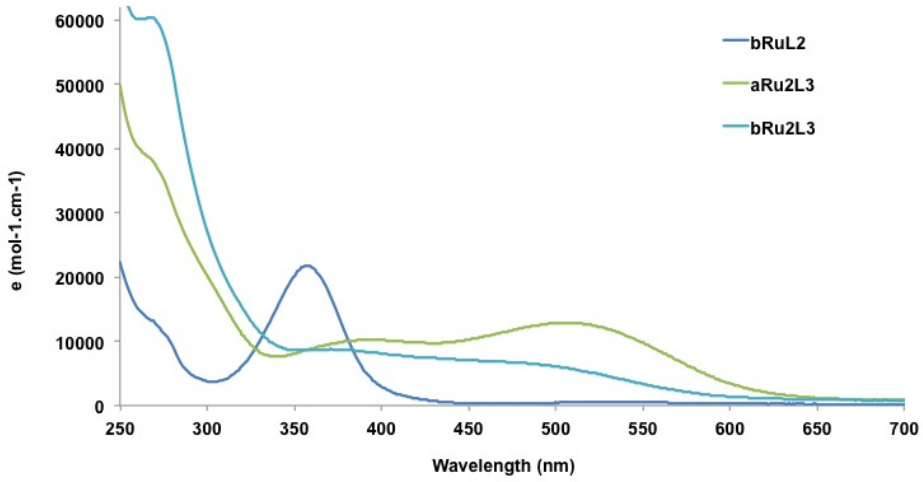

Figure 3.15: UV-Vis. spectra for the *s*-tetrazine complexes in chloroform

The electronic spectra of the complexes are characterized by intense high energetic bands in the range of 250-290 nm, alongside with low energy bands in the range of 300 to 600 nm, depending on the ligand. For complex **bRuL2**, two low energy electronic transitions at 357 and 531 nm, resembling the free ligand, are observed. For the higher energy, occurring at 357 nm, the electronic spectra of this complex show a red shift by 8 nm, comparatively with the free ligand, consistent with a low π-backdonation from the metal centre, as already suggested by the FTIR spectra and NMR data. The lower energy band is attributed to the forbidden n-$\pi^{\star}$ transition characteristic of tetrazine-based

Table 3.6: Selected ^{13}C-NMR data for the *s*-tetrazine complexes

	^{13}**C-RMN** δ /ppm [b]		
Comp.	**bRuL2**	**aRu$_2$L3**	**bRu$_2$L3**
Cp	83.60	84.17	86.52
C$_3$	170.37 (0.44)	162.10 (-1.35)	163.47 (0.02)
C$_6$	170.37 (13.98)	162.10 (-1.35)	163.47 (0.02)
C$_{1'}$	[c]	137.87 (-1.58)	139.47 (0.00)
C$_{2'}$		121.31 (-0.38)	121.71 (0.02)
C$_{3'}$	150.61 (0.91)	159.43 (7.85)	151.60 (0.02)
C$_{4'}$	109.16 (0.11)		
C$_{5'}$	141.79 (0.60)	159.43 (7.85)	151.60 (0.02)
C$_{6'}$	13.79 (0.44)	121.31 (-0.38)	121.71 (0.02)
C$_{7'}$	12.85 (0.64)		
C$_{1''}$	[c]	139.47 (-1.58)	139.47 (0.02)
C$_{2''}$	103.92 (-15.98)	121.31 (-0.38)	121.71 (0.02)
C$_{3''}$	115.38 (-4.52)	159.43 (0.91)	151.60 (0.02)
C$_{5''}$		159.43 (7.85)	151.60 (0.02)
C$_{6''}$		121.31 (-0.38)	121.71 (0.02)

[a] all ^{13}C NMR values values in DMSO-*d* ^{6}; [b] in parenthesis the difference between the coordinated and the free ligand resonances $\delta_{(coord)} - \delta_{(free)}$
[c] not observed

compounds.

Dinuclear complexes **aRu$_2$L3** and **bRu$_2$L3** present very broad, low-lying electronic transitions that consists of, at least, two electronic transitions. The energy of the transitions is in accordance with the electron donating properties of the phosphane co-ligands, for which κ^2-dppe provides lower energy transfers than PPh_3. These bands, clearly result

from the coordination of the **L3** ligand to the metal centre and, hence, are attributed to metal-to-ligand charge transfer. In fact, as it will be shown later, DFT calculations corroborate such assumptions. Characteristic n-$\pi^\star$ electronic transition from the tetrazine ligand are not observed due to overlap with the MLCT bands.

Table 3.7: Uv-Vis absorption maxima for the *s*-tetrazine complexes

λ /nm ($\epsilon\times10^4$(mol^{-1}cm^{-1}))		
Compound	Chloroform	DMF
bRuL2	357 (2.2)	353 (2.1)
	531 (0.05)	525 (0.09)
aRu$_2$L3	266 (0.8)	391 (1.4)
	393 (1.2)	461 (1.0)
	507 (1.3)	527 (0.8)
bRu$_2$L3	481 (sh)	490 (0.7)
	371 (0.9)	378 (0.8)

The solvatochromic behaviour of the complexes was studied by measuring spectra in chloroform and DMF. Although complex **bRuL2** presents a negative solvatochromic behaviour, the dinuclear complexes show a slight red shift of the electronic transition with the increasing solvent polarity. In particular, complex **aRu$_2$L3** shows a red shift by 20 nm when going from chloroform to DMF suggesting an increase of the dipole moment of the molecule upon photo-excitation. Hence, higher hyperpolarizabilities are expected for this complex comparatively to the other two, according to the TLM, and the previous spectroscopic data.[88,91,92]

3.2.4 Quadratic Hyperpolarizabilities of the Complexes

Although no hyperpolarizability measurements were performed in the *s*-tetrazine complexes were made, some remarks can be made concerning the spectroscopic data of the complexes and according to the TLM.

For complex **bRuL2**, the spectroscopic data suggests that moderate to low hyperpolarizability values should be obtained. Judging from the FTIR and NMR data, no sig-

nificative π-backdonation is estimated upon ligand coordination to the metal centre and hence, only moderate improvement of the hyperpolarizabilities are expected. Furthermore, the linear optical data suggests that no significative metal-to-ligand charge transfer is present. The negative solvatochromic behaviour further corroborates this assumptions.

For complexes **aRu$_2$L3** and **bRu$_2$L3**, the spectroscopic data also suggest that moderate to low hyperpolarizabilities should be obtained. The determined nonlinear optical data should, however, be enhanced comparatively to the former complex due to the presence of low-lying electronic trasitions in the UV-Vis. spectra of the **L3**-based complexes. Moreover, the FTIR and NMR data suggest a significative amount of π-backdonation from the metal centre, that should enhance the nonlinear optical properties of the complexes, in particular for the case of **aRu$_2$L3**. In fact, DFT calculations show that this complex provide the highest estimated β value of the three synthesized complexes (*vide infra*).

3.3 Density Functional Theory Studies

As previously stated, the choice of functional is crucial when one is dealing with the interpretation and comparison of theoretical data with the obtained experimental results. For that matter DFT calculations on all the tetrazine-based compounds were performed using the same functionals (B3LYP, CAM-B3LYP and M06) and basis sets (6-31G(d,p) for light atoms, and LANL2DZ ECP for transition metal and phosphorous atoms) used in **Chapter 2**. It has been recently shown that the reliable theoretical study of *s*-tetrazines must be performed taking into account solvent-solute interactions, since they have a direct influence on the estimated UV spectra, in particular in the characteristic $n \rightarrow \pi^\star$ transitions.[93] Hence, all calculations were made taking into account solvent effects by the Polarizable Continuum model (PCM) using chloroform as solvent.[94]

3.3.1 DFT studies of the Ligands

3.3.1.1 Geometry and optical data

The optimized structures of ligands **L1** - **L5** are shown in **Figure 3.16**. **Table 3.8** shows the selected bond distances and bond angles for all compounds. Since the ligands present different substituents, comparison between the obtained structures will only be

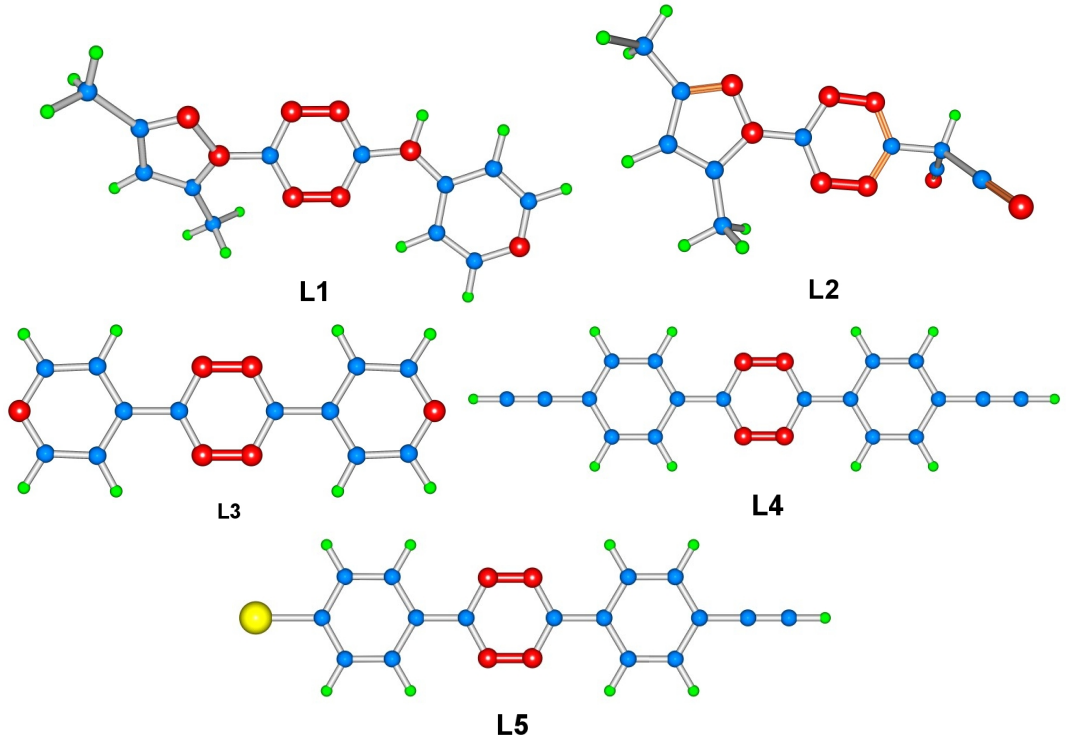

Figure 3.16: B3LYP optimized structures of **L1**-**L5**.

No significative differences were obtained with other functionals.

made by comparing the structural differences in tetrazine ring. Furthermore, since no crystallographic data was obtained for these ligands, the DFT optimized structures will be compared to the crystallographic structure of 3,6-bis(diphenyl)-*s*-tetrazine, obtained by Ahmed *et al.* and whose structural data is shown in **Figure 3.17**.[95] Finally, the BLA parameter is not presented also because of the difference in the ligands structures.

The optimized structures for the ligands show that the molecules present different symmetries, depending on the substituents in the tetrazine ring. In particular, the asymmetric ligands **L1**, **L2** and **L5** belong to C_1 symmetry group, whereas ligands **L3** and **L4** belong to the C_{2v} symmetry group.

The average carbon–nitrogen bond length in 3,6-bis(diphenyl)-*s*-tetrazine is 1.345 Å, while the nitrogen–nitrogen bond lengths are 1.314 Å. An interesting feature of this molecule is its slight deviation from the regular hexagonal shape presented by pure benzenoid structures, where N-N-C and C-N-N angles of 117.5° and 120.6° are observed, respectively, together with a N-C-N angle of 121.8°. In general, the three functionals

reproduce very well the average carbon-nitrogen bond length, particularly the M06 functional for which an average carbon-nitrogen bonds of 1.344 Å were obtained. B3LYP overestimates the average carbon-nitrogen bond by *ca.* 0.003 Å whereas for CAM-B3LYP the opposite behaviour is observed, that is, a slight underestimation of *ca.* 0.002 Å. In the case of the average nitrogen-nitrogen bond, CAM-B3LYP and M06 functionals underestimate this bond by 0.006 and 0.009 Å, respectively, while B3LYP overestimates the same bond by 0.002 Å. The bond angles are also in general well reproduced, although overestimated for all functionals.

Some remarks considering the ligand substituents can also be made. Comparing **L1** and **L2**, shorter X_1-C_6 bond length are observed for the latter as a result of the presence of the strong electron withdrawing dycianovynil group. Conversely, shorter C_3-X_2 bond lengths are observed for **L1**. However, care must be taken when analysing these results since they refer to different bond types: C_3-X_2 is a C-N bond for **L1**, whereas it is a C-C bond for **L2**. The position of the 3,6-bis(3,5-dimethylpyrazolyl) group is also different for both ligands. The fact that **L2** presents a lower Dh_1 dihedral angle suggests a higher delocalized system between the *s*-tetrazine ring and the 3,6-bis(3,5-dimethylpyrazolyl) group, consistent with the shorter X_1-C_6 bond length. As expected, ligands **L3**, **L4** and **L5** present planar geometries in good accordance with 3,6-bis(diphenyl)-*s*-tetrazine, with both dihedral angles very close to 180° for all ligands. However, much larger X_1-C_6 and C_3-X_2 bond lengths are observed when compared with the model compound, suggesting a lower electronic delocalization throughout the molecule, even when electron donor groups are present. This fact is rather surprising since the presence of the alkynyl electron donor groups in **L4** and **L5** should promote a higher electronic delocalization towards the *s*-tetrazine ring.

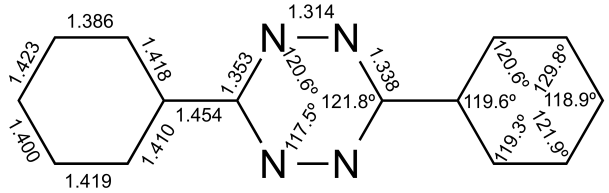

Figure 3.17: Bond angles and bond lengths of 3,6-bis(diphenyl)-*s*-tetrazine.

Double bonds were ommited for clarity

Table 3.8: Selected bond distances and bond angles for the tetrazine ligands

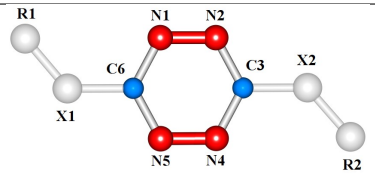

Func.	B3LYP					CAM-B3LYP					M06				
Comp.	**L1**	**L2**	**L3**	**L4**	**L5**	**L1**	**L2**	**L3**	**L4**	**L5**	**L1**	**L2**	**L3**	**L4**	**L5**
							Bond Distances (Å)								
$\mathbf{X_1}$-$\mathbf{C_6}$	1.3970	1.3805	1.4789	1.4742	1.4751	1.3954	1.3787	1.4790	1.4754	1.4759	1.3915	1.3768	1.4716	1.4670	1.4676
$\mathbf{C_6}$−$\mathbf{N_1}$	1.3542	1.3543	1.3487	1.3513	1.3507	1.3455	1.3438	1.3394	1.3414	1.3410	1.3495	1.3527	1.3440	1.3466	1.3460
$\mathbf{N_1}$-$\mathbf{N_2}$	1.3004	1.3129	1.3123	1.3112	1.3113	1.2920	1.3049	1.3047	1.3040	1.3041	1.2937	1.3014	1.3059	1.3046	1.3047
$\mathbf{N_2}$-$\mathbf{C_3}$	1.3636	1.3377	1.3487	1.3513	1.3513	1.3563	1.3302	1.3394	1.3414	1.3414	1.3587	1.3373	1.3440	1.3466	1.3465
$\mathbf{C_3}$−$\mathbf{N_4}$	1.3439	1.3354	1.3487	1.3513	1.3513	1.3340	1.3279	1.3394	1.3414	1.3414	1.3378	1.3261	1.3440	1.3466	1.3465
$\mathbf{N_4}$-$\mathbf{N_5}$	1.3225	1.3116	1.3123	1.3112	1.3113	1.3157	1.3039	1.3047	1.3040	1.3041	1.3164	1.3111	1.3059	1.3046	1.3047
$\mathbf{N_5}$-$\mathbf{C_6}$	1.3333	1.3509	1.3487	1.3513	1.3507	1.3231	1.3412	1.3394	1.3414	1.3410	1.3484	1.3409	1.3440	1.3466	1.3460
$\mathbf{C_3}$-$\mathbf{X_2}$	1.3655	1.5282	1.4781	1.4742	1.4743	1.3612	1.5207	1.4790	1.4754	1.4759	1.3617	1.5185	1.4716	1.4670	1.4676
							Bond Angles (°)								
$N_1N_2C_3$	118.22	118.10	118.26	118.50	118.50	118.25	118.13	118.29	118.52	118.50	118.19	118.17	118.15	118.40	118.36
$N_2C_3N_4$	124.10	125.20	123.48	123.01	123.01	123.92	124.99	123.41	122.97	122.97	124.28	125.32	123.70	123.21	123.21
$C_3N_4N_5$	117.15	117.72	118.26	118.50	118.48	117.26	117.78	118.29	118.52	118.51	118.27	117.51	123.70	118.40	118.39
$N_4N_5C_6$	118.30	117.34	118.26	118.50	118.48	118.36	117.44	118.29	118.52	118.51	118.27	117.35	118.15	118.40	118.39
$N_5C_6N_1$	124.73	124.75	123.48	123.01	123.05	124.60	124.71	123.41	122.97	123.00	124.84	124.97	123.70	123.21	123.25
$C_6N_1N_2$	117.38	116.83	118.26	118.50	118.48	117.51	116.94	118.39	118.52	118.51	117.31	116.66	118.15	118.40	118.40
							Diedral Angles (°)								
$\mathbf{Dh_1}$[b]	149.07	179.37	180.00	179.56	-179.97	145.60	168.36	180.00	180.00	-179.96	152.24	-171.91	180.00	180.00	179.99
$\mathbf{Dh_2}$[b]	-179.86	119.61	180.00	179.98	-179.99	179.83	116.21	180.00	179-98	179-98	-179.35	170.84	180.00	180.00	180.00

[a] X_1 and X_2 represent the ligands substituents in the same position as defined in Figure 3.16. [b] Dh_1 = R_1-X_1-C_6-N_5 and Dh_2 = N_2-C_3-X_2-R_2. R_1 represents the atom prior to X_1 (R_1 = N for **L1** and **L2**, and C for the remaining ligands; R_2 represents the atom after X_2, which is C for all ligands)

The *s*-tetrazine family is the most interesting six-membered heteroaromatic ring, since it presents strong electronic transitions in all three perpendicular directions of the cartesian axes. In fact, the electronic spectra of *s*-tetrazines is, by far, the most studied feature of these compounds, both theoretically and experimentally.[93,96,97] For example, the three isomers of the bis(pyrydil)-*s*-tetrazine family belong to different symmetry groups: 3,6-bis(4-pyridyl)-*s*-tetrazine belongs to the C_{2v} group; 3,6-bis(3-pyridyl)-*s*-tetrazine belongs to either C_{2v} or C_{2h} groups (depending on the conformation it adopts) and 3,6-bis(2-pyridyl)-*s*-tetrazine belongs to the C_i group of symmetry. The difference in the symmetry of the molecules has enormous influence their electronic spectra, and it is observed that 3,6-bis(4-pyridyl)-s-tetrazine is a purple solid whereas 3,6-bis(2-pyridyl)-*s*-tetrazine is a red solid.[98] Another interesting feature of *s*-tetrazines is that the composition of their HOMO and HOMO-1 orbitals is dependant on the substituents.[99] A systematic study on the nature of the HOMO's orbital of different compounds has proven that, in many cases, the energy of the orbital containing the four non-bonding electrons of the nitrogen atoms in the *s*-tetrazine ring is close to the energy of the orbital of the π-electrons of the aromatic system of the substituent. It was observed that, in one hand, if the substituent is a weak electron donor (or eventually an electron acceptor), such as chlorine or alkoxy groups, the inductive effects are not sufficient for the orbital mixing, the HOMO-1 remains with π-character and the HOMO remains centred on the non-bonding lone pairs of the nitrogens in the tetrazine ring (n-orbitals). On the other hand, if the substituent is a good electron donor (such as aromatic systems, amines or alkylthio groups), a high degree of mixing in this two orbitals can occur, and they rearrange in a form that the character of the HOMO-1 and HOMO is reversed. As for the LUMO, its energy is only slightly affected by the nature of the substituents since this $\pi^\star$ orbital its located entirely in the four nitrogen atoms of the *s*-tetrazine ring.[100]

In order to get a better understanding of the electronic properties of the synthesized tetrazine ligands, TD-DFT calculations were performed in ligands **L1**-**L5**. **Table 3.9** shows the selected optical data and the orbitals involved are showed in **Figure 3.18**.

Table 3.9: Relevant TD-DFT results for tetrazine-based ligands

Ligand	Functional	λ_{max} (nm) [a]	f [b]	Major Contributions
L1	B3LYP	554	0.0047	HOMO-1→LUMO (65%)
		457	0.0130	HOMO→LUMO (94%)
		305	1.1109	HOMO→LUMO+1 (87%)
	CAM-B3LYP	509	0.0058	HOMO-2→LUMO (78%)
		273	1.2131	HOMO→LUMO+1 (87%)
	M06	604	0.0041	HOMO-1→LUMO (88%)
		297	1.1507	HOMO→LUMO+1 (88%)
L2	B3LYP	566	0.0044	HOMO-1→LUMO (100%)
		400	0.0096	HOMO→LUMO (97%)
		283	0.7991	HOMO-2→LUMO+1 (95%)
	CAM-B3LYP	515	0.0056	HOMO-2→LUMO (87%)
		321	0.0230	HOMO-1→LUMO (75%)
		257	0.6703	HOMO-1→LUMO+1 (54%)
	M06	616	0.0039	HOMO→LUMO (96%)
		295	0.7946	HOMO-2→LUMO+1 (91%)
L3	B3LYP	577	0.0045	HOMO→LUMO (100%)
		304	1.1731	HOMO-3→LUMO+1 (98%)
	CAM-B3LYP	526	0.0055	HOMO→LUMO (99%)
		262	0.1207	HOMO-2→LUMO+1 (81%)
		251	0.1952	HOMO-2→LUMO (97%)
	M06	629	0.0039	HOMO→LUMO (100%)
		300	1.1293	HOMO-5→LUMO+1 (96%)
L4	B3LYP	583	0.0043	HOMO-1→LUMO (100%)
		379	1.6386	HOMO→LUMO+1 (99%)
	CAM-B3LYP	532	0.0053	HOMO-1→LUMO (99%)
		320	1.8676	HOMO→LUMO+1 (90%)
	M06	637	0.0039	HOMO-1→LUMO (100%)
		370	1.6526	HOMO→LUMO+1 (97%)
		317	0.1213	HOMO-3→LUMO (99%)
L5	B3LYP	583	0.0043	HOMO-1→LUMO (100%)
		365	1.4673	HOMO→LUMO+1 (98%)
	CAM-B3LYP	532	0.0053	HOMO-1→LUMO (99%)
		312	1.6866	HOMO→LUMO+1 (99%)
	M06	637	0.0037	HOMO-1→LUMO (100%)
		359	1.4956	HOMO→LUMO+1 (97%)

[a] Absorption wavelength of the main transitions; [b] Oscillator strength;

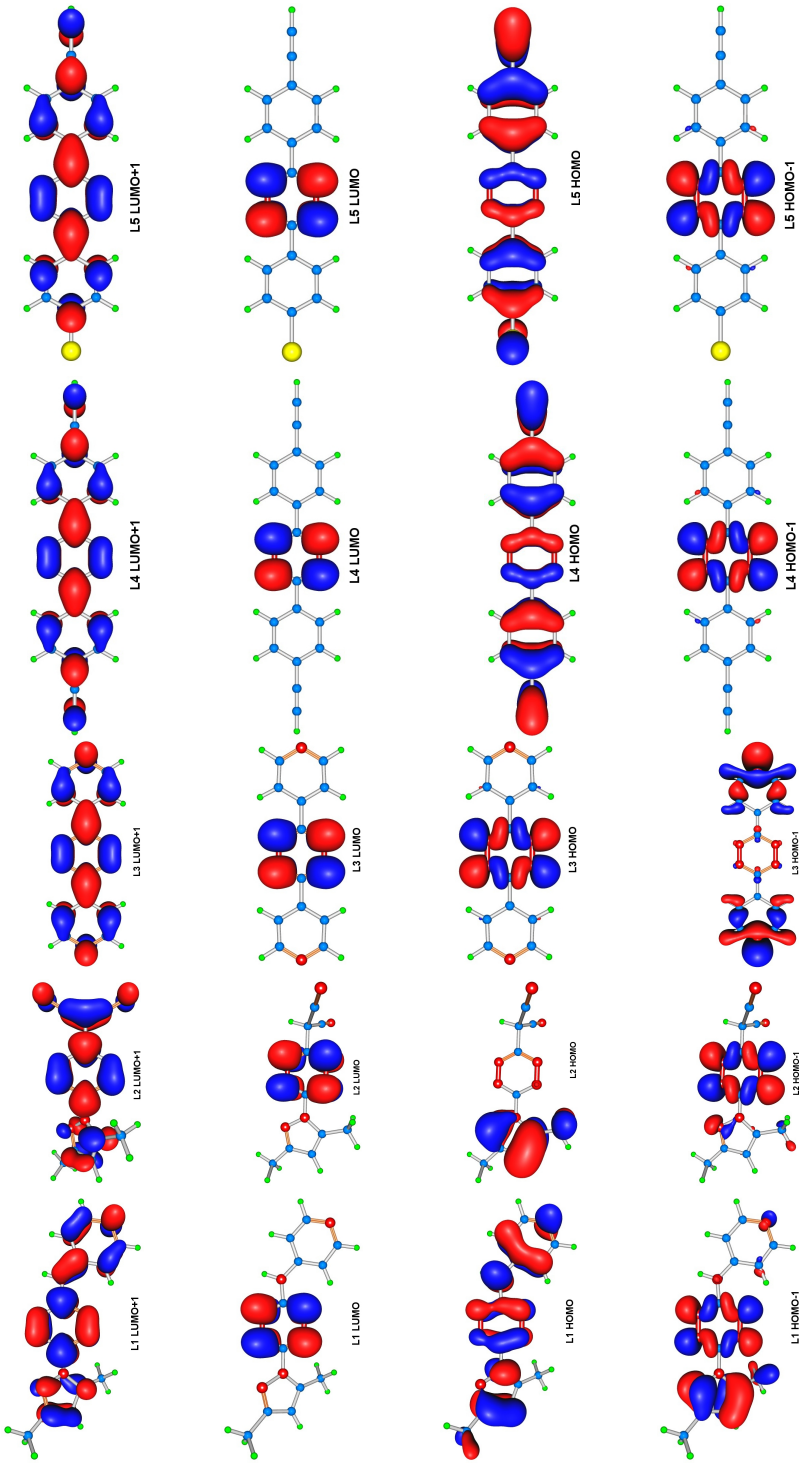

Figure 3.18: HOMO-1, HOMO and LUMO densities for ligands **L1**–**L5**.
(contour = 0.003 a.u.)

The lowest-energy electronic transition can be attributed to HOMO→LUMO or HOMO-1→LUMO transition, depending on the ligand. An analysis of the orbitals involved shows that, for **L1**, **L4** and **L5**, the HOMO is almost spread over the entire molecule whereas for **L2** and **L3** it is mainly located at the pyrazolyl group and tetrazine ring, respectively. For HOMO-1s subtle changes is observed. For **L2**, **L4** and **L5** this orbital is located at the tetrazine ring whereas for **L1** it is mainly located at pyrazolyl group and tetrazine ring. In case of **L3**, the electron density is clearly located at pyridine groups. The $\pi^\star$ LUMO orbital is centred in the tetrazine ring for all the ligands. **Figure 3.19** shows the energy diagram of these orbitals for all ligands. The diagram shows that, as expected, the energy of these orbitals depends on the groups bonded to the tetrazine moiety. It is interesting to note that for ligands **L2**, **L4** and **L5** the HOMO and HOMO-1 orbitals are almost degenerate.

Yhe highest-energy electronic transition can be attributed to HOMO→LUMO+1 (for **L1**, **L4** and **L5**),

The representative simulated spectra, obtained using B3LYP functional, for all ligands are shown in **Figure 3.20**.

The simulated spectra are characterized by a low intensity band in visible region (λ_{max} = 500-620 nm) attributed to a forbidden $n\rightarrow\pi^\star$ transition, characteristic of the tetrazine ring, and by a dominant strong band in the UV region (λ_{max} = = 250-370 nm, depending on the used functional) attributed to a $\pi\rightarrow\pi^\star$ transition. Ligand **L1** presents an additional transition at 457 nm, predicted only by B3LYP, in good accordance with the experimental spectrum. The spectra show that the experimental energy and relative intensity of these bands are dependent on the nature of the substituents adjacent to the *s*-tetrazine ring, in particular their donor/acceptor properties. This behaviour is more noticeable for the UV band rather than for the visible band, which is known to be weakly sensitive to the substituent effects, as shown for several *s*-tetrazine-based compounds.[78] The DFT results show that, within the same functional, the UV band is, in fact, much more sensitive to the substituent of the tetrazine ring. For the three functionals, **L4**, possessing only electron donating group, present the UV band red-shifted by *ca.* 70 nm comparatively to **L3**, possessing only electron withdrawing substituents in the tetrazine ring. The energy of the UV band for **L1** and **L5** falls in the range of the energy reported for **L4** and **L3** ligands, since these compounds have electron donating and electron withdrawing groups. In addition, a general hyperchromic effect is also observed with the increasing character

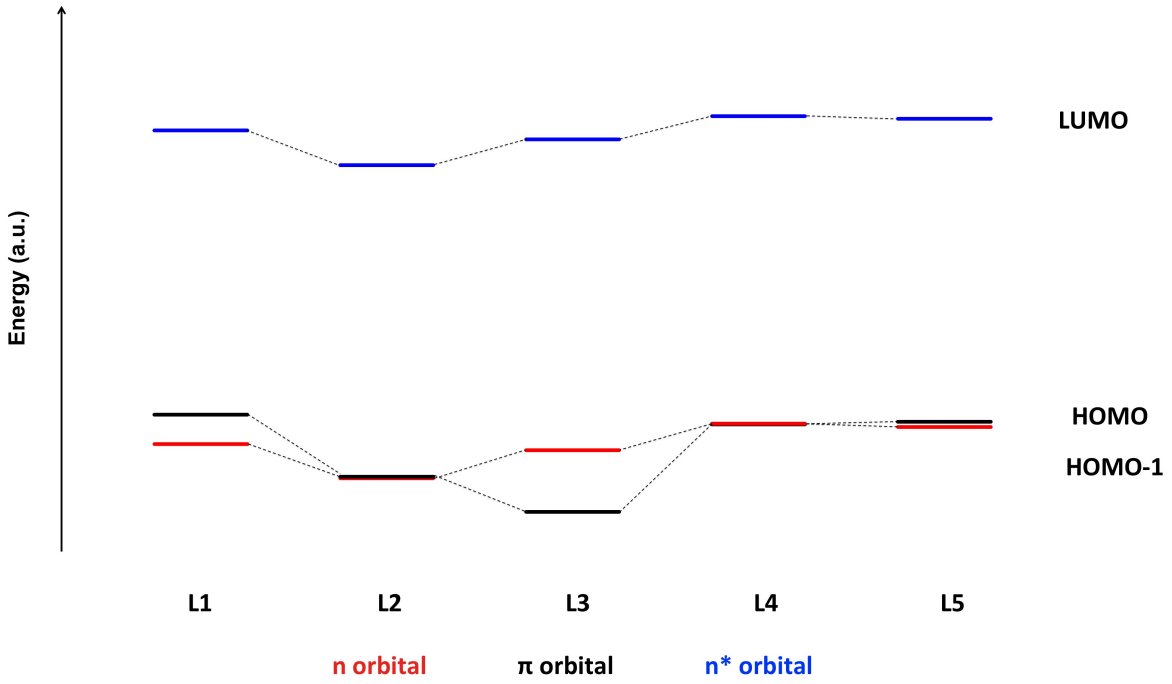

Figure 3.19: Energy of the HOMO-1, HOMO and LUMO orbitals for ligands **L1**–**L5**. Orbitals with the same character are represented by the same color.

of the electron donation properties of the substituents, where higher oscillator strengths are observed for **L4**. Concerning the position and intensity of the band in the visible region, it is clear that the donor/acceptor properties of the substituents in the tetrazine ring weakly affects its energy, as showed by the energy of the transition for ligands **L3**, **L4** and **L5** ($\lambda_{max,B3LYP}$(**L4**) = $\lambda_{max,B3LYP}$(**L5**) = 583 nm; $\lambda_{max,B3LYP}$(**L3**) = 577 nm). Similar results are observed for the other functionals. Except for ligand **L2**, the functionals have a good overall performance in predicting the both the intensity and energy of the electronic transitions of the ligands, in particular for **L1** where dierences of 5 and 3 nm are observed for the B3LYP and M06 functionals, respectively. However, these two functionals underestimate the energy of the transition for L4 and L5 by *ca.* 50 nm in the case of **L4** and ca. 35 nm in the case of **L5**. The energy of the transition for ligand **L2** is overestimated by all functionals, in particular for CAM-B3LYP, which provides a deviation from the experimental wavelength of 92 nm (B3LYP and M06 provides a deviation of 60 nm).

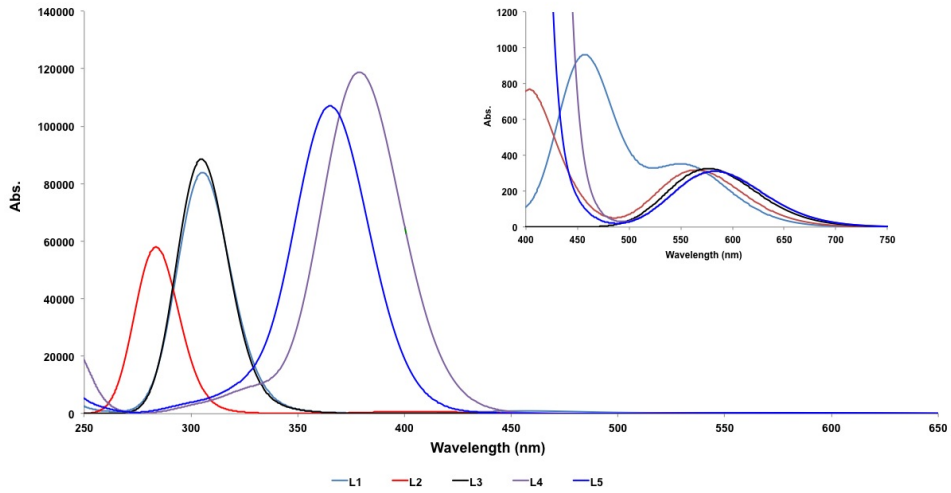

Figure 3.20: TD-DFT simulated spectra for the tetrazine ligands **L1**-**L5** using B3LYP

3.3.1.2 Nonlinear Optical Properties of the Ligands

The hyperpolarizability tensors and the estimated total hyperpolarizability (β_{tot}) for the ligands are shown in **Table 3.10**. The hyperpolarizability values are relatively low for ligands **L1**, **L2** and **L5**, and null for the case of **L3** and **L4**. The results for the latter ligands are expected and are a consequence of their symmetry.

In the case of the asymmetric **L1**, **L2** and **L5** it is observed that β_{tot} is dominated by tensor β_{xxx}, along the conjugated backbone of the ligand. As showed previously, the analysis of the orbital involved in the lowest energy transition (HOMO, HOMO-1 and LUMO) for ligand **L1** shows that the charge transfer arise from the the tetrazine substituents to the central tetrazine ring. In the case of **L2** results show that mainly the pyrazolyl group and the tetrazine ring are involved. This fact, suggest that a higher variation of the transition dipole moment is expected for **L2** upon photo-excitation, resulting in a higher hyperpolarizability value. In fact, the three functionals predict that the hyperpolarizability for **L2** is higher than **L1** by a 2-fold factor. Concerning ligands **L3**, **L4** and **L5**, the analysis of the orbitals show that the low lying energy transition occurs mainly centred at the tetrazine ring, hence resulting in a null variation of the transition dipole moment upon photo-excitation. The low hyperpolarizability value of **L5** could be related to the asymmetry of the molecule.

The estimated β_{tot} values for the three ligands, using the three functionals, are very similar, in particular for **L1**. For ligand **L2**, B3LYP provides the highest hyperpolarizability whereas CAM-B3LYP provides the lowest. Since the tetrazine ligands present a relatively short charge transfer transitions, the CAM-B3LYP should, in fact, perform worst, accounting the fact that this functional was developed for correctly weight long charge transfers in molecules.

Table 3.10: Hyperpolarizability tensors β_{iii} and total htperpolarizability β_{tot} for the tetrazine ligands

		Hyperpolarizability tensors ($\times 10^{-30}$ esu)										
Funct.	Comp.	β_{xxx}	β_{xxy}	β_{xyy}	β_{yyy}	β_{xxz}	β_{xyz}	β_{yyz}	β_{xzz}	β_{yzz}	β_{zzz}	β_{tot}
	L1	-10.12	4.08	-0.20	-2.19	-1.18	-0.46	-0.02	-0.02	0.10	0.19	10.57
	L2	36.01	-0.35	-0.70	-2.00	-0.09	-0.02	-0.09	-0.37	0.36	0.05	35.00
B3LYP	**L3**	0.00	0.00	0.00	0.00	0.00	0.00	0.00	0.00	0.00	0.00	0.00
	L4	0.00	0.00	0.00	0.00	0.00	0.00	0.00	0.00	0.00	0.00	0.00
	L5	-1.20	0.00	0.09	0.00	0.00	0.00	0.00	-0.83	0.00	0.00	1.94
	L1	-6.39	4.22	-0.12	-2.01	-0.44	-0.40	0.62	0.00	0.06	0.17	6.90
	L2	-26.40	-0.09	0.53	-1.75	-0.53	0.08	-0.46	0.29	0.19	0.30	25.64
CAM-B3LYP	**L3**	0.00	0.00	0.00	0.00	0.00	0.00	0.00	0.00	0.00	0.00	0.00
	L4	0.00	0.00	0.00	0.00	0.00	0.00	0.00	0.00	0.00	0.00	0.00
	L5	3.27	0.00	-0.09	0.00	0.00	0.00	0.0	0.66	0.00	0.00	3.84
	L1	9.62	3.63	-0.02	-2.09	0.28	-0.26	0.05	-0.24	0.11	0.00	9.51
	L2	30.65	1.09	-0.27	-1.25	-1.16	-0.12	-0.13	-0.48	-0.13	0.03	31.40
M06	**L3**	0.00	0.00	0.00	0.00	0.00	0.00	0.00	0.00	0.00	0.00	0.00
	L4	0.00	0.00	0.00	0.00	0.00	0.00	0.00	0.00	0.00	0.00	0.00
	L5	-5.50	0.00	0.35	0.00	0.01	0.00	0.00	-0.69	0.00	0.00	5.86

3.3.2 DFT studies of the Complexes

Like in the case of the DFT studies for the tetrazine-based ligands, the formerly used methods for the DFT studies of the benzo[c]thiophene-based complexes (**Chapter 2**) were applied, that is, the same level of theory (DFT and TD-DFT), functionals and basis sets. It was also shown that the use of model phosphanes provide a good approximation with lower computational time and effort. For this reason, only model phosphanes were tested. Also, as aforementioned, the inclusion of solvation models in theoretical calculations tetrazines were found to be crucial for obtaining adequate results. Hence, all calculations involving the organometallic complexes were also performed using solvation methods, namely the polarizable continuum model (PCM) using chloroform as solvent.

The calculations of the tetrazine-based complexes was not as successful as the ligands. Several SCF convergence problems were encountered either during geometry optimizations or during the estimation of the nonlinear optical properties of the complexes. In particular, the energy minimum for complex **bRu$_2$L3** was not achieved. Attempts to overcome these problems were made by the use of a quadratically convergent SCF procedure (QC) or a double quadratic convergent procedure (XQC). Also, usage of the previously failed calculations as initial guess for subsequent geometry optimization attempts alongside the request of force constants at the initial step were tested. None of these additional features of the calculation resulted in the minimization of the energy of the complex. Hence, since no optimized geometry was obtained, no results will be presented for this complex. Hyperpolarizability calculations on the **aRu$_2$L3** complex were also not successfully achieved due to convergence problems. The same problem was encountered for **bRuL3** using the CAM-B3LYP and M06 functionals. Extending the number of cycles for the SCF cycle proved to be insufficient to obtain the required convergence.

3.3.2.1 Geometry and optical data

The solvated B3LYP optimized structures of the model organometallic complexes are shown in **Figure 3.21**. No significative differences were observed for the other functionals. **Table 3.11** shows the selected bond distances and bond angles for all the studied compounds.

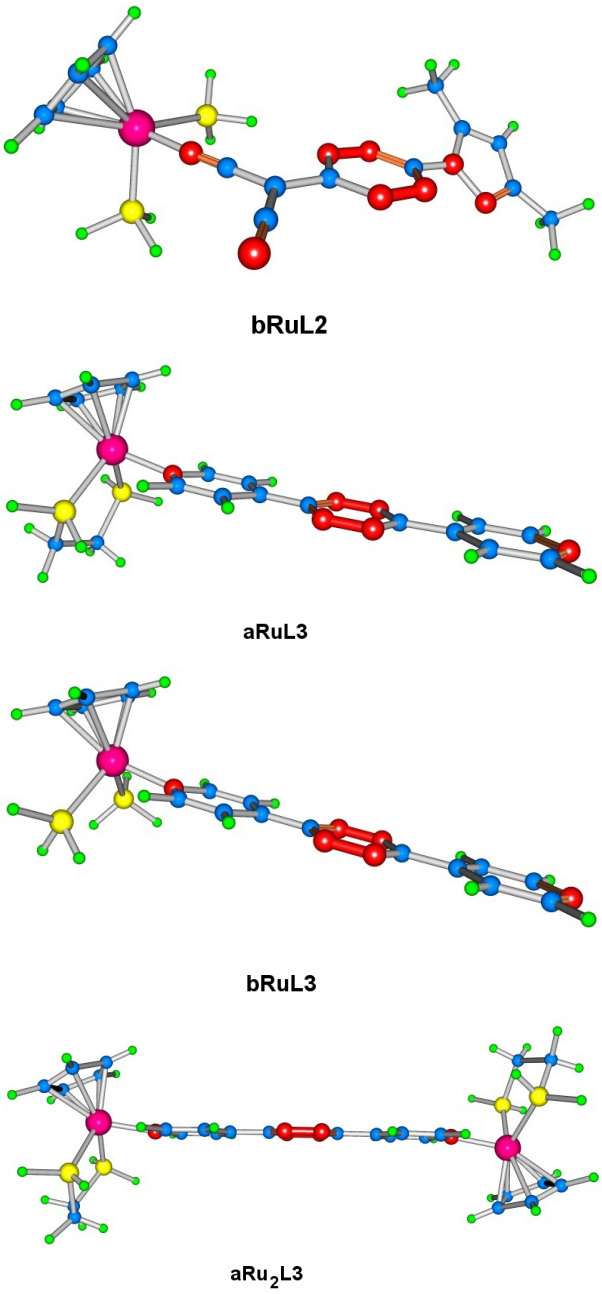

Figure 3.21: B3LYP solvated structures for the studied complexes

Table 3.11: Selected Bond Distances and Bond Angles for the studied complexes

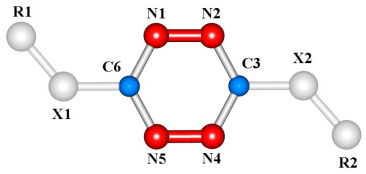

Comp.	B3LYP				CAM-B3LYP				M06			
	bRuL2	aRuL3	bRuL3	aRu_2L3	bRuL2	aRuL3	bRuL3	aRu_2L3	bRuL2	aRuL3	bRuL3	aRu_2L3
Bond Distances (Å)												
M_1-Cp[a]	1.8859	1.8983	1.8892	1.8991	1.9100	1.8738	1.8671	1.8739	1.8862	1.8467	1.8391	1.8470
M_2-Cp[a]				1.8981				1.8739				1.8470
M_1-P[b]	2.4314	2.4231	2.4374	2.4221	2.4074	2.4122	2.4262	2.4130	2.4074	2.4156	2.4313	2.4163
M_2-P[b]				2.4220				2.4130				2.4163
M_1-N	2.0779	2.1694	2.1740	2.1674	2.0633	2.1643	2.1686	2.1629	2.0633	2.1765	2.1728	2.1698
M_2-N				2.1674				2.1629				2.1698
X_1-C_6	1.4049	1.4781	1.4782	1.4772	1.3912	1.4791	1.4161	1.4787	1.3886	1.4141	1.4706	1.4696
C_6−N_1	1.3656	1.3471	1.3489	1.3484	1.3688	1.3375	1.3715	1.3386	1.3742	1.3784	1.3423	1.3437
N_1-N_2	1.3127	1.3119	1.3119	1.3118	1.3222	1.3045	1.3268	1.3044	1.3278	1.3324	1.3050	1.3048
N_2-C_3	1.3388	1.3500	1.3501	1.3483	1.3498	1.3406	1.3413	1.3386	1.3575	1.3470	1.3464	1.3437
C_3−N_4	1.3454	1.3500	1.3501	1.3485	1.3437	1.3406	1.3502	1.3386	1.3508	1.3586	1.3452	1.3437
N_4-N_5	1.3070	1.3118	1.3118	1.3112	1.3270	1.3043	1.196	1.3043	1.3312	1.3231	1.3054	1.3048
N_5-C_6	1.3689	1.3471	1.3470	1.3485	1.3639	1.3376	1.3764	1.3386	1.3699	1.3841	1.3422	1.3437
C_3-X_2	1.4302	1.4775	1.4776	1.4772	1.4139	1.4780	1.3943	1.4787	1.4143	1.3915	1.4702	1.4696
Bond Angles (°)												
Cp-M_1-N[a]	127.73	104.63	123.41	123.97	127.52	124.00	123.46	124.02	129.93	124.26	123.42	124.16
Cp-M_2-N[a]				123.87				124.03				124.16
P-M_1-P	92.45	82.10	90.71	82.17	92.95	82.17	90.84	82.22	91.37	81.67	90.24	81.66
P-M_2-P				82.13				82.22				81.66
M-N-Tet[c]	146.03	170.07	176.60	171.27	138.51	170.91	171.75	171.48	143.47	168.49	170.13	167.81
Npy-Tet-Npy[c]		177.35	179.02	170.32		178.48	179.14	180.00		177.52	179.86	179.99
Ru-Tet-Ru[c]				178.60				180.00				179.99
$N_1N_2C_3$	118.12	118.29	118.23	118.14	118.58	118.26	118.25	118.16	118.36	118.12	118.11	118.04
$N_2C_3N_4$	124.91	123.43	123.80	123.70	124.31	123.40	123.42	123.70	124.68	123.66	123.69	123.94
$C_3N_4N_5$	117.84	118.23	118.23	118.16	118.23	118.25	118.25	118.14	117.99	118.12	118.12	118.03
$N_4N_5C_6$	118.24	118.17	118.15	118.15	118.48	118.20	118.17	118.16	118.30	118.05	118.03	118.03
$N_5C_6N_1$	122.84	123.73	123.80	123.70	122.25	123.72	123.75	123.70	122.57	123.95	124.00	123.94
$C_6N_1N_2$	117.90	118.16	118.15	118.15	118.10	118.18	118.17	118.14	117.87	118.05	118.05	118.03
Dh1[d]	179.23	-179.95	178.37	-178.81	179.53	179.43	178.22	178.81	-179.88	-179.78	176.63	179.76
Dh2[e]	-137.52	179.70	179.31	179.46	−141.65	-149.05	179.37	-178.80	-145.04	-179.75	178.82	-179.76

[a] M = Ru(II); Values refer to the centroid of the cyclopentadienyl ring; [b] Average M-P bond distance; [c] Tet refers to the centroid of the tetrazine ring; [d] Dh1 refers to the C4-C5-C6-C7 dihedral angle; [e] Dh2 refers to the C12-C13-C14-C15 dihedral angle

The ruthenium complexes adopt a three-legged piano-stool geometry around the metal centre, with the η^5-cyclopentadienyl ring occupying three coordinating positions. The remaining three positions are occupied by the phosphane co-ligand and ligands **L2**, in the case of **bRuL2**, and **L3**, in the case of the mononuclear **aRuL3** and **bRuL3** and binuclear **aRu$_2$L3** complexes. The binuclear complex adopt a transoid structure in which the η^5-cyclopentadienyl rings of both metal centre are in opposite plans of the molecules. In all complexes the Ru-Cp and the Ru-P bond lengths are consistent with other experimental crystal data for parent η^5-monocyclopentadienyl-ruthenium(II) complexes, like the case of the previously studied benzo[c]thiophene derivatives and other found in the literature.[71]The structures of the binuclear complexes are also in good agreement with other dinuclear η^5-cyclopentadienylmetal complexes.[101]

Comparatively to the complexes bearing ligand **L3**, the **bRuL2** complex present a longer M-Cp bond length consitent with the less positively charged ruthenium centre. In order to investigate the structure of this complex, DFT calculations were also made for the C-bound analogue. **Figure 3.22** shows the B3LYP optimized geometry for the C-bound complex together with some of its structural parameters. The structure of the N-bound complex **bRuL2** was included for comparison. The tetrazine ligand was omitted for simplification.

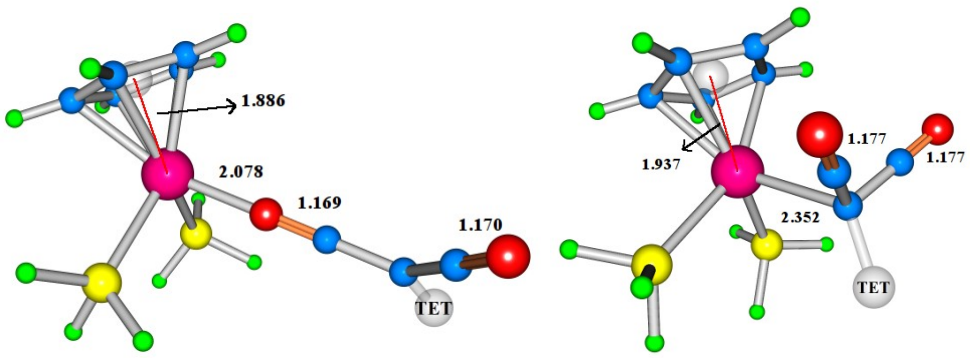

Figure 3.22: Structural features of the N-bound and C-bound optimized geometries of ruthenium (II) complexes bearing ligand **L2**

It is clear that the coordination mode of ligand **L2** has significative influence on the structural features of the N- and C-bound complexes. In particular, longer M-Cp bond distances are observed in the C-bound complex due to the coordination of the ruthenium centre at the anionic carbon atom of the dicyanomethyl group, hence affording, formally,

a neutral complex. Also, the N≡C bond lengths of both structures are sligthly different. The N-bound complex shows a slightly shorther N≡C bonds when compared with the C-bound complex (*ca* 0.007 Å). However, both complexes show that N≡C bond distances of the two nitrile groups are identical (only a difference of 0.001 Å was found for the N-bound complex). It was hypothesized that the σ donnor effect of the bonded N≡C group to the Ru metal centre is compensated by the π-backdonation, which leads to an almost unchanged N≡ bond energy upon coordination. Experimental FTIR spectroscopic data (*vide supra*) supports this observation since no significative change on the ≡ stretching energy was observed upon ligand coordination. DFT calculations also determined that the N-bound complex is more stable than the C-bound complex by 28.6 kcal/mol, corroborating the hypothesized structure of a N-bound coordination mode for the synthesized complex.

DFT calculations were made on the carboanionic ligand to further support these observations. Results show that N≡C bond length for the N-bound complex is more similar to the anionic form of the ligand, than the C-bound complex (N≡C for the anionic **L2**: 1.1711 Å; N≡C for **L2**: 1.1593 Å). According to the ^{13}C-NMR data presented in Section 3.2.3, it was hypothesized that complex **bRuL2** presented, in fact, two distinct nitrile groups.

As a result of the coordination to the organometallic fragments, the bond lengths and bond angles of the tetrazine ring in the organometallic complexes are slightly different comparatively to the free ligands. However, for **bRuL2** the X_1-C_6 and C_3-X_2 bond lengths are not comparable due to the difference in the structure of the coordinated and free ligand. For the mononuclear complexes , and as a general behaviour for all functionals, shorter X_1-C_6 and C_3-X_2 are observed. In particular, the X_1-C_6 present a shortening of 0.001 Å upon metal coordination for M06, but remains unchanged for the B3LYP and CAM-B3LYP functionals. A similar behaviour is observed for the C_3-X_2 bond length. The structural data suggests that the coordination of a single metal centre to ligand **L3** results in a weak π-backdonation from the metal centre. For the dinuclear complex, the shortening of the X_1-C_6 and C_3-X_2 bonds is slightly more pronounced than for the mononuclear complexes. For complex **aRu$_2$L3** a shortening of 0.002 Å is observed for B3LYP and M06, whereas CAM-B3LYP provides a similar bond length. The weak π-backdonation from the metal centre(s) for both the mono- and dinuclear complexes is also observed in the deviation of the N_{py}-TET-N_{py} angle from its full planarity, where differences in

the 1°–2° and 1°–4° ranges are obtained for the mononuclear and dinuclear complexes, respectively. Noteworthy is also the fact that the deviations are in accordance with the well known electron donation abilities of the phosphanes, that is, higher deviations are observed for the κ^2-dppe than for PPh_3.

Considering the different functionals, B3LYP is the functional that provides higher bond distances in the organometallic fragment, followed by CAM-B3LYP and M06. This trend is not observed in the structural data for the ligand, in which M06 now outcomes CAM-B3LYP providing higher bond distances.

The linear optical data was obtained by performing TD-DFT calculations on the optimized geometries of the complexes. **Table 3.12** shows the selected optical data whereas **Figure 3.23** shows the simulated spectra using B3LYP functional as a typical behaviour for these complexes.

The simulated spectra of the mononuclear complexes (**bRuL2**, **aRuL3** and **bRuL3**) resembles those of the corresponding free ligands, that is, are characterized by a very low intensity band in visible region (λ_{max} = 500 - 620 nm) and by a strong band in the UV region (λ_{max} = 250 - 370 nm) which energies depends on the coordinated ligands or phosphane co-ligand. These bands result from a combination of electronic transitions, close in energy, which difficult the charge transfer analysis based on the involved orbitals. For this reason, only the orbitals involved in relevant transitions are presented in the following discussion. These orbitals are showed in **Figure 3.24 - 3.26**.

The analysis of the orbitals involved in the charge transfer processes (both lowest energy and highest energy bands) for **bRuL2** (**Figure 3.24**) resembles almost those of the corresponding free ligands (see **Figure 3.18** and **Table 3.9**). The main difference is that the organometallic moiety enhances the π-delocalized system and its contribution to the excitations leads to changes on the observed band, in particular their energy. The lowest energy band of this complex can be attributed to a combination of a MLCT and an ILCT. In both cases the tetrazine ring has clearly higher contribution than the pyrazolyl group in these excitations. A red shift of this band (48 nm) is observed upon coordination of the **L2** ligand. In the case of the highest energy band, it can be attributed mainly to an ILCT with an enhanced contribution of the pyrazolyl group. Also, a red shift (*ca* 60 nm) is observed on this band upon ligand coordination.

For **aRuL3** (**Figure 3.25**) the lowest energy band can be clearly attributed to an

Table 3.12: Selected TD-DFT results for the studied complexes

Ligand	Functional	λ_{max} (nm) [a]	f [b]	Major Contributions
bRuL2	B3LYP	602	0.0053	HOMO-1→LUMO (88%)
		582	0.0022	HOMO→LUMO (96%)
		363	0.0457	HOMO-1→LUMO+2 (31%)
		342	0.8774	HOMO→LUMO+2 (84%)
	CAM-B3LYP	595	0.0024	HOMO→LUMO (93%)
		357	0.0259	HOMO-1→LUMO+2 (76%)
		342	0.8659	HOMO-1→LUMO+2 (86%)
		326	0.0299	HOMO-2→LUMO+1 (26%)
	M06	601	0.0025	HOMO→LUMO (98%)
		376	0.0278	HOMO-2→LUMO+3 (57%)
		347	0.8018	HOMO→LUMO+2 (83%)
aRuL3	B3LYP	521	0.0052	HOMO-3→LUMO (99%)
		391	0.0241	HOMO→LUMO+3 (49%)
		326	0.0265	HOMO-2→LUMO+3 (36%)
		323	0.2662	HOMO-1→LUMO (73%)
		302	0.7020	HOMO-2→LUMO (75%)
	CAM-B3LYP	524	0.0052	HOMO-3→LUMO+1 (99%)
		370	0.0185	HOMO-1→LUMO+5 (41%)
		318	0.2327	HOMO-1→LUMO (69%)
		297	0.6855	HOMO-2→LUMO (76%)
	M06	626	0.0036	HOMO-3→LUMO (10%)
		465	0.0919	HOMO-1→LUMO+1 (90%)
		434	0.2770	HOMO-2→LUMO+1 (98%)
		402	0.0182	HOMO-1→LUMO+4 (90%)
		301	0.8808	HOMO-6→LUMO+1 (92%)
bRuL3	B3LYP	574	0.0042	HOMO-3→LUMO (100%)
		467	0.0888	HOMO-1→LUMO+1 (96%)
		406	0.3028	HOMO-2→LUMO+1 (85%)
		306	0.8415	HOMO-6→LUMO+1 (91%)
	CAM-B3LYP	523	0.0052	HOMO-3→LUMO+1 (99%)
		387	0.0117	HOMO-1→LUMO+4 (46%)
		375	0.0269	HOMO→LUMO+3 (59%)
		311	0.3510	HOMO-1→LUMO (78%)
		292	0.6775	HOMO-2→LUMO (73%)
	M06	626	0.0037	HOMO-3→LUMO (100%)
		450	0.1489	HOMO-1→LUMO+1 (88%)
		439	0.0295	HOMO-1→LUMO+4 (38%)
		418	0.2073	HOMO-2→LUMO+3 (74%)
		404	0.0324	HOMO→LUMO+3 (70%)
		301	0.9116	HOMO-6→LUMO+1 (90%)
aRu$_2$L3	B3LYP	572	0.0039	HOMO-6→LUMO (99%)
		542	0.1614	HOMO-2→LUMO+1 (97%)
		464	0.5786	HOMO-4→LUMO+1 (97%)
		311	0.1451	HOMO-11→LUMO (67%)
		300	0.1054	HOMO-5→LUMO+2 (93%)
		281	0.7274	HOMO-13→LUMO+1 (94%)
	CAM-B3LYP	519	0.0048	HOMO-6→LUMO+1 (99%)
		382	0.0403	HOMO-2→LUMO (27%)
		344	0.5407	HOMO-2→LUMO (74%)
		319	0.7116	HOMO-4→LUMO (75%)
	M06	624	0.0034	HOMO-6→LUMO+1 (100%)
		515	0.2574	HOMO-2→LUMO+1 (93%)
		481	0.4661	HOMO-4→LUMO+1 (93%)
		302	0.1021	HOMO-11→LUMO (48%)
		298	0.1461	HOMO-7→LUMO+1 (55%)
		295	0.2642	HOMO-9→LUMO+1 (47%)

[a] Absorption wavelength of the main transitions; [b] Oscillator strength;

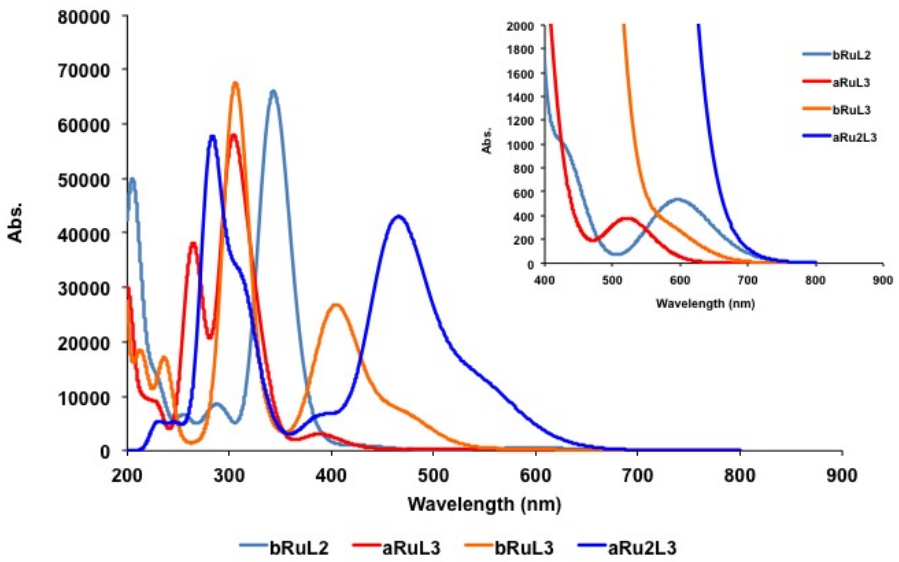

Figure 3.23: B3LYP TD-DFT spectra of the complexes

.Inset: Expansion of the 400-900 nm range.

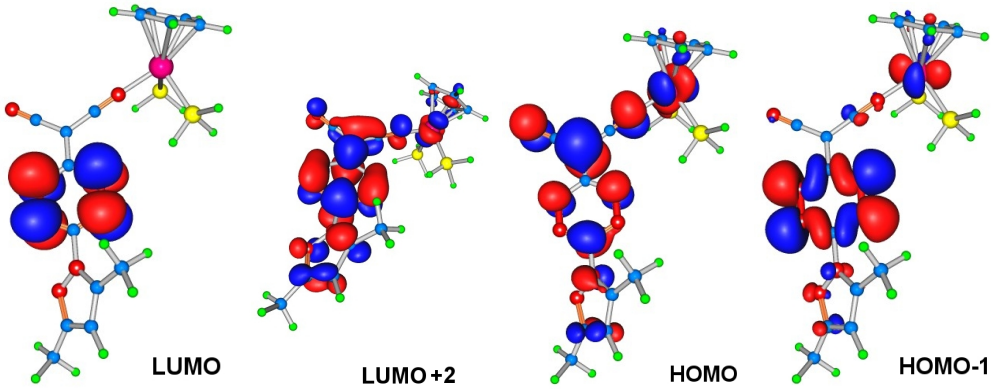

Figure 3.24: Orbitals involved in the relevant optical transitions of complex **bRuL2** obtained by B3LYP (contour: 0.046 au)

ILCT involving the tetrazine ring. The character of this charge transfer clearly resembles that of the free ligand (see **Figure 3.18** and **Table 3.9**). The main change observed on this excitation is a blue shift (45 nm) upon coordination of the ligand to the metal centre. In the case of the highest energy band, it can be clearly attributed to a MLCT (from metal centre to the tetrazine ring) with a minor contribution of a transition centred

at the organometallic moiety. Compared to the highest energy band of the free ligand, a red shift is observed upon ligand coordination (*ca* 20-30 nm).

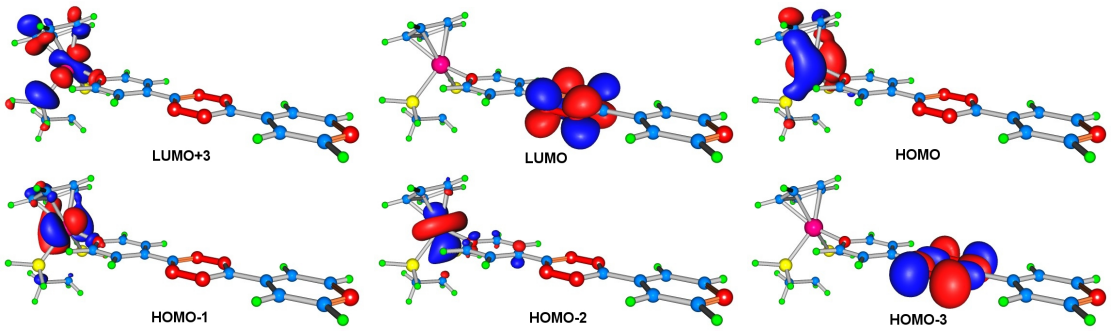

Figure 3.25: Orbitals involved in the relevant optical transitions of complex **aRuL3** obtained by B3LYP (contour: 0.046 au)

For **bRuL3** (**Figure 3.26**) a main difference is observed when comparing the spectra of the **aRuL3** complex. Changing the κ^2-dppe coligand by 2 PH_3 leads to the emerging of a new broad charge transfer process centred at (λ_{max} = 406 nm) which can be assigned as a MLCT according to the orbitals involved (HOMO-2→LUMO+1 and HOMO-1→LUMO+1). An ILCT involving the tetrazine ring, also present in the **bRuL3** complex and the free **L3** ligand, appears at λ_{max} = 574 nm. In the case of the highest energy band (λ_{max} = 306 nm), it can be attributed to an ILCT involving both tetrazine ring and pyridine groups with some contribution of the metal centres. The character of this transition resembles that of the highest-energy transition of the free **L3** ligand (see **Figure 3.18** and **Table 3.9**). Compared to the corresponding energy of the free ligand, this transition shows a slight red shift (2 nm) upon ligand coordination. It is interesting to note that, compared to the highest-energy transition of the κ^2-dppe complex (**aRuL3**) which has clearly MLCT character, for the present 2 PH_3 derivative this transition became an ILCT.

The simulated spectra of the binuclear complex **aRu2L3** using B3LYP shows two strong and complex bands being one of them in the visible region (λ_{max} = 464 nm) with a shoulder centred at *ca* 542 nm and the second in the UV region (λ_{max} = 281 nm), also with a shoulder centred at $\lambda_{max} \approx$ 305 nm. An analysis of the orbitals involved (**Figure 3.27**) shows that the broad lowest-energy band has contributions of an intense transition clearly assigned to MLCT excitation (λ_{max} = 464 nm) and a shoulder which has a component assigned also to MLCT transition (λ_{max} = 542 nm) and an ILCT (λ_{max} = 572 nm). It

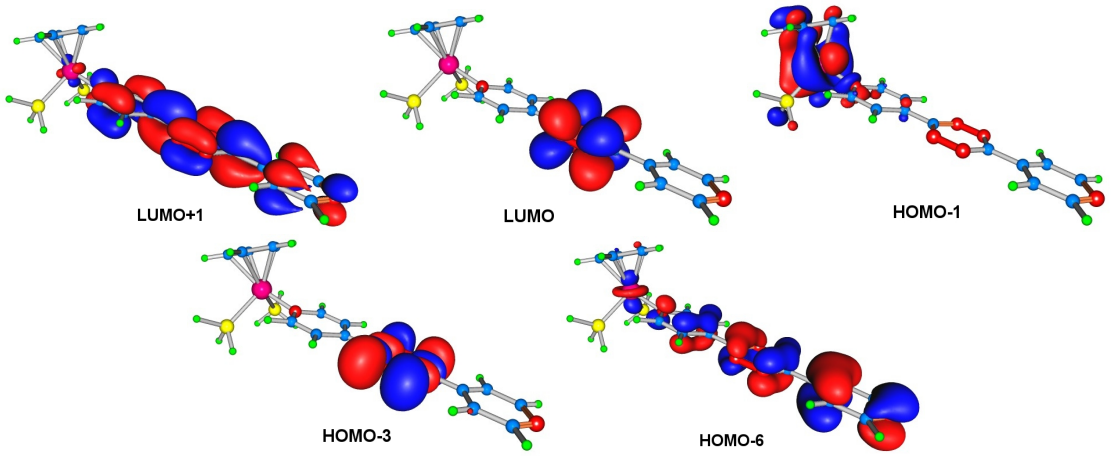

Figure 3.26: Orbitals involved in the relevant optical transitions of complex **bRuL3** obtained by B3LYP (contour: 0.046 au)

can be seen that the main MLCT transition results in an effective charge transfer from the metal centres (HOMO-4) to both the tetrazine and pyridine groups (LUMO+1). The same character is found in the MLCT component of the shoulder. Finally, the ILCT component of the shoulder is clearly assigned with a charge transfer within the tetrazine ring which resembles the lowest-energy transition of the free **L3** ligand (see **Figure 3.18** and **Table 3.9**). Compared to the corresponding energy of the free ligand, this transition shows a slight blue shift (5 nm) upon ligand coordination. In the case of the highest energy band, the main transition (λ_{max} = 281 nm) can be attributed to an ILCT involving both tetrazine ring and pyridine groups with some contribution of the metal centres. The character of this transition resembles that of the highest-energy transition of the free **L3** ligand. Compared to the corresponding energy of the free ligand, this transition shows a blue shift (23 nm) upon ligand coordination. Finally, the shoulder centred at λ_{max} = 305 nm has a component assigned as a MLCT (mainly from metal centres to the pyridine groups) and an ILCT (from pyridine groups to the tetrazine rings) also present in the free ligand.

Thus, as an overall conclusion it can be assumed that the coordination of the ligand **L3** to the organometallic moieties in the binuclear complex leads to the appearance of new transitions assigned to MLCT besides the chromophore based ILCTs.

At this point, the overall DFT results should be commented. Comparison with experimental data can only be performed between the linear optical spectra and the TD-DFT

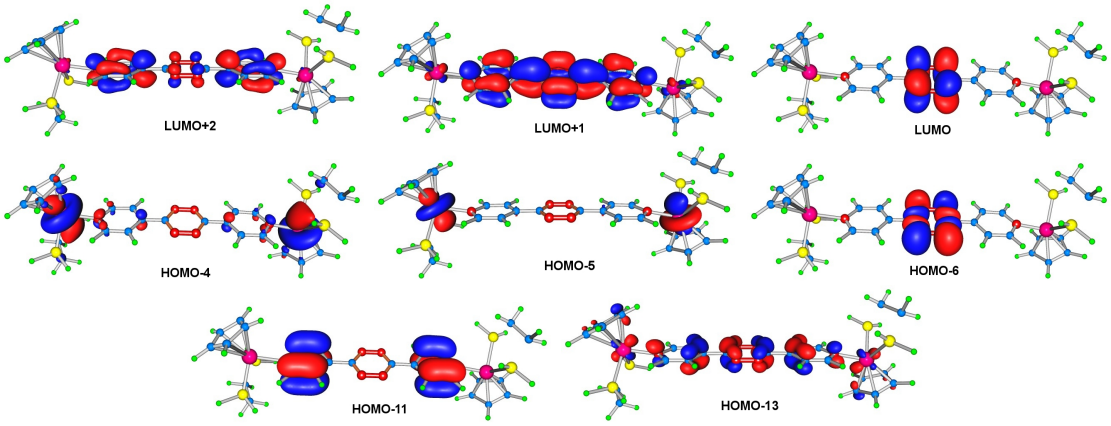

Figure 3.27: Orbitals involved in the relevant optical transitions of complex **aRu2L3** obtained by B3LYP (contour: 0.046 au)

results for both the ligands and complexes **bRuL2** and **aRu$_2$L3**. For both cases, it is impossible to establish an unambiguous relation between the functionals performance in the reproduction of the experimental data. For exemple, analysis of the TD-DFT performance for the three functionals for complex **bRuL2** shows that no significative differences are obtained – all functionals overestimate the lowest energy transition by *ca.* 60 nm and underestimate the highest energy transition by *ca.* 10 nm. Concerning **aRu$_2$L3**, it is clear that CAM-B3LYP outperforms both the B3LYP and M06 functionals, for which higher deviations in comparison with the experimental data are obtained. In particular, for the lowest energy band, CAM-B3LYP slightly underestimates the energy of the transition by *ca* 12 nm whereas an underestimation of 35 and 62 nm are observed for the B3LYP and M06 functionals respectively. For the highest energy transition, higher overestimations are observed for B3LYP and M06 ($\approx$ 95 nm) than for CAM-B3LYP ($\approx$ 45 nm).

Calculations of the nonlinear optical properties of the complexes were performed. As mentioned previously, no hyperpolarizabilities were obtained for the binuclear complexes due to successive convergence failure of the SCF procedure. The rst hyperpolarizabilities of the mononuclear complexes **bRuL2**, **aRuL3** and **bRuL3** are shown in **Table 3.13**.

Table 3.13: Hyperpolarizability tensors β_{iii} and total htperpolarizability β_{tot} for the tetrazine-based complexes

Funct.	Comp.	Hyperpolarizability tensors ($\times 10^{-30}$ esu)										
		β_{xxx}	β_{xxy}	β_{xyy}	β_{yyy}	β_{xxz}	β_{xyz}	β_{yyz}	β_{xzz}	β_{yzz}	β_{zzz}	β_{tot}
B3LYP	**bRuL2**	11.59	-6.17	11.11	-5.43	-6.14	6.86	-5.22	5.26	-3.45	-7.60	36.98
	aRuL3	-109.46	7.18	1.10	3.19	-0.04	0.04	0.38	0.77	1.88	0.13	108.28
	bRuL3	93.36	1.26	-1.15	1.57	-3.70	0.16	-2.71	-1.38	-0.51	-3.32	91.38
CAM-B3LYP	**bRuL2**	19.47	-9..61	4.25	2.50	1.80	0.57	-0.28	0.66	-0.38	6.04	26.61
	aRuL3	18.95	1.80	-0.19	2.29	0.19	0.00	-0.30	-0.22	0.94	-0.01	19.20
	bRuL3	14.95	0.44	-0.55	0.91	-1.63	0.09	-1.64	-0.55	-0.16	-2.68	15.13
M06	**bRuL2**	29.76	-7.24	5.94	2.34	-1.03	0.82	-0.58	-0.16	-0.51	7.39	36.41
	aRuL3	-119.73	8.28	1.14	1.24	-0.23	0.01	0.44	1.15	1.57	0.09	117.96
	bRuL3	104.00	1.17	-1.53	1.51	-3.81	0.25	-2.18	-1.83	-0.47	-2.64	101.03

The estimated hyperpolarizabilities for all complexes are functional dependent. The observed trend on β_{tot} by varying the used functionals is maintained for all complexes: CAM-B3LYP < M06 ≈ B3LYP.

As general behaviour, the calculated hyperpolarizabilities for the organometallic complexes are higher than those for the free ligands. It can be show that, in the case of **bRuL2** complex, the calculated hyperpolarizability is only slightly higher than that of the corresponding free ligand, **L2**. On the basis of the analysis of the orbitals involved in the charge transfer processes for this complex discussed above, the character of both lowest energy and highest energy bands almost resembles those of the corresponding free ligands, with a small contribution of the organometallic moiety. Thus, the minor change on the hyperpolarizability upon coordination for this complex can be related to the small participation of organometallic moiety in the charge transfer processes. In particular, the lowest energy band has a small contribution of a MLCT transition and a red shift was observed upon coordination of the **L2** ligand. For **aRuL3** and **bRuL3** a significant change on hyperpolarizabilities was obtained upon **L3** coordination. Considering that the symmetric free ligand presents a null hyperpolarizability, it is clear that the observed hyperpolarizability on the complexes results from the coordination to the metal centres which breaks the symmetry of the chromophore. In the case of **aRuL3**, and on the basis of the analysis of the orbitals involved in the charge transfer processes discussed above, the observed β_{tot} cannot be explained by the lowest energy band since it is clearly attributed to an ILCT involving the tetrazine ring and a blue shift was observed upon coordination of the ligand to the metal centre. Probably, the highest energy band of this complex, attributed mainly to a MLCT, plays a role. Also, a red shift of this band is observed upon ligand coordination which favours the quadratic hyperpolarizability properties.

In the case of **bRuL3**, the observed β_{tot} can be mainly related with the charge transfer process centred at (λ_{max} *approx* 406 nm) which was clearly assigned as a MLCT according to the orbitals involved and discussed above. Compared to the main charge transfer processes contributing to β_{tot} for **bRuL3** and **aRuL3** it is supposed that former should give a higher hyperpolarizability value. However both values are quite similar being **aRuL3** with the best value. Probably the highest energy band of **bRuL3** also contributes to the observed hyperpolarizability. As discussed above this band can be assigned as ILCT for this complex whereas for **aRuL3** it is a MLCT. Thus, a somewhat hampering effect on the observed hyperpolarizability for **bRuL3** can be present. It is interesting to note that

a higher estimated hyperpolarizability for complex **aRuL3** had been already suggested by DFT structural data, in which a higher π-backdonation interaction have been observed.

Some remarks considering the applicability of the well-known TLM to describe the quadratic hyperpolarizabilities of these mononuclear complexes can be made. For **aRuL3** and **bRuL3** the observed β_{tot} is clearly dominated by the β_{xxx} tensor (along the conjugated backbone of the chromophore). However, at least two electronic transitions seem to play a role indicating that β_{tot} cannot be describe by a single excited state. For **bRuL2**, also two electronic transitions seem to govern the observed β_{tot}. In addition, it is clear from the hyperpolarizability tensors (**Table 3.13**) that all tensors cannot be negligible in the contribution of the overall hyperpolarizability.

Although no hyperpolarizabilities were obtained for the binuclear complex **aRu$_2$L3**, some remarks can be made. On the basis of the analysis of the orbitals involved in the charge transfer processes discussed above, the main electronic transitions can be attributed to MLCT which electronic density change arises from the metal centres to the tetrazine ring or the overall chromophore, hence being of opposite directions. Hence, null or low hyperpolarizability is expected for this complex.

3.3.3 Redox switching

The second-order NLO redox switching abilities of the complexes were investigated. The complexes were tested towards oxidation of the metal centre. Hence, unrestricted calculations of the one-electron-oxidized species were performed. Geometries were optimized in condensed phase using PCM solvation method and chloroform as solvent. TD-DFT and hyperpolarizabilities calculations were performed using the same methodology as previously described.

Calculations of the one-oxidized complexes have proven to be more hard than for the non-oxidized counterparts. In particular, similar problems in the convergence of the SCF procedure was observed in geometry optimization of the dinuclear complexes. Again, attempts to avoid this problem by the same methods described for the non-oxidized complexes were performed. None of the attempts resulted in the minimization of the energy of the complexes. For that reason, no results for the dinuclear organometallic complexes are presented.

Figure 3.28 and **Table 3.14** show the obtained B3LYP optimized geometries and selected structural data for the tested compounds upon oxidation, respectively.

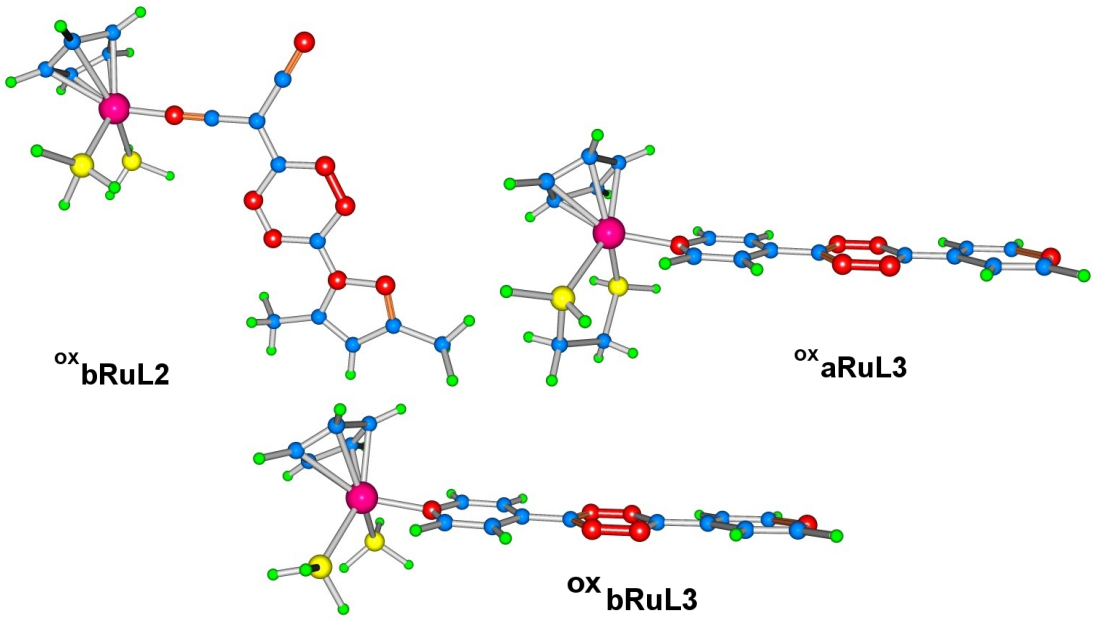

Figure 3.28: B3LYP optimized geometries for the oxidized complexes

Table 3.14: Selected Bond Distances and Bond Angles for oxidized complexes

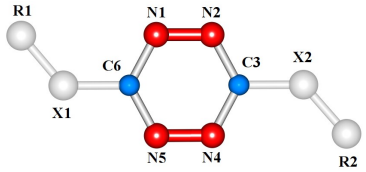

Comp.	B3LYP			CAM-B3LYP			M06		
	^{ox}bRuL2	^{ox}aRuL3	^{ox}bRuL3	^{ox}bRuL2	^{ox}aRuL3	^{ox}bRuL3	^{ox}bRuL2	^{ox}aRuL3	bRuL3
				Bond Distances (Å)					
M_1-Cp[a]	1.9557	1.9405	1.9367	1.9311	1.9112	1.8946	1.9196	1.9020	1.8947
M_1-P[b]	2.4391	2.4659	2.4866	2.4277	2.4547	2.4657	2.4269	2.4463	2.4662
M_1-N	1.9746	2.1788	2.1790	1.9594	2.1650	2.1700	1.9699	2.1657	2.1700
X_1-C_6	1.4430	1.4801	1.4801	1.4422	1.4802	1.4726	1.4375	1.4727	1.4728
C_6−n_1	1.3698	1.3449	1.3446	1.3585	1.3360	1.3400	1.3677	1.3403	1.3404
N_1-N_2	1.3282	1.3117	1.3120	1.3199	1.3038	1.3050	1.3228	1.3049	1.3050
N_2-C_3	1.3722	1.3515	1.3515	1.3591	1.3420	1.3468	1.3686	1.3469	1.3468
C_3−n_4	1.3624	1.3515	1.3517	1.3498	1.3420	1.3468	1.3564	1.3471	1.3468
N_4-N_5	1.3341	1.3111	1.3109	1.3268	1.3042	1.3046	1.3309	1.3052	1.3040
N_5-C_6	1.3642	1.3452	1.3452	1.3524	1.3359	1.3403	1.3611	1.3406	1.3403
C_3-X_2	1.3771	1.4759	1.4758	1.3759	1.4765	1.4682	1.3737	1.4685	1.4682
				Bond Angles (°)					
Cp-M_1-N[a]	128.28	127.69	126.92	128.71	127.32	126.72	131.39	127.75	126.72
P-M_1-P	90.20	80.24	84.54	80.29	89.53	83.99	87.69	79.98	83.99
M-N-Tet[c]	148.02	171.52	171.60	151.27	172.55	121.90	153.99	170.45	170.67
Npy-Tet-Npy[c]		178.21	177.50		178.48	176.73		177.91	176.73
$N_1n_2C_3$	117.39	118.17	118.20	118.04	117.95	118.05	117.38	118.06	118.05
$N_2C_3n_4$	124.28	123.45	123.42	124.13	124.31	123.68	124.39	123.69	123.68
$C_3n_4n_5$	117.96	118.16	118.20	117.55	118.49	118.00	117.93	118.03	117.98
$N_4n_5C_6$	118.13	118.08	118.07	118.66	117.91	118.00	118.12	117.96	118.00
$N_5C_6n_1$	123.60.	124.06	124.02	123.41	122.84	124.27	123.5	124.27	124.27
$C_6n_1n_2$	118.63	118.05	118.09	118.19	118.44	117.93	118.65	117.97	117.93
Dh1[d]	-179.18	-179.76	174.98	-178.83	179.57	177.16	-177.72	178.71	177.16
Dh2[e]	-175.64	177.73	175.51	-164.33	-176.72	173.83	-177.20	176.74	173.83

[a] M = Ru(II); Values refer to the centroid of the cyclopentadienyl ring; [b] Average M-P bond distance; [c] Tet refers to the centroid of the tetrazine ring; [d] Dh1 refers to the C4-C5-C6-C7 dihedral angle; [e] Dh2 refers to the C12-C13-C14-C15 dihedral angle

By comparison of **Tables 3.11** and **3.14** it is seen that the oxidized species present similar structural features of their non-oxidized counterparts. The most distinct features of the oxidized compounds are the relative position of the Cp ring, which bond is also lengthened comparatively to the non-oxidized compounds. A similar behaviour is found for the Ru-P bonds.

For the ^{ox}**bRuL2** complex, the one-electron oxidation results in the shortening of the M-N bond length, suggesting a higher coupling between the dicyanomethyl group and the metal centre. Furthermore, this effect is also noticeable in the dihedral angles of the ligand, that show improved planarity in both substituents. For the ^{ox}**aRuL3** and ^{ox}**bRuL3** a slight shortening of the M-N bond is also observed. However, no significant improved planarity is observed in the ligand.

Considering the tetrazine ring, ^{ox}**bRuL2** complex provides shorter X_1-C_6 and C_3-X_2 bond length than its non-oxidized counterparts, corroborating the hypothesis of an enhancement coupling of the metal centre with the tetrazine ligand. Shorter X_1-C_6 and C_3-X_2 bond lengths are also observed for the ^{ox}**aRuL3** and ^{ox}**bRuL3** comparatively to their non-oxidized counterparts.

The linear optical data for the oxidized complexes was obtained by TD-DFT calculations in condensed phase using chloroform as solvent. The obtained spectra for the three tested compounds, using B3LYP, is showed in **Figure 3.29** whereas the selected optical data is summarized in **Table 3.15**.

Compared to its non-oxidized counterpart, the main optical feature of complex ^{ox}**bRuL2** is the presence of a broad and very low energy band occurring in the NIR region attributed mainly to a βHOMO$\rightarrow\beta$LUMO transition. Results show that CAM-B3LYP provides the lowest energy transfer whereas for B3LYP and M06 similar results are obtained. An analysis of the orbitals involved, which electronic densities were obtained using B3LYP functional and typifies the behaviour observed for this transition (**Figure 3.30**), this charge transfer arises mainly from tetrazine ring and pyrazolyl group to the organometallic fragment. Thus, the nature of the lowest energy band is significantly altered upon oxidation. In fact, for **bRuL2**, this band was attributed to a combination of a MLCT and an ILCT whereas for ^{ox}**bRuL2** it becomes a LMCT. This fact suggests that, upon oxidation, the organometallic fragment becomes a stronger σ-electron withdrawing group. This feature is supported by the shorter M-N bond length observed for this complex comparatively to its non-oxidized counterpart.

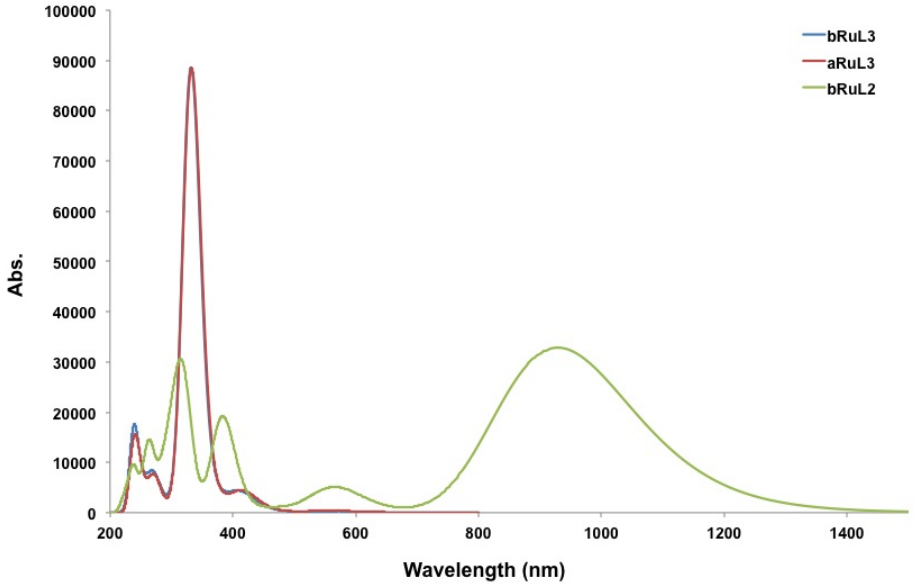

Figure 3.29: TD-DFT spectra of the oxidized complexes using B3LYP

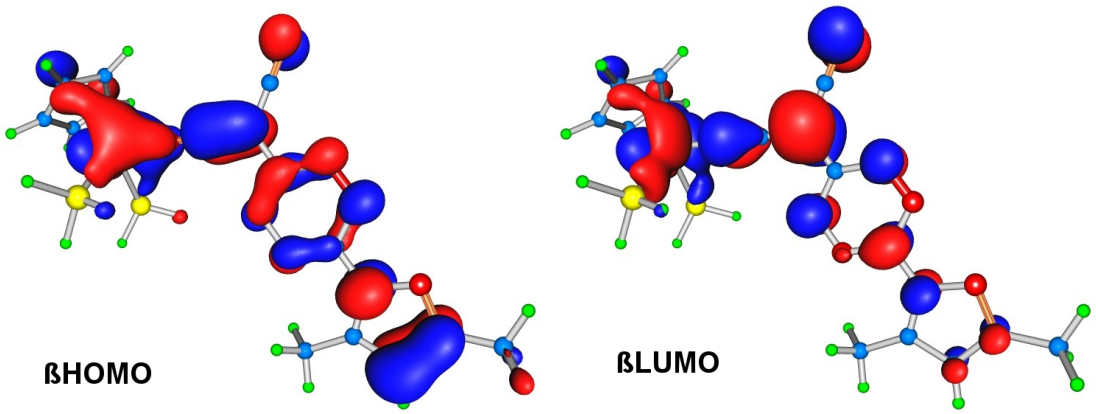

Figure 3.30: Contour plots of the βHOMO and βLUMO orbitals for ^{ox}**bRuL2** complex

Complexes ^{ox}**aRuL3** and ^{ox}**bRuL3** are characterized by the presence an intense band centred at $\lambda \approx 300$ nm (for B3LYP). TD-DFT results shows that this band has contributions of several electronic transitions with very similar energy. This fact makes the analysis of the charge transfer process very complex, and for that reason, the results are discussed based on the relevant transitions that should be responsible for the nonlinear

Table 3.15: Relevant TD-DFT results for the oxidized complexes

Comp.	Functional	λ_{max} (nm) [a]	f [b]	Major Contributions
^{ox}**bRuL2**	B3LYP	930	0.4364	βHOMO→βLUMO (96%)
		827	0.0153	βHOMO-5→βLUMO (81%)
		563	0.0656	βHOMO-4→βLUMO (83%)
		408	0.0116	αHOMO-3→αLUMO (66%)
		382	0.2285	αHOMO→αLUMO+3 (47%)
		323	0.1133	αHOMO-4→αLUMO+2 (14%)
		319	0.1625	βHOMO-4→βLUMO (83%)
		304	0.1499	βHOMO-10→βLUMO (58%)
	CAM-B3LYP	1076	0.4906	βHOMO→βLUMO (93%)
		414	0.0360	βHOMO-3→βLUMO (56%)
		357	0.0123	βHOMO→βLUMO+1 (62%)
		354	0.0635	αHOMO-2→αLUMO+2 (19%)
		345	0.0195	βHOMO→βLUMO+4 (43%)
		348	0.2187	αHOMO→αLUMO+2 (17%);βHOMO-3→βLUMO (16%)
		339	0.0138	αHOMO-5→αLUMO+3 (27%); βHOMO-5→βLUMO+4 (26%)
	M06	1351	0.0145	βHOMO-4→βLUMO (27%)
		1194	0.0225	βHOMO-4→βLUMO (26%)
		887	0.3345	βHOMO→βLUMO (61%)
		530	0.0744	βHOMO-5→βLUMO (89%)
		408	0.0139	αHOMO-3→αLUMO+3(58%)
		385	0.1534	αHOMO→αLUMO+3 (41%)
		371	0.0558	βHOMO→βLUMO+2 (38%)
^{ox}**aRuL3**	B3LYP	422	0.0143	αHOMO-4→αLUMO+3 (24%)
		417	0.0201	αHOMO-4→αLUMO+3 (38%); βHOMO-4→βLUMO+3 (21%)
		406	0.0246	αHOMO-4→αLUMO+3 (48%)
		337	0.3143	αHOMO-4→αLUMO (32%)
		333	0.3071	αHOMO-4→αLUMO (22%)
		329	0.2238	αHOMO-1→αLUMO+2 (50%)
		328	0.1492	αHOMO-4→αLUMO (31%); βHOMO-6→βLUMO+1 (25%)
	CAM-B3LYP	391	0.0236	αHOMO-4→αLUMO+2 (33%); βHOMO-4→βLUMO+3 (19%)
		335	0.0112	βHOMO-11→βLUMO+3 (56%)
		314	0.0309	αHOMO-7→αLUMO+2 (17%); βHOMO-5→βLUMO+3 (24%)
		296	0.0985	βHOMO-3→βLUMO (21%)
		294	0.0565	βHOMO-1→βLUMO (49%)
		283	1.0694	αHOMO-3→αLUMO (35%); βHOMO-3→βLUMO+1 (37%)
	M06	395	0.0269	αHOMO-4→αLUMO+2 (30%)
		387	0.0148	αHOMO-4→αLUMO+3 (26%)
		380	0.0209	αHOMO-4→αLUMO+3 (35%)
		331	0.0130	βHOMO-11→βLUMO (57%)
		294	0.1168	βHOMO-3→βLUMO (54%)
		291	0.1050	αHOMO-7→αLUMO+3 (26%); βHOMO-5→βLUMO+4 (22%)
		287	1.0592	αHOMO-3→αLUMO (36%); βHOMO-3→βLUMO+1 (38%)
^{ox}**bRuL3**	B3LYP	418	0.0352	αHOMO-4→αLUMO (63%)
		402	0.0126	αHOMO-2→αLUMO+1 (37%)
		364	0.0132	αHOMO-4→αLUMO+3 (70%)
		343	0.0795	βHOMO-5→αLUMO+3 (23%)
		331	1.1198	αHOMO-3→αLUMO+1 (46%); βHOMO-3→βLUMO+1 (63%)
	CAM-B3LYP	395	0.0478	αHOMO-4→αLUMO+1 (65%)
		381	0.0113	αHOMO-4→αLUMO+3 (62%)
		320	0.0229	αHOMO-7→αLUMO+1 (21%); βHOMO-5→βLUMO+3 (23%)
		295	0.0412	αHOMO-7→αLUMO+3 (24%); βHOMO-5→βLUMO+4 (22%)
		283	1.2055	αHOMO-3→αLUMO (38%); βHOMO-3→βLUMO+1 (41%)
	M06	445	0.0170	αHOMO-4→αLUMO (40%)
		435	0.0154	αHOMO-4→αLUMO+3 (52%)
		348	0.0192	αHOMO-2→αLUMO+1 (43%); βHOMO-5→βLUMO+3 (46%)
		332	0.0683	αHOMO-6→αLUMO+3 (33%)
		325	1.1665	αHOMO-3→αLUMO+1 (41%); βHOMO-3→βLUMO+1 (46%)

[a] Absorption wavelength of the main transitions; [b] Oscillator strength;

optical properties of the complexes. **Figures 3.31** and **3.32** show the orbitals involved in the dominant electronic transitions for these complexes.

For ^{ox}**aRuL3** the mentioned band has two main contributions: a MLCT (from the metal centre to the ligand, in particular to tetrazine ring and pyridine group bonded to the metal) and a LMCT (from the terminal pyridine group to the organometallic moiety).

The former is also present in the non-oxidized counterpart but with a lower contribution of the pyridine groups. Thus, the new electronic transition that arises from the oxidation of the complexes can be assigned to the mentioned LMCT in which the terminal pyridine group behaves clearly as a donor to the organometallic fragment. No significant change of the energy of the overall band is observed upon oxidation. For ^{ox}**bRuL3** the relevant band can be assigned to an ILCT with some contribution of the organometallic moiety. A band with similar character is also present in the non-oxidized counterpart at almost same energy. The main difference from the non-oxidized counterpart is the vanishing of the MLCT which was observed in the visible region for **bRuL3**.

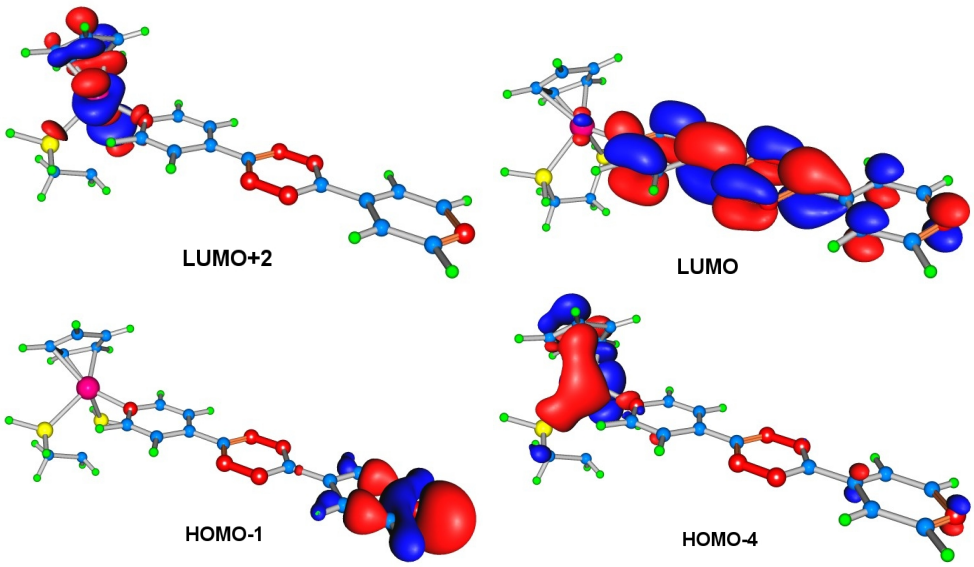

Figure 3.31: Contour plots of the HOMO and LUMO orbitals for ^{ox}**aRuL3** complex

The optical nonlinearities were computed for the three complexes. Results are showed in **Table 3.16**. The estimated hyperpolarizabilities show that different behaviours upon one-electron oxidation for the studied complexes are obtained.

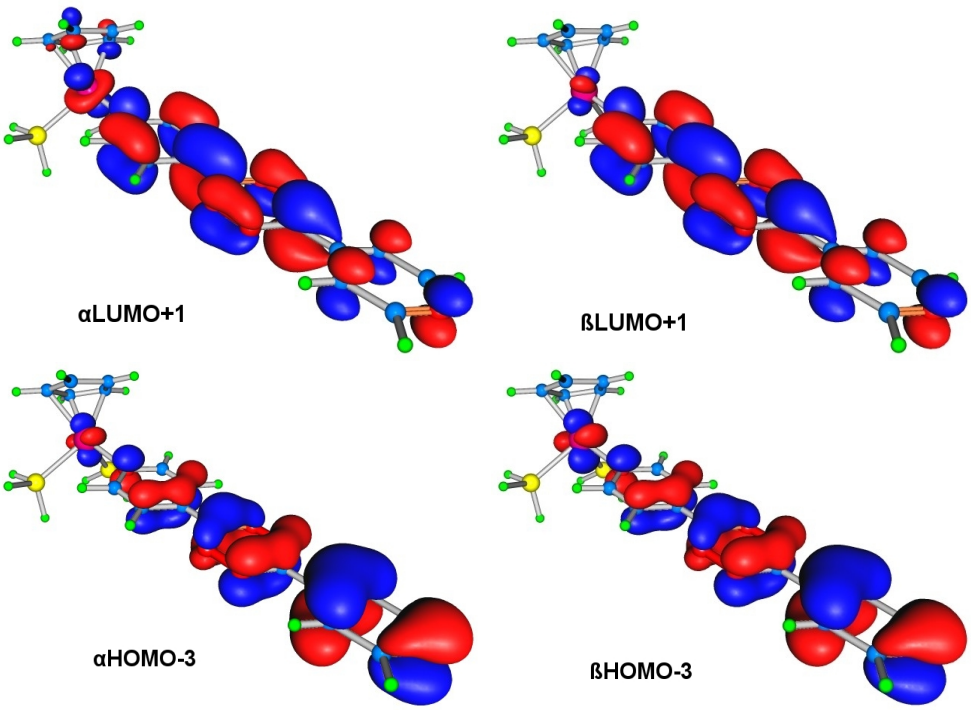

Figure 3.32: Contour plots of the HOMO and LUMO orbitals for ^{ox}**bRuL3** complex

Table 3.16: Hyperpolarizability tensors β_{iii} and total htperpolarizability β_{tot} for the tetrazine-based oxidized complexes

		Hyperpolarizability tensors($\times 10^{-30}$ esu)										
Funct.	Comp.	β_{xxx}	β_{xxy}	β_{xyy}	β_{yyy}	β_{xxz}	β_{xyz}	β_{yyz}	β_{xzz}	β_{yzz}	β_{zzz}	β_{tot}
	^{ox}**bRuL2**	-396.44	205.20	24.22	-4.81	1.67	-0.11	0.16	-1.69	-2.71	0.550	422.95
B3LYP	^{ox}**aRuL3**	-58.27	-1.46	0.97	-1.27	0.35	0.16	0.13	0.05	-0.27	-0.67	57.33
	^{ox}**bRuL3**	-61.85	-0.69	0.14	-0.39	-0.17	0.14	0.89	-0.42	-0.22	-0.33	62.14
	^{ox}**bRuL2**	571.48	390.51	135.49	32.85	-29.08	-8.55	-2.02	-0.40	-1.21	0.10	823.66
CAM-B3LYP	^{ox}**aRuL3**	-215.45	8.34	-1.03	-40.92	0.75	3.96	-12.10	-1.85	14.89	-19.13	221.17
	^{ox}**bRuL3**	-37.08	-0.16	0.18	-1.30	-0.19	0.65	-0.92	0.58	0.33	-0.08	36.35
	^{ox}**bRuL2**	-281.19	133.18	8.83	-10.92	12.47	1.34	1.29	-0.71	-1.81	1.26	298.83
M06	^{ox}**aRuL3**	-46.27	-1.12	0.46	-1.45	0.85	0.07	0.17	0.07	-0.41	-0.52	45.82
	^{ox}**bRuL3**	50.97	-1.03	-0.07	-0.75	-1.66	0.045	0.83	-0.00	-0.19	0.03	50.93

For ^{ox}**bRuL2**, a high enhancement of the estimated hyperpolarizability is observed upon one-electron oxidation (up to 31-fold, depending on the used functional). This behaviour can be explained by the appearance of a low energy band occurring in the NIR region attributed to a LMCT, as discussed above. Comparison with the non-oxidized counterpart indicate that, for this complex, a red shift of the lowest-energy transition occurs for all functionals. In particular CAM-B3LYP provides a red shift by *ca.* 730 nm whereas for B3LYP and M06 a red shift of 588 and 540 nm are obtained. This red shift is accompanied by a lowering of the correspondent oscillator strength by approximately 50% in all cases. Hence, in the case of complex ^{ox}**bRuL2**, the increasing of the estimated hyperpolarizability upon oxidation is justied by red-shift of the relevant electronic transition. In fact, the CAM-B3LYP functional provides the higher enhancement of the hyperpolarizability that correlates with the lowest-energy of this transition.

In the case of complexes ^{ox}**aRuL3** and ^{ox}**bRuL3** opposite trends are observed when using dierent functionals: a diminishing of the hyperpolarizability upon one-electron oxidation of the complexes by ca a 2-fold factor is observed for B3LYP and M06 whereas an enhancement of the hyperpolarizability using CAM-B3LY3P by ca a 11-fold factor for complex ^{o}x**aRuL3** and by a 2.5-fold factor for complex ^{ox}**bRuL3** are observed.

The behaviour observed on the change of the hyperpolarizability upon one-electron oxidation using B3LYP (and M06) can be easily understood on the basis of the character of the electronic transitions involved and discussed previously. For ^{ox}**aRuL3** the decrease in β_{tot} value can be related to the emerging of a new transition assigned to LMCT, which charge transfer occurs in opposite direction of that of MLCT (also present in the oxidized and non-oxidized counterpart). The almost unchanged energy of the overall band upon oxidation further supports this observation. For ^{ox}**bRuL3** the decrease in β_{tot} value can be due to the vanishing of a MLCT band which was observed in the visible region for the non-oxidized counterpart. Besides, the presence of an ILCT, a band with similar character that is also present in the non-oxidized counterpart at almost same energy, further supports this observation.

Some remarks considering the behaviour found using CAM-B3LYP functional for the **L3** based complexes can be addressed. As stated above this functional gives an enhanced β_{tot} values upon oxidation in opposite trend of that is observed using B3LYP and M06 functionals. **Figure 3.33** shows the orbitals involved in the main electronic transition for ^{ox}**aRuL3** (similar orbital contours are observed for ^{ox}**bRuL3**). It can be observed that

this transition can be assigned to an ILCT with some contribution of the metal centre. With CAM-B3LYP, the LMCT, present in ^{ox}**aRuL3** complex using B3LYP (and M06) functionals and responsible for lowering the hyperpolarizability upon oxidation, is absent. Thus, an expected enhancing effect on β_{tot} is observed with CAM-B3LYP. For ^{ox}**bRuL3**, this functional gives almost the same character of the relevant CT than that obtained with B3LYP (and M06). In this case, a somewhat higher oscillator strength of this band can play a role on the observed enhancing effect on β_{tot} upon oxidation.

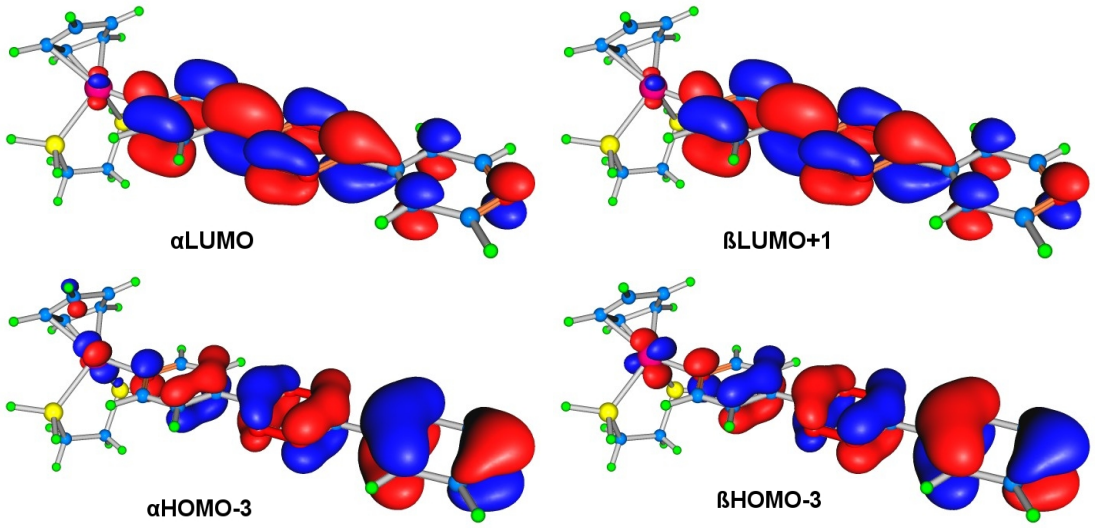

Figure 3.33: Contour plots of the HOMO and LUMO orbitals for ^{ox}**aRuL3** complex using CAM-B3LYP

Concerning the overall data for the three complexes, the results for complex ^{ox}**bRuL2** are noteworthy. According to DFT calculations, this complex seems to be the most promising candidate for NLO-switching by redox means. The fact that oxidation lead to improved hyperpolarizabilities should be further commented here. It is well-known that most of the metal-organic compounds studied for SONLO switching follows the well-known type I switching mechanism. According to this mechanism, in a typical push-pull D-π-A system, the donor becomes a competing acceptor moiety upon oxidation thus leading to lower hyperpolarizability. In the case of this complex, with a more likely less studied D-π-D feature, the oxidation lead to the achievement of a D-π-A structure, in which the organometallic moiety becomes an acceptor, and hence an expected increase on the corresponding quadratic hyperpolarizability. As for the case of the previously studied

benzo[c]thiophene complexes (**Chapter 2**), this complex present an unusual switching behaviour in which the on state corresponds to the oxidized form of the complex and the o form corresponds to its non-oxidized form. However a subtle difference can be envisaged between these two kinds of complexes. In the case of benzo[c]thiophene complexes, the oxidation lead to the achievement of a D-π-A structure in which the donor character of the organometallic moiety is enhanced. In case of the tetrazine based complex, the oxidation also lead to the achievement of a D-π-A structure but in which the acceptor character of the organometallic moiety is improved.

The different behaviour found on quadratic hyperpolarizability upon one-electron oxidation for **L3** based complexes, depending on the used functionals, shows that we must be careful in the characterization of the NLO-redox switching properties of these complexes. In that sense, only additional experimental work could help in the evaluation of the accurateness of the DFT calculations and to decide which functional works better in the studied complexes. In particular, the determination of the optical nonlinearities of the complexes in their non-oxidized and oxidized forms (of the isolated compounds or generated in situ during NLO measurements) accompanied with the study of their electrochemical reversibility towards oxidation are of major importance.

The DFT estimated enhancement/diminishing of the hyperpolarizabilities of the complexes in their non-oxidized and oxidized forms can only be interpreted as trends in the expected behaviour of the complexes.

3.4 Conclusions

This chapter deal with synthesis, spectroscopical studies and density functional theory calculations of tetrazine-based organic ligands and their correspondent organometallic compounds.

Synthesis of the tetrazine ligands **L1** and **L2** were performed by nucleophilic aromatic substitution on the initial 3,6-bis(3,5-dimethylpyra-zol-1-yl)-*s*-tetrazine in good yields. Ligand **L3** was synthesized by Pinner's reaction starting from 4-cianopyridyne also in good yields. The unprecedented ligands **L4** and **L5** were synthesized by Sonogashira cross-coupling reactions between 3,6-bis(4-bromophenyl)-*s*-tetrazine and 2-methyl-3-butyn-2-ol. The developed synthetic procedure allowed the obtention of either one of the ligands by controlling the experimental conditions.

Attempts of coordination of the synthesized ligands were performed in the presence of thalium trifluoromethanesulfonate. Other typical halogen abstractor salts have shown to be unsuccessful reagents for the synthesis of tetrazine-based organometallic complexes. Complexes of ligands **L2** (**bRuL2**) and **L3** (**aRu$_2$L3** and **bRu$_2$L3**) were obtained in moderate yields and were spectroscopically characterized. As far as this work is concerned, complex **bRuL2** is the first example of a zwitterionic complexes bearing a tetrazine ring. The spectroscopic data confirmed the zwitterionic structure of the complex due to the anionic nature of the ligand and the absence of the counter-anion. Dinuclear complexes **aRu$_2$L3** and **bRu$_2$L3** are also one of the few examples of non-polymeric linear complexes bearing tetrazine ligands.

Density functional theory calculations were used in order to give more insight on the electronic properties of both the ligands and complexes, and more importantly, to estimate their nonlinear optical properties and nonlinear optical redox switching abilities of the complexes. Results show that the compounds present moderate to low hyperpolarizabilities, which are functional dependent (β_{tot} = 0 - 35 $\times 10^{-30}$ esu for the ligands; β_{tot} = 15 - 108 $\times 10^{-30}$ esu for the complexes). The complexes presented higher estimated hyperpolarizability values in comparison with the free ligands. For complex **bRuL2**, minor changes on the hyperpolarizability upon coordination are expected whereas for **aRuL3** and **bRuL3** significant change on hyperpolarizabilities are predicted. The difference in the hyperpolarizabilities values of the latter complexes were justified based on the character of the electronic transitions involved in the photo-excitaion of the compounds. Density functional theory calculations allow to clearly state that tetrazine-based complexes present remarkable potential for nonlinear optical application, and in particular for nonlinear optical redox switching. In particular, complex **bRuL2** presents an enhancement of the first-order hyperpolarizability by 8- to 31-fold (depending on the functional) in comparison with its non-oxidized counterpart. The enhancement of the hyperpolarizability for this complex is attributed to a very low energy band attributed a ligand to metal charge transfer electronic transition, caused by the presence of the organometallic fragment. This complex present an unusual switching behaviour in which the "on" state corresponds to the oxidized form of the complex and the "off" form corresponds to its non-oxidized form. For complexes bearing ligand **L3**, a lowering of the estimated hyperpolarizability is observed for B3LYP and M06 fucntionals whereas CAM-B3LYP predicts an enhancement of the nonlinear optical properties, upon electron oxidation.

3.5 Experimental

Synthesis of the ligands were performed in standard conditions, unless otherwise stated. Commercial reagents were used as received and without further purification. 3,6-Bis(3,5-dimethylpyrazol-1-yl)-*s*-tetrazine and 3,6-di(pyridin-4-yl)-*s*-tetrazine were prepared following published procedures with some modifications, either in the oxidation step or in the purification method (see details below).[64] All synthesis involving organometallic complexes, including the Sonogashira coupling reactions, were carried out under nitrogen atmosphere using current Schlenk techniques. The details of the synthesis of the starting organometallic complexes and the characterization methods are described in **Chapter 5**.

3.5.1 Synthesis of ligands L1 and L2

3.5.1.1 Synthesis of triaminoguanidine monohydrochloride (1)

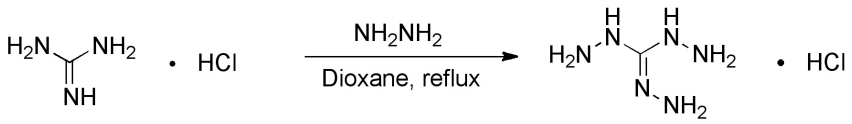

To a suspension of guanidine hydrochloride (26.1 g, 0.267 mol) in 150 mL of 1,4-dioxane was added a solution of hydrazine monohydrate at 80% (45 mL, 0.91 mol) with stirring. The mixture was heated to reflux for 2 hours. During that time a large amount of white solid precipitates. After cooling to room temperature, the solid were collected by filtration, washed with dioxane and dried to give pure triaminoguanidine monohydrochloride in quantitative yield. Due to the low solubility of the product only FTIR analysis was made.

FTIR: ν**(KBr)/cm^{-1}**: 3322 and 3214 (NH), 1682 (N=C), 1330, 1132, 960.

3.5.1.2 Synthesis of 3,6-bis(3,5-dimethylpyrazol-1-yl)-1,2-dihydro-*s*-tetrazine (2)

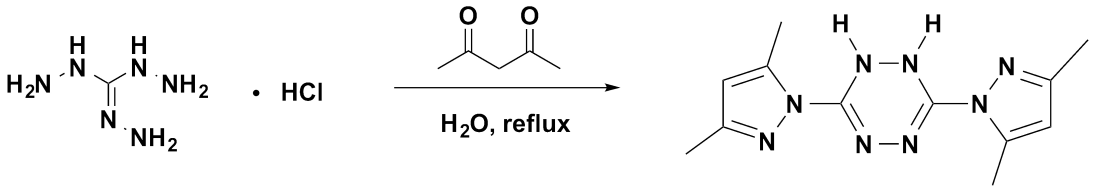

The entire amount of the triaminoguanidine monohydrochloride (**1**) (27 grs.; 0.19 mol) obtained in the previous step was dissolved in the minimum amount of water (≈ 150 mL). The reaction flask was kept in a cold water bath and 2,4-pentanedione (52.5 mL, 0.506 mol) was added dropwise. The temperature was maintained bellow 30°C during this stage. After the addition is completed, the reaction is allowed to stir for 30 minutes at room temperature and then was heated to reflux for 4 hours. During that time, the dark yellow 3,6-bis(3,5-dimethylpyrazol-1-yl)-1,2-dihydro-*s*-tetrazine precipitates. The solid was collected by filtration, washed with water and dried in vacuum. The desired product was obtained in 40 % yield.

^{1}H-NMR (400 MHz, $CDCl_3$, 25°C): 2.20 and 2.47 (s, 6H, CH_3), 5.95 (s, 2H, CH) and 8.10 (s, 2H, NH) ppm;

^{13}C-NMR (100 MHz, $CDCl_3$, 25°C): 13.40 (C7' and C7"), 13.74 (C6' and C6"), 109.77 (C4' and C4"), 142.19 (C3' and C3"), 145.69 (C5' and C5"), 149.85 (C3 and C6) ppm.

3.5.1.3 Synthesis of 3,6-bis(3,5-dimethylpyrazol-1-yl)-*s*-tetrazine (3)

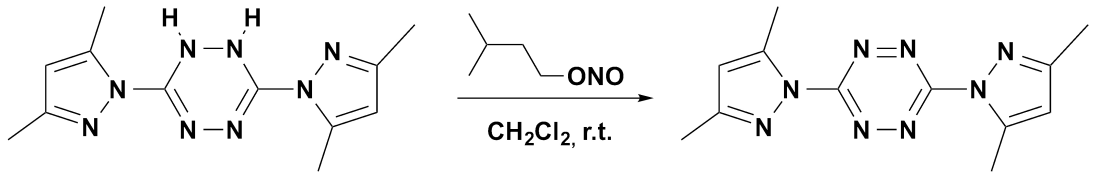

3,6-bis(3,5-dimethylpyrazol-1-yl)-1,2-dihydro-*s*-tetrazine (**2**) (7 g; 0.026 mol) were dissolved in the minimum amount of dichloromethane. An excess of isoamyl nitrite (7 mL; 0.042 mol) was then added dropwise. The solution was allowed to stir at room temperature for 4 hrs. to ensure full oxidation. The solution was then washed with water and dried under anhydrous magnesium sulphate. After evaporation of the solvent, bright red 3,6-bis(3,5-dimethylpyrazol-1-yl)-*s*-tetrazine was obtained in 56 % yield.

FTIR: ν(KBr)/cm^{-1}: 3085 (CH, aromatic), 2993 and 2933 (CH, aliphatic), 1579 (C=C), 1483 and 1425 (C=N), 1079 and 970 (N=N);

^{1}H-NMR (400 MHz, DMSO, 25°C): 2.28 (s, 3H, H7' and H7"), 2.60 (s, 3H, H6' and H6"), 6.37 (s, 1H, H4' and H4") ppm;

^{13}C-NMR (100 MHz,DMSO, 25°C): 13.85 (C7' and C7"), 14.05 (C6' and C6"), 111.37 (C4' and C4"), 143.49 (C5' and C5"), 152.97 (C3' and C3"), 159.16 (C3 and C6) ppm;

UV-Vis. ($CHCl_3$, λ_{max}/nm ($\epsilon\times10^4$/M^{-1}cm^{-1})): 300 (2.9); 376 (0.1); 537 (0.04);

3.5.1.4 Synthesis of 6-(3,5-dimethyl-1H-pyrazol-1-yl)-N-(pyridin-4-yl)-*s*-tetrazin-3-amine (L1)

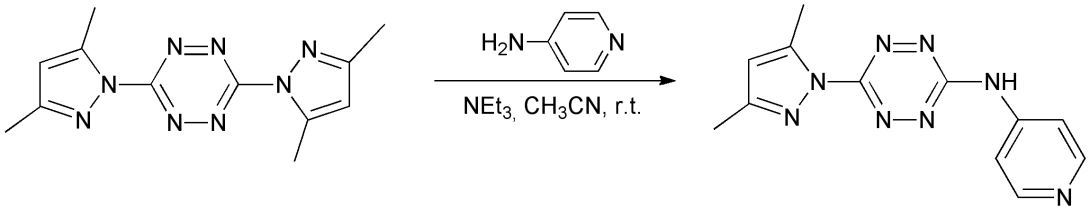

To 40 mL of dried acetonitrile was added 0.5 g (1,8 mmol) of 3,6-bis(3,5-dimethylpyrazol-1-yl)-*s*-tetrazine (**3**), followed by 0.435 g of 4-aminopyridine (3,7 mmol, 2 eq.) and 3 mL of triethylamine (22 mmol, 12 eqs). The mixture was heated in an oil bath at 40°C and allowed to stir overnight. The solvent was evaporated and the bright orange solid was chromatographed in a short column using neutral aluminium oxide as solid phase and a mixture of chloroform:ethanol (9:1) as eluent. The desired product was obtained in 72% yield.

FTIR (ν(KBr)/cm^{-1}): 3236 (NH), 3088 (CH, aromatic), 2964 and 2952 (CH, aliphatic), 1596 (C=C), 1479 and 1423 (C=N), 1075 and 1043 (N=N);

^{1}H-NMR (400 MHz, DMSO, 25°C): 2.25 (s, 3H, H6'), 2.50 (s, 3H, H7'), 6.27 (s, 1H, H4'), 7.75 (d, $^{3}J_{H,H}$=5.92 Hz, 2H, H3" and H6"), 8.50 (d, $^{3}J_{H,H}$=5.92 Hz, 2H, H4" and H5") and 11.45 (s, 1H, H1") ppm;

^{13}C-NMR (100 MHz, DMSO, 25°C): 12.92 (C7'), 13.44 (C6'), 109.59 (C4'), 113.17 (C4" and C5"), 142.04 (C5'), 145.35 (C2"), 150.49 (C3" and C6"), 151.09 (C3'), 157.21 (C6), 160.58 (C3) ppm;

UV-Vis. ($CHCl_3$, λ_{max}/nm ($\epsilon\times10^4$/ M^{-1}cm^{-1})): 300 (2.9), 414 (0.09), 530 (0.005);

3.5.1.5 Synthesis of 2-(6-(3,5-dimethyl-1H-pyrazol-1-yl)-*s*-tetrazin-3-yl)malononitrile (L2)

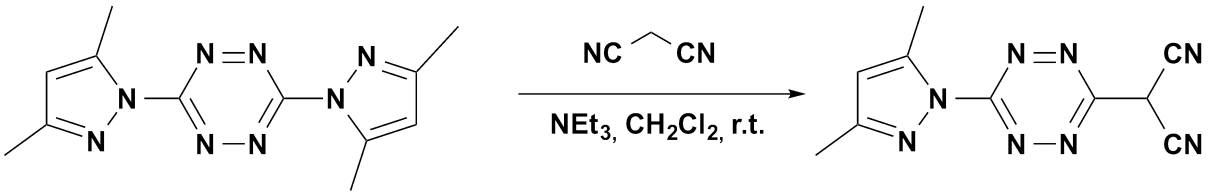

Malononitrile (79 mg, 1.2 mmol) and triethylamine (0.101 g; 1.0 mmol) were added to a suspension of 3,6-bis(3,5-dimethylpyrazol-1-yl)-*s*-tetrazine (**3**) (1.0 mmol) in dry toluene (15 ml) and stirred for 2 hrs. at room temperature. The solvent was evaporated and the resulting purple solid was washed by by adding 50 mL of a 10% hydrochloric acid aqueous solution. The dark-violet precipitate was filtered, washed with water and dry in vacuum, affording the desired product in 85% yield.

FTIR ν(KBr)/cm^{-1}: 2207 and 2176 (N≡C);

^{1}H-NMR (400 MHz, DMSO, 25°C): 2.21 (s, 3H, H6'), 2.37 (s, 3H, H7'), 6.15 (s, 1H, H4') ppm;

^{13}C-NMR (100 MHz, DMSO, 25°C): 12.21 (C7'), 13.36 (C6'), 108.27 (C4'),

119.91 (C2" and C3"), 139.45 (C1"), 141.19 (C5'), 149.75 (C3"), 156.40 (C5'), 156.39 (C6), 169.93 (C3) ppm;

UV-Vis. ($CHCl_3$, λ_{max}/nm ($\epsilon \times 10^4$/$M^{-1}cm^{-1}$)): 349 (2.4), 516 (2.4), 638 (2.4);

3.5.2 Synthesis of ligand L3

3.5.2.1 Synthesis of 3,6-di(pyridin-4-yl)-*s*-tetrazine

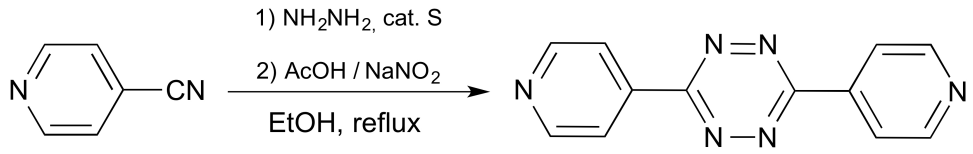

4-Cyanopyridine (2 g; 19.20 mmol) were dissolved in the minimum amount of absolute ethanol (15 mL). Powdered sulphur (0.45 g; 14.00 mmol) was then suspended in the previous solution and 7 mL of a 80% solution of hydrazine in water were added carefully. After stirring at room temperature for 1 hr., the dark-brown solution was refluxed overnight. The pale yellow precipitated was collected by vacuum filtration and washed with cold ethanol. After drying, the solid was dissolved in 100 mL of dichloromethane and 20 mL of glacial acetic acid were added. Sodium nitrite (0.25 g; 3.6 mmol) was then added portionwise over the period of 2 hrs. After stirring overnight, vacuum filtration afforded a purple solid that was purified by column chromatography (silica gel; eluent: dichloromethane). The desired product was obtained in 56% yield.

FTIR ν(KBr)/cm^{-1}: 3034 (CH, aromatic), 1590 and 1562 (C=C), 1411 and 1388 (N=C), 1112 and 1056 (N=N);

^{1}H-NMR (400 MHz, DMSO, 25°C): 8.46 (d, $^3J_{H,H}$= 5.3 Hz, 4H, H2', H2", H6' and H6"), 8.96 (d, $^3J_{H,H}$= 8.8 Hz, 4H, H3', H2", H5' and H5") ppm;

^{13}C-NMR (100 MHz, DMSO, 25°C): 121.69 (C2', C2", C6' and C6"), 139.45 (C1' and C1"), 151.58 (C3', C3", C5' and C5"),163.45 (C3 and C6) ppm;

UV-Vis. ($CHCl_3$, λ_{max}/nm ($\epsilon \times 10^4$/ $M^{-1}cm^{-1}$)): 274 (3.7), 544 (0.07);

3.5.3 Synthesis of ligands L4 and L5

3.5.3.1 Synthesis of 3,6-bis(4-bromophenyl)-*s*-tetrazine (4)

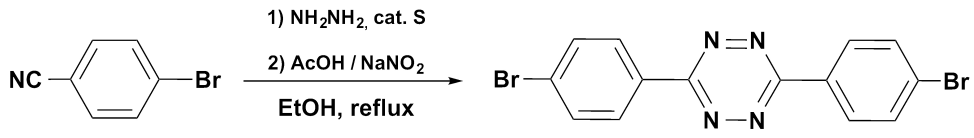

4-bromobenzonitrile (3 g; 16.47 mmol) was dissolved in the minimum amount of absolute ethanol (50 mL). Powdered sulphur (0.45 g; 14.00 mmol) was then suspended in the previous solution and 7 mL of a 80% solution of hydrazine in water were added carefully. After stirring at room temperature for 2 hrs., the dark-brown solution was refluxed overnight. The yellow precipitated was collected by vacuum filtration and washed with cold ethanol. After drying for a few minutes, the solid was placed into a second flask and 100 mL of dichloromethane were added together with 20 mL of glacial acetic acid. Sodium nitrite (0.25 grs.; 3.6 mmol) was then added portionwise over the period of 2hrs. After stirring overnight, vacuum filtration afforded a purple solid, insoluble in all tested solvents. Yield: 67%

FTIR ν(KBr)/cm^{-1}: 3089 (CH, aromatic), 1588 (C=C), 1406 (N=C), 1106, 1070, 1008 (N=N);

3.5.3.2 General Procedure for the Sonogashira Coupling Reaction

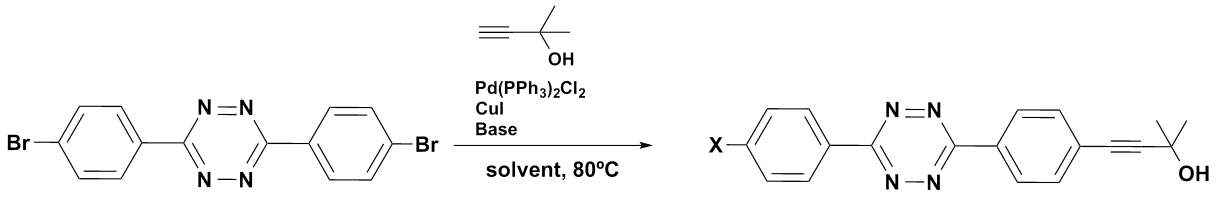

Conditions:
(7) (X = Methylbut-3-yn-2-ol): Solvent = DMF, Base = ^{i}prop-amine
(8) (X = Br): Solvent = THF, Base = ^{i}prop-amine

A degassed two-necked, round-bottomed flask was charge with 1 mmol of 3,6-bis(4-bromophenyl)-*s*-tetrazine (**4**) followed by Bis(triphenylphosphine)palladium(II) dichloride (20 mmol%). The solvent (20mL) and the base (3 mL) were then added and the mixture was allowed to stir at room temperature for 30 minutes. Copper (I) iodide (20 mmol%) was then added and the mixture was allowed to stir at the adequate temperature overnight. After this period, the reaction mixture was filtered, the organic phases were diluted in 50 mL of dichloromethane and washed with water. The organic phase was dried with anhydrous magnesium sulphate and evaporated. The purple solid was the chromatographed (silica gel: dichloromethane) affording the desired products.

- **Characterization data for (7)**

  FTIR ν(KBr)/cm^{-1}: 3478 (OH), 2983 (CH, aliphatic), 1603 (C=C), 1399 (N=C), 1153 and 1103 (N=N);

  ^{1}H-NMR (400 MHz, DMSO, 25°C): 1.51 (s, 12H, CH_3), 5.61 (s, 2H, OH), 7.70 (d, $^{3}J_{H,H}$=8.30 Hz, 4H, H3', H3", H5' and H5"), 8.55 (d, $^{3}J_{H,H}$= 8.29 Hz, 4H, H2', H2", H6' and H6") ppm;

  ^{13}C-NMR (100 MHz, DMSO, 25°C): 31.48 (C10', C11' and C10", C11"), 63.74 (C9' and C9"), 79.96 (C7' and C7"), 99.47 (C8' and C8"),126.80 (C1' and C1"), 127.75 (C2', C6' and C2", C6"), 131.32 (C4' and C4"), 132.29 (C3', C5' and C3", C5"), 163.00 (C3 and C6) ppm;

- **Characterization data for (8)**

  FTIR ν(KBr)/cm^{-1}: 3285 (OH), 3094 (CH, aromatic), 2993 (CH, aliphatic), 1603 and 1589 (C=C), 1399 (N=C), 1106 and 1069 (N=N);

  ^{1}H-NMR (400 MHz, DMSO,25°C): 1.51 (s, 6H, CH_3), 5.60 (s, 1H, OH), 7.69 (d, $^{3}J_{H,H}$=8.38 Hz, 2H, H3" and H5"), 7.91 (d, $^{3}J_{H,H}$= 8.57 Hz, 2H, H3' and H5'), 8.46 (d,$^{3}J_{H,H}$= 8.57 Hz, 2H, H2' and H6'), 8.52 (d, $^{3}J_{H,H}$ = 8.38 Hz, 2H, H2" and H6") ppm;

  ^{13}C-NMR (100 MHz, DMSO, 25°C): 31.48 (C10" and C11"), 63.75 (C9"), 79.95 (C7"), 99.51 (C8"), 126.75 (C4"), 126.83 (C4'), 127.76 (C2" and C6"), 129.51 (C2' and C6'), 131.12 (C1'), 131.29 (C1"), 132.30 (C3" and C6"), 132.66 (C3' and C6'), 162.72 (C6), 162.94 (C3) ppm;

3.5.3.3 General Procedure for the Deprotection of Acetylide Tetrazines

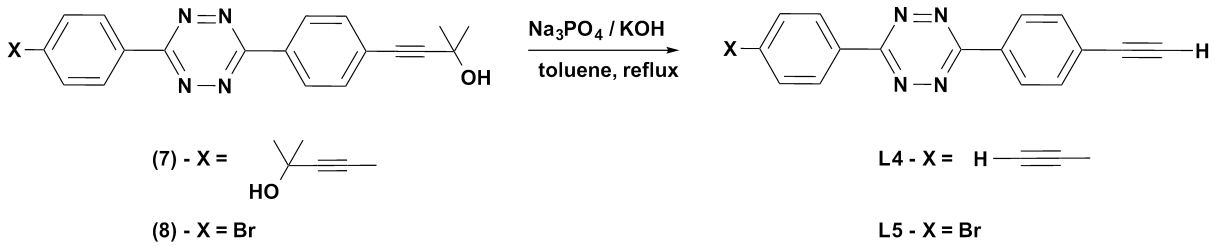

In a typical procedure, a 50 mL flask containing 20 mL of dry toluene was charged with the protected acetylene (1 mmol), sodium phosphate (1 eq. per protective group) and sodium hydroxide (1 eq. per protective group). The mixture was placed in a pre-heated oil bath at 120 °C and allowed to reflux (see times bellow). After cooling at room temperature, 20 mL of DCM was added and the mixture was filtered to remove the yellowish inorganic solids. The organic phase was dried with anhydrous magnesium sulphate and evaporated. The purple solid was the chromatographed (silica gel: dichloromethane) affording the desired product.

- **Characterization data for L4**

  Conditions / Yield: reflux overnight, 43%;

  FTIR ν(KBr)/cm^{-1}: 3286 (CC-H);

  ^{1}H-NMR (400 MHz, DMSO, 25°C): 1.51 (s, 6H, CH_3), 4.52 (s, 1H, H8' and H8"), 7.80 (d, $^{3}J_{H,H}$= 7.73 Hz, 4H, H3, H3", H5' and H5"), 8.55 (d, $^{3}J_{H,H}$= 7.73 Hz, 4H, H2, H2", H6' and H6") ppm;

  ^{13}C-NMR (100 MHz, DMSO, 25°C): 55.31 (C8' and C8"), 126.27 (C1' and C2"), 128.17 (C2' and C2"), 132.19 (C3', C3", C5' and C5"), 132.41 (C2', C2", C6' and C6") ppm;

  UV-Vis. ($CHCl_3$, λ_{max}/nm ($\epsilon\times10^4$/ M^{-1}cm^{-1})): 319 (2.5); 549 (0.05)

- **Characterization data for L5**

  Conditions / Yield: reflux 6 hrs., 76%;

  FTIR ν(KBr)/cm^{-1}: 3270 (CC-H);

  ^{1}H-NMR (400 MHz, ($CDCl_3$),25°C): 4.54 (s, 2H, H8'), 7.80 (d, $^{3}J_{H,H}$= 8.00 Hz, H3" and H5"), 7.92 (d, $^{3}J_{H,H}$= 8.0 Hz, H3' and H5'), 8.47 (d, $^{3}J_{H,H}$= 8.0 Hz, H2' and H6'), 8.55 (d, $^{3}J_{H,H}$= 8.00 Hz, H2" and H6") ppm;

  UV-Vis. ($CHCl_3$, λ_{max}/nm ($\epsilon\times10^4$/ M^{-1}cm^{-1})): 328 (3.7); 551 (0.04)

3.5.4 Synthesis of [CpM(PP)(L)]OTf complexes (L=tetrazine ligand)

3.5.4.1 Attempt of the synthesis of complexes of general formula [M(η^5-C_5H_5)(PP)(L1)]OTf

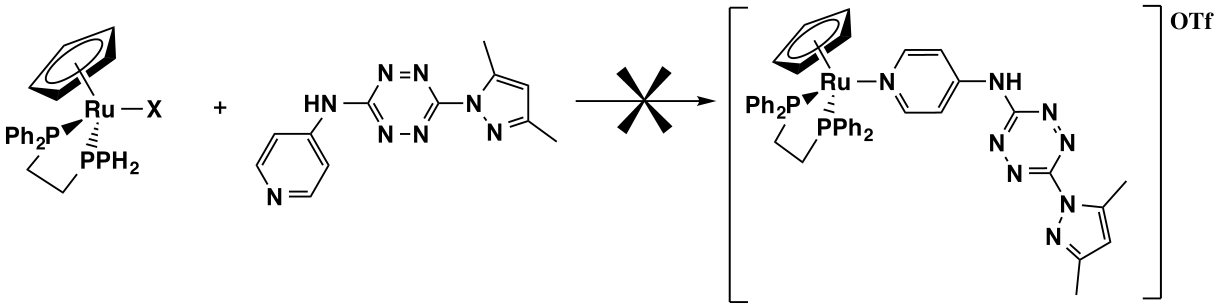

A mixture of the adequate [M(η^5-C_5H_5)(PP)X] complex (0.5 mmol), TlOTf (1.5 eq.) and ligand **L1** (1.1 eq.) were placed in a degassed Schlenk. Freshly dried dichloromethane (25 mL) was added and the resulting solution was allowed to stir at room temperature overnight. An aliquot was extracted and analysed by NMR showing that no reaction occurred. The solution was then heated to reflux and was left with stirring for another 16hrs. A second aliquot was extracted and analysed by NMR showing the presence of only decomposition products.

In a second attempt, a mixture of [M(η^5-C_5H_5)(PP)X] (0.5 mmol), TlOTf (1.5 eq.) and ligand **L1** (1.1 eq.) were placed in a degassed Schlenk. Freshly dried dichloromethane (15 mL) and THF (15 mL) was added and the resulting solution was allowed to stir at 50 °C overnight. An aliquot was extracted and analysed by NMR showing that no reaction occurred. No further attempts were made.

3.5.4.2 Synthesis of complexes of general formula [M(η^5-C_5H_5)(PP)(L2)]

A mixture of the adequate [Ru(η^5-C_5H_5)(κ^2-dppe)Cl] (0.5 mmol), TlOTf (1.5 eq.) and ligand **L2** (1.1 eq.) were placed in a degassed Schlenk. Freshly dried dichloromethane (25 mL) was added and the resulting solution was allowed to stir at room temperature

overnight. An aliquot was extracted and analysed by NMR showingthe presence of only decomposition products.

In a similar fashion, a mixture of [M(η^5-C_5H_5)(PPh_3)Cl] (0.5 mmol), TlOTf (1.5 eq.) and ligand **L2** (1.1 eq.) were placed in a degassed Schlenk. Freshly dried dichloromethane (25 mL) was added and the resulting solution was allowed to stir at room temperature overnight. The solvent was then removed under reduced pressure and the resulting dark purple solid was recrystalized by slow diffusion of a dichloromethane/hexane mixture afforded complex **bRuL2** as a purple solid.

Dark red. 361 mg, 62 % yield. ν(KBr)/cm^{-1}: 2209 and 2173 (N≡C).

^{1}H NMR (400 MHz, DMSO, 25C): 2.24 (s, 3H, H6'), 2.43 (s, 3H, H7'), 4.46 (s, 5H, η^5-C_5H_5), 6.21 (s, 3H, H4'), 7.14 (t, $^3J_{H,H}$= 4.6 Hz, 12H, H_{ortho}-Ph), 7.27 (t, $^3J_{H,H}$= 7.3 Hz, 12H, H_{meta}-Ph), 7.37 (t, $^3J_{H,H}$= 7.1 Hz, 6H, H_{para}-Ph) ppm.

^{13}C NMR (100 MHz, $(CD_3)_2CO$, 25C): 12.85 (C6'), 13.79 (C7'), 83.54 (η^5-C_5H_5),103.92 (C2"), 109.16 (C4'), 115.38 (C3"), 128.56 (t, $^3J_{C,P}$ = 9.1 Hz, C_{meta}-Ph), 130.06 (s, C_{para}-Ph), 133.34 (t, $^2J_{C,P}$= 10.3 Hz, C_{ortho}-Ph), 136.43 (t, $^1J_{C,P}$= 19.2 Hz, C_{ipso}-Ph), 141.79 (C5'), 150.61 (C3'), 170.37 (C3 and C6) ppm.

UV-Vis. ($CHCl_3$): λ_{max}/nm ($\epsilon\times10^4$/ $M^{-1}cm^{-1}$): 357 (2.2), 531 (0.05) .

3.5.4.3 Synthesis of complexes of general formula [M(η^5-C_5H_5)(PP)(L3)]OTf

A mixture of the adequate [M(η^5-C_5H_5)(PP)X] (0.5 mmol), TlOTf (1.5 eq.) and ligand **L3** (1.1 eq.) were placed in a degassed Schlenk. Freshly dried dichloromethane (25 mL) was added and the resulting solution was allowed to stir at room temperature overnight. An aliquot was extracted and analysed by NMR showing that the formation a mixture of mono- and dinuclear complexes. The solvent was evaporated dark red solid was recrystalized by slow diffusion of a dichloromethane/hexane mixture affording **aRu_2L3** and **bRu_2L3**.

Attempt ofsynthesizing the mononuclear complexes was performed by mixing the adequate (η^5-C_5H_5)Ru(PP)X (0.5 mmol) and TlOTf (1.5 eq.) in toluene (25 mL). Ligand **L3** was added portionwise every two hours and the reaction was allowed to stir at room temperature overnight. The solvent was evaporated dark red solid was recrystalized by slow diffusion of a dichloromethane/hexane mixture affording only the dinuclear **aRu_2L3** and **bRu_2L3**. No mononuclear complexes were isolated.

- **Characterization data for aRu_2L3**

Dark red, 42 % yield. ν(KBr)/cm^{-1}: 1283 (OT^-).

^{1}H NMR (400 MHz, DMSO, 25C): 3.04 and 3.14 (m, 4H, CH_2), 4.74 (s, 5H, η^5-C_5H_5), 7.23 (t, $^3J_{H,H}$=8.0 Hz, 4H, H_{orto}-Ph), 7.34 (t, $^3J_{H,H}$=8.0 Hz, 8H, H_{meta}-Ph), 7.37 (d, $^3J_{H,H}$=4.1 Hz, 4H, H3', H5', H3" and H5"), 7.47 (t, $^3J_{H,H}$=8.0 Hz, 4H, H_{orto}-Ph), 7.63 (t, $^3J_{H,H}$=8.0 Hz, 4H, H_{para}-Ph), 7.95 (d, $^3J_{H,H}$=6.5 Hz, 4H, H2', H6', H2" and H6") ppm.

^{13}C NMR (100 MHz, DMSO, 25C): 84.17 (η^5-C_5H_5), 121.31 (C3', C5', C3" and C5"), 128.96 (t, $^2J_{C,P}$= 9.2 Hz, C_{meta}-Ph), 129.21 (t, $^2J_{C,P}$= 10.0 Hz, C_{orto}-Ph), 130.18 (t, $^2J_{C,P}$= 9.2 Hz, C_{meta}-Ph), 130.70 (t, $^2J_{C,P}$= 11.0 Hz, C_{ortho}-Ph), 133.27 (C_{para}-Ph), 137.27 (C1' amd C1"), 159.43 (C2', C6', C2" and C6"), 162.10 (C3 and C6) ppm.

UV-Vis. ($CHCl_3$): λ_{max}/nm ($\epsilon\times10^4$/ $M^{-1}cm^{-1}$): 393 (1.2), 507 (1.3), .

- **Characterization data for bRu_2L3**

  Dark brown, 34 % yield. ν(KBr)/cm^{-1}: 1270 (OTf^-).

  ^{1}H NMR (400 MHz, DMSO, 25C): 4.93 (s, 5H, η^5-C_5H_5), 7.09 (t, $^3J_{H,H}$=5.0 Hz, 12H, H_{orto}-Ph), 7.34 (t, $^3J_{H,H}$=7.1 Hz, 12H, H_{meta}-Ph), 7.47 (t, $^3J_{H,H}$=8.5 Hz, 6H, H_{para}-Ph), 8.46 (d, $^3J_{H,H}$=4.1 Hz, 4H, H2', H6', H2" and H6"), 8.96 (d, $^3J_{H,H}$=4.1 Hz, 4H, H3', H5', H3" and H5") ppm

  ^{13}C NMR (100 MHz, DMSO, 25C): 86.52 (η^5-C_5H_5), 121.71 (C3', C5', C3" and C5"), 128.96 (t, $^2J_{C,P}$= 9.8 Hz, C_{meta}-Ph), 128.73 (t, $^2J_{C,P}$= 10.0 Hz, C_{para}-Ph), 133.81 (s, C_{orto}-Ph), 136.43 (t, $^1J_{C,P}$= 22.0 Hz, C_{ipso}-Ph), 139.47 (C1' and C1"), 151.60 (C2', C6', C2", C6"), 163.47 (C3 and C6) ppm.

  UV-Vis. ($CHCl_3$): λ_{max}/nm ($\epsilon\times10^4$/ $M^{-1}cm^{-1}$): 371 (0.9), 481 (0.8).

3.5.4.4 Attempt of the synthesis of complexes of general formula [M(η^5-C_5H_5)(PP)(L4)]OTf

A mixture of Ru(η^5-C_5H_5)(κ^2-DPPE)Cl (0.5 mmol), NH_4PF_6 (1.5 eq.) and ligand **L4** (1.1 eq.) were placed in a degassed Schlenk. Freshly dried THF (25 mL) was added and the resulting solution was allowed to stir at room temperature overnight. An aliquot was extracted and analysed by NMR showing that no reaction occurred.

An first attempt to deprotonate the ligand was made by dissolving the **L4** (0,1 mmol) with 2.5 eqs. of potassium tert-butoxide in 20 mL of THF. After stirring overnight, an NMR sample revealed the presence of only the starting materials. In a second attempt, ligand **L4** (0,1 mmol) was dissolved in 25 mL of dried THF and was placed at -50 °C. *n*-Butyllithium was added (3 eqs.) and the solution was to stir for 30 minutes at -50 °C and allowed to warm to room temperature. Additional stirring for 1hr. afforded a yellowish solution. The solvent was removed under reduced pressure. The resulting yellow solid, was transfered carefully to a second Schlenk containing 0.5 eqs of Ru(η^5-C_5H_5)(κ^2-DPPE)Cl and TlOTf (0.6 eq.) in 20 mL of dried THF. The reaction was then allowed to stir at room temperature overnight. The solvent was again removed under reduced pressure and the solid was analysed by NMR. Results showed only decomposition products.

3.5.4.5 Attempt of the synthesis of complexes of general formula [M(η^5-C_5H_5)(PP)(L5)]OTf

A mixture of Ru(η^5-C_5H_5)(κ^2-DPPE)Cl (0.5 mmol), NH_4PF_6 (1.5 eq.) and ligand **L5** (1.1 eq.) were placed in a degassed Schlenk. Freshly dried THF (25 mL) was added and the resulting solution was allowed to stir at room temperature overnight. An aliquot was extracted and analysed by NMR showing that no reaction occurred. The solution was then heated to reflux and was left with stirring for another 16hrs. A second aliquot was extracted and analysed by NMR showing.

In a single attempt to deprotonate the ligand, **L5** (0,1 mmol) was dissolved in 20 mL of dried THF and with 1.2 eqs. of potassium tert-butoxide were added. After stirring overnight, an NMR sample revealed the presence of only the starting materials.

References

[1] Jochen Kerth and Stefan Löbbecke. Synthesis and characterization of 3,3-azobis(6-amino-1,2,4,5-tetrazine) daat – a new promising nitrogen-rich compound. *Propellants, Explosives, Pyrotechnics*, 27(3):111–118, 2002.

[2] Nurullah Saracoglu. Recent advances and applications in 1,2,4,5-tetrazine chemistry. *Tetrahedron*, 63(20):4199 – 4236, 2007.

[3] Thomas M. Klapotke, Davin G. Piercey, Jörg Stierstorfer, and Michael Weyrauther. The synthesis and energetic properties of 5,7-dinitrobenzo-1,2,3,4-tetrazine-1,3-dioxide (dnbtdo). *Propellants, Explosives, Pyrotechnics*, 37(5):527–535, 2012.

[4] Thermal behavior and combustion mechanism of high-nitrogen energetic materials dht and btatz. *Thermochimica Acta*, 535(0):48 – 57, 2012.

[5] Xiao-Hong Li, Rui-Zhou Zhang, and Xian-Zhou Zhang. Theoretical studies on vibrational spectra, thermodynamic properties, and detonation properties for 1,2,4,5-tetrazine derivatives. *Canadian Journal of Chemistry*, 91(8):662–670, 2013.

[6] Jadwiga Sołoducho, Jacek Doskocz, Joanna Cabaj, and Szczepan Roszak. Practical synthesis of bis-substituted tetrazines with two pendant 2-pyrrolyl or 2-thienyl groups, precursors of new conjugated polymers. *Tetrahedron*, 59(26):4761 – 4766, 2003.

[7] Gilles Clavier and Pierre Audebert. *s*-Tetrazines as building blocks for new functional molecules and molecular materials. *Chemical Reviews*, 110(6):3299–3314, 2010.

[8] Cassandre Quinton, Valérie Alain-Rizzo, Cécile Dumas-Verdes, Gilles Clavier, Fabien Miomandre, and Pierre Audebert. Design of new tetrazine–triphenylamine bichromophores – fluorescent switching by chemical oxidation. *European Journal of Organic Chemistry*, 2012(7):1394–1403, 2012.

[9] Da-Shuai Zhang, Ze Chang, Ying-Bin Lv, Tong-Liang Hu, and Xian-He Bu. Construction and adsorption properties of microporous tetrazine-based organic frameworks. *RSC Advances*, 2:408–410, 2012.

[10] Yujin Chen, Chao Li, Pan Zhang, Yaowen Li, Xiaoming Yang, Liwei Chen, and Yingfeng Tu. Solution-processable tetrazine and oligothiophene based linear A–D–A small molecules: Synthesis, hierarchical structure and photovoltaic properties. *Organic Electronics*, 14(5):1424 – 1434, 2013.

[11] Guo-Wu Rao and Wei-Xiao Hu. Synthesis, structure analysis, and antitumor activity of 3,6-disubstituted-1,4-dihydro-1,2,4,5-tetrazine derivatives. *Bioorganic and Medicinal Chemistry Letters*, 16(14):3702 – 3705, 2006.

[12] Neal K. Devaraj and Ralph Weissleder. Biomedical applications of tetrazine cycloadditions. *Accounts of Chemical Research*, 44(9):816–827, 2011.

[13] Shaun Stairs, André A. Neves, Henning Stöckmann, Yelena A. Wainman, Heather Ireland-Zecchini, Kevin M. Brindle, and Finian J. Leeper. Metabolic glycan imaging by isonitrile–tetrazine click chemistry. *ChemBioChem*, 14(9):1063–1067, 2013.

[14] André A. Neves, Henning Stöckmann, Yelena A. Wainman, Joe C-H. Kuo, Sarah Fawcett, Finian J. Leeper, and Kevin M. Brindle. Imaging cell surface glycosylation in vivo using "double click" chemistry. *Bioconjugate Chemistry*, 24(6):934–941, 2013.

[15] Alan R. Katritzky, Christopher A. Ramsden, Eric F.V. Scriven, and Richard Taylor, editors. *Comprehensive Heterocyclic Chemistry*, volume 3. Elsevier Science Ltd., 2008.

[16] Robert J. Forster and Tia E. Keyes. Tetrazine bridged osmium dimers: electrochemical vs photoinduced electron transfer. *The Journal of Physical Chemistry B*, 105(37):8829–8837, 2001.

[17] H. Neunhoeffer. 2.21 - tetrazines and pentazines. In : Editors in Chief: Alan R. Katritzky and Charles W. Rees, editors, *Comprehensive Heterocyclic Chemistry*, pages 531 – 572. Pergamon, Oxford, 1984.

[18] A. Pinner. Ueber die einwirkung von hydrazin auf imidoäther. *Berichte der deutschen chemischen Gesellschaft*, 26(2):2126–2135, 1893.

[19] Richard Wiley, C. Jarboe, Jr., and F. Hayes. Heterocyclic analogs of terphenyl: 3,6-diaryl-1,2,4,5-tetrazines. *The Journal of Organic Chemistry*, 22(7):835–836, 1957.

[20] Jun Yang, Mark R. Karver, Weilong Li, Swagat Sahu, and Neal K. Devaraj. Metal-catalyzed one-pot synthesis of tetrazines directly from aliphatic nitriles and hydrazine. *Angewandte Chemie International Edition*, 51(21):5222–5225, 2012.

[21] Jun Yang, Mark R. Karver, Weilong Li, Swagat Sahu, and Neal K. Devaraj. Metal-catalyzed one-pot synthesis of tetrazines directly from aliphatic nitriles and hydrazine. *Angewandte Chemie International Edition*, 51(21):5222–5225, 2012.

[22] L.V. Myznikov, K.A. Esikov, T.V. Artamonova, and G.I. Koldobskii. Tetrazoles XLV: Amidoalkylation of 5-substituted tetrazoles. *Russian Journal of Organic Chemistry*, 39(5):731–734, 2003.

[23] Farid Fouad, Brett Ellman, Scott Bunge, Patrik Miller, and Robert Twieg. Liquid crystalline symmetrical 3,6-diaryl-1,2,4,5-tetrazines. *Molecular Crystals and Liquid Crystals*, 582(1):34–42, 2013.

[24] W. Zieliński and W. Czardybon. The synthesis of 3,6-diaryl-dihydrotetrazines and tetrazines. *Polish Journal of Applied Chemistry*, Vol. 44, nr 1:37–40, 2000.

[25] Thorsten Lifka and H. Meier. 3,6-bis(2-arylethenyl)-1,2,4,5-tetrazine – synthese, flüssigkristallinität und photochemie. *Journal für Praktische Chemie/Chemiker-Zeitung*, 337(1):641–646, 1995.

[26] Haixuan Liu and Yunyang Wei. Novel synthesis of 3,6-disubstituted-1,2,4,5-tetrazine derivatives from hydrazones by using [hydroxyl(tosyloxy)iodo]benzene. *Tetrahedron Letters*, 54(35):4645 – 4648, 2013.

[27] Qing Zhou, Pierre Audebert, Gilles Clavier, Fabien Miomandre, and Jie Tang. New unsymmetrical alkyl-s-tetrazines: original syntheses, fluorescence and electrochemical behaviour. *RSC Advances*, 4:7193–7195, 2014.

[28] Pierre Audebert, Fabien Miomandre, Gilles Clavier, Marie-Claude Vernières, Sophie Badré, and Rachel Méallet-Renault. Synthesis and properties of new tetrazines substituted by heteroatoms: Towards the world's smallest organic fluorophores. *Chemistry – A European Journal*, 11(19):5667–5673, 2005.

[29] Subas M. Sakya, Kelley K. Groskopf, and Dale L. Boger. Preparation and inverse electron demand diels-alder reactions of 3-methoxy-6-methylthio-1,2,4,5-tetrazine. *Tetrahedron Letters*, 38(22):3805 – 3808, 1997.

[30] Marty C. Wilkes. "Azaphilic addition" of methyl lithium to 3,6-bisalkylthio-1,2,4,5-tetrazines: A remarkable dichotomy. *Journal of Heterocyclic Chemistry*, 28(4):1163–1164, 1991.

[31] János Faragó, Zoltán Novák, Gitta Schlosser, Antal Csámpai, and András Kotschy. The azaphilic addition of organometallic reagents on tetrazines: scope and limitations. *Tetrahedron*, 60(9):1991 – 1996, 2004.

[32] Scott C. Benson, Lily Lee, Lydie Yang, and John K. Snyder. Intramolecular inverse electron demand diels–alder reactions of tryptamine with tethered heteroaromatic azadienes. *Tetrahedron*, 56(9):1165 – 1180, 2000.

[33] Alberto Mangia, Fulvio Bortesi, and Umberto Amendola. 3-monosubstituted and 3,6-unsymmetrically disubstituted 1,2,4,5-tetrazines. a general method of synthesis. *Journal of Heterocyclic Chemistry*, 14(4):587–593, 1977.

[34] Beatrix Bostai, Zoltán Novák, Attila C. Bényei, and András Kotschy. Quinoidal tetrazines: formation of a fascinating compound class. *Organic Letters*, 9(17):3437–3439, 2007.

[35] Zoltán Novák and András Kotschy. First cross-coupling reactions on tetrazines. *Organic Letters*, 5(19):3495–3497, 2003.

[36] Flavia Pop, Jie Ding, Latevi Max Lawson Daku, Andreas Hauser, and Narcis Avarvari. Tetrathiafulvalene-s-tetrazine: versatile platform for donor-acceptor systems and multifunctional ligands. *RSC Advances*, 3:3218–3221, 2013.

[37] David E. Chavez and Michael A. Hiskey. 1,2,4,5-tetrazine based energetic materials. *Journal of Energetic Materials*, 17(4):357–377, 1999.

[38] DavidE. Chavez, MichaelA. Hiskey, and DarrenL. Naud. Tetrazine explosives. *Propellants, Explosives, Pyrotechnics*, 29(4):209–215, 2004.

[39] Shunichi Fukuzumi, Junpei Yuasa, and Tomoyoshi Suenobu. Scandium ion-promoted reduction of heterocyclic NN double bond. Hydride transfer vs electron transfer. *Journal of the American Chemical Society*, 124(42):12566–12573, 2002.

[40] My Hang V. Huynh, Michael A. Hiskey, David E. Chavez, Darren L. Naud, and Richard D. Gilardi. Synthesis, characterization, and energetic properties of diazido heteroaromatic high-nitrogen CN compound. *Journal of the American Chemical Society*, 127(36):12537–12543, 2005.

[41] M.B. Talawar, R. Sivabalan, N. Senthilkumar, Gurumallesh Prabhu, and S.N. Asthana. Synthesis, characterization and thermal studies on furazan- and tetrazine-based high energy materials. *Journal of Hazardous Materials*, 113(1–3):11 – 25, 2004.

[42] Wolfgang Kaim. The coordination chemistry of 1,2,4,5-tetrazines. *Coordination Chemistry Reviews*, 230(1–2):127 – 139, 2002.

[43] Wolfgang Kaim and Stephen Kohlmann. Design and evaluation of conjugated bridging π systems. Molecular orbital characterization and electrochemical determination of the pentacarbonyltungsten binding site in two new ambidentate ligands. *Inorganic Chemistry*, 29(10):1898–1902, 1990.

[44] Matthew A. Withersby, Alexander J. Blake, Neil R. Champness, Paul A. Cooke, Peter Hubberstey, Wan-Sheung Li, and Martin Schröder. Solvent control in the synthesis of 3,6-bis(pyridin-3-yl)-1,2,4,5-tetrazine-bridged cadmium(II) and zinc(II) coordination polymers. *Inorganic Chemistry*, 38(10):2259–2266, 1999.

[45] Thomas Scheiring, Jan Fiedler, and Wolfgang Kaim. Structure and spectroelectrochemistry (UV/Vis, IR, EPR) of the acceptor-bridged heterodinuclear complex [(^{5}-C_5Me_5)ClRh(μ-bptz)Re(CO)$_3$Cl](PF_6), bptz = 3,6-bis(2-pyridyl)-1,2,4,5-tetrazine. *Organometallics*, 20(7):1437–1441, 2001.

[46] Matthew A. Withersby, Alexander J. Blake, Neil R. Champness, Peter Hubberstey, Wan-Sheung Li, and Martin Schröder. Anion control in bipyridylsilver(I) networks: A helical polymeric array. *Angewandte Chemie International Edition in English*, 36(21):2327–2329, 1997.

[47] Y. K. Gunko and H. Hayden. Synthesis and photochemical studies of cu(I) complex with 1,4-bis(3,5-dimethylpyrazol-1yl)tetrazine ligand. *Proceedings of the SPIE*, 5826:628–635, 2005.

[48] Juergen Poppe, Michael Moscherosch, and Wolfgang Kaim. An unusually weak intervalence transition in a very stable bis chelate analog of the ruthenium mixed-valent Creutz-Taube ion. UV/visible/near-IR and EPR spectroelectrochemistry of $[(NH_3)_4Ru(\mu\text{-bptz})Ru(NH_3)_4]^{n+}$ (bptz = 3,6-bis(2-pyridyl)-1,2,4,5-tetrazine; n = 3-5). *Inorganic Chemistry*, 32(12):2640–2643, 1993.

[49] Mónica M. Vergara, Mónica E. García Posse, Florencia Fagalde, Néstor E. Katz, Jan Fiedler, Biprajit Sarkar, Monika Sieger, and Wolfgang Kaim. Mixed-valency with cyanides as terminal ligands: Diruthenium(III,II) complexes with the 3,6-bis(2-pyridyl)-1,2,4,5-tetrazine bridge and variable co-ligands (CN vs. bpy or NH_3). *Inorganica Chimica Acta*, 363(1):163 – 167, 2010.

[50] Stuart R. Batten, Jens Bjernemose, Paul Jensen, Ben A. Leita, Keith S. Murray, Boujemaa Moubaraki, Jonathan P. Smith, and Hans Toftlund. Designing dinuclear iron(ii) spin crossover complexes. Structure and magnetism of dinitrile-, dicyanamido-, tricyanomethanide-, bipyrimidine- and tetrazine-bridged compounds. *Dalton Transations*, pages 3370–3375, 2004.

[51] Ivo Cacelli, Silvio Campanile, Gianfranco Denti, Alessandro Ferretti, and Milena Sommovigo. $[(NH_3)_5Ru(1,2,4,5\text{-tetrazine})]^{2+}$: Synthesis and experimental and theoretical study of its solvatochromism in the visible spectral region. *Inorganic Chemistry*, 43(4):1379–1387, 2004.

[52] Silvia Tampucci, Marisa Belicchi Ferrari, Lucia Calucci, Giorgio Pelosi, and Gianfranco Denti. μ-1,2,4,5-tetrazine-N1:N4-bis(pentaammineruthenium) tetracation: Synthesis and X-ray structure. *Inorganica Chimica Acta*, 360(8):2814 – 2818, 2007.

[53] Animesh Nayak, Srikanta Patra, Biprajit Sarkar, Sandeep Ghumaan, Vedavati G. Puranik, Wolfgang Kaim, and Goutam Kumar Lahiri. Tetrazine derived mononuclear $Ru^{II}(acac)_2(l)$ (1), $[ru^{II}(bpy)_2(l)](clo_4)_2$ (2) and $[ruII(bpy)(l)_2](clo_4)_2$ (3) (3-amino-6-(3,5-dimethylpyrazol-1-yl)-1,2,4,5-tetrazine, acac=acetylacetonate, bpy=2,2-bipyridine): syntheses, structures, spectra and redox properties. *Polyhedron*, 24(2):333 – 342, 2005.

[54] Leslie M. Werbel, Dennis J. Mcnamara, Norman L. Colbry, Judith L. Johnson, Margaret J. Degnan, and Barbara Whitney. Synthesis and antimalarial effects of n,n-dialkyl-6-(substituted phenyl)-1,2,4,5-tetrazin-3-amines. *Journal of Heterocyclic Chemistry*, 16(5):881–894, 1979.

[55] Duong Nhu, Sandra Duffy, Vicky M. Avery, Andrew Hughes, and Jonathan B. Baell. Antimalarial 3-arylamino-6-benzylamino-1,2,4,5-tetrazines. *Bioorganic and Medicinal Chemistry Letters*, 20(15):4496 – 4498, 2010.

[56] Wei-Xiao Hu, Guo-Wu Rao, and Ya-Quan Sun. Synthesis and antitumor activity of s-tetrazine derivatives. *Bioorganic and Medicinal Chemistry Letters*, 14(5):1177 – 1181, 2004.

[57] Guo-Wu Rao and Wei-Xiao Hu. Synthesis, X-ray crystallographic analysis, and antitumor activity of 1-acyl-3,6-disubstituted phenyl-1,4-dihydro-1,2,4,5-tetrazines. *Bioorganic and Medicinal Chemistry Letters*, 15(12):3174 – 3176, 2005.

[58] Guo-Wu Rao, Yan-Mei Guo, and Wei-Xiao Hu. Synthesis, structure analysis, and antitumor evaluation of 3,6-dimethyl-1,2,4,5-tetrazine-1,4-dicarboxamide derivatives. *ChemMedChem*, 7(6):973–976, 2012.

[59] Pierre Audebert, Samp Sadki, Fabien Miomandre, and Gilles Clavier. First example of an electroactive polymer issued from an oligothiophene substituted tetrazine. *Electrochemistry Communications*, 6(2):144 – 147, 2004.

[60] Izabela Janowska, Fabien Miomandre, Gilles Clavier, Pierre Audebert, Janusz Zakrzewski, Khuyen Hoang Thi, and Isabelle Ledoux-Rak. Donor-Acceptor-Donor tetrazines containing a ferrocene unit: Synthesis, electrochemical and spectroscopic properties. *The Journal of Physical Chemistry A*, 110(47):12971–12975, 2006.

[61] Yuna Kim, Eunkyoung Kim, Gilles Clavier, and Pierre Audebert. New tetrazine-based fluoroelectrochromic window; modulation of the fluorescence through applied potential. *Chemical Communications*, pages 3612–3614, 2006.

[62] Yuna Kim, Jaekwon Do, Eunkyoung Kim, Gilles Clavier, Laurent Galmiche, and Pierre Audebert. Tetrazine-based electrofluorochromic windows: Modulation of the fluorescence through applied potential. *Journal of Electroanalytical Chemistry*, 632(1–2):201 – 205, 2009.

[63] Michael D. Coburn and Donald G. Ott. An improved synthesis of 3,6-diamino-1,2,4,5-tetrazine. *Journal of Heterocyclic Chemistry*, 27(7):1941–1945, 1990.

[64] M. D. Coburn, G. A. Buntain, B. W. Harris, M. A. Hiskey, K.-Y. Lee, and D. G. Ott. An improved synthesis of 3,6-diamino-1,2,4,5-tetrazine. II – from triaminoguanidine and 2,4-pentanedione. *Journal of Heterocyclic Chemistry*, 28(8):2049–2050, 1991.

[65] G.L. Rusinov, N.I. Latosh, I.I. Ganebnykh, R.I. Ishmetova, N.K. Ignatenko, and O.N. Chupakhin. Synthesis of 1,2,4,5-tetrazines, symmetrically and unsymmetrically 3,6-disubstituted by N-nucleophiles. *Russian Journal of Organic Chemistry*, 42(5):757–765, 2006.

[66] S.G. Tolshchina, R.I. Ishmetova, N.K. Ignatenko, A.V. Korotina, P.A. Slepukhin, G.L. Rusinov, and V.N. Charushin. Synthesis and transformations of cyanomethyl-1,2,4,5-tetrazines. *Chemistry of Heterocyclic Compounds*, 49(4):604–617, 2013.

[67] Achim Wieczorek, Tiago Buckup, and Richard Wombacher. Rigid tetrazine fluorophore conjugates with fluorogenic properties in the inverse electron demand diels-alder reaction. *Org. Biomol. Chem.*, 12:4177–4185, 2014.

[68] Rafael Chinchilla and Carmen Nájera. The Sonogashira Reaction: A booming methodology in synthetic organic chemistry. *Chemical Reviews*, 107(3):874–922, 2007.

[69] Rafael Chinchilla and Carmen Najera. Recent advances in sonogashira reactions. *Chemical Society Reviews*, 40:5084–5121, 2011.

[70] Marc Schilz and Herbert Plenio. A guide to sonogashira cross-coupling reactions: The influence of substituents in aryl bromides, acetylenes, and phosphines. *The Journal of Organic Chemistry*, 77(6):2798–2807, 2012.

[71] Tiago J. L. Silva, Paulo J. Mendes, Ana M. Santos, M. Helena Garcia, M. Paula Robalo, J. P. Prates Ramalho, A. J. Palace Carvalho, Marina Büchert, Christian Wittenburg, and Jürgen Heck. Mono(η^5-cyclopentadienyl)metal(II) complexes with thienyl acetylide chromophores: Synthesis, electrochemical studies, and first hyperpolarizabilities. *Organometallics*, 33(18):4655–4671, 2014.

[72] Jie Li and Pengcheng Huang. A rapid and efficient synthetic route to terminal arylacetylenes by tetrabutylammonium hydroxide- and methanol-catalyzed cleavage of 4-aryl-2-methyl-3-butyn-2-ols. *Beilstein Journal of Organic Chemistry*, 7:426 – 431, 2011.

[73] Alexey Smeyanov and Andreas Schmidt. K_3PO_4-KOH mixture as efficient reagent for the deprotection of 4-aryl-2-methyl-3-butyn-2-ols to terminal acetylenes. *Synthetic Communications*, 43(20):2809–2816, 2013.

[74] Glenn H. Spencer, Paul C. Cross, and Kenneth B. Wiberg. *s*Tetrazine. II – infrared spectra. *The Journal of Chemical Physics*, 35(6):1939–1945, 1961.

[75] Cyril Herbivo, Alain Comel, G. Kirsch, A. Maurício C. Fonseca, M. Belsley, and M. Manuela M. Raposo. Synthesis and characterization of novel, thermally stable 2-aryl-5-dicyanovinylthiophenes and 5-aryl-5-dicyanovinyl-2,2-bithiophenes as potentially promising non-linear optical materials. *Dyes and Pigments*, 86(3):217 – 226, 2010.

[76] Andreia Valente, Sophie Royer, Milan Narendra, Tiago J.L. Silva, Paulo J.G. Mendes, M. Paula Robalo, Manuel Abreu, Jürgen Heck, and M. Helena Garcia. Synthesis of new Fe(II) and Ru(II) η^5-monocyclopentadienyl compounds showing significant second order NLO properties. *Journal of Organometallic Chemistry*, 736(0):42 – 49, 2013.

[77] Jacek Waluk, Jens Spanget-Larsen, and Erik W. Thulstrup. Electronic states of symmetrically disubstituted s-tetrazines. *Chemical Physics*, 200(1–2):201 – 213, 1995.

[78] Ewa Kurach, David Djurado, Jan Rimarcik, Aleksandra Kornet, Marek Wlostowski, Vladimir Lukes, Jacques Pecaut, Malgorzata Zagorska, and Adam Pron. Effect of substituents on redox, spectroscopic and structural properties of conjugated diaryltetrazines – A combined experimental and theoretical study. *Physical Chemistry Chemical Physics*, 13:2690–2700, 2011.

[79] Manish Chandra, Abhaya Nand Sahay, Daya Shankar Pandey, M.Carmen Puerta, and Pedro Valerga. Synthetic, spectral and structural aspects of some mono- and binuclear (homo/hetero) Ru(II) hydrido carbonyl complexes. *Journal of Organometallic Chemistry*, 648(1–2):39 – 48, 2002.

[80] Xian-He Bu, He Liu, Miao Du, Lei Zhang, Ya-Mei Guo, Mitsuhiko Shionoya, and Joan Ribas. New mononuclear, cyclic tetranuclear, and 1-D helical-chain Cu(II) complexes formed by metal-assisted hydrolysis of 3,6-di-2-pyridyl-1,2,4,5-tetrazine (dptz): crystal structures and magnetic properties. *Inorganic Chemistry*, 41(7):1855–1861, 2002.

[81] Robert J. Forster, Tia E. Keyes, and Alan M. Bond. Protonation effects on the structure and homogeneous charge transport dynamics of solid state osmium bis(bipyridyl)tetrazine chloride films. *The Journal of Physical Chemistry B*, 104(27):6389–6396, 2000.

[82] Sylvia D. Ernst and Wolfgang Kaim. Energy level tailoring in ruthenium(II) polyazine complexes based on calculated and experimental ligand properties. *Inorganic Chemistry*, 28(8):1520–1528, 1989.

[83] Sangjoon Hahn, Dongho Kim, and Minhaeng Cho. Nonlinear optical properties of the linear quadrupolar molecule: Structure-Function relationship based on a three-state model. *The Journal of Physical Chemistry B*, 103(39):8221–8229, 1999.

[84] Tânia S. Morais, Filipa Santos, Leonor Côrte-Real, Fernanda Marques, M. Paula Robalo, Paulo J. Amorim Madeira, and M. Helena Garcia. Biological activity and cellular uptake of [Ru(η^5-C_5H_5)(PPh_3)(Me_2bpy)][CF_3SO_3] complex. *Journal of Inorganic Biochemistry*, 122(0):8 – 17, 2013.

[85] Tânia S. Morais, Filipa C. Santos, Tiago F. Jorge, Leonor Côrte-Real, Paulo J. Amorim Madeira, Fernanda Marques, M. Paula Robalo, António Matos, Isabel Santos, and M. Helena Garcia. New water-soluble ruthenium(II) cytotoxic complex: Biological activity and cellular distribution. *Journal of Inorganic Biochemistry*, 130(0):1 – 14, 2014.

[86] Takeshi Naota, Akio Tannna, Shigeaki Kamuro, Masayuki Hieda, Kazuki Ogata, Shun-Ichi Murahashi, and Hikaru Takaya. Switchable c- and n-bound isomers of transition-metal cyanocarbanions: Synthesis and interconversions of cyclopentadienyl ruthenium complexes of phenylsulfonylacetonitrile anions. *Chemistry A European Journal*, 14(8):2482–2498, 2008.

[87] Aibing Xia and John P. Selegue. Highly polarized ruthenium alkynyls with nitrothienyl substituents. *Inorganica Chimica Acta*, 334(0):219 – 224, 2002. Protagonists in Chemistry: Andrew A. Wojcicki.

[88] M. Helena Garcia, M. Paula Robalo, Alberto R. Dias, M. Teresa Duarte, Wim Wenseleers, G. Aerts, Etienne Goovaerts, Marie P. Cifuentes, Steph Hurst, Mark G. Humphrey, Marek Samoc, and Barry Luther-Davies. Synthesis and nonlinear optical properties of η^5-Monocyclopentadienyliron(II) acetylide derivatives. X-ray crystal structures of [Fe(η^5-C_5H_5)(DPPE)(p-C≡C$C_6H_4NO_2$)] and [Fe(η^5-C_5H_5)(DPPE)((E)-p-C≡CC_6H_4C(H)C(H)$C_6H_4NO_2$)]. *Organometallics*, 21(10):2107–2118, 2002.

[89] Maria Helena Garcia, Pedro Florindo, Maria de Fátima M. Piedade, Stefano Maiorana, and Emanuela Licandro. New organometallic Ru(II) and Fe(II) complexes with tetrathia-[7]-helicene derivative ligands. *Polyhedron*, 28(3):621 – 629, 2009.

[90] M. Helena Garcia, Pedro Florindo, M. Fátima M. Piedade, M. Teresa Duarte, M. Paula Robalo, Etienne Goovaerts, and Wim Wenseleers. Synthesis and structural characterization of ruthenium(ii) and iron(ii) complexes containing 1,2-di-(2-thienyl)-ethene derived ligands as chromophores. *Journal of Organometallic Chemistry*, 694(3):433 – 445, 2009.

[91] M. H. Garcia, P. J. Mendes, M. P. Robalo, M. T. Duarte, and N. Lopes. Synthesis and electrochemical studies of η^5-monocyclopentadienylruthenium(II) complexes with substituted thiophene nitrile ligands. crystal structure of $[Ru(\eta^5\text{-}C_5H_5)(dppe)(NC\{SC_4H_2\}_2NO_2)][PF_6]$. *Journal of Organometallic Chemistry*, 694(18):2888 – 2897, 2009.

[92] Nathan E. Schultz, Yan Zhao, and Donald G. Truhlar. Density functionals for inorganometallic and organometallic chemistry. *The Journal of Physical Chemistry A*, 109(49):11127–11143, 2005.

[93] Carlo Adamo and Vincenzo Barone. A TD-DFT study of the electronic spectrum of *s*-tetrazine in the gas-phase and in aqueous solution. *Chemical Physics Letters*, 330(1–2):152 – 160, 2000.

[94] Giovanni Scalmani and Michael J. Frisch. Continuous surface charge polarizable continuum models of solvation. I – general formalism. *The Journal of Chemical Physics*, 132(11):–, 2010.

[95] N. A. Ahmed and A. I. Kitaigorodsky. Experimental and theoretical determination of the crystal structure of 3,6-diphenyl-s-tetrazine. *Acta Crystallographica Section B*, 28(3):739–742, 1972.

[96] H. Alyar, M. Bahat, Z. Kantarc, and E. Kasap. Torsional potential and nonlinear optical properties of phenyldiazines and phenyltetrazines. *Computational and Theoretical Chemistry*, 977(13):22 – 28, 2011.

[97] Marcel Plugge, Valérie Alain-Rizzo, Pierre Audebert, and Albert M. Brouwer. Excited state dynamics of 3,6-diaryl-1,2,4,5-tetrazines. experimental and theoretical studies. *Journal of Photochemistry and Photobiology A: Chemistry*, 234(0):12 – 20, 2012. ¡ce:title¿In honour of Monique M. Martin¡/ce:title¿.

[98] J. Spanget-Larsen, E.W. Thulstrup, and J. Waluk. Electronic states of diphenyl- and dipyridyl-s-tetrazines: linear and magnetic circular dichroism, and quantum chemical calculations. *Chemical Physics*, 254(2–3):135 – 149, 2000.

[99] Rolf Gleiter, Volker Schehlmann, Jens Spanget-Larsen, Hans Fischer, and Franz A. Neugebauer. Photoelectron spectra of disubstituted 1,2,4,5-tetrazines. *The Journal of Organic Chemistry*, 53(24):5756–5762, 1988.

[100] Yong-Hua Gong, Fabien Miomandre, Rachel Méallet-Renault, Sophie Badré, Laurent Galmiche, Jie Tang, Pierre Audebert, and Gilles Clavier. Synthesis and physical chemistry of *s*-tetrazines: Which ones are fluorescent and why? *European Journal of Organic Chemistry*, 2009(35):6121–6128, 2009.

[101] Richard L. Cordiner, Deborah Corcoran, Dmitri S. Yufit, Andres E. Goeta, Judith A. K. Howard, and Paul J. Low. Cyanoacetylenes and cyanoacetylides: versatile ligands in organometallic chemistry. *Dalton Trans.*, pages 3541–3549, 2003.

Chapter 4

Suplementar published work

During the period of this Ph.D., other work was performed in collaboration with other group members of the Organometalic Chemistry Group of Faculdade de Ciências da Universidade de Lisboa and/or with other national and international groups. These works resulted in the publications of five peer-reviewed papers in international journals, whose first pages are reproduced in **Figures 4.1 – 4.5** In this Chapter, the mentioned works are briefly presented. Four topics are summarized: the experimental determination of the nonlinear optical properties; the mechanistic studies of a Ring Opening Polymerization (ROP) reaction; the bond dissociation energies of Ruthenium (II) organometallic compounds ; and finally the charge decomposition analysis Ruthenium (II) organometallic compounds containing bidentate N,O and N,N-heteroaromatic ligands.

4.1 Hyperpolarizability measurement

Hyperpolarizability measurements by hyper-Rayleigh Scattering was performed in the University of Hamburg, Germany, under the supervision of Prof. Jürgen Heck. A total of 27 compounds were analysed for their nonlinear optical properties. Among the compounds were the three benzo[c]thiophene complexes discussed in **Chapter 1**. Several other η^5-monocyclopentadienyliron (II), ruthenium (II) and nickel (II) thienyl-based organometallic complexes, alongside η^5-monocyclopentadienylruthenium(II) complexes bearing 4-butoxybenzonitrile and N-(3-cyanophenyl)formamide) as ligands and the binuclear iron(II) complex containing the (E)-2-(3-(4-nitrophenyl)allylidene)malononitrile ligand were also tested. Except for the case of the binuclear complex and the ruthenium(II)

complexes bearing 4-butoxybenzonitrile, Density Functional Theory calculations were performed in order to get a better understanding of the experimental linear and nonlinear optical data. The front pages of the two manuscripts are reproduced in **Figures4.1** and **4.2**.

4.2 Mechanistic Study of ROP

Several other ruthenium (II) complexes with general formula $[Ru(\eta^5\text{-}C_5H_5)(\eta^6\text{-substituted-arene})]^+[PF_6]^-$ (substituted arene = 2-phenylpyridine, dibenzosuberone and toluene) were used for the polymerization of ϵ-caprolactone. DFT calculations were undertaken for the first time in a Ring Opening Polymerization study. Results show that the polymerization proceeds via a living Activated Monomer mechanism (AM) involving an η^6 -η^4 change of the coordination mode of the arene ligand.

The front page manuscript is reproduced in **Figure 4.3**.

4.3 Estimation of Bond Dissociation Energies

Theoretical calculations were performed at the density functional theory (DFT) level using two different functionals (B3LYP and M06L) to estimate the dissociation energies (D) of η^5-monocyclopentadienylruthenium(II) complexes with N-coordinated ligands. The obtained D values of RuL_N and RuL_P were compared with the experimental data. For the imidazole-derived ligands the energy trend was rationalized in terms of the increasing extension of the σ-donation/π-backdonation effect.The M06L functional afforded values of D closer to the experimental values.

The front page manuscript is reproduced in **Figures4.4**.

4.4 Charge Decomposition Analysis Studies

Density functional theory (DFT) calculations were performed in a η^5-monocyclopentadienylruthenium(II) complex in with bidentate N,O-heteroaromatic ligands. DFT results showed that this compound revealed an enhanced metal-ligand binding, strengthened by an electronic flow from the metal centre to the σ bonded ligand, in good accordance with the experimental data.

The front page manuscript is reproduced in **Figure 4.5**.

ORGANOMETALLICS

Article

pubs.acs.org/Organometallics

Mono(η^5-cyclopentadienyl)metal(II) Complexes with Thienyl Acetylide Chromophores: Synthesis, Electrochemical Studies, and First Hyperpolarizabilities

Tiago J. L. Silva,[†] Paulo J. Mendes,*[,‡] Ana M. Santos,[†] M. Helena Garcia,[†] M. Paula Robalo,[§,∥] J. P. Prates Ramalho,[‡] A. J. Palace Carvalho,[‡] Marina Büchert,[⊥] Christian Wittenburg,[⊥] and Jürgen Heck[⊥]

[†]Centro de Ciências Moleculares e Materiais, Faculdade de Ciências, Universidade de Lisboa, Ed. C8, Campo Grande, 1749-016 Lisboa, Portugal

[‡]Centro de Química de Évora, Departamento de Química, Escola de Ciências e Tecnologia, Universidade de Évora, Rua Romão Ramalho 59, 7002-554 Évora, Portugal

[§]Centro de Química Estrutural, Instituto Superior Técnico, Universidade Técnica de Lisboa, Av. Rovisco Pais, 1049-001 Lisboa, Portugal

[∥]Área Departamental de Engenharia Química, Instituto Superior de Engenharia de Lisboa, Rua Conselheiro Emídio Navarro, 1, 1959-007 Lisboa, Portugal

[⊥]Institut für Anorganische und Angewandte Chemie, Universität Hamburg, Martin-Luther-King-Platz 6, D-20146 Hamburg

Supporting Information

ABSTRACT: A series of mono(η^5-cyclopentadienyl)metal-(II) complexes with nitro-substituted thienyl acetylide ligands of general formula $[M(\eta^5\text{-}C_5H_5)(L)(C{\equiv}C\{C_4H_2S\}_nNO_2)]$ (M = Fe, L = κ^2-DPPE, n = 1, 2; M = Ru, L= κ^2-DPPE, 2 PPh_3, n = 1, 2; M = Ni, L = PPh_3, n = 1, 2) has been synthesized and fully characterized by NMR, FT-IR, and UV−Vis spectroscopy. The electrochemical behavior of the complexes was explored by cyclic voltammetry. Quadratic hyperpolarizabilities (β) of the complexes have been determined by hyper-Rayleigh scattering (HRS) measurements at 1500 nm. The effect of donor abilities of different organometallic fragments on the quadratic hyperpolarizabilities was studied and correlated with spectroscopic and electrochemical data. Density functional theory (DFT) and time-dependent DFT (TDDFT) calculations were employed to get a better understanding of the second-order nonlinear optical properties in these complexes. In this series, the complexity of the push−pull systems is revealed; even so, several trends in the second-order hyperpolarizability can still be recognized. In particular, the overall data seem to indicate that the existence of other electronic transitions in addition to the main MLCT clearly controls the effectiveness of the organometallic donor ability on the second-order NLO properties of these push−pull systems.

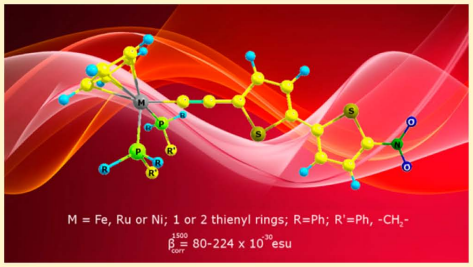

INTRODUCTION

Organometallic compounds have given rise to a great deal of interest owing to their application in the field of nonlinear optics (NLO).[1−11] Organometallic complexes (and organic molecules) have been shown as potential alternatives to the traditional inorganics due to fast and large NLO response, high optical damage thresholds, and structural diversity. In comparison to organic chromophores, organometallics can offer additional flexibility due to the presence of metal−ligand charge transfer excitations, usually at low energy and of high intensity, which are tunable due to the diversity of metal centers, oxidation states, ligand environments, and coordination geometries.

In order to obtain high second-order responses (molecular quadratic hyperpolarizability, β), strongly asymmetric systems are needed. These systems can be obtained by combining a π-conjugated chain with electron donor and/or acceptor groups (D-π-A) in which metal centers can behave either as acceptor or donor groups by simply varying the metal and/or its oxidation state. During the last two decades, it has been found that high β values could be found for molecules in which the metal center is coplanar with the π-conjugated chain. Concerning this feature, systematic studies were made by our group and others on mono(η^5-cyclopentadienyl)metal and pseudo-octahedral complexes with benzene- or thiophene-

Special Issue: Organometallic Electrochemistry

Received: February 11, 2013
Published: February 21, 2014

dx.doi.org/10.1021/om4001204 | Organometallics 2014, 33, 4655−4671

Figure 4.1: Front page of Silva *et al.*

(DOI: 10.1021/om4001204)

Journal of Organometallic Chemistry 736 (2013) 42–49

Contents lists available at SciVerse ScienceDirect

Journal of Organometallic Chemistry

journal homepage: www.elsevier.com/locate/jorganchem

Synthesis of new Fe(II) and Ru(II) η^5-monocyclopentadienyl compounds showing significant second order NLO properties

Andreia Valente [a], Sophie Royer [b], Milan Narendra [a], Tiago J.L. Silva [a,c], Paulo J.G. Mendes [c], M. Paula Robalo [b,d], Manuel Abreu [e], Jürgen Heck [f], M. Helena Garcia [a,*]

[a] Centro de Ciências Moleculares e Materiais, Faculdade de Ciências da Universidade de Lisboa, Campo Grande, 1749-016 Lisboa, Portugal
[b] Centro de Química Estrutural, Complexo I, Instituto Superior Técnico, Av. Rovisco Pais, 1049-001 Lisboa, Portugal
[c] Centro de Química de Évora, Universidade de Évora, Rua Romão Ramalho 59, 7002-554 Évora, Portugal
[d] Área Departamental de Engenharia Química, Instituto Superior de Engenharia de Lisboa, Av. Conselheiro Emídio Navarro, 1, 1959-007 Lisboa, Portugal
[e] Laboratorio de Óptica, Lasers e Sistemas, Departamento de Física, Faculdade de Ciências da Universidade de Lisboa, Campo Grande, 1749-016 Lisboa, Portugal
[f] Institut für Anorganische und Angewandte Chemie, Universität Hamburg, Martin-Luther-King-Platz 6, D-20146 Hamburg, Germany

ARTICLE INFO

Article history:
Received 22 November 2012
Received in revised form
15 February 2013
Accepted 21 February 2013

Keywords:
Cyclopentadienyl complexes
Quadratic hyperpolarizabilities
Hyper-Rayleigh scattering
Kurtz powder technique
Second-order nonlinear optical

ABSTRACT

A series of new ruthenium(II) complexes of the general formula [Ru(η^5-C_5H_5)(PP)(L)][PF_6] (PP DPPE or 2PPh_3, L 4-butoxybenzonitrile or N-(3-cyanophenyl)formamide) and the binuclear iron(II) complex [Fe(η^5-C_5H_5)(PP)(μ-L)(PP)(η^5-C_5H_5)Fe][PF_6]$_2$ (L (*E*)-2-(3-(4-nitrophenyl)allylidene)malononitrile, that has been also newly synthesized) have been prepared and studied to evaluate their potential in the second harmonic generation property. All the new compounds were fully characterized by NMR, IR and UV–Vis spectroscopies and their electrochemistry behaviour was studied by cyclic voltammetry. Quadratic hyperpolarizabilities (β) of three of the complexes have been determined by hyper-Rayleigh scattering (HRS) measurements at fundamental wavelength of 1500 nm and the calculated static β_0 values are found to fall in the range 65–212 $\times 10^{-30}$ esu. Compound presenting β_0 212 $\times 10^{-30}$ esu has revealed to be 1.2 times more efficient than urea standard in the second harmonic generation (SHG) property, measured in the solid state by Kurtz powder technique, using a Nd:YAG laser (1064 nm).

1. Introduction

There is current research interest in the development of second-order nonlinear optical (NLO) materials exhibiting large first hyperpolarizabilities β because of their applications in laser frequency conversion, optical parameter oscillators and signal communication and the inherent employ in electrooptic devices [1–9]. The most intensively studied NLO chromophores are based in highly polarizable conjugated backbones presenting an electron donor and an acceptor group attached to both ends of the backbone in order to create an asymmetric "push–pull" system. Coordination of such systems to organometallic moieties bring additional possibilities to enhance high hyperpolarizabilities due to the occurrence of low energy ligand to metal or metal to ligand charge transfer. In this frame, the organometallic moiety forms an alternative type of donor or acceptor group for the traditional push–pull system. Additional advantages of complexes are related with the variation of coligands that can fine tune the energy of these charge transfer transitions besides the introduction of other variables related with size, nature and redox ability of the transition metal.

Our approach in the search of organometallic molecular materials with strong NLO properties has been based on "MCp" pianostool structures where the chromophores are linked to the metal centre (Fe^{II}, Ru^{II}, Ni^{II} and Co^{III}) by functional groups such as nitrile (N≡C) or acetylide (C≡C) that allow interactions of the suitable metal *d* orbitals with the two π sets of orthogonal π and π^* orbitals of the functional group, leading consequently to an extension of the π-electron system between the metal and the terminal donor/acceptor substituting group of the ligand. Experimental values of the hyperpolarizabilities obtained by Hyper Rayleigh Scattering measurements were corroborated by our theoretical calculations, showing that "FeCp" and "RuCp" were the best partners for this kind of interaction, behaving more efficiently as electron donors than the traditional donor groups (such as alkyl substituted amine groups) [10]. Within this prospective to search for a large NLO response in molecular materials, we continue to explore the field and we report here our recent results concerning four new compounds. As new approaches for structural diversity and

* Corresponding author. Tel.: +351 217500972; fax: +351 217500088.
E-mail address: lena.garcia@fc.ul.pt (M.H. Garcia).

0022-328X/$ – see front matter © 2013 Elsevier B.V. All rights reserved.
http://dx.doi.org/10.1016/j.jorganchem.2013.02.028

Figure 4.2: Front page of Valente *et al.*

(DOI: 10.1016/j.jorganchem.2013.02.028)

4. Charge Decomposition Analysis Studies

Journal of Molecular Catalysis A: Chemical 346 (2011) 102–110

Contents lists available at ScienceDirect

Journal of Molecular Catalysis A: Chemical

journal homepage: www.elsevier.com/locate/molcata

Polymerization of ε-caprolactone using ruthenium(II) mixed metallocene catalysts and isopropyl alcohol: Living character and mechanistic study

Andreia Valente[a,b,c,d,e], Philippe Zinck[a,b,c,d], André Mortreux[a,b,c,d], Marc Visseaux[a,b,c,d], Paulo J.G. Mendes[f], Tiago J.L. Silva[e,f], M. Helena Garcia[e,*]

[a] Univ Lille Nord de France, F-59000 Lille, France
[b] ENSCL, UCCS, CCM, F-59652 Villeneuve d'Ascq, France
[c] USTL, UCCS, CCM, F-59655 Villeneuve d'Ascq, France
[d] CNRS, UMR8181, F-59652 Villeneuve d'Ascq, France
[e] Centro de Ciências Moleculares e Materiais, Departamento de Química e Bioquímica, Faculdade de Ciências da Universidade de Lisboa, Campo Grande, 1749-016, Lisboa, Portugal
[f] Centro de Química de Évora, Departamento de Química da Escola de Ciências e Tecnologia da Universidade de Évora, Rua Romão Ramalho 59, 7002-554 Évora, Portugal

ARTICLE INFO

Article history:
Received 28 April 2011
Received in revised form 28 June 2011
Accepted 30 June 2011
Available online 6 July 2011

Keywords:
ε-Caprolactone polymerization
ROP
Activated Monomer mechanism
Mixed sandwich
Ruthenium(II) complexes
Density Functional Theory

ABSTRACT

A series of ruthenium(II) complexes with the general formula [Ru(η^5-C_5H_5) (η^6-substituted arene)]$^+$[PF_6]$^-$ (substituted arene = 2-phenylpyridine (**1**), dibenzosuberone (**2**) and toluene (**3**)), in combination with isopropyl alcohol were used for the polymerization of ε-caprolactone. The polymerization was found to be quantitative and controlled, with PDI in the range 1.1–1.3. By means of MALDI-ToF analyses, functionalization studies with D,L-lactide and NMR monitoring techniques, it has been found that the polymerization proceeds via a *living* Activated Monomer mechanism (AM) involving an η^6–η^4 change of the coordination mode of the arene. These experimental results were corroborated by DFT studies. The growth of several polymer chains per ruthenium atom highlights interesting potentialities for molecular weight control and catalyst economy. The stability of the ruthenium complexes allows their recovery at the end of the polymerization, which can be viewed as a further advance in a green chemistry frame.

1. Introduction

Ring-opening polymerization (ROP) of polar monomers has an important impact in modern polymer chemistry due to the widespread medical applications, biocompatibility and biodegradability of the final polymers [1]. The catalysts used more often in this type of polymerization are mainly based on oxophilic metal derivatives, containing tin [2], aluminum [3,4], lithium [5], titanium [6] and rare earths [4,7]. Their activity relies on their ability to form active species, which depends on the involved mechanism. While in classical living ROP one initiator leads to the growth of one polymer chain, via Coordination Insertion (CI) [4,8] and Activated Monomer (AM) [1a,9–17] based ROP several macromolecular chains can be generated per initiator. In this case the initiator becomes a true "catalyst". This is achieved via introduction of protic compounds in addition to the catalyst, mostly alcohols. Transfer reactions are then occurring, as reported in the pioneering work of Inoue et al. [18]. Chain-end functionalization and catalyst economy can thus be achieved via these pathways. Although ruthenium based catalysts are nowadays very well established [19], their use in ring-opening polymerization of lactones is still an emerging field [20]. It is known that ruthenium complexes display a great variety of properties, such as high electron transfer ability, high Lewis acid properties and stability of reactive metallic species which make this metal a good candidate to this chemistry. The ability for transfer reactions to alcohols in ε-caprolactone polymerization was observed using the $RuCl_2(PPh_3)_3$/1,3-propanediol system (T = 150 °C; 30 h) via a Coordination-Insertion mechanism [20a]. The same authors also studied the ligand influence in the ruthenium sphere of coordination using TpRuCl(L)(L′) complexes (Tp = HB(pz)$_3$ = hydrotris(pyrazolyl)borate, L = L′ = PPh_3, L = PPh_3 and L′ = $PHPh_2$, L = L′ = PMe_2Ph, L = PPh_3 and L′ = PMe_2Ph) [20b]. Better catalytic activities were obtained using these catalysts instead of $RuCl_2(PPh_3)_3$, together with the occurrence of transfer reactions to alcohols. Finally, another research group studied a more simple catalytic system based on ruthenium(III) chloride in bulk, which suggested an Activated Monomer mechanism [20c].

In this paper we have performed the ring-opening polymerization of ε-caprolactone using three Ru(II) cationic complexes of the general formula [Ru(η^5-C_5H_5)(η^6-substituted arene)]$^+$[PF_6]$^-$ (substituted arene = 2-phenylpyridine (**1**), dibenzosuberone (**2**), and

* Corresponding author. Tel.: +351 936269186; fax: +351 217500088.
E-mail address: lena.garcia@fc.ul.pt (M.H. Garcia).

1381-1169/$ – see front matter © 2011 Elsevier B.V. All rights reserved.
doi:10.1016/j.molcata.2011.06.015

Figure 4.3: Front page of Valente *et al.*

(DOI: 10.1016/j.molcata.2011.06.015)

Research Article

Rapid Communications in Mass Spectrometry

Received: 15 March 2012 Revised: 10 May 2012 Accepted: 11 May 2012 Published online in Wiley Online Library

Rapid Commun. Mass Spectrom. **2012**, *26*, 1675–1686
(wileyonlinelibrary.com) DOI: 10.1002/rcm.6276

Gas-phase behaviour of Ru(II) cyclopentadienyl-derived complexes with N-coordinated ligands by electrospray ionization mass spectrometry: fragmentation pathways and energetics

Paulo J. Amorim Madeira[1*,†], Tânia S. Morais[2†], Tiago J. L. Silva[2,3], Pedro Florindo[2] and M. Helena Garcia[2]

[1]Centro de Química e Bioquímica, Departamento de Química e Bioquímica, Faculdade de Ciências da Universidade de Lisboa, Campo Grande, 1749-016 Lisboa, Portugal
[2]Centro de Ciências Moleculares e Materiais, Departamento de Química e Bioquímica, Faculdade de Ciências da Universidade de Lisboa, Campo Grande, 1749-016 Lisboa, Portugal
[3]Centro de Química de Évora, Departamento de Química da Escola de Ciências e Tecnologia da Universidade de Évora, Rua Romão Ramalho 59, 7002-554 Évora, Portugal

RATIONALE: The gas-phase behaviour of six Ru(II) cyclopentadienyl-derived complexes with N-coordinated ligands, compounds with antitumor activities against several cancer lines, was studied. This was performed with the intent of establishing fragmentation pathways and to determine the Ru–L_N and Ru–L_P ligand bond dissociation energies. Such knowledge can be an important tool for the postulation of the mechanisms of action of these anticancer drugs.
METHODS: Two types of instruments equipped with electrospray ionisation were used (ion trap and a Fourier transform ion cyclotron resonance (FTICR) mass spectrometer). The dissociation energies were determined using energy-variable collision-induced dissociation measurements in the ion trap. The FTICR instrument was used to perform MS^n experiments on one of the compounds and to obtain accurate mass measurements. Theoretical calculations were performed at the density functional theory (DFT) level using two different functionals (B3LYP and M06L) to estimate the dissociation energies of the complexes under study.
RESULTS: The influence of the L_N on the bond dissociation energy (*D*) of RuCp compounds with different nitrogen ligands was studied. The lability order of L_N was: imidazole < 1-butylimidazole < 5-phenyl-1*H*-tetrazole < 1-benzylimidazole. Both the functionals used gave the following ligand lability order: imidazole < 1-benzylimidazole < 5-phenyl-1*H*-tetrazole 1-butylimidazole. It is clear that there is an inversion between 1-benzylimidazole and 1-butylimidazole for the experimental and theoretical lability orders. The M06L functional afforded values of *D* closer to the experimental values. The type of phosphane (L_P) influenced the dissociation energies, with values of *D* being higher for Ru–L_N with 1-butylimidazole when the phosphane was 1,2-bis(diphenylphosphino)ethane. The Ru–L_P bond dissociation energy for triphenylphosphane was independent of the type of complex.
CONCLUSIONS: The *D* values of Ru–L_N and Ru–L_P were determined for all six compounds and compared with the values calculated by the DFT method. For the imidazole-derived ligands the energy trend was rationalized in terms of the increasing extension of the σ-donation/π-backdonation effect. The bond dissociation energy of Ru–PPh_3 was independent of the fragmentations. Copyright © 2012 John Wiley & Sons, Ltd.

Ruthenium compounds have attracted a great deal of attention largely because of their ability to inhibit the growth of cancer cells. Biological studies carried out *in vitro* and *in vivo* revealed that ruthenium-containing compounds were interesting potential candidates for anticancer drugs.[1–6] An important topic of research is the interaction of these compounds with DNA and serum proteins in order to understand the possible mechanisms of action. A fundamental issue for these studies is the ligand exchange chemistry inherent to the Ru-coordination compounds, knowledge of which will certainly help in the overall understanding of the process. Thus, studies of the metal–ligand bond strength together with preferred pathways for fragmentation of the potential drug candidates can be an important tool for determining their mechanisms of action.

Electrospray ionization (ESI) is a useful technique for the study of organometallic compounds in the gas phase. This technique[7,8] has gained recognition as a versatile way of transferring intact organometallic complexes from

* *Correspondence to:* P. J. A. Madeira, Centro de Química e Bioquímica, Departamento de Química e Bioquímica, Faculdade de Ciências da Universidade de Lisboa, Campo Grande, 1749-016 Lisboa, Portugal.
E-mail: pmadeira@fc.ul.pt

† These authors contributed equally to this work.

Figure 4.4: Front page of Madeira *et al.*

(DOI: 10.1002/rcm.6276)

4. Charge Decomposition Analysis Studies

Journal of Inorganic Biochemistry 114 (2012) 65–74

Contents lists available at SciVerse ScienceDirect

Journal of Inorganic Biochemistry

journal homepage: www.elsevier.com/locate/jinorgbio

Synthesis of organometallic ruthenium(II) complexes with strong activity against several human cancer cell lines

Tânia S. Morais [a], Tiago J.L. Silva [a,b], Fernanda Marques [c], M. Paula Robalo [d,e], Fernando Avecilla [f], Paulo J. Amorim Madeira [g], Paulo J.G. Mendes [b], Isabel Santos [c], M. Helena Garcia [a,*]

[a] Centro de Ciências Moleculares e Materiais, Faculdade de Ciências da Universidade de Lisboa, Campo Grande, 1749-016 Lisboa, Portugal
[b] Centro de Química de Évora, Universidade de Évora, Rua Romão Ramalho 59, 7002-554 Évora, Portugal
[c] Unidade de Ciências Químicas e Radiofarmacêuticas, Instituto Tecnológico e Nuclear, Estrada Nacional 10, 2686-953 Sacavém, Portugal
[d] Área Departamental de Engenharia Química, Instituto Superior de Engenharia de Lisboa, Av. Conselheiro Emídio Navarro 1, 1959-007 Lisboa, Portugal
[e] Centro de Química Estrutural, Instituto Superior Técnico, Av. Rovisco Pais, 1049-001 Lisboa, Portugal
[f] Departamento de Química Fundamental, Universidade da Coruña, Campus de A Zapateria 15071, A Coruña, Spain
[g] Centro de Química e Bioquímica, Faculdade de Ciências da Universidade de Lisboa, Campo Grande, 1749-016 Lisboa, Portugal

ARTICLE INFO

Article history:
Received 23 February 2012
Received in revised form 24 April 2012
Accepted 24 April 2012
Available online 2 May 2012

Keywords:
Ruthenium(II)
Cyclopentadienyl
Heteroaromatic ligand
Organometallic
Cytotoxicity
DFT calculations

ABSTRACT

A new family of "RuCp" (Cp = η^5-C_5H_5) derivatives with bidentate N,O and N,N′-heteroaromatic ligands revealed outstanding cytotoxic properties against several human cell lines namely, A2780, A2780CisR, HT29, MCF7, MDAMB231, and PC3. IC_{50} values were much lower than those found for cisplatin. Crystal structure of compound **4** was determined by X-ray diffraction studies. Density functional theory (DFT) calculations performed for compound **1** showed electronic flow from the ruthenium center to the coordinated bidentate ligand, in agreement with the electrochemical studies and the existence of a metal-to-ligand charge-transfer (MLCT) band evidenced by spectroscopic data.

1. Introduction

Study of ruthenium organometallic complexes became, in the recent years, a particular attractive area for the search of new antitumor drugs. The advantage of ruthenium based pharmaceuticals, relatively to antitumor platinum(II) complexes currently used in clinic [1–4], can derive on the reduced toxicity of ruthenium compounds. This crucial feature can be originated on the ability of ruthenium to mimic the iron in binding to biological molecules. Furthermore, the non-cross-resistance and a novel mechanism of action found for ruthenium complexes [5,6] in cisplatin-resistant cancer cells together with the prospect of a different spectrum of activity [7,8], put forward this promising area of research.

Our studies in this field, pioneered the family of 'Ru(η^5-C_5H_5)' based complexes as presenting potent cytotoxicity against a range of human tumor cell lines [9–11] together with the extensively studied families of compounds based on 'Ru(η^6-arene)' fragment [12–21]. In addition, the compounds derived of 'Ru(η^5-C_5H_5)(CO)' with pyridocarbazole ligands revealed strong and selective inhibitors of protein kinases GSK-3 and Pim-1 [22,23] showing also their potentiality as anticancer drugs. Therefore, an important prospective is certainly foreseen for ruthenium half sandwich structured complexes. In fact, the stabilization of the metal center by an aromatic ligand such as 'η^5-C_5H_5' or 'η^6-C_6H_6' occupying three coordination positions, constitutes the base for the design of these molecules. The remaining coordination sites can be used by the ligand that can impart the required antitumor activity together with ligands that can control the electronic properties at the ruthenium center.

We have been interested in the coordination of N-heteroaromatic molecules to 'Ru(η^5-C_5H_5)' systems and particularly for the complex with the N,N′-bipyridyl bidentate ligand we found interesting properties of stability aside the excellent cytotoxicity against several cancer cell lines [11], thus suggesting the effectiveness of a chelate ligand for our purpose. Having this in mind, our strategy was then the selection of some N,O-heteroaromatic molecules, which present other coordination sites than nitrogen, as bidentate ligands. We found that this new

* Corresponding author at: Faculdade de Ciências da Universidade de Lisboa, Edifício C8, Campo Grande, 1749-016 Lisboa, Portugal. Tel.: +351 217500972; fax: +351 217500088.
E-mail address: lena.garcia@fc.ul.pt (M.H. Garcia).

0162-0134/$ – see front matter © 2012 Elsevier Inc. All rights reserved.
doi:10.1016/j.jinorgbio.2012.04.014

Figure 4.5: Front page of Morais *et al.*

(DOI: 10.1016/j.jinoorgbio.2012.04.014)

Chapter 5

Experimental

5.1 Characterization Methods

Commercial reagents were used without further purification. Monocyclopentadiene was obtained by thermal cracking of dicyclopentadiene and used immediately. All organometallic synthesis were carried out under nitrogen atmosphere using Schlenk techniques. The solvents used were dried and distilled according to common literature procedures.[1] Organometallic starting materials were prepared following the methods described in the literature: (η^5-C_5H_5)Fe(κ^2-dppe)I],[2] (η^5-C_5H_5)Ru(PPh_3)$_2$Cl and (η^5-C_5H_5)Ru(κ^2-dppe)Cl.[3]

5.1.1 Spectroscopic Techniques

FT-IR spectra were recorded in a Mattson Satelite FTIR spectrophotometer in dry KBr pellets. The spectra were obtained by accumulation of 32 scans with a 1 cm^{-1} resolution.

UV-Vis spectra were recorded in a Jasco V-660 in using quartz cells in the range of 200-900 nm. All used solvents were spectroscopic grade or dried and distilled prior to use.

^{1}H , ^{13}C and ^{31}P-NMR spectra were recorded on a Bruker Avance 400 spectrometer at probe temperature using comercialy available deuterated solvents. The ^{1}H and ^{13}C chemical shifts (s = singlet; d = duplet; t = triplet; m = multiplet for 1H) are reported in parts per million (ppm) downfield from the residual solvent peak and the ^{31}P NMR spectra are reported in ppm downfield from external standard, 85% H_3PO_4. Coupling constants are reported in Hz. All assignments were attributed using HMBC, HMQC and COSY 2D-RMN techniques.

5.1.2 Hyper-Rayleigh Scattering (HRS)

First hyperpolarizabilities (β) measurements were performed at a fundamental wavelength of 1500 nm as described elsewhere, using a Q-switched Nd:YAG laser operating in the 10 Hz repetition range.[4] Fluo-

rescence checks were made by replacement of the interference filter at the entrance of the photomultiplier tube using filters with the transmittances at 650, 700 and 800 nm. The $10^{-3} - 10^{-5}$ M chloroform solutions of the complexes were placed into a 4 cm long fluorimetric cell, after being carefully filtered through a 0.2 μm filter in order to eliminate the white light noise resulting from microburning of any the remaining dust particles by the incoming laser beam. Disperse Red 1 (DR1) was used as external standard and was measured also in chloroform solutions. The reference hyperpolarizability of DR1 in $CHCl_3$ was measured by comparison of the slopes of $I_{2\omega}$ vs. concentration plots of the standard in CH_2Cl_2 and $CHCl_3$. Using the hyperpolarizability of DR1 in dichloromethane (β_{DR1} (CH_2Cl_2) = 70×10^{-30} esu the hyperpolarizability of DR1 in $CHCl_3$ was estimated to be 80×10^{-30} esu, which is very close to the published value of 74×10^{-30} esu.[4,5] Assuming that the scattering contribution from the solvent is negligibly small, this external reference method is used to calculate the β values of complexes according to equation 5.4:

$$\beta = \sqrt{\frac{S_{sample}}{S_{ref.}}} \times \beta_{ref.} \tag{5.1}$$

where S is the slope of the appropriate $I_{2\omega}$ vs. concentration plot and $\beta_{ref.}$ is the orientational average of the first hyperpolarizability of the reference sample.

5.1.3 Cyclic Voltammetry (CV)

Electrochemical measurements were performed on an EG&G Princeton Applied Research Potentiostat-Galvanostat Model 273A equipped with Electrochemical PowerSuite v2.51 software for electrochemical analysis, in anhydrous dichloromethane or acetonitrile with tetrabutylammonium hexafluorophosphate (0.1 M) as supporting electrolyte. The electrochemical cell was a home made three electrode configuration cell with a platinum-disc working electrode (1.0 mm) probed by a Luggin capillary connected to a silver-wire pseudo-reference electrode and a platinum wire auxiliary electrode. All experiments were performed in nitrogen atmosphere at room temperature. All the potentials reported were measured against the ferrocene/ferrocenium redox couple as internal standard and normally quoted relative to SCE (using the ferrocenium/ferrocene redox couple $Ep_{1/2}$ = 0.46 or 0.40 V versus SCE for dichloromethane or acetonitrile, respectively).[6] The electrochemical grade electrolyte was purchased from Aldrich Chemical Co. and stored under nitrogen atmosphere. All used solvents were dried, purified by standard procedures and distilled under nitrogen atmosphere before use.

5.1.4 Elemental Analysis (EA)

Elemental analyses were obtained at Laboratório de Análises, Instituto Superior Técnico, using a Fisons Instruments EA1108 system. Data acquisition, integration and handling were performed using a PC with the software package EAGER-200 (Carlo Erba Instruments).

5.2 Density Functional Calculations

All calculations were performed at the DFT level using the Gaussian 09 package[7]. The B3LYP (Beckes three parameter functional with Lee-Yang-Parr exchange-correlations) CAM-B3LYP (Coulomb-attenuating method applied to B3LYP) and M06 functionals were used for the calculations.[8–11] As a compromise between accuracy and computational effort we have adopted the 6-31G* basis set (for geometry optimizations) and the 6-31+G* basis set (for the calculation of hyperpolarizabilities) for C, H, N, O and H and the LANL2DZ effective core potential basis set for S, P, Fe and Ru .[12,13] In the case of the hyperpolarizability calculations the LANL2DZ basis set was also augmented with a polarization function (exponents of 0.496 and 0.364) and a diffuse function (exponents of 0.0347 and 0.0298) for elements S and P, respectively.[14,15] Geometry optimizations were performed without any symmetry constraints. In all cases, the Hessian was computed to confirm the stationary points of the potential energy surfaces (PES) as true minima. In the case of the oxidized and reduced species, spin unrestricted calculations were done. Condensed phase calculations were performed using the Polarizable Continuum Model (PCM) as implemented in Gaussian.[16] The static first hyperpolarizability, β_{tot} and β_{HRS}, for all compounds were calculated as implemented in the Gaussian 09 program package by using the following equation:

$$\beta_{to} = \sqrt{\beta_x^2 + \beta_y^2 + \beta_z^2} \tag{5.2}$$

with

$$\beta_i = \frac{1}{3}\sum\left(\beta_{iii}^2 + \beta_{ijj}^2 + \beta_{ikk}^2\right), \quad with \quad i,j,k = x,y,z \tag{5.3}$$

and

$$\langle\beta_{HRS}^2\rangle = \langle\beta_{ZZZ}^2\rangle + \langle\beta_{XZZ}^2\rangle \tag{5.4}$$

with

$$\langle\beta_{ZZZ}^2\rangle = \frac{1}{7}\sum_i \beta_{iii}^2 + \frac{6}{35}\sum_{i\neq j}\beta_{iii}\beta_{ijj} + \frac{9}{35}\sum_{i\neq j}\beta_{iij}^2 + \frac{12}{35}\sum_{ijk,cyclic}\beta_{ijk}^2 \tag{5.5}$$

$$\begin{aligned}\langle\beta_{XZZ}^2\rangle = \frac{1}{35}\sum_i \beta_{iii}^2 - \frac{2}{105}\sum_{i\neq j}\beta_{iii}\beta_{ijj} + \frac{11}{105}\sum_{i\neq j}\beta_{iij}^2 \\ - \frac{2}{105}\sum_{ijk,cyclic}\beta_{iij}\beta_{jkk}^2 + \frac{8}{35}\beta_{ijk}^2\end{aligned} \tag{5.6}$$

Time-dependent density functional theory (TD-DFT)[17,18] was used to compute the electronic spectra of the studied molecules applying the same theory level and basis sets used for the calculation of the hyperpolarizabilities. The first 24 lower excitation energies were computed in the case of Chapter 2 whereas 120 lower excitation energies was used for Chapter 3. The simulated absorption bands were obtained by convolution of Gaussian functions centred at the calculated excitation energies using the

GaussSum (version 2.2.4) software.[19] Chemcraft program (version 1.6) was used for the visualization of the computed results, including the representation of the geometries and the orbitals.

References

[1] W.L.F. Armarego and C. Chai. *Purification of Laboratory Chemicals*. Elsevier Science, 2012.

[2] M. Helena Garcia, Paulo J. Mendes, M. Paula Robalo, A. Romão Dias, Jochen Campo, Wim Wenseleers, and Etienne Goovaerts. Compromise between conjugation length and charge-transfer in nonlinear optical η^5-monocyclopentadienyliron(II) complexes with substituted oligo-thiophene nitrile ligands: Synthesis, electrochemical studies and first hyperpolarizabilities. *Journal of Organometallic Chemistry*, 692(14):3027 – 3041, 2007.

[3] Chun-Guang Liu, Xiao-Hui Guan, and Zhong-Min Su. Computational study on redox-switchable 2D second-order nonlinear optical properties of pushpull mono-tetrathiafulvalene-bis(salicylaldiminato) zn(II) schiff base complexes. *The Journal of Physical Chemistry C*, 115(13):6024–6032, 2011.

[4] Stefan Stadler, Roland Dietrich, Grant Bourhill, Christoph Bruchle, Andreas Pawlik, and Walter Grahn. First hyperpolarizability measurements via hyper-rayleigh scattering at 1500 nm. *Chemical Physics Letters*, 247(3):271 – 276, 1995.

[5] Junes Ipaktschi, Javad Mohseni-Ala, Ansgar Dlmer, Stefan Steffens, Christian Wittenburg, and Jrgen Heck. Addition of ynamines to the tungsten 1-vinylidene complexes (5-c5h5)(no)(co)wcc(h)r. *Organometallics*, 23(21):4902–4909, 2004.

[6] Neil G. Connelly and William E. Geiger. Chemical redox agents for organometallic chemistry. *Chemical Reviews*, 96(2):877–910, 1996. PMID: 11848774.

[7] M. J. Frisch, G. W. Trucks, H. B. Schlegel, G. E. Scuseria, M. A. Robb, J. R. Cheeseman, G. Scalmani, V. Barone, B. Mennucci, G. A. Petersson, H. Nakatsuji, M. Caricato, X. Li, H. P. Hratchian, A. F. Izmaylov, J. Bloino, G. Zheng, J. L. Sonnenberg, M. Hada, M. Ehara, K. Toyota, R. Fukuda, J. Hasegawa, M. Ishida, T. Nakajima, Y. Honda, O. Kitao, H. Nakai, T. Vreven, J. A. Montgomery, Jr., J. E. Peralta, F. Ogliaro, M. Bearpark, J. J. Heyd, E. Brothers, K. N. Kudin, V. N. Staroverov, R. Kobayashi, J. Normand, K. Raghavachari, A. Rendell, J. C. Burant, S. S. Iyengar, J. Tomasi, M. Cossi, N. Rega, J. M. Millam, M. Klene, J. E. Knox, J. B. Cross, V. Bakken, C. Adamo, J. Jaramillo, R. Gomperts, R. E. Stratmann, O. Yazyev, A. J. Austin, R. Cammi, C. Pomelli, J. W.

Ochterski, R. L. Martin, K. Morokuma, V. G. Zakrzewski, G. A. Voth, P. Salvador, J. J. Dannenberg, S. Dapprich, A. D. Daniels, Ö. Farkas, J. B. Foresman, J. V. Ortiz, J. Cioslowski, and D. J. Fox. Gaussian 09 Revision B.01. Gaussian Inc. Wallingford CT 2009.

[8] Axel D. Becke. Densityfunctional thermochemistry. iii. the role of exact exchange. *The Journal of Chemical Physics*, 98(7):5648–5652, 1993.

[9] Chengteh Lee, Weitao Yang, and Robert G. Parr. Development of the colle-salvetti correlation-energy formula into a functional of the electron density. *Phys. Rev. B*, 37:785–789, Jan 1988.

[10] Takeshi Yanai, David P Tew, and Nicholas C Handy. A new hybrid exchange–correlation functional using the coulomb-attenuating method (cam-b3lyp). *Chemical Physics Letters*, 393(1–3):51 – 57, 2004.

[11] Yan Zhao and DonaldG. Truhlar. The m06 suite of density functionals for main group thermochemistry, thermochemical kinetics, noncovalent interactions, excited states, and transition elements: two new functionals and systematic testing of four m06-class functionals and 12 other functionals. *Theoretical Chemistry Accounts*, 120(1-3):215–241, 2008.

[12] P. Jeffrey Hay and Willard R. Wadt. Ab initio effective core potentials for molecular calculations. potentials for the transition metal atoms sc to hg. *The Journal of Chemical Physics*, 82(1):270–283, 1985.

[13] P. Jeffrey Hay and Willard R. Wadt. Ab initio effective core potentials for molecular calculations. potentials for k to au including the outermost core orbitals. *The Journal of Chemical Physics*, 82(1):299–310, 1985.

[14] Catherine E. Check, Timothy O. Faust, John M. Bailey, Brian J. Wright, Thomas M. Gilbert, and Lee S. Sunderlin. Addition of polarization and diffuse functions to the lanl2dz basis set for p-block elements. *The Journal of Physical Chemistry A*, 105(34):8111–8116, 2001.

[15] Karen L. Schuchardt, Brett T. Didier, Todd Elsethagen, Lisong Sun, Vidhya Gurumoorthi, Jared Chase, Jun Li, and Theresa L. Windus. Basis set exchange: a community database for computational sciences. *Journal of Chemical Information and Modeling*, 47(3):1045–1052, 2007. PMID: 17428029.

[16] Alessandro Corozzi, Benedetta Mennucci, Roberto Cammi, and Jacopo Tomasi. Structure versus solvent effects on nonlinear optical properties of pushpull systems: A quantum-mechanical study based on a polarizable continuum model. *The Journal of Physical Chemistry A*, 113:14774–14784, 2009.

[17] Mark E. Casida, Christine Jamorski, Kim C. Casida, and Dennis R. Salahub. Molecular excitation energies to high-lying bound states from time-dependentdensity-functionalresponsetheory: Characterizationand correctionofthetime-dependentlocaldensityapproximation ionization threshold. *The Journal of Chemical Physics*, 108(11):4439–4449, 1998.

[18] R.F. Nalewajski. *Perspectives in Electronic Structure Theory*. Springer Berlin Heidelberg, 2012.

[19] Noel M. O'boyle, Adam L. Tenderholt, and Karol M. Langner. cclib: A library for package-independent computational chemistry algorithms. *Journal of Computational Chemistry*, 29(5):839–845, 2008.

Chapter 6

Conclusion

The main goal of this thesis was the synthesis, characterization and density functional studies of novel η^5-monocyclopentadienyl complexes for molecular nonlinear optical switching purposes. Two dierent families of ligands, benzo[c]thiophene and s-tetrazine based chromophores, were synthesized giving a total of seven compounds. The further coordination to η^5-monocyclopentadienyliron(II) and/or ruthenium(II) metal centres afforded six novel organometallic compounds.

The synthesis of the benzo[c]thiophene ligands have proven to be troublesome in the sense that the achievement of the core structure was challenging. Subsequent functionalization of the core with the initially intended acetylene linker was unsuccessful due to a failure in the bromination reactions step. Coordination to the metal centres was hence made by a nitrile linkage. Insertion of an electron-withdrawing nitro group in view to obtain more asymmetric structures was also unsuccessful. The nonlinear optical properties of the synthetized complexes, besides a series of other families of complexes mentioned in Chapter 4, were studied by hyper-Rayleigh scattering in the University of Hamburg during a stay of three months. Based of density functional theory calculations, all the studied complexes present electronic features that distinguish them among the existent compounds with nonlinear optical redox-switching properties. In particular, the results showed that, upon one-electron oxidation, the hyperpolarizabilities are predicted to be enhanced, contrarily to the usually accepted behaviour that is a diminishing of this property. Unfortunately the oxidation form of the complexes was found to be unstable to allow the evaluation of the experimental nonlinear optical redox-switching properties and to confirm the predicted behaviour from theoretical studies.

Future perspectives in this benzo[c]thiophene based complexes include the synthesis of complexes with enhanced stability, the determination of the hyperpolarizabilities of both the oxidized and non-oxidized isolated complexes, or generated *in situ* during experimental hyperpolarizability determination, and the measurement of the bulk nonlinear optical properties of both the oxidized and non-oxidized species. The stability of the oxidized form complexes can be achieved by several ways keeping in mind the stabilization of the metal centre in a higher formal oxidation state, namely using the η^5-pentamethylcyclopentadienyl moiety, insertion of good electron-donor substituents in the chromophore and fine tune the electron density at the metal centre by varying the co-ligands.

Tetrazines recently rebirth to the eyes of chemists. Their nonlinear optical properties are fairly un-

known and a deep exploitation either in their spectroscopic or electrochemical properties is still required. The present work provided new compounds that are one of the few examples of non-polymeric linear tetrazine based complexes. As far as this work is concerned, it is the only dealing with the NLO-switching properties of tetrazine-based organometallic compounds.

The major flaw of this work is the lack of the electrochemical properties of the synthesized tetrazine compounds which would greatly improve the overall results, in particular the investigation of the reversibility of the redox processes that allows to give an insight of the stability of the oxidized species and enable a switch to be obtained. Also, the experimental hyperpolarizabilities could not be measured. However, the nonlinear optical redox-switching properties of some of the studied compounds were evaluated by density functional theory calculations. Results show that NLO molecular switches bearing tetrazine rings can be developed. As for the benzo[c]thiophene based complexes, the results showed that, upon one-electron oxidation, the hyperpolarizabilities are predicted to be significantly enhanced, depending on the chromophore structure, contrarily to the mentioned usually accepted behaviour.

Currently, the classification of the nonlinear optical switching mechanisms by redox means is based on molecules that possesses highly asymmetric structures in their non-oxidized form. In this work, If the theoretical data of the present work could be confirmed by experimental results in the near future, this work could prove that it is also possible to achieve efficient nonlinear optical redox switches based on symmetric (or less asymmetric) structures in their non-oxidized form. So far, this kind of strategy is much less studied in this field and future perspectives could be envisaged to keeping efforts in this strategy, also exploring other π-spacers and/or donor and acceptor groups.